Assessing the fidelity of the marine sedimentary magnetic record: Preservation and diagenetic alteration of magnetic mineral assemblages in upwelling regions off western Africa

Dissertation

Zur Erlangung des Doktorgrades der Naturwissenschaften
am Fachbereich Geowissenschaften
der Universität Bremen

submitted for the doctoral degree in natural sciences
at the faculty of Geosciences
of Bremen University

vorgelegt von
by

Melanie Dillon

Bremen,
März/March 2008

Tag des Kolloquiums:

30. Mai 2008

Gutachter:

Herr Prof. Dr. Ulrich Bleil

Frau PD Dr. Sabine Kasten

Prüfer:

Herr Prof. Dr. Tobias Mörz

Herr Prof. Dr. Heiner Villinger

Content

Introduction

Magnetic particles usually occur in very minor concentrations in igneous and sedimentary rocks, soils, volcanic ashes, dusts and even in living organisms. Many of these magnetic grains are capable of carrying a stable permanent magnetization and therefore act as recorders of the recent and ancient Earth´s magnetic field. Thus paleomagnetism refers to the study of this remanent magnetization in sedimentary and volcanic rocks through time. From this magnetization, directional intensity information can be recovered concerning the geomagnetic field that prevailed at the sample location at the time of the rock formation.

Through time the Earth´s magnetic field varies in both, its orientation and intensity. Based on numerous global studies of basaltic lava flows, it has been shown that the Earth´s magnetic field reverses irregularly at intervals ranging from tens of thousands to many millions of years. The last event, the so-called "Matuyama-Brunhes" reversal, has been dated from lava successions ~780 thousand years ago (e.g. *Spell and McDougall*, 1992). Paleomagnetic studies have contributed to the present theories of polar wandering, continental drift and sea floor spreading and a global geomagnetic polarity time scale has been established (e.g. *Cande and Kent*, 1995). However, volcanic activity occurs only sporadically and therefore lava successions do not yield a continuous sequence of paleomagnetic information.

Aquatic sediments comprise continuous records of directional and intensity changes of the Earth´s magnetic field. It was found that sediments which accumulated continuously, such as deep-sea sediments, have also recorded polarity changes in detail. Investigations by *Ninkovich et al*. (1966), *Heirtzler et al*. (1968), *Opdyke and Glass* (1969) rapidly confirmed the land-based polarity time scale. High-quality relative paleointensity records were determined from deep-sea sediments e.g. by *Tauxe and Wu* (1990), *Valet and Meynadier* (1993), *Thibal et al*. (1995) *Guyodo and Valet* (1999) and *Valet* (2005). In the deep-sea, sedimentation rates are generally relatively low, typically ~1 cm/kyr or even less (e.g. *Schmieder*, 2004). This constraints the time resolution of the magnetic signal but on the other hand extents the archive further back in time.

The magnetic parameter on which such paleomagnetic studies are based is the natural remanent magnetization (NRM). It describes the magnetization in sedimentary and igneous rocks, resulting from the orientation of the particles magnetizations within the Earth´s magnetic field at the time of the sediment/rock formation. The mechanism of the NRM acquisition depends on the mode of deposition and on the individual history of the rock, as well as on the specific characteristics of the magnetic minerals. The remanent magnetization acquired by sediments is a mechanical process termed detrital remanent magnetization (DRM). During their passage through the water column and ultimate settling at the water sediment interface the magnetic particles will act like small magnets with a preferred orientation in alignment with the direction of the ambient magnetic field. This original orientation may be preserved during the depositional process, resulting in a NRM that is parallel to the field at the time of deposition. In most cases the DRM is not completely fixed until the sediment has been compacted and consolidated by the weight of later deposits ("lock-in depth"). Until this point is reached the unconsolidated sediments are often affected by further disturbance through bioturbation or mechanical slumping, which may modify the recorded direction (e.g. *Kent*, 1973). If the primary DRM is modified after deposition, the magnetization is then called post-depositional remanent magnetization pDRM.

Even during intervals of constant polarity the geomagnetic field shows irregular behaviour with short-term changes in its direction and intensity (e.g. secular variations). High-quality magnetic records provide a powerful tool for dating and correlating sediment sequences over the past few thousands of years. To achieve such temporally high resolution records, deposits characterized by high sedimentation rates are needed. The highest sedimentation rates are usually found in continental margin regions with magnitudes of several cm per thousand years. These sediments have recorded the changes of the geomagnetic field over recent geological history. With an average sedimentation rate of 10 cm/kyr a ten metre long sediment sequence would therefore cover the last 100.000 years which is geologically speaking a relatively short time interval. Therefore the rapidly deposited marine sediments which occur along continental margins potentially offer continuous high resolution records of geomagnetic secular variation.

Magnetic studies can not only be used for dating and correlation of whole sequences or specific geologic horizons by their magnetic reversal records, magnetic grains also act as sensitive recorders of paleoclimatic and paleoenvironmental changes. In recent years, where global warming is one of the most pressing challenges facing mankind, paleoclimatic studies have become increasingly important. The mineral influx from eroded continental bedrock debris into marine sediments involves a variety of geological processes: physical and chemical weathering, aeolian and fluvial transport, deposition and re-deposition by ocean currents, and the overprint by early diagenesis. The identification of particle sources, transport pathways and post-depositional mineral alteration provides important information about these climatically triggered variations. The changes in magnetic mineralogy, concentration and grain-size are influenced by environmental conditions prevailing at the sediment source and the depositional area. Magnetic mineral assemblages in marine sediments are suitable archives for reconstructions of the paleoenvironment, since their concentration, mineralogy, grain-size and coercivity are indicative of the genesis of the magnetic components and the geological processes they were subjected to. The properties of magnetic minerals have been used as proxy parameters for paleoclimate, paleoceanographic or provenance studies in sediments (e.g. *Kent,* 1982; *Bloemendal et al*., 1992; *Schmidt et al*., 1999; *Schmieder et al*., 2000; *Watkins and Maher*, 2003; *Bleil and von Dobeneck*, 2004*; Funk et al*., 2004; *Franke et al*., 2007) forming the field of environmental magnetism.

For marine environments *Thompson and Oldfield* (1986) distinguished four potential magnetic components of different origin: (1) cosmogeneous compounds which are of atmospheric and extraterrestrial origin (e.g. cosmic spherules), (2) lithogenous components which originate from land erosion and/or submarine volcanoes, (3) biogenic compounds (e.g. magnetosomes of magnetotactic bacteria) and (4) authigenic / diagenetic components (Fig. 1). In particular the influx of terrigenous magnetic components into marine sedimentary deposits depends on the individual geographic setting and typically comprises various lithogenic minerals and their weathering products. The sediment magnetic properties are in general dominated by ferrimagnetic (magnetite, titanomagnetite, maghemite, titano-maghemite) and antiferromagnetic (hematite, titanohematite) iron-titanium oxides. Iron sulfides (greigite, phyrrotite) and iron hydroxides (goethite) may also be of significance. Authigenic and diagenetic magnetic phases were found to be quite common in marine sediments (e.g. *Frederichs et al*., 2003). Their formation is often related to drastic changes in the accumulation rate and the availability of organic matter, which in turn depend on

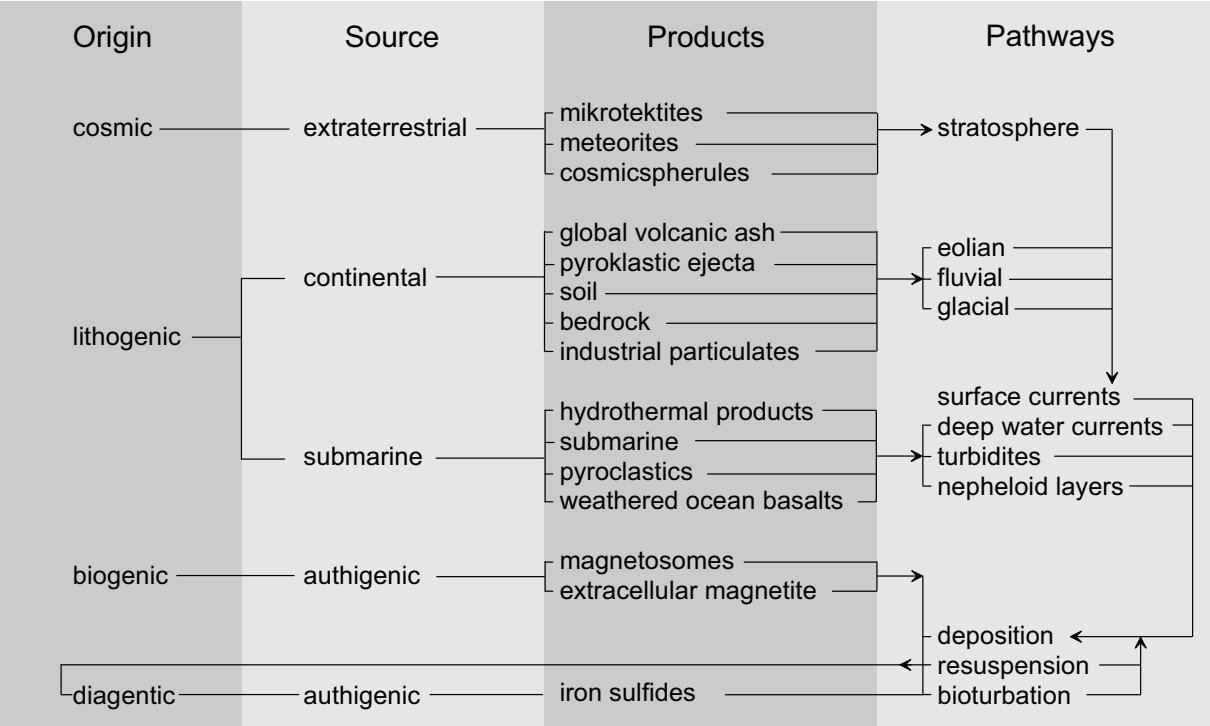

Fig. 1 Roots and tracks of magnetic minerals to the marine environment (redrawn after *Frederichs et al*., 1999)

climate conditions. In continental margin regions the remanence acquisition process is complicated by post-depositional modifications of the original magnetic material. The primary NRM may be erased either partly or completely and additional secondary components may be added by several other processes. These subsequent overprints are referred to as secondary magnetizations. One major task in all paleomagnetic investigations is to identify and, if possible, separate all components by their primary or secondary characteristics (e.g. viscous remanent magnetization (VRM) or chemical remanent magnetization (CRM)).

In marine and continental environments, an important cause of diagenesis is the decomposition of organic matter by microbial oxidation (e.g. *Berner*, 1981). After their deposition magnetic minerals can be altered or new magnetic phases can be formed. Consequently the original NRM might be obscured or even fully erased. The process of diagenesis and authigenesis may thus seriously compromise paleomagnetic interpretation. Therefore our knowledge of the geomagnetic field behavior based on sediment records from continental margin regions remains limited. To obtain fully reliable information about the geomagnetic field or paleoenvironmental conditions from continental margin regions, the effect of early diagenetic processes occurring after deposition of the sediment must be understood in detail.

The marine realm of the NW and W African continental margin

Continental margins are ideal study areas for geoscientific investigations since they provide the main accumulation zones for terrigenous sediments. Passive continental margins such as most of the Atlantic coastal regions are characterized by wide and shallow shelves, with thick sedimentary wedges derived from the long term erosion of the adjacent continent. There is no collision or subduction taking place, hence tectonic activity is minimal and the accumulation of thick sedimentary deposits on the relatively wide continental shelves occurs quasi-continuously through

time. Mass flow occurs across the land-sea boundary by river and wind transport. After deposition further distribution or redistribution of the material is driven by the ocean currents. The quantity and composition of the terrigenous fraction transported into the oceans is strongly influenced by the climate and vegetation in the hinterland that control the nature and the degree of weathering and also the mode of material supply (*Weaver et al*., 2000).

The African climate system is a result of its geographical position which is almost completely in the subtropical and equatorial latitudes of the northern and southern hemisphere. The climate of NW and Central Africa exhibits different regimes (Fig. 2). The North is dominated by the arid Saharan desert, while in Central Africa rainforests with highly humid conditions exist (*Nicholson*, 2000). Overall approximately 39% of the continent is covered by desert, 10% by semi-desert, 35% by savannah and only 10% equatorial rainforest. The seasonal latitudinal shift of the Intertropical Convergence Zone (ITCZ) plays an important role in controlling NW African atmospheric conditions. During boreal summers the ITCZ moves to its northernmost position at ~19°N and in boreal winter to its southernmost position at ~5°S (*Nicholson*, 2000). Thus the centre of transatlantic aeolian dust transport migrates seasonally. Besides this general pattern, regional differences are found, e.g., the Canary Island Region is mainly influenced by the dry winter monsoons, whereas the Niger deep sea fan area is situated in reach of the wet summer monsoons.

The Niger River is the main river in western Africa and along with the Congo River further south the major fluvial source of continental detritus into the tropical Atlantic (Fig. 2). The Niger originates in SW Guinea and flows over a length of 4180 km generally eastward into a vast delta on the Gulf of Guinea. The modern drainage area ($\sim 1.55 \cdot 10^6$ km^2) of the Niger extends from the sub-Sahara, through the savannah grassland and finally the dense forest regions (*Boeglin and Probst*, 1998). Due to the relatively high rates of annual rainfall (~1250 mm/year) in the drainage area, the Niger River transports about 154 km^3 water into the eastern tropical South Atlantic each year, but because of the low-relief gradient of the lateritic river basin, which prevents an intensive erosion, the complete suspended material amounts only to ~26 g/m^3. The suspension load consists mainly of highly weathered solids (*Konta*, 1985 and references therein). Overall fluvial supply into the North Atlantic Ocean is restricted to the Moroccan margin, where short-living rivers derived from the Atlas Mountains are responsible for sediment transport. Further south on the NW African coast the fluvial discharge into the ocean is strongly reduced (*Weaver et al*., 2000), instead aeolian dust is the most important contributor of lithogenic material to the marine sediments (Fig. 2).

One of the most important global source regions of airborne mineral dust is the Saharan-Sahel area (*Harrison et al*., 2001). The aeolian dust transport over the NW African continent and the eastern tropical Atlantic is driven by two main wind systems: the Saharan Air Layer (SAL) and the Trade winds (*Mayewski et al*., 1997). The SAL is a mid-tropospheric zonal wind system related to the African Easterly Jet and occurs at altitudes between 1500 and 5000 m (*Prospero*, 1990). It accounts for most of the transport of Saharan and Sahelian dust (*Bergametti et al*., 1989). The lower altitudes (< 1500 m) are dominated by the seasonal NE Trade winds, blowing parallel to the African coast. The dust load of these Trade winds originates mainly from the northern Sahara and the Atlas Mountains (*Chiapello et al*., 1995).

The Trade winds also dominate the dynamics of the North and Equatorial Atlantic surface water circulation. The major surface ocean current along the NW African margin is the cold, southwestward flowing Canary Current (CC) (Fig. 2). It is part of the Eastern Boundary Current

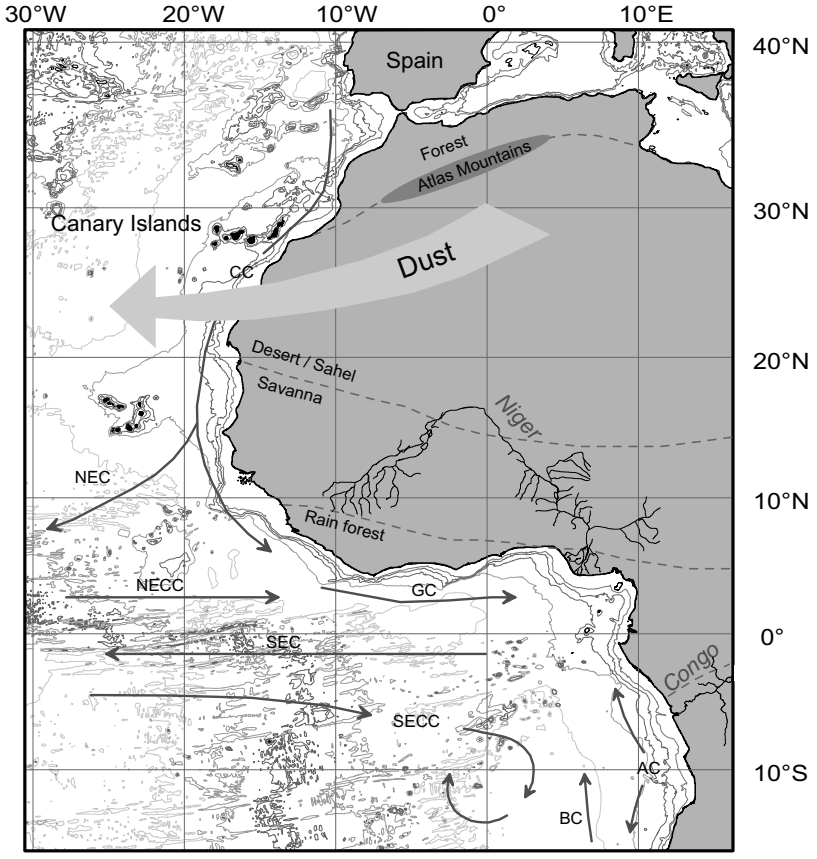

Fig. 2 Overview of the main study area, situated in around NW Africa and the Equatorial Atlantic. Coastlines and isobaths at 1000 m intervals are given according to the *Intergovernmental Oceanographic Commission* (1994). Black arrows mark the major surface currents for the region: Canary Current (CC), North Equatorial Atlantic (NEC), North Equatorial Countercurrent (NECC), Guinea Current (GC), South Euqatorial Current (SEC), South Equatorial Countercurrent (SECC), Benguela Current (BC), and Angola Current (AC). The large grey arrow denotes the major wind direction triggered by zonal winds. Also shown are the different general vegetation zones reflecting the prevailing climatic conditions on the African continent (*deMenocal et al*., 1993). The Niger and Congo River are the major fluvial sources.

System, which in turn originates from the North Atlantic drift. At approximately 15°N the Canary Current diverges: driven by the Trade winds most of this fraction turns west, forming the westward flowing North Equatorial Current (NEC). A minor part of the CC continues on southwards along the coast, until further south it becomes the Guinea Current (GC) which joins the Equatorial Countercurrent (ECC) at approximately 6°N (*Sarntheim et al*., 1982). Besides the Guinea Current, the Southern Equatorial Atlantic Current (SEC) and the Benguela Current (BC) form the surface water circulation in the tropical eastern Atlantic (*Peterson and Stramma*, 1991). The modern oceanic circulation pattern off NW Africa and the tropical eastern Atlantic are described comprehensively by e.g. *Sarntheim et al*. (1982) and *Peterson and Stramma* (1991).

One of the most important responses of the ocean to the surface winds is the coastal upwelling of nutrient rich water from the subsurface. Particularly the eastern continental ocean margins are characterized by this process. This oceanographic phenomenon involves wind-driven motion of warmer, usually nutrient-depleted surface water off the coast. As the surface water is pushed offshore, deeper water is drawn from

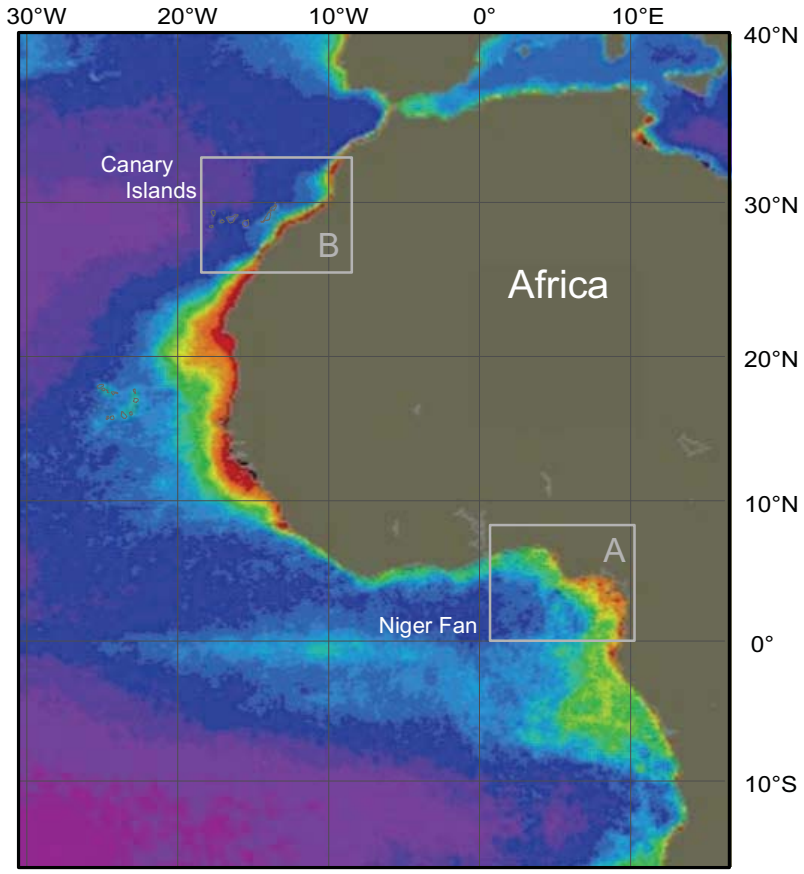

Fig. 3 Biogenic primary productivity visualized by the phytoplankton pigment concentration, values increase from lilac to red (http://seawifs.gsfc.nasa.gov; data collected over the time period November 1978 – June 1986). The study areas (A) in the eastern Equatorial Atlantic and (B) in the upwelling region off NW Africa are marked by rectangles.

below to replace it, this upward movement is termed upwelling. Upwelling regions are characterized by primary production in the newly formed surface waters which reach higher levels than in other areas of the open ocean. Regions with high marine productivity in the surface waters are characterized by elevated biogenic accumulation rates. It has been shown, that such areas are often associated with the occurrence of diagenetic processes in the sedimentary deposits (*Bloemendal et al*., 1992; *Garming et al*., 2005; *Dillon and Bleil*, 2006).

Coastal upwelling and the associated high productivity off Northwest and West Africa is generally concentrated along the outer shelf (Fig. 3). Between 20° and 25°N, the regional trade winds are strong and persist throughout the year, leading to continuous coastal upwelling and high productivity (*Mittelstaedt,* 1991; *Van Camp et al*, 1991). Maximum intensities are observed during spring and autumn when the NE Trade winds reach their peak. North of 25°N, upwelling occurs during summer and autumn, while south of 20°N upwelling occurs in the winter and spring. Upwelling in the eastern equatorial Atlantic Ocean is strongest during boreal summer, when the SE trade winds are strongest and also the wind-driven South Equatorial Current (SEC) reaches an annual maximum in velocity (*Philander and Pacanowsi*, 1986).

Early diagenesis and redox zonation

The preservation of the magnetic signal in marine sediments, either as information concerning the Earth´s magnetic field or paleoenvironmental conditions, has been

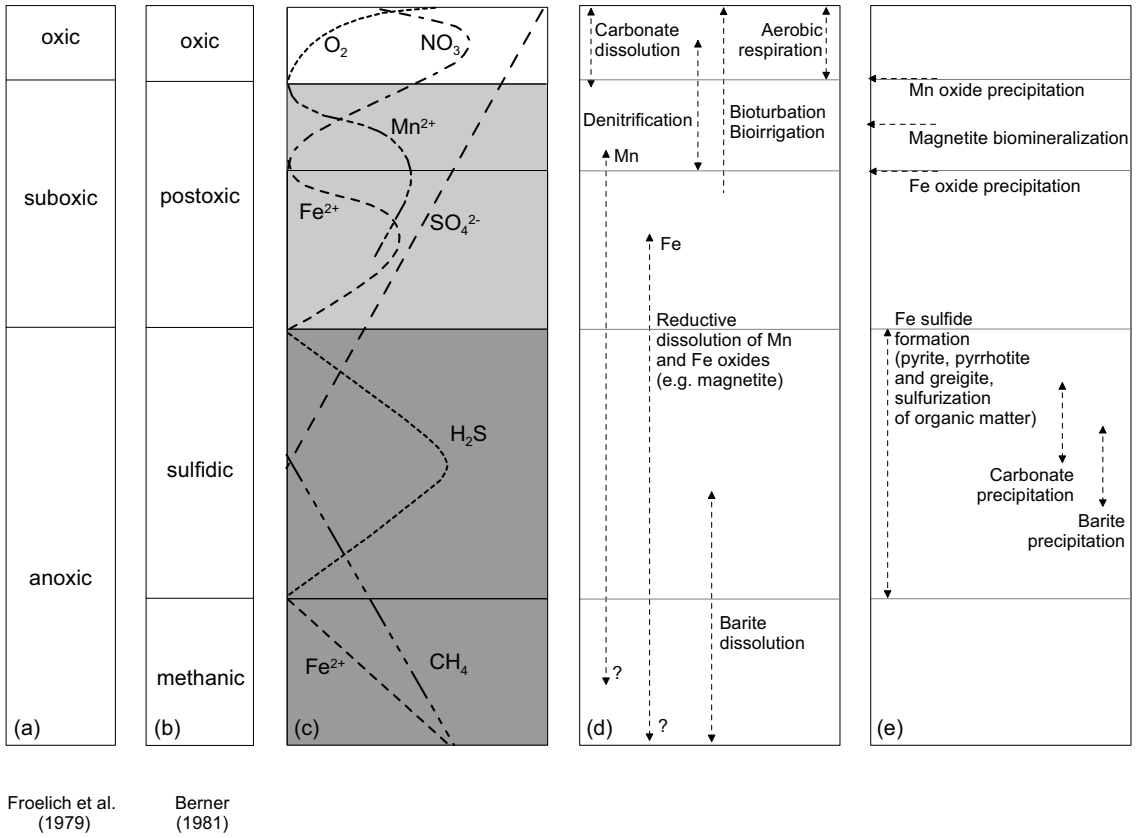

Fig. 4 Classification of early diagenetic environments in marine sediments according to (a) *Froelich et al*. (1979) and (b) *Berner* (1981) combined with (c) schematic pore water profiles of dissolved terminal electron acceptors. Processes of early diagenesis which can overprint the primary signal are delineated for (d) dissolution and (e) authigenesis (modified from *Kasten et al*. (2004)).

the focus of many studies during the past decades. In that context early microbially degradation of organic matter in the course of diagenetic processes has been of special interest. Numerous investigations (e.g. *Karlin*, 1990a, *Leslie et al*., 1990; *Tarduno*, 1994; *Tarduno and Wilkinson*, 1996) have shown that reductive diagenesis may strongly modify the magnetic mineral inventory by dissolution of primary iron oxides and the subsequent formation of authigenic iron sulfides such as greigite, pyrrhotite and pyrite. The oxidation of organic compounds provides energy for the microorganisms to maintain their metabolism. This process follows a well defined sequence of successive terminal electron acceptors in the sediment column (*Froehlich et al*., 1979), starting with oxygen in the top layer followed downwards by nitrate, Mn-oxides, Fe-oxides, sulfate and methane fermentation (Fig. 4). This sequence of oxidants reflects the quantity of energy per mole of organic carbon available for the microbial degradation.

Marine environments that contain measurable dissolved oxygen in the pore water are termed oxic (*Berner*, 1981). Accordingly, anoxic environments are those in which the sediments interstitial waters contain no more measurable dissolved oxygen. A further distinction is made between suboxic and sulphidic anoxic environments (Fig. 4). The magnetic record of a sediment succession can usually be regarded as entirely unchanged at the levels where oxidative organic matter decomposition, denitrification and reduction of manganese oxides occur. But in the iron reduction zone even well crystallized ferrimagnetic iron oxides of detrital or biogenic origin become chemically unstable (*Karlin and*

Levi, 1985; *Leslie et al.*, 1990), resulting in a systematic change of the sediment´s magnetic properties, in particular the primary paleomagnetic signal recorded in the marine sediments. The post-depositional evolution of most continental margin sediments depends strongly upon their organic matter content, the sedimentation rate and level of deep-water circulation, which leads to oxygen-poor conditions in the bottom water (*Karlin und Levi*, 1985; *Canfield and Berner*, 1987; *Leslie et al*., 1990; *Robinson*, 2000). These sedimentary conditions define the depth below which the reducing conditions become established in the sediment column.

Under oxic conditions, the authigenic formation of magnetite has been recognized near the Fe-redox boundary (e.g., *Karlin et al*., 1987; *Tarduno*, 1994) as well as in the vicinity of oxidation fronts (e.g., *Dekkers et al*., 1994; *Langereis et al*., 1997). Shifts of the depth extent of the oxidation and redox zonation due to changing environmental conditions can thus largely compromise (paleo-)magnetic records (e.g. *Karlin*, 1990b).

In the course of anoxic diagenesis, various secondary iron and manganese minerals can form in the sediment, which are often paramagnetic at room temperature and therefore unable to carry a NRM. Among these authigenic minerals are e.g. pyrite (iron sulphide Fe_2S), siderite (iron carbonate $FeCO_3$) or rhodochrosite (manganese carbonate $MnCO_3$) (*Frederichs et al*., 2003). Their formation is often related to dramatic changes in the accumulation rate and the availability of organic matter. They are typical for anoxic environments and indicative of geochemical conditions where the ferric iron oxides usually dissolve (*Canfield et al*., 1992) e.g. authigenic iron sulfide mineralization occurs deeper in the sediment column, where ferrous iron reacts with H_2S originating from sulphate-methane reduction. As a consequence of sulfidic diagenesis, anoxic sediments are often almost completely depleted in magnetic minerals.

The chemical pathway of pyrite formation involves intermediate magnetic iron sulfide phases (*Roberts and Turner*, 1993) such as the ferrimagnetic minerals pyrrhotite (Fe_7S_8) and greigite (Fe_3S_4). These metastable iron sulfides are thought to gradually transform to pyrite upon progressive diagenesis. The preservation of these iron sulfides is possibly the result of an incomplete pyritisation process limited by the concentration of dissolved sulfate, organic or iron compounds (*Berner*, 1984). Especially in rapidly accumulated marine sediments, pyrrhotite and greigite may be well preserved, when the geochemical equilibrium is not yet reached.

Aim and methods of this study

The aim of this project was to develop a comprehensive understanding of the primary magnetic mineral inventory in the marine sediments of coastal upwelling regions off NW and W Africa, its origins and its potential subsequent alterations after deposition. Therefore diagenetically altered sediments from the eastern Equatorial Atlantic and from the NW African continental slope (Fig. 3) were analyzed. Due to upwelling along the entire W African coast, both investigation areas are characterized by enhanced biological productivity in the surface waters, leading to high fluxes of organic material to the sea floor and virulent diagenetic processes in the sedimentary deposits. Thus these study areas present suitable environments to investigate the modifications of the primary magnetic mineral inventory during the course of reductive diagenesis.

The first study area (Fig. 3 (A)), in the eastern Equatorial Atlantic, was selected based on prior geochemical analyses performed by *Zabel et al*. (2001) and *Heuer* (2003) and focuses on organic-rich Late Quaternary deposits of the Niger deep-sea fan. The geochemistry provided detailed results of pore water and solid phase analyses and the inferred redox

zonation, which are crucial for the unambiguous interpretation of the subsequent magnetic studies. The sedimentary deposits are dominated by terrigenous components supplied by the Niger River reflecting the climate history of its drainage area (*Zabel et al*., 2001). Aeolian contributions are of minor importance in this region, comprising only 7 to 15% of the lithogenic fraction. Fluvial material is therefore the dominant terrigenous input, reflecting the mechanical weathering conditions of the hinterland.

The second study area (Fig. 3(B)), the Canary Island region, was selected because it accommodates one of the World's most prominent upwelling systems. Accumulation in this region offshore NW Africa is strongly influenced by dust components transported from the semi-arid and arid areas of the African continent to the subtropical and tropical Atlantic by the south westerly Trade winds (*Sarntheim et al*., 1982).

The magnetic properties of rocks and sediments arise from the specific properties of their constituent minerals. Typically, only a small fraction (<< 1 ‰) of the bulk marine sediment consists of magnetic minerals (*Frederichs et al*., 1999). However, it is this small fraction that determines the bulk rock magnetic properties of the sediment as a whole. The remaining constituents in marine sediments are "non-magnetic". They are either referred to as the diamagnetic (e.g. silicates or feldspars) or paramagnetic (e.g. iron bearing clay minerals) fraction. Dia- and paramagnetic minerals acquire a weak induced magnetization in the presence of a magnetic field, but they can not carry a remanent i.e. permanent magnetization. In general, magnetic studies focus on minerals that are ferri- or antiferromagnetic at room temperature, i.e. to minerals that are able to carry a stable remanent magnetization under ambient conditions. These magnetic minerals embrace iron titanium oxides, iron sulfides and iron oxyhydroxides.

The rock magnetic parameters which are employed in the following chapters vary as a function of the magnetomineralogy, magnetic grain-size and concentration. Therefore these rock magnetic parameters are diagnostic of the mineral type and often allow an interpretation of their origin. Thus such investigations can be used to characterize the magnetic mineral assemblage in sediments and its related early diagenetic modifications. Besides a suite of well established room-temperature rock magnetic parameters, a focus was placed on low-temperature magnetic measurements performed on a superconducting Quantum Design ´Magnetic Property Measurement System` (MPMS) at the University of Bremen (www.geophysik.uni-bremen.de). The applied measurements on the MPMS are highly sensitive and non-destructive, with the advantage that low-temperature experiments do not alter the sample chemically during cooling, so that the specimen can be treated several times. This becomes particularly important when the magnetic mineral content in a bulk sediment is very low and the sample material is limited.

Low-temperature techniques can not completely replace conventional thermomagnetic methods, but they offer a useful and often valuable complementary tool. A suite of magnetic minerals, such as magnetite, pyrrhotite and hematite undergo magnetic order-disorder transitions or crystallographic phase transitions below room temperature (*Verwey*, 1939; *Morin*, 1950; *Dekkers et al*., 1989) that can be used as diagnostic indicators of a mineral´s presence or absence. All these transition temperatures are known to be sensitive to non-stoichiometry, domain state and thus grain-size and "vacancy defects". In some cases the transitions can be totally suppressed (*Aragón et al.,* 1985; *Kakol et al.*, 1994; *Dunlop and Özdemir*, 1997). But even when such diagnostic remanence transitions and/or susceptibility peaks are not obviously apparent in low-temperature

data - which is often the case for natural marine sediment samples - careful comparisons of the data reveal important relevant information. This information can then be used to characterize the magnetic mineral phases in a sediment sample and therefore results in a detailed paleo-environmental understanding.

Summary of this thesis

High-resolution rock magnetic analyses of marine sediments from the NW and W African continental slope were performed, in order to understand in detail the complex diagenetic processes affecting the primary magnetic mineral inventory under reducing conditions in this region. The applied techniques included room-temperature remanence acquisition and demagnetization experiments, thermomagnetic low-temperature remanence, susceptibility and hysteresis measurements on bulk sediment samples and magnetic extracts. The data sets provide detailed information concerning variations in magnetic mineral concentration, grain-size and coercivity of the mineral phases. Additionally scanning electron microscopy (SEM) analyses were performed on magnetic extracts, to visualize the specific morphology of the magnetic particles and to determine their elemental composition.

Chapter 2 considers the strong influence of reductive diagenesis on the magnetic inventory in marine sediments originating from the Niger deep-sea fan. A well defined redox zonation was employed to determine, how the rock magnetic parameters change across the modern iron-redox boundary and the transition from the suboxic to anoxic environment. High- and low-temperature thermomagnetic analyses of selected bulk sediments and magnetic extracts from the oxic, suboxic and anoxic sulfidic environments have been performed to identify the magneto-mineralogical composition of the samples from the different geochemical environments. It was found that diagenetic alteration is not only a grain-size selective process, but also critically depends on the Ti-content of the mineral phases, in particular compounds with low Ti-concentrations are less resistant to diagenetic dissolution. Titanomagnetites and titanohematites with intermediate Ti-content thus persist as the predominant magnetic mineral fraction in the sulfidic anoxic sediments.

Chapter 3 deals with a new modelling procedure using linear combinations of end-members to represent coercivity spectra and thus does not rely on any specific distribution function. Unlike other mixture models, however, type curves are not required and there is no assumption that pure end-member curves must be contained in the measured data set. Instead, the method determines both the form of the end-members and their abundances using only the input remanence curves. The study demonstrates the ability of such an approach to derive both, coercivity components and their abundances, based solely upon the variability in the investigated data set. The effects of diagenetic alteration on the detrital mineral assemblage of the Niger deep-sea fan was successfully traced in terms of changes across geochemical fronts and more gradual modifications as a function of depth.

Chapter 4 demonstrates that it is possible to distinguish between titanomagnetites ($Fe_{3-x}Ti_xO_4$, $0 \le x \le 1$) and titanohematites ($Fe_{2-y}Ti_yO_3$, $0 \le y \le 1$) identified in magnetic extracts from suboxic and anoxic environments using a novel combination of low-temperature magnetic experiments and element dispersive X-ray spectroscopy (EDS). Large contrasts in the low-temperature magnetic remanence and hysteresis measurements between the samples from suboxic and anoxic layers emphasize that the Fe-Ti oxide phases occur in different proportions in the two identified geochemical environments. EDS analysis was used to discriminate between these two mineral phases on the basis of the element intensity ratio Fe/Ti and to calculate a close approximate elemental

composition for each particle. Element spectra with high Fe/Ti intensity ratios were found to be rather typical for titanomagnetites while low Fe/Ti ratios are indicative for titanohematites. Due to its high intrinsic stability titanohematite was found to persist as the predominant magnetic mineral fraction in the sulfidic anoxic sediments.

Chapter 5 considers the diagenetic impact on sedimentary sequences from the continental margin region off Cape Ghir. These alteration processes are related to the upwelling system off NW Africa and their imprint was encountered in a specific restricted depth interval. Low-temperature remanence experiments identified coarse grained magnetite as the dominant magnetic phase in these reduced sediments. The magnetic properties suggest a magnetite composition close to stoichiometry. In contrast to findings in other marine environments of intense diagenetic alteration, magnetite apparently withstands the reductive diagenetic processes. Therefore these sediments are suitable for paleointensity studies, which is shown in the following chapter.

Chapter 6 deals with so-called relative paleointensity, which is determined by normalizing the natural remanent magnetization by the concentration of the magnetic carriers. A new high-resolution Holocene paleomagnetic record for NW Africa is presented, which comprises a high quality declination, inclination and relative paleointensity record for this region. This provides detailed information on the variability of the Earth´s magnetic field vector for the last seven kyrs.

References

Aragón, R., D. J. Buttrey, J. P. Shepherd, and I. M. Honig (1985), Influence of nonstoichiometry on the Verwey transition, *Phys. Rev., B, 31*, 430-436.

Bergametti, G., L. Gomes, G. Coude-Gaussen, P. Rognon, and M.-N. le Coustumer (1989), African dust observed over Canary Islands: Source-regions identification and transport pattern for some summer situations, *J. Geophys. Res., 94*, 14855-14864.

Berner, R. A. (1981), A new geochemical classification of sedimentary environments, *J. Sed. Petrol., 51,* 359-365.

Berner, R. A. (1984), Sedimentary pyrite formation: an update, *Geochim. Cosmochim. Acta, 48*, 605-615.

Bleil, U., and T. von Dobeneck (2004), Late Quaternary terrigenous sedimentation in the western equatorial Atlantic: South American versus African provenance discriminated by magnetic mineral analyses, in *The South Atlantic in the Late Quaternary*, edited by G. Wefer et al., pp. 213-236, Springer-Verlag, Berlin, Heidelberg.

Bloemendal, J., J. W. King, F. R. Hall, and S.-J. Doh (1992), Rock magnetism of late Neogene and Pleistocene deep-sea sediments: relationship to source, diagenetic processes, and sediment lithology, *J. Geophys. Res., 97*, 4361-4375.

Boeglin, J.-L., and J.-L. Probst (1998), Physical and chemical weathering rates and CO_2 consumption in a tropical lateritic environment: the upper Niger basin, *Chem. Geol., 148*, 137-156.

Cande, S. C., and D. V. Kent (1995), Revised calibration of the geomagnetic polarity timescale for the late Cretaceous and Cenozoic, *J. Geophys. Res., 100,* 6093-6095.

Canfield, D. E., and R. A. Berner (1987), Dissolution and pyritization of magnetite in anoxic marine sediments, *Geochim. Cosmochim. Acta, 51*, 645-659.

Canfield, D. E., R. Raiswell, and S. Bottrell (1992), The reactivity of sedimentary iron minerals toward sulphide, *Am. J. Sci., 292*, 659–683.

Chiapello, I., G. Bergametti, L. Gomes, B. Chatenet, F. Dulac, J. Pimenta, and E. Santos Suares (1995), An additional low layer transport of Sahelian and Saharan dust over the North-Eastern Tropical Atlantic, *Geophys. Res. Lett., 22*, 3191-3194.

Dekkers, M. J., J.-L Mattéi, G. Fillion, and P. Rochette (1989), Grain-size dependence of the magnetic behavior of pyrrhotite during its low-temperature transition at 34 K, *Geophys. Res. Lett., 16*, 855-858.

Dekkers, M. J., C. G. Langereis, S. P. Vriend, P. J. M. van Santvoort, and G. J. de Lange (1994), Fuzzy c-means cluster analysis of

early diagenetic effects on natural remanent magnetization acquisition in a 1.1 Myr piston core from the central Mediterranean, *Phys. Earth Planet. Inter., 85*, 155-171.

deMenocal, P. B., W. F. Ruddiman, E. M. Pokras (1993), Influences of high- and low-latitude processes on African terrestrial climate: Pleistocene eolian records from equatorial Atlantic Ocean Drilling Programm Site 663, *Paleoceanography, 8*, 209-242.

Dillon, M., and U. Bleil (2006), Rockmagnetic signatures in diagenetically altered sediments from the Niger deep-sea fan, *J. Geophys. Res., 111*, B03105, doi:10.1029/ 2004JB003540.

Dunlop, D. J., and Ö. Özdemir (1997), *Rock Magnetism: Fundamentals and Frontiers*, 573 pp., Cambridge University Press, Cambridge.

Franke, C., T. von Dobeneck, M. R. Drury, J. D. Meeldijk, and M. J. Dekkers, (2007), Magnetic petrology of Equatorial Atlantic sediments: Electron microscopic results and their environmental magnetic implications, *Paleoceanography, 22*, PA4207, doi:10.1029/2007PA001442.

Frederichs, T., U. Bleil, K. Däumler, T. von Dobeneck, and A. M. Schmidt (1999), The magnetic view on the marine paleoenvironment: parameters, techniques and potential of rock magnetic studies as a key to paleoclimatic and paleoceanographic changes. In *Use of Proxies in Paleoceanography: Examples from the South Atlantic*, edited by G. Fischer and G. Wefer, pp. 575–599, Springer-Verlag, Berlin, Heidelberg.

Frederichs, T., T. von Dobeneck, U. Bleil, and M. J. Dekkers (2003), Towards the identification of siderite, rhodochrosite, and vivianite in sediments by their low-temperature magnetic properties, *Phys. Chem. Earth., 28*, 669-679.

Froelich, P. N., G. B. Klinkenhammer, M. L. Bender, N. A. Luedtke, G. R. Heath, D. Cullen, B. Hartmann, and V. Maynard (1979), Early oxidation of organic matter in pelagic sediments of the eastern equatorial Atlantic: suboxic diagenesis, *Geochim. Cosmochim. Acta, 43*, 1075-1090.

Funk, J. A., T. von Dobeneck, and A. Reitz (2004), Integrated rock magnetic and geochemical quantification of redoxomorphic iron mineral diagenesis in late Quaternary sediments from the equatorial Atlantic, in *The South Atlantic in the Late Quaternary*, edited by G. Wefer et al., pp. 237-260, Springer-Verlag, Berlin, Heidelberg.

Garming, J. F. L., U. Bleil, and N. Riedinger (2005), Alteration of magnetic mineralogy at the sulphate-methane transition: analysis of sediments from the Argentine continental slope, *Phys. Earth Planet. Inter., 151*, 290-308.

Guyodo Y., and J.-P. Valet (1999), Global changes in intensity of the Earth's magnetic field during the past 800 kyr, *Nature,* 399, 249–252.

Harrison, S. P., K. E. Kohfeld, C. Roelandt, and T. Claquin (2001), The role of dust in climate changes today, at the last glacial maximum and in the future, *Earth-Sci. Rev.*, 54, 43-80.

Heirtzler, J. R., G. O. Dickson, E. M. Herron, W. C. Pittman III, and X. LePichon (1968), Marine magnetic anomalies, geomagnetic field reversals, and motions of the ocean floor and continents, *J. Geophys. Res*., 73, 2119-2136.

Heuer, V. (2003), Spurenelemente in Sedimenten des Südatlantik. Primärer Eintrag und frühdiagenetische Überprägung. Berichte, Fachbereich Geowissenschaften, Universität Bremen, *209*.

Intergovernmental Oceanographic Commission (1994), GEBCO Digital Atlas (CD-Rom), *Intergov. Oceanogr. Comm.*, Int. Hydrogr. Org., Birkenhead, U. K.

Kakol, Z., J. Sabol, A. Kozlowski, J. M. Honig (1994), Influence of titanium doping on the magnetocrystalline anisotropy of magnetite, *Phys. Rev. B, 49*, 12,767-12,772.

Karlin, R. (1990a), Magnetite diagenesis in marine sediments from the Oregon continental margin, *J. Geophys. Res., 95*, 4405-4419.

Karlin, R. (1990b), Magnetic mineral diagenesis in suboxic sediments at Betis Site N-W, NE Pacific Ocean, *J. Geophys. Res., 95*, 4421-4436.

Karlin, R., and S. Levi (1985), Geochemical and sedimentological control of the magnetic properties of hemipelagic sediments, *J. Geophys. Res., 90*, 10373-10392.

Karlin, R., M. Lyle, and G. R. Heath (1987), Authigenic magnetic formation in suboxic marine sediments, *Nature, 326*, 490-493.

Kasten, S., M. Zabel, V. Heuer, and C. Hensen (2004), Processes and signals of nonsteady-state diagenesis in deep-sea sediments and their pore waters, in *The South Atlantic in the Late Quaternary*, edited by G. Wefer et al., pp. 431-459, Springer-Verlag, Berlin, Heidelberg.

Kent, D. V. (1973), Post-depositional remanent magnetisation in deep-sea sediments, *Nature, 246*, 32-34.

Kent, D. V. (1982), Apparent correlation of palaeomagnetic intensity and climatic records in deep-sea sediments, *Nature, 299*, 538-539.

Konta, J. (1985), Mineralogy and chemical maturity of suspended matter in major rivers sampled under the SCOPE/UNEP Project, in *Transport of carbon and minerals in major world rivers, Part 3*, edited by E. T. Degend et al., pp. 569-592, Mitteilung des Geologisch-Paläontologischen Instituts der Universität Hamburg, Hamburg.

Langereis, C. G., M. J. Dekkers, G. J. de Lange, M. Paterne, and P. J. M. van Santvoort (1997), Magnetostratigraphic and astronomical calibration of the last 1.1 Myr from an eastern Mediterranean piston core and dating of short events in the Brunhes, *Geophys. J. Int.*, *129*, 75-94.

Leslie, B. W., D. E. Hammond, W. M. Berelson, and S.P. Lund (1990), Diagenesis in anoxic sediments from the California continental borderland and its influence on iron, sulfur and magnetite behaviour, *J. Geophys. Res., 95*, 4453-4470.

Mayewski, P. A., L. D. Meeker, M. S. Twickler, S. Whitlow, Q. Yang, W. B. Lyons, and M. Prentice (1997), Major features and forcing of high-latitude northern hemisphere atmospheric circulation using a 110,000-year-long glaciochemical series, *J. Geophys. Res., 102*, 26345-26366.

Mittelstaedt, E (1991), The ocean boundary along the northwest African coast: Circulation and oceanographic properties at the sea surface, *Progr. Ocean., 26*, 307-355.

Morin, T. (1950), Magnetic susceptibility of αFe_2O_3 and αFe_2O_3 with added titanium, *Phys. Rev., 78*, 819-820.

Nicholson, S. E. (2000), The nature of rainfall variability over Africa on time scales of decades to millennia, *Global Planet. Change, 26*, 137-158.

Ninkovich, D., N. Opdyke, B. C. Heezen, and J. H. Foster (1966), Paleomagnetic stratigraphy, rates of deposition and tephrachronology in north Pacific deep-sea sediments, *Earth Planet. Sci. Lett., 1,* 476–492.

Opdyke, N. D., and B. P. Glass (1969), The paleomagnetism of sediment cores from the Indian Ocean, *Deep-Sea Research, 16*, 249-261.

Peterson, R. G., and L. Stramma (1991), Upper-level circulation in the South Atlantic Ocean, *Prog. Oceanog., 26*, 1-73.

Philander, S. G. H., and R. C. Pacanowsi (1986), A model of the seasonal cycle in the tropical Atlantic Ocean, *J. Geophys. Res., 91*, 14,192–14,206.

Prospero, J. M., (1990), Mineral-aerosol transport to the North Atlantic and North Pacific: The impact of African and Asian sources, in *The long-range atmospheric transport of natural and contaminant substances, Mathematical and Physical Sciences*, edited by A. H. Knap, pp.59-86, Kluwer Academic Publishers, Dodrecht.

Roberts, A. P., and G. M. Turner (1993), Diagentic formation of ferrimagnetic iron sulphides minerals in rapidly deposited marine sediments, South Island, New Zealand, *Earth Planet. Sci. Lett., 115*, 257-273.

Robinson, S. G., J. T. S. Sahota, and F. Oldfield (2000), Early diagenesis in North Atlantic abyssal plain sediments characterized by rock-magnetic and geochemical indices, *Mar. Geology, 163*, 77-107.

Sarnthein, M., J. Thiede, U. Pflaumann, H. Erlenkeuser, D. Fütterer, B. Koopmann, H. Lange, and E. Seibold (1982), Atmospheric and oceanic circulation patterns off Northwest Africa during the past 25 million years. In: *Geology of the Northwest African Continental Margin*, edited by U. von Rad et al., pp. 545-604, Springer, Berlin, Heidelberg.

Schmidt, A. M., T. von Dobeneck, and U. Bleil (1999), Magnetic characterization of Holocene sedimentation in the South Atlantic, *Paleoceanography*, *14*, 465-481.

Schmieder, F. (2004), Magnetic signals in Plio-Pleistocene sediments of the South

Atlantic: Chronostratigraphic usability and paleoceanographic implications. In *The South Atlantic in the Late Quaternary*, edited by G. Wefer et al., pp. 261-277, Springer, Berlin, Heidelberg.

Schmieder, F., T. von Dobeneck, and U. Bleil (2000), The Mid-Pleistocene climate transition as documented in the deep South Atlantic Ocean: Initiation, interim state and terminal event, *Earth Planet. Sci. Lett., 179*, 539-549.

Spell, T. L., and I. McDougall (1992), Revisions to the age of the Brunhes-Matuyama boundary and the pleistocene geomagnetic polarity timescale, *Geophys. Res. Lett.*, *19* (12), 1181–1184.

Tarduno, J. A. (1994), Temporal trends of magnetic dissolution in the pelagic realm: Gauging paleoproductivity?, *Earth Planet. Sci. Lett*., 123, 39-48.

Tarduno, J. A., and S. L. Wilkinson (1996), Non-steady state magnetic mineral reduction, chemical lock–in, and delayed remanence acquisition in pelagic sediments, *Earth Planet. Sci. Lett., 144*, 315-326.

Tauxe, L., and G. Wu (1990), Normalized remanence in sediments in the western equatorial Pacific: Relative paleointensity of the geomagnetic field, *J. Geophys. Res., 95*, 12337-12350.

Thibal, J., J.-P. Pozzi, V. Barthés, and G. Dubuisson (1995), Continuous record of geomagnetic field intensity between 4.7 and 2.7 Ma from downhole measurements, *Earth Planet. Sci. Lett.*, 136, 541-550.

Thompson, R., and F. Oldfield (1986), *Environmental Magnetism*, 227 pp., Allen and Unwin, London.

Valet, J.-P., and L. Meynardier (1993), Geomagetic field intensity and reversals during the past four million years, *Nature, 399*, 91-95.

Valet, J.-P., L. Meynadier, and Y. Guyodo (2005), Geomagnetic dipole strength and reversal rate over the past two million years, *Nature, 435*, doi:10.1038/nature03674.

Van Camp, L., L. Nykjaer, E. Mittelstaedt, and P. Schlittenhardt (1991), Upwelling and boundary circulation off Northwest Africa as depicted by infrared and visible satellite observations, *Prog. Ocean., 26*, 357-402.

Verwey, E. J. W. (1939), Electronic conduction of magnetite (Fe_3O_4) and its transition point at low temperatures, *Nature, 44*, 327-328.

Watkins, S. J., and B. M. Maher (2003), Magnetic characterisation of present-day deep-sea sediments and sources in the North Atlantic, *Earth Planet. Sci. Lett., 214*, 379-394.

Weaver, P. P. E., R. B. Wynn, N. H. Kenyon, and J. Evans (2000), Continental margin sedimentation, with special reference to the north-east Atlanic margin, *Sedimentology, 47*, 239-256.

Zabel, M., R. R. Schneider, T. Wagner, A. T. Adegbie, U. de Vries, S. Kolonic, (2001), Late Quaternary climate changes in central Africa as inferred from terrigenious input to the Niger Fan, *Quat. Res., 56,* 1-11.

JOURNAL OF GEOPHYSICAL RESEARCH, VOL. 111, B03105, doi:10.1029/2004JB003540, 2006

Rock magnetic signatures in diagenetically altered sediments from the Niger deep-sea fan

Melanie Dillon[1] and Ulrich Bleil[1]

Received 16 November 2004; revised 8 September 2005; accepted 22 November 2005; published 28 March 2006.

[1] Diagenesis has extensively affected the magnetic mineral inventory of organic-rich late Quaternary sediments in the Niger deep-sea fan. Changes in concentration, grain size, and coercivity document modifications of the primary magnetic mineral assemblages at two horizons. The first front, the modern iron redox boundary, is characterized by a drastic decline in magnetic mineral content, coarsening of the grain size spectrum, and reduction in coercivity. Beneath a second front, the transition from the suboxic to the sulfidic anoxic domain, a further but less pronounced decrease in concentration and bulk grain size occurs. Finer grains and higher coercive magnetic constituents substantially increase in the anoxic environment. Low- and high-temperature experiments were performed on bulk sediments and on extracts which have also been examined by X-ray diffraction. Thermomagnetic analyses proved ferrimagnetic titanomagnetites of terrigenous provenance as the principal primary magnetic mineral components. Their broad range of titanium contents reflects the volcanogenic traits of the Niger River drainage areas. Diagenetic alteration is not only a grain size selective process but also critically depends on titanomagnetite composition. Low-titanium compounds are less resistant to diagenetic dissolution. Intermediate titanium content titanomagnetite thus persists as the predominant magnetic mineral fraction in the sulfidic anoxic sediments. At the Fe redox boundary, precipitation of authigenic, possibly bacterial, magnetite is documented. The presence of hydrogen sulfide in the pore water suggests a formation of secondary magnetic iron sulfides in the anoxic domain. Grain size–specific data argue for a gradual development of a superparamagnetic and single-domain iron sulfide phase in this milieu, most likely greigite.

Citation: Dillon, M., and U. Bleil (2006), Rock magnetic signatures in diagenetically altered sediments from the Niger deep-sea fan, *J. Geophys. Res.*, *111*, B03105, doi:10.1029/2004JB003540.

1. Introduction

[2] Numerous environmental magnetism studies have used magnetic characteristics of marine sediments to address a variety of paleoclimatic and paleoceanographic issues. For example, analyses of the magnetic mineral assemblage allowed source region identification, discrimination of fluvial versus eolian pathways of terrigenous components and their climate induced variations [e.g., *Bloemendal et al.*, 1992; *Bleil and von Dobeneck*, 2004]. A prerequisite to achieve accurate results with these methods is a complete understanding of the primary magnetic mineral inventory, its origins and particularly its potential subsequent modifications.

[3] The influx of terrigenous magnetic components into marine sedimentary deposits depends on the individual geographic setting and typically comprises various lithogenic minerals and their weathering products. In regions of elevated biologic productivity like upwelling regions, where high amounts of organic material (C_{org}) reach the seafloor, diagenetic processes affect the magnetic mineral inventory. Only at the level of oxidative organic matter decomposition, denitrification and reduction of manganese oxides [*Froelich et al.*, 1979] the magnetic record is left unchanged. At more advanced suboxic to anoxic (sulfate reducing) diagenetic stages, detrital and authigenic magnetic iron oxides will be dissolved. As repeatedly documented since early investigations [*Karlin and Levi*, 1983, 1985; *Canfield and Berner*, 1987; *Karlin*, 1990a, 1990b; *Leslie et al.*, 1990a, 1990b], such conditions are encountered at shallow depths in high sedimentation rate continental margin areas, but were also observed in the open ocean realm [e.g., *Funk et al.*, 2004]. These findings are of critical importance, given that multiple high-resolution paleomagnetic directional and relative paleointensity records have been derived from such deposits. In this respect a biotic or abiotic precipitation of magnetic iron oxides or sulfides at depth in the sediment column is of even more concern.

[4] The reductive diagenic sequence of iron oxide dissolution and precipitation followed by iron monosulfide, magnetic iron sulfide (pyrrhotite, Fe_7S_8 or greigite, Fe_3S_4) and last by pyrite formation is in principle well understood [*Canfield and Berner*, 1987]. The main location of authi-

[1]Fachbereich Geowissenschaften, Universität Bremen, Bremen, Germany.

0148-0227/06/2004JB003540$09.00

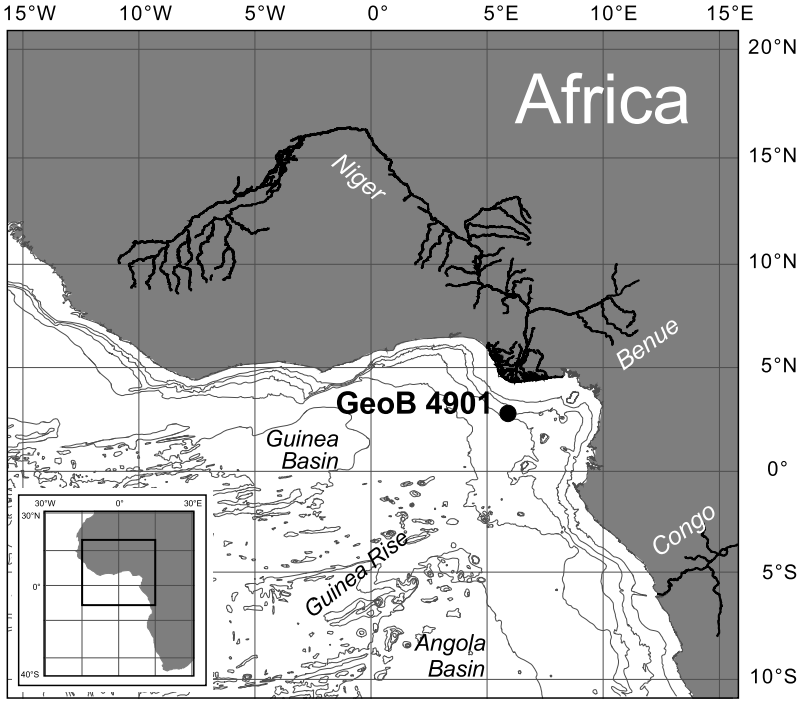

Figure 1. Location of sediment coring site GeoB 4901 in 2184 m water depth on the southeastern flank of the Niger deep-sea fan (02°40.7′N, 06°43.2′E). Isobaths are at 1000 m intervals according to *Intergovernmental Oceanographic Commission* [1994].

genic (possibly also bioauthigenic) iron sulfide mineralization is deep in the sediment column, where ferrous iron reacts with H_2S originating from sulfate reduction. Greigite was identified in various marine sediments though mostly in particular settings [*Suttill et al.*, 1982; *Hallam and Maher*, 1994; *Lee and Jin*, 1995; *Oda and Torii*, 2004]. Pyrrhotite so far has been mostly recognized in uplifted, subaerial marine sediment sequences [*Linssen*, 1988; *Roberts and Turner*, 1993; *Horng et al.*, 1998, *Dinarès-Turell and Dekkers*, 1999; *Weaver et al.*, 2002]. Marine sedimentary greigites and pyrrhotites were traditionally interpreted as diagenetic products. Their preservation is attributed to arrested pyritization reactions resulting from limited concentrations of dissolved sulfate, organic matter and/or iron compounds [*Berner*, 1984; *Reynolds et al.*, 1994]. More recently this view has been questioned. *Jiang et al.* [2001] demonstrated that greigite can form in late diagenetic processes, *Weaver et al.* [2002] suggested tectonically driven fluid migration as a possible mechanism. *Dinarès-Turell and Dekkers* [1999] proposed a late diagenetic precipitation also for pyrrhotite.

[5] The objective of this study is to fully characterize the complex reductive diagenetic processes affecting the magnetic mineral inventory in an expanded, geochemically well defined redox sequence of late Quaternary Niger deep-sea fan sediments. Especially in the sulfidic anoxic strata major emphasis was on assessing the potential importance of authigenic magnetic sulfide minerals.

2. Study Area and Materials

[6] Gravity core GeoB 4901-8 was recovered during R/V METEOR Cruise M 41/1 [*Schulz et al.*, 1998] from 2184 m water depth on the southeastern flank of Niger deep-sea fan (02°40.7′N, 06°43.2′E; see Figure 1). The sediment series of 20.30 m total length reach into marine oxygen isotope stage (MIS) 7 near the base of the core [*Adegbie*, 2001; *Zabel et al.*, 2001] (Figure 2). Sedimentation rates vary between about 5 and 12 cm/kyr. The 10 cm sample spacing for bulk rock magnetic measurements hence corresponds to an average temporal resolution of 1.3 ka. *Zabel et al.* [2001] have documented that the deposits are dominated by terrigenous components supplied by the Niger River reflecting the climate history in its drainage area. Comprising 7 to 15% of the lithogenic fraction, eolian contributions are of minor importance. Carbonate content is relatively low (16.3 wt%), but shows a distinct 0.1 to 36.1 wt% climate variability. Enhanced marine productivity during cold periods is attributed to the combined effects of riverine nutrient supply and zonal trade wind intensity [*Zabel et al.*, 2001].

[7] Only the top 10 cm of the sediment column are oxic. The suboxic interval, characterized by dissolved manganese in the pore water, extends to 12.50 m depth. The position of the suboxic/sulfidic anoxic transition has been defined on evidence of dissolved hydrogen sulfide (H_2S) in the pore water produced by anaerobic oxidation of methane [*Heuer*, 2003]. Linearly extrapolating the sulfate gradient, *Heuer* [2003] estimated the complete sulfate consumption and thus the top of the methanic zone in 26.70 m depth at the coring site. From top to bottom very dark sediments reveal no distinctive color changes that would indicate transitions in redox conditions [*Lyle*, 1983].

[8] Organic carbon content varies between 0.65 and 1.95 wt%, indicating a significant input and preservation of organic matter [*Kolonic*, 1999; *Holtvoeth et al.*, 2005]. *Kolonic* [1999] inferred that on average about one third of

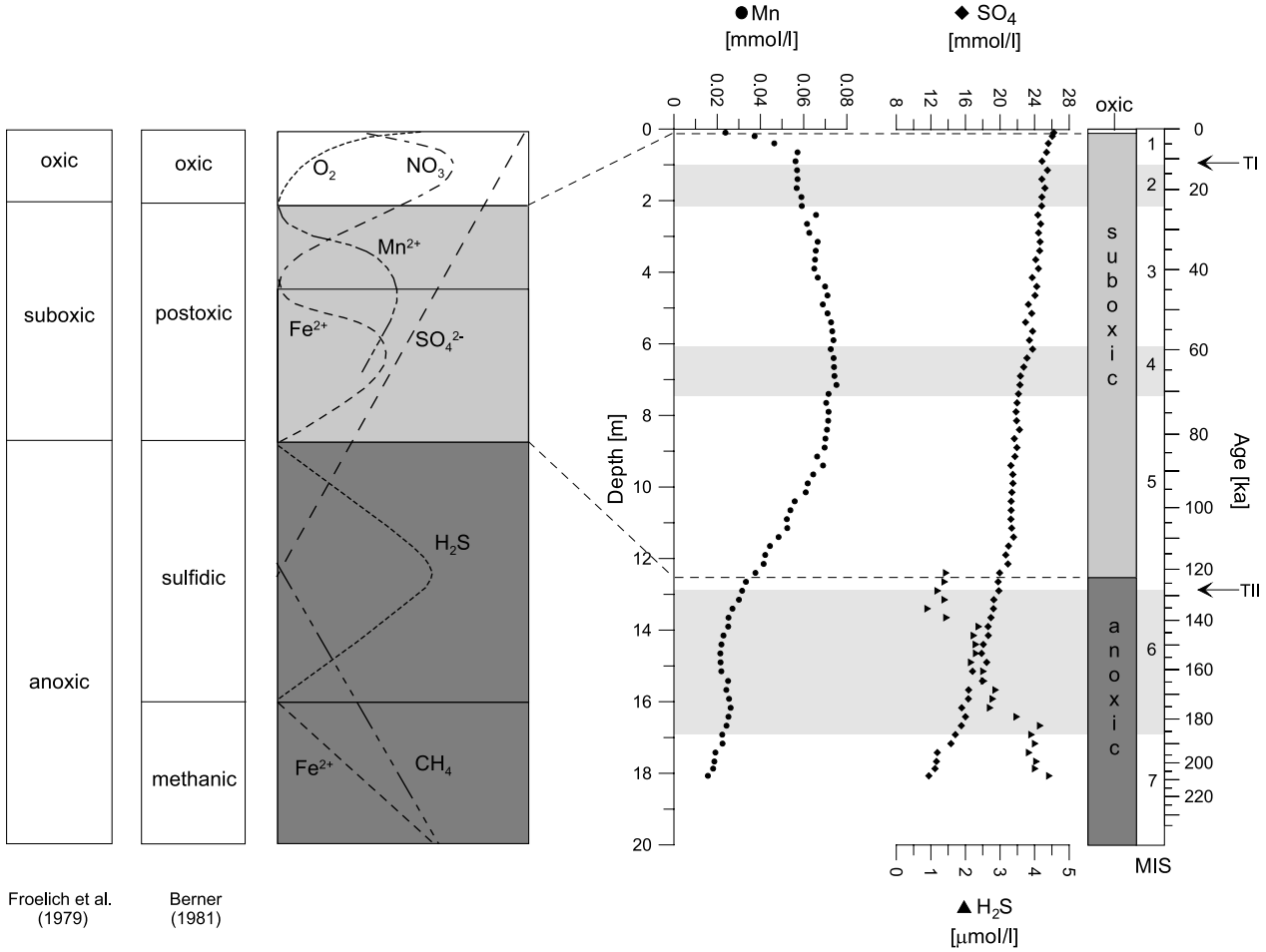

Figure 2. (left) Classification of early diagenetic environments in marine sediments according to *Froelich et al.* [1979] and *Berner* [1981] together with schematic pore water profiles of dissolved terminal electron acceptors (modified from *Kasten et al.* [2004] with kind permission of the author and Springer Science and Business Media). (right) Pore water chemistry at site GeoB 4901 [*Heuer*, 2003] plotted on a linear depth scale and a nonlinear age scale [*Adegbie*, 2001], including marine oxygen isotope stages and terminations TI and TII. Gray shading indicates cold periods. Dashed lines mark the oxic/suboxic and suboxic/anoxic transitions.

the original C_{org} has been degraded by sulfate reduction. Iron concentrations are relatively uniform, the mean of 40.8 g/kg corresponds to on average 5.8 wt% Fe_2O_3. They show no relationship to the present redox zonation, but are associated with the lithogenic sediment fraction as indicated by a close correlation to aluminum (r = 0.92, Pearson) [*Heuer*, 2003].

3. Analytical Methods

[9] Bulk rock magnetic measurements have been performed on cube specimens (6.2 cm^3) sampled in 10 cm depth intervals. Magnetic volume susceptibility κ was determined with a *Geofyzica Kappabridge* KLY 2 supplementing a κ log (1 cm spacing) recorded with a *Bartington* MS2 spot sensor on the split core half.

[10] Acquisition of isothermal remanent magnetization (IRM) in 18 steps to 0.3 T and anhysteretic remanent magnetization (ARM), imparted by superimposing a gradually decaying alternating field of 0.3 T maximum amplitude on a constant biasing field of 40 μT was followed by incremental triaxial IRM and ARM alternating field demagnetization. All remanences have been measured on a *2G Enterprises* 755R DC SQUID cryogenic magnetometer system (noise level $\sim 10^{-12}$ Am^2), the fields were generated with its built-in facilities. By limiting the maximum field amplitudes to 0.3 T, rock magnetic parameters deduced from these data characterize the low coercivity ferrimagnetic (titano)magnetite mineral fraction. To estimate concentrations of high-coercivity iron oxides and oxyhydroxides (hematite, goethite) from the hard isothermal remanent magnetization HIRM [*Stoner et al.*, 1996] 0.3 T backfields were applied to 2.5 T remanences imparted with a pulse magnetizer.

[11] Magnetic hysteresis and backfield measurements limited to a maximum field of 0.3 T were performed with a *PMC* M2900 alternating-gradient force magnetometer (noise level $\sim 10^{-12}$ Am^2). For data processing, the program '*Hystear*' [*von Dobeneck*, 1996] was used to determine mass-specific saturation magnetization σ_s and remanent saturation magnetization σ_{rs}, coercive force B_c and remanent coercivity B_{cr}, all specifying the characteristics of the ferrimagnetic mineral components. Additionally, the non-

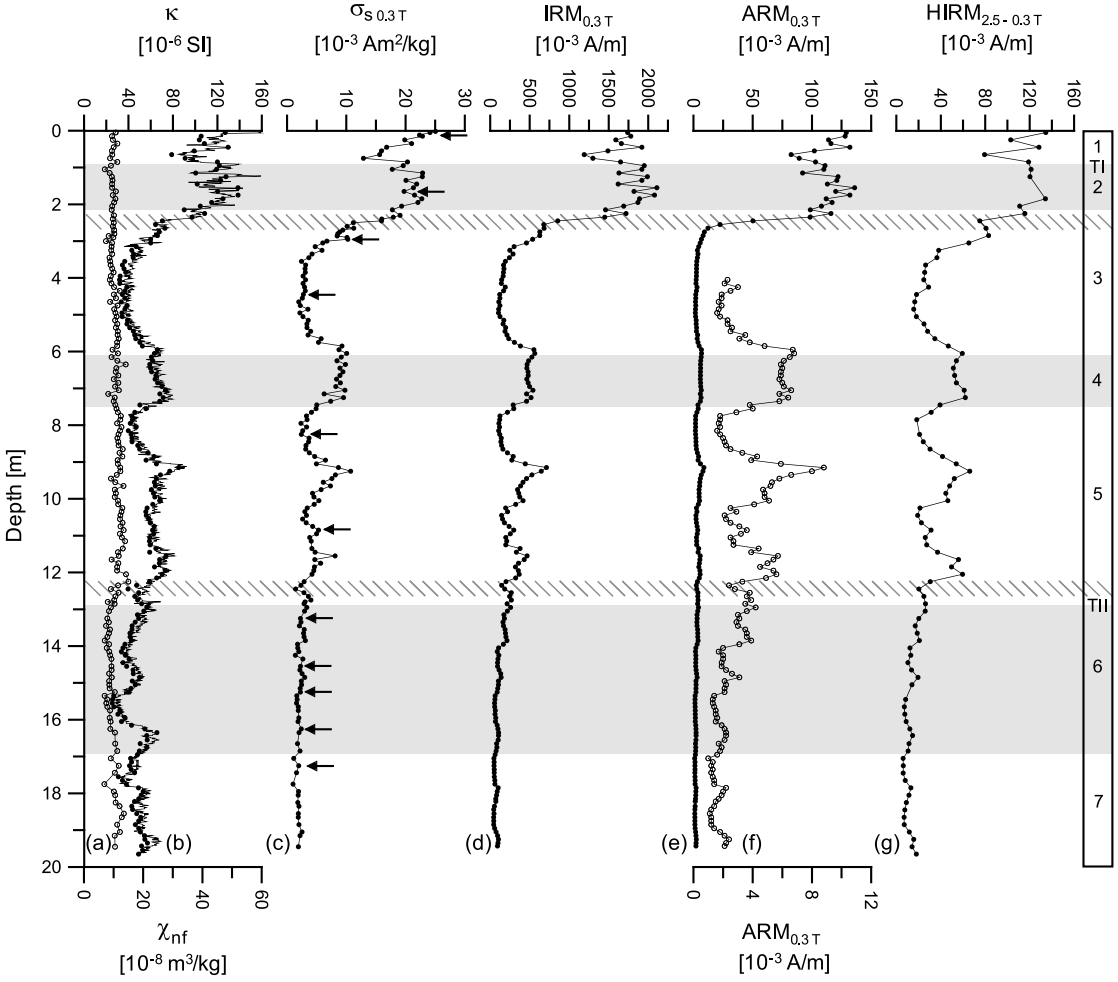

Figure 3. Depth profiles of rock magnetic attributes delineating variations in concentration of magnetic minerals: nonferromagnetic susceptibility χ_{nf} (curve a, open symbols) and bulk susceptibility κ (curve b; full symbols refer to single samples and the continuous line to core logging measurements), saturation magnetization σ_s (curve c), isothermal remanent magnetization IRM (curve d), anhysteretic remanent magnetization ARM (curves e and f; open symbols refer to the lower scale), and hard isothermal remanent magnetization HIRM (curve g). HIRM assesses the content of antiferromagnetic iron oxide and hydroxide (hematite, goethite); all other magnetizations relate to ferrimagnetic (titano)magnetite. Arrows at the σ_s profile denote horizons, where high- and/or low-temperature magnetic analyses have been performed (see Figures 5–7). Horizontal hatched bars mark the modern iron redox boundary (at around 2.5 m depth) and the suboxic/sulfidic anoxic transition (at around 12.5 m depth). For further details see Figure 2.

ferromagnetic susceptibility χ_{nf}, quantifying paramagnetic and diamagnetic contributions of the sedimentary matrix to susceptibility has been derived from an approach-to-saturation analysis [*von Dobeneck*, 1996].

[12] Low-temperature experiments were accomplished with the facilities of a *Quantum Design* Magnetic Property Measurement System (noise level $\sim 10^{-11}$ Am^2). Thermal demagnetization of low-temperature remanence was monitored for selected bulk sediments and magnetic extracts after zero field cooling (ZFC) and applying a 2.5 T field at 5 K as well as after field cooling (FC) in a 2.5 T field. For magnetic extracts also variations of in-phase susceptibility (1000 Hz) were determined at 10 degree increments between 5 and 300 K.

[13] Miniature samples for hysteresis and low-temperature analyses have been prepared using techniques described by *von Dobeneck* [1996] and *Frederichs et al.* [2003], respectively. The method of *Petersen et al.* [1986] was applied to collect magnetic extracts.

[14] High-temperature thermomagnetic measurements between room temperature and 720°C were performed at Utrecht University (Netherlands) with a horizontal translation-type Curie balance (noise level $\sim 10^{-9}$ Am^2) [*Mullender et al.*, 1993] on selected bulk sediments at heating rates of 10 and cooling rates of 15°C per minute.

4. Room Temperature Analyses

4.1. Mineralogy and Concentration

[15] Magnetic volume susceptibility κ indicates an overall notably low magnetic mineral content (Figure 3, curve b). The most remarkable feature of the record is a distinct drop

(67%) between about 2.0 and 3.5 m depth. Below this level, κ variations are minor with slightly declining amplitudes at greater depths. In clear contrast, the nonferromagnetic susceptibility χ_{nf} (Figure 3, curve a), which magnetically characterizes the sediment matrix, remains fairly constant over the entire sediment column. It is strongly correlated to the lithogenic elements iron (r = 0.76) and aluminum (r = 0.78), documenting that the sediment matrix is dominated by terrigenous constituents and that iron is largely bound in paramagnetic mineral phases, most probably iron rich clays [*Zabel et al.*, 2001]. In deeper strata, up to 80% of the remaining bulk susceptibility signal originates from these sediment matrix compounds.

[16] Mass-specific saturation magnetization σ_s (Figure 3, curve c) and susceptibility display notably similar variations down to 12.5 m. Below, in the sulfidic anoxic zone, σ_s decreases by another 15% evincing that only tiny fractions of the ferrimagnetic (titano)magnetite minerals last the progressive diagenetic alteration. With a room temperature–specific saturation magnetization of 92 Am^2/kg for magnetite [*Dunlop and Özdemir*, 1997] the ferrimagnetic mineral content is estimated to diminish from approximately 0.02 wt% in the top sediments to 0.002 wt% in the sulfidic anoxic layers.

[17] Isothermal remanent magnetization IRM (Figure 3, curve d) refers to the entire grain size spectrum of remanence carrying ferrimagnetic mineral phases. Its almost perfect correlation to saturation magnetization (r = 0.97) suggests that superparamagnetic (SP) components should not be of sizable importance.

[18] Anhysteretic remanent magnetization ARM is very predominantly acquired by the (titano)magnetite single-domain (SD) and fine pseudo-single-domain (PSD) grain size fractions. ARM intensities abruptly decline in a narrow depth interval around 2.5 m (Figure 3, curve e). Following this almost 90% loss, the amplitudes of ARM variations, although small, conform in detail to those observed for the other concentration indicative parameters (Figure 3, curve f). In the deep anoxic zone, the fine grained ferrimagnetic mineral fraction is reduced to less than 2% of its initial concentration.

[19] Hard isothermal remanent magnetization HIRM, assessing contents of hematite and goethite, is also drastically reduced in the upper suboxic layers. In the anoxic zone ultimately only some 10% of the top part HIRM remains (Figure 3, curve g). Using a hematite saturation remanence of 1 kA/m [*Thompson and Oldfield*, 1986] the antiferromagnetic mineral content is calculated to diminish from approximately 0.01 to 0.002 wt% down the sediment column. This provides only minimum estimates, because the 2.5 T field applied is insufficient to saturate hematite and particularly goethite. Their relative variation should be reasonably assessed, however.

4.2. Grain Size and Coercivity

[20] The grain size indicative ratio of anhysteretic to isothermal remanent magnetization ARM/IRM [*Maher*, 1988] reveals high concentrations of fine SD/PSD (titano)-magnetite in the primary magnetic mineral assemblage of the top sediment layers. Within a narrow interval at around 2.5 m depth a distinct shift to much coarser grain size spectra documents an almost complete dissolution of the fine ferrimagnetic fraction (Figure 4, curve a). Respective coarsening trends in the bulk magnetogranulometric ratios of saturation remanence to saturation magnetization, σ_{rs}/σ_s, (Figure 4, curve b) and coercivity of remanence to coercive field, B_{cr}/B_c, (Figure 4, curve c) are less pronounced and extend over a broader depth range.

[21] Deeper in the suboxic field B_{cr}/B_c remain at an approximately constant level. On average slightly decreasing σ_{rs}/σ_s values suggest a continuous minor coarsening followed by some fining in the lowest suboxic section which is also apparent in the B_{cr}/B_c and ARM/IRM ratios. In the anoxic layers beneath 12.5 m depth σ_{rs}/σ_s and B_{cr}/B_c indicate a further coarsening of the bulk magnetic grain size spectrum, while an opposite ARM/IRM trend implies increasing concentrations of fine grained components.

[22] Coercive field B_c (Figure 4, curve d) and coercivity of remanence B_{cr} (Figure 4, curve f) as well as the IRM median destructive field MDF_{IRM} (Figure 4, curve e) hint at a uniform bulk magnetic stability of the primary ferrimagnetic mineral assemblage. Their drop in the upper suboxic zone and overall slight further reduction complies with the general coarsening of the (titano)magnetite component presuming that coercivity is predominantly grain size controlled. As confirmed by an inverse correlation of the short-term grain size and coercivity variations, this premise holds over the entire suboxic sediment series including its lowermost part, where the trends reverse to smaller grain sizes and higher coercivities attaining about the same level at the suboxic/anoxic transition as in the top sediments. The increase in B_c, B_{cr}, and MDF_{IRM} on average persists in the anoxic layers, whereas in clear contrast the σ_{rs}/σ_s and B_{cr}/B_c ratios document an additional coarsening.

4.3. Summary

[23] Room temperature magnetic analyses of bulk sediments document significant modifications of the primary magnetic mineral assemblages across two discrete horizons. The first in about 2.50 m depth is interpreted as the modern iron redox boundary. Standard criteria to identify its exact position, the onset of dissolved Fe^{2+} in the pore water or the transition from a reddish/brownish to grayish/greenish sediment color, could not be applied because of the lack of respective information. Magnetic characteristics of the upper diagenetic front are a drastic decline in magnetic mineral content (Figure 3), a marked overall coarsening of the grain size spectrum and a minor reduction in coercivity (Figure 4). This mode of reductive diagenesis in suboxic environments is a distinctly grain size selective process proceeding from an initial dissolution of the finest fraction to the progressing destruction of the coarser grains [e.g., *Karlin and Levi*, 1983, 1985; *Robinson et al.*, 2000]. Accordingly, the actual position of the Fe redox boundary should approximately coincide with the top of the narrow zone, where ARM drops by almost 90% (Figure 3, curve e) and grain sizes abruptly coarsen (Figure 4, curve a) over a depth range of a few decimeters.

[24] Massive dissolution of both the antiferromagnetic (~80%) and bulk ferrimagnetic (~75%) mineral fractions directly below the Fe redox boundary could imply similar reactions to diagenetic alteration. Yet, the HIRM decline clearly extends over a broader depth interval (Figure 3, curve g) than IRM (Figure 3, curve d) and specifically ARM

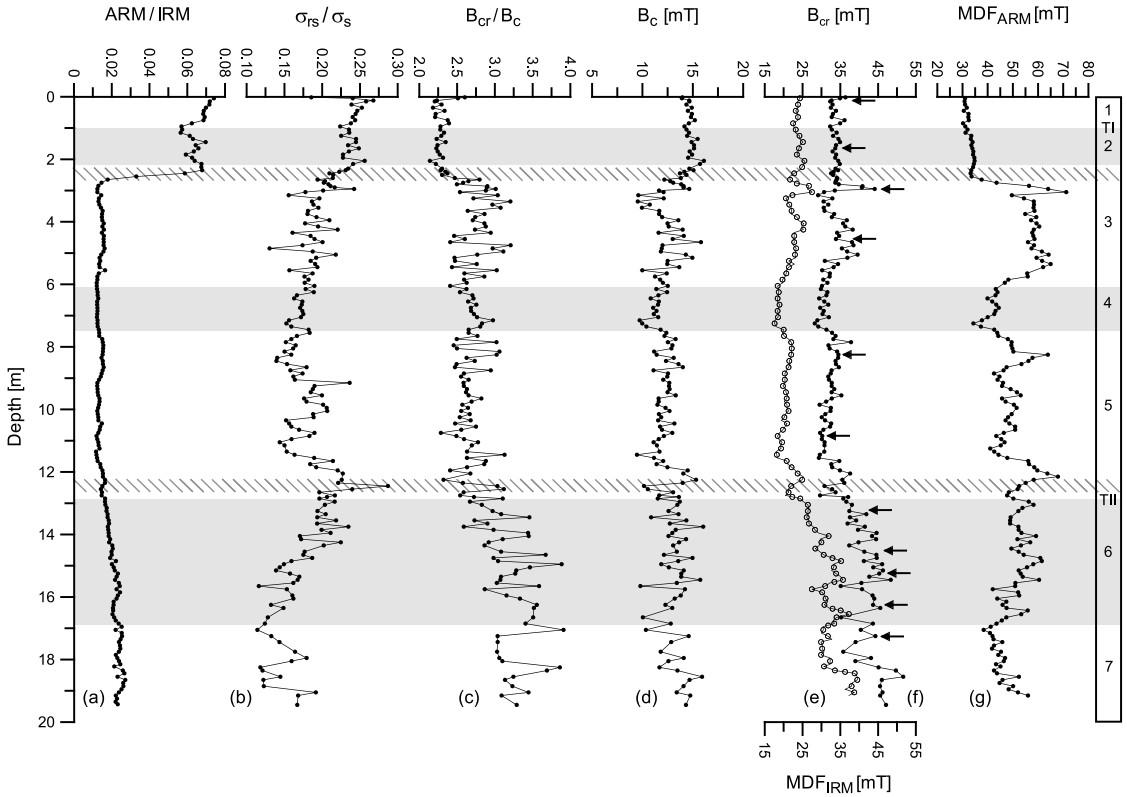

Figure 4. Depth profiles of rock magnetic attributes delineating variations in grain size and coercivity of the ferrimagnetic mineral inventory. Magnetogranulometric ratios include anhysteretic to isothermal remanent magnetization ARM/IRM (curve a), saturation remanence to saturation magnetization σ_{rs}/σ_s (curve b), and coercivity of remanence to coercive field B_{cr}/B_c (curve c). Coercivity parameters include coercive field B_c (curve d), IRM and ARM median destructive field MDF_{IRM} (curve e, open symbols), coercivity of remanence B_{cr} (curve f, solid symbols), and IRM and ARM median destructive field MDF_{ARM} (curve g). Arrows at the B_{cr} profile denote horizons, where high- and/or low-temperature magnetic analyses have been performed (see Figures 5–7). For further details, see Figure 2.

(Figure 3, curve e). This pattern fully agrees with a number of recent studies reporting that hematite is more resistant against diagenetic alteration than (titano)magnetite [*Hilgenfeldt*, 2000; *Robinson et al.*, 2000; *Yamazaki et al.*, 2003; *Liu et al.*, 2004; *Emiroğlu et al.*, 2004; *Garming et al.*, 2005]. Relevant geochemical concepts are rather controversial, however. According to *Canfield et al.* [1992] hematite should be more reactive to diagenetic dissolution than magnetite, whereas *Cornell and Schwertmann* [1996] state that Fe^{3+} is more tightly bonded to the oxide mineral structure than Fe^{2+}, conforming with the available magnetic evidence for the magnetite versus hematite diagenetic reactions. For iron-titanium oxides increasing Ti contents enhance the diagenetic stability [*Emiroğlu et al.*, 2004; *Garming et al.*, 2005]. An interesting observation in this context is the around twofold rise of the ARM median destructive field MDF_{ARM} just below the almost complete loss of the fine grained ferrimagnetic fraction (Figure 4, curve g). This superior magnetic stability of the residual fine grained components most likely reflects the better preservation of higher coercive medium to high Ti titanomagnetite [*Day*, 1977] as compared with low Ti titanomagnetite and pure magnetite.

[25] Precipitation of fine grained authigenic magnetite was repeatedly observed just above the Fe redox boundary [*Karlin*, 1990b; *Tarduno*, 1994; *Reitz et al.*, 2004]. Slightly finer grain sizes and somewhat elevated coercivities (Figure 4) suggest that such a process may be in progress in the Niger Fan deposits. Much more prominent is the coercivity maximum located just below the Fe redox boundary (Figure 4). Interpreted to result from authigenic, most likely bacterial magnetite precipitation [*Tarduno*, 1994], it must have formed, when the Fe redox boundary was below this position in a relatively shallower depth than today. The higher marine productivity in the Niger Fan area during the last glacial [*Thomson et al.*, 1984; *Zabel et al.*, 2001] should have been favorable to establish an appropriate redox zonation. The rearrangement to the present setting must have occurred fairly recently and abruptly to preserve the fine grained magnetite in an environment of currently strong active iron oxide dissolution.

[26] In the deeper suboxic strata diagenetic effects on the magnetic mineral assemblage are relatively limited. Only a slight further coarsening of the bulk grain size spectrum (σ_{rs}/σ_s ratio, Figure 4, curve b) and a minor increase of the fine grained fraction (ARM/IRM ratio, Figure 4, curve a) indicate some progressing alteration.

[27] Below the second diagenetic horizon, the suboxic/sulfidic anoxic transition in about 12.50 m depth, magnetic sediment characteristics document further modifications of

the magnetic mineral fractions which endured the suboxic environment. Different from conditions at the upper diagenetic front, where the impact is most drastic directly beneath the Fe redox boundary, processes in the anoxic domain proceed more gradually producing the strongest effects in the deepest layers. Concentrations of both ferrimagnetic and antiferromagnetic components systematically decrease to greater depths. Grain sizes reveal two opposite trends. While the bulk grain size spectrum further coarsens (σ_{rs}/σ_s ratio, Figure 4, curve b; B_{cr}/B_c ratio, Figure 4, curve c), relative contents of the fine grained portion rise continuously (ARM/IRM ratio, Figure 4, curve a). Simultaneously, bulk coercivities (B_c, Figure 4, curve d; B_{cr}, Figure 4, curve f; and MDF_{IRM}, Figure 4, curve e) evince increasingly higher magnetic stabilities. These features can obviously not be solely explained by grain size selective progressive dissolution of a uniform magnetic mineralogy. Either diagenetic alteration additionally results in the formation of an authigenic, possibly sulfidic magnetic mineral phase or it preferentially removes components of lower coercivity.

[28] To differentiate these two options, high- and low-temperature thermomagnetic analyses of selected bulk sediments and magnetic extracts from the oxic, suboxic and anoxic sulfidic environments have been performed.

5. Thermomagnetic Analyses

5.1. High-Temperature Cycling

[29] Sediments from the oxic top layer revealed but a single significant Curie temperature of around 600°C, confirming magnetite as a major primary magnetic mineral component (Figure 5). A smooth continual reduction of magnetization upon heating possibly hints at additional titanomagnetite with varying titanium contents. Such compounds have been reported from the Cameroon volcanics in the drainage area of the Niger River tributaries [*Herrero-Bervera et al.*, 2004; *Ubangoh et al.*, 2005]. Heating cycles of all sediments from the suboxic and anoxic strata are characterized by an increase and subsequent decrease in magnetization between 350°C and 600°C with more or less clearly developed discrete peaks at about 450°C and/or 500°C, respectively. The width of these humps remains practically unchanged, but their amplitudes build up in the suboxic zone reaching maxima around the anoxic boundary. *Passier et al.* [2001] found the same phenomenon in the youngest eastern Mediterranean Sea sapropel (S1). They interpret the double peak to result from pyrite oxidation upon heating in air, framboidal aggregates being oxidized below, euhedral crystals above 450°C.

[30] In none of the thermomagnetic cycles there is clear evidence for a magnetic iron sulfide [*Dekkers et al.*, 2000] or an iron hydroxide phase. Faint signals of hematite are at the limits of resolution. Up to 720°C primary ferrimagnetic Fe oxides and secondary pyrite oxidation products are largely altered to hematite in air. Lower magnetizations should hence prevail upon cooling. This is in fact observed in the oxic top layer and also less distinct in the suboxic section. In the sulfidic anoxic part opposite trends are found (Figure 5). Similar patterns in sapropel S1 were attributed to Fe oxides which newly formed at high temperatures [*Passier et al.*, 2001].

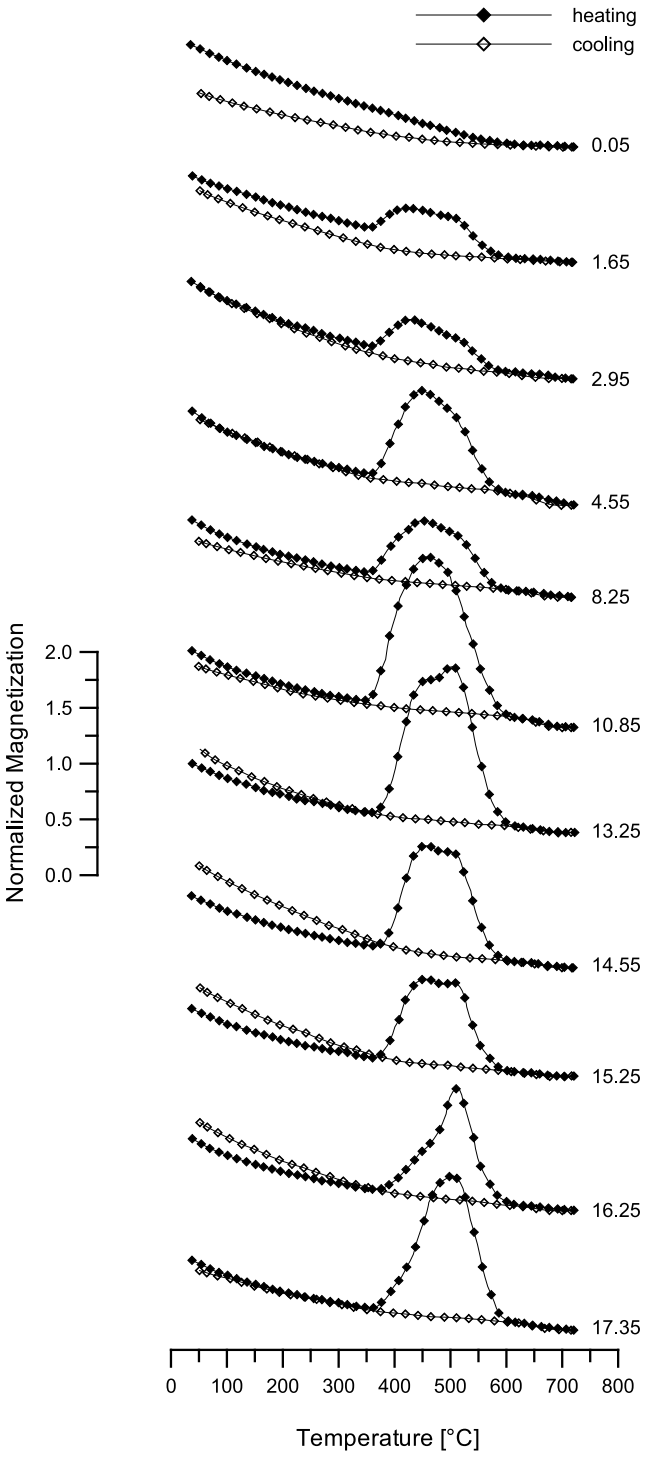

Figure 5. High-temperature thermomagnetic cycles measured on a translation-type Curie balance in air. Numbers on the right denote sample depths in meters.

5.2. Low-Temperature Cycling: Bulk Sediments

[31] Low-temperature remanences of the bulk sediments are notably higher at 5 K after cooling from 300 K in a 2.5 T field (FC) than after zero field cooling (ZFC) through the same temperature interval and applying a 2.5 T field (Figure 6a). In the oxic layer the difference amounts to about one third, decreases to ~20% in the upper suboxic

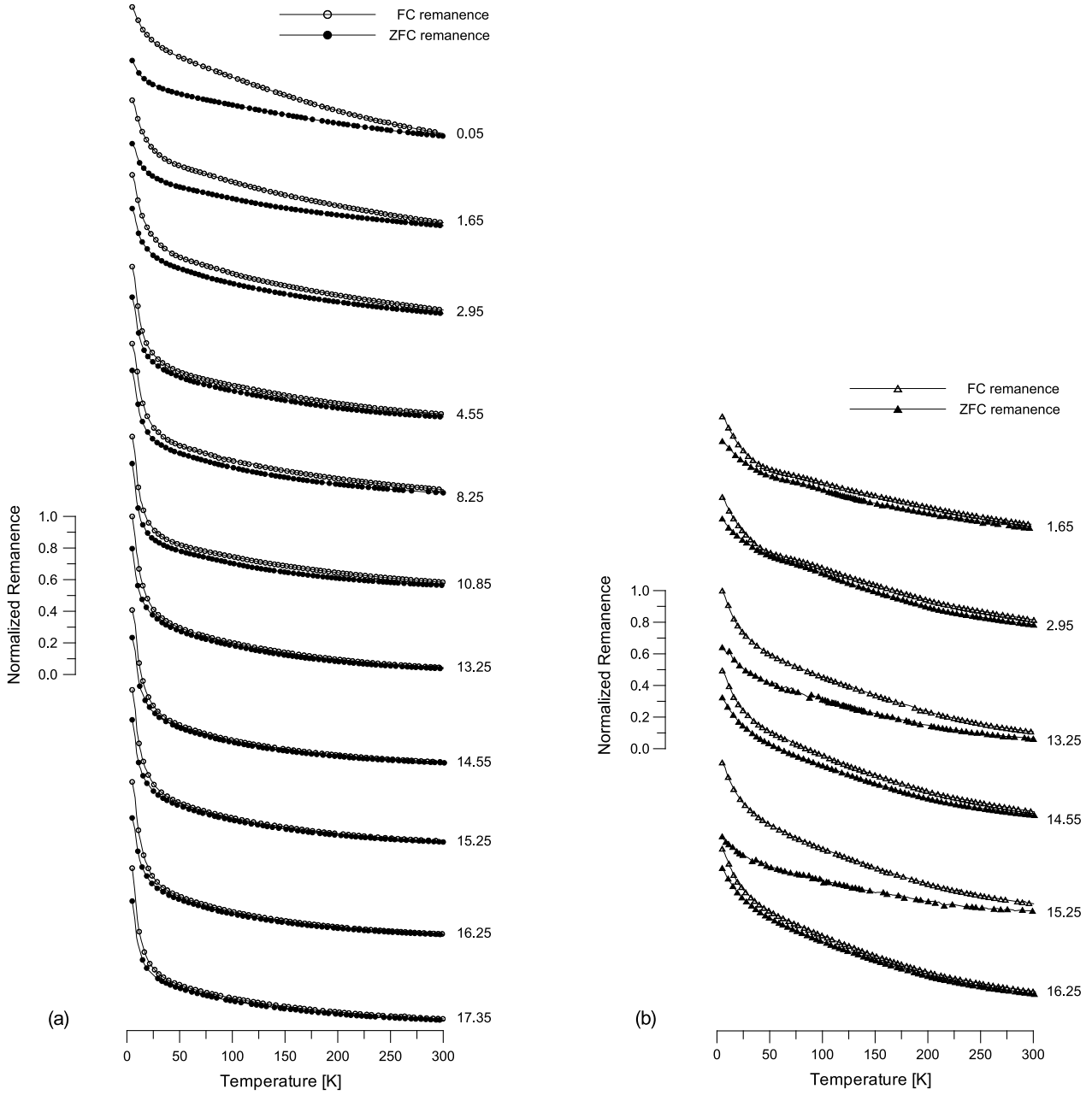

Figure 6. Low-temperature thermal demagnetization of normalized remanences acquired at 5 K after cooling from 300 K in a 2.5 T field (FC) and after zero field cooling (ZFC) through the same temperature interval and applying a 2.5 T field: (a) bulk sediments and (b) magnetic extracts. Numbers on the right denote sample depths in meters.

section and remains at this level in the lower suboxic and anoxic strata. Thermal demagnetization to 300 K reveals that separate effects contribute to this discrepancy. Between 5 and 50 K the gap between FC and ZFC remanences is practically unchanged in the oxic sediments. Respective reductions to 15% in the suboxic and to less than 10% in the anoxic sections indicate that progressing diagenetic alteration causes significant modifications of remanence properties in this temperature interval.

[32] Differences between FC and ZFC remanences in the oxic sediments must be due to specific characteristics of the primary magnetic mineral assemblage. Parts of it acquire a thermal remanence in the applied field, when cooling through their Curie temperature, SP/SD threshold or a particular magnetic transition below 300 K. These mineral phases can obviously not be completely saturated in a 2.5 T field at 5 K. A likely candidate is magnetite, although FC and ZFC warming curves revealed no indications of the Verwey structural phase transition (Figure 6a). However, the Verwey transition is highly sensitive to nonstoichiometry, cation substitution and grain size effects and is thus often obscured or missing in natural bulk material. Potential contributions could also originate from titanomagnetites ($Fe_{3-x}Ti_xO_4$; $0 \leq x \leq 1$) with high titanium contents ($x \gtrsim$

0.75) which have Curie temperatures below 300 K and high magnetic stabilities at low temperature [*Schmidbauer and Readman*, 1982] or titanohematites ($Fe_{2-y}Ti_yO_3$; $0 \leq y \leq 1$) with similar magnetic properties for high-Ti ($y \gtrsim 0.75$) compounds [*Bozorth et al.*, 1957; *Ishikawa et al.*, 1985].

[33] For sediments from above the Fe redox boundary less than 40% of the ZFC remanences are demagnetized between 5 and 50 K (Figure 6a). Below the Fe redox boundary this proportion rises sharply to >60% and more gradually to about 70% in the lower suboxic and anoxic sections. FC remanences show the same trends at somewhat higher percentages. Results obtained from synthetic samples with the same experimental setting [*Moskowitz et al.*, 1998] yield small ZFC remanence losses (<5%) in the 5 to 50 K interval for pure magnetite and Ti-rich ($x \approx 0.6$) titanomagnetites increasing for intermediate compositions with a maximum of about 75% for $x \approx 0.3$. Accordingly, titanomagnetite of variable Ti contents should be an important primary magnetic mineral phase in the Niger deep-sea fan sediments.

[34] In the lower suboxic and anoxic strata, where more than 60% of the remanences are lost below 50 K, minerals formed in the course of diagenetic processes should play a major role. Another possibility to consider are superparamagnetic mineral fractions [*Smirnov and Tarduno*, 2000].

5.3. Low-Temperature Cycling: Magnetic Extracts

[35] Magnetic extracts from the suboxic zone above (1.65 m) and below (2.95 m) the Fe redox boundary yield much smaller differences between FC and ZFC remanences at 5 K than the corresponding bulk sediments (Figure 6b). Upon warming minor gaps left at 50 K remain almost unchanged to 300 K. Low-temperature changes in remanence properties are hence relatively insignificant confirming the above assumption that in bulk sediments they may be largely due to mineral phases which are paramagnetic at ambient temperature and therefore present only in small amounts in magnetic extracts. With the much enhanced concentration of ferrimagnetic components, variations in slope of ZFC and FC demagnetization reveal a suppressed Verwey transition. Ti-poor or slightly oxidized titanomagnetite thus is a substantial component of the primary magnetic mineral inventory. This conclusion complies with the results of high-temperature measurements (Figure 5) and also with the convex shaped susceptibility dependence (Figure 7) observed during warming from 5 to 300 K [*Moskowitz et al.*, 1998]. Furthermore, the Verwey transition identified at 2.95 m depth supports the explanation that the singular maximum in coercivity at this horizon results from authigenic bacterial magnetite formation.

[36] Results of low-temperature measurements on bulk sediments and magnetic extracts from the anoxic layers are largely contrasting. The steep decrease (~70%) of FC and ZFC remanences between 5 and 50 K observed for bulk sediments diminishes to less than 40% for the extracts. These ratios are unrelated to the differences between FC and ZFC remanences at 5 K, which are about 20% for bulk sediments, but extremely variable for magnetic extracts, ranging from ~50% at 15.25 m to ~10% at 16.25 m depth. Independent of the width of the gap at 5 K, on average 60% are closed to 50 K, 30% between 50 and 300 K and 10% remain at room temperature. This strongly suggests that in each case basically the same mineral phases responsible for the changes in remanent properties below 50 K and between 50 and 300 K are magnetically separated. Their variable relative amounts presumably reflect individual arrangements of minerals at a given depth. Diagenesis products, probably most important for the effects in the 5 to 50 K temperature range, may be extracted at room temperature as intergrowths with or overgrowths on magnetic oxides which they have partly substituted. Similarly, high Ti titanomagnetite ($x \gtrsim 0.75$) or titanohematite ($y \gtrsim 0.75$) compounds, which should mainly account for the FC to ZFC differences between 50 and 300 K, could be extracted as intergrowths with other magnetic minerals or included in a silicate matrix also containing magnetic phases.

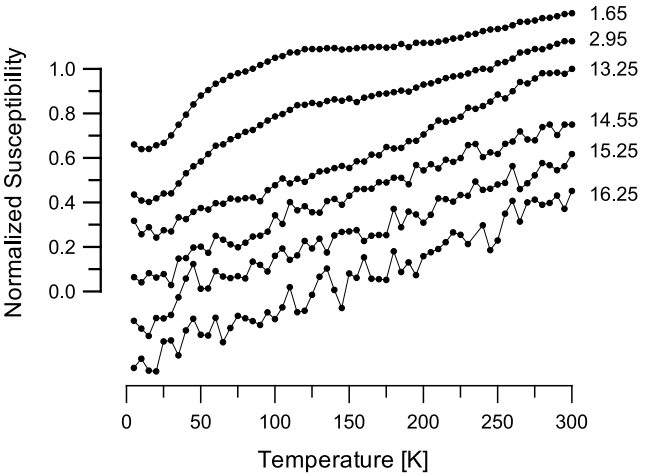

Figure 7. Normalized low-temperature in-phase susceptibility of magnetic extracts measured at 1000 Hz during warming from 5 to 300 K. Numbers on the right denote sample depths in meters.

[37] In the anoxic layers no indications of a suppressed Verwey transition are present. Instead, an approximately linear increase of susceptibility between 5 and 300 K (Figure 7) argues for titanomagnetite of intermediate compositions ($x \approx 0.4$ to 0.6) as the predominant remaining magnetic mineral phase [*Moskowitz et al.*, 1998]. XRD analyses of magnetic extracts from 14.55 and 15.25 m depth (not shown) could positively identify only 'titanomagnetite' and 'titanohematite', but their limited resolution did not allow a quantitative assessment of titanium and iron contents. Neither low-temperature thermomagnetic nor XRD analyses of the extracts provided any evidence for magnetic sulfides. Hence they should not be present in sizable amounts. In particular, thermal demagnetization of FC and ZFC remanences to 300 K (Figure 6) lacks convincing indications for the pyrrhotite low-temperature magnetic transition at 30–35 K [*Dekkers et al.*, 1989].

6. Conclusions

6.1. Primary Magnetic Mineral Inventory

[38] As in most areas of the western South Atlantic [*Schmidt et al.*, 1999], concentrations of magnetic minerals are remarkably low in recent sediments of the Niger deep-sea fan. Estimates based on saturation magnetization and saturation remanence data yield 0.02 wt% and 0.01 wt% of

the bulk sediment to be magnetite and hematite, respectively. Distributed according to this 2:1 ratio, the average total iron content of 40.8 g/kg [*Heuer*, 2003] would correspond to 3.8 wt% magnetite and 1.9 wt% hematite. Therefore only tiny portions of detrital iron are bound in magnetic oxides, a fractionation that should be significantly influenced by prevailing climate conditions causing intense weathering on the African continent.

[39] High-temperature cycling of bulk sediments (Figure 5) as well as low-temperature remanence and susceptibility experiments of magnetic extracts (Figures 6 and 7) identified magnetite as a major component of the primary magnetic mineral assemblage in the Niger deep-sea fan deposits. These measurements also provided conclusive evidence for titanomagnetite of variable composition, most probably derived from the Cameroon volcanics [*Herrero-Bervera et al.*, 2004; *Ubangoh et al.*, 2005]. High coercive hematite was identified from hard isothermal remanent magnetization (Figure 3, curve g) to which iron hydroxides like goethite should also contribute, but could not be appropriately assessed with the available analytical means.

[40] Fine grained ferrimagnetic (titano)magnetite dominates the primary magnetic mineralogy. The ARM/IRM ratio (Figure 4, curve a) documents a substantial single-domain fraction [*Maher*, 1988]. Average grain sizes defined by the σ_{rs}/σ_s (Figure 4, curve b) and B_{cr}/B_c (Figure 4, curve c) ratios fall into the finer grained pseudo-single-domain field [*Day et al.*, 1977]. Superparamagnetic components estimated from the frequency dependence of susceptibility are of minor importance in the upper about 2.5 m ($\kappa_{fd} \approx$ 3%). Because of its limited resolution, this method could not be applied in the magnetically depleted sediments below the Fe redox boundary.

6.2. Diagenetic Alteration

[41] Diagenetic alteration of the iron oxide mineral assemblage in the suboxic environment below the Fe redox boundary confirms all the characteristics previously described in similar settings. Both the ferrimagnetic and antiferromagnetic mineral components are drastically reduced in concentration. Dissolution of hematite evolves in a noticeably slower reaction than that of magnetite [*Cornell and Schwertmann*, 1996; *Hilgenfeldt*, 2000; *Robinson et al.*, 2000; *Yamazaki et al.*, 2003; *Liu et al.*, 2004]. On the other hand, increasing titanium content stabilizes titanomagnetite compounds [*Karlin*, 1990b; *Emiroğlu et al.*, 2004; *Garming et al.*, 2005] because Ti^{4+} substitution correspondingly reduces the number of Fe^{3+}, the acting electron acceptor under anaerobic conditions. Diagenetic alteration of the magnetic mineral assemblage is therefore not only a grain size selective process, but also critically discriminates different mineralogies and compositions of iron-titanium oxides. The resulting shift in ferrimagnetic compounds from magnetite above to titanomagnetite is first reflected below the Fe redox boundary in a distinctly higher magnetic stability of the residual fine grained fraction (MDF_{ARM}, Figure 4, curve g) as coercivity increases with rising titanium content [*Day*, 1977]. In the iron reducing environment magnetite could definitely be identified only just below the presently active Fe redox boundary (Figure 6b) at a single spot of noticeable elevated coercivity (Figure 4). With reference to similar observations [*Karlin*, 1990b; *Tarduno*, 1994; *Reitz et al.*, 2004], this horizon is interpreted to indicate the former position of the Fe redox boundary. Additional major coercivity excursions found deeper in the suboxic domain could represent analogous paleoredox signals of climate controlled, non–steady state C_{org} fluxes and sedimentation rates as in pelagic carbonates of the western equatorial Pacific [*Tarduno*, 1994].

[42] In the anoxic sulfidic sediments magnetite is no more traceable in low-temperature remanence experiments (Figure 6b). An about linear temperature dependence of in-phase susceptibility between 5 and 300 K (Figure 7) implies that titanomagnetite of variable intermediate compositions persist as the predominant ferrimagnetic phase [*Moskowitz et al.*, 1998]. Bulk grain sizes (σ_{rs}/σ_s and B_{cr}/B_c ratios, Figure 4, curves b and c) substantially coarsen on average to greater depth in the anoxic sulfidic layers whereas bulk coercivity (B_c, B_{cr}, Figure 4, curves d and f) continuously increases. These trends can evidently not be explained by a grain size selective dissolution of a monotype magnetic mineral inventory. Instead, constituents of the titanomagnetite solid solution series are selectively dissolved according to their individual content of Fe^{3+} ions. Stability against diagenetic alteration hence increases together with the Ti content and in turn results in a higher magnetic stability.

[43] Conspicuous differences between FC and ZFC remanences at 5 K in the entire sediment column regardless of the diagenetic regime (Figure 6) should to substantial amounts originate from high Ti content iron oxides which are paramagnetic at ambient temperature and have high coercivities at low temperature. As titanomagnetites of respective compositions ($x \gtrsim 0.75$) are quite uncommon natural compounds [*Petersen and Bleil*, 1982], it appears more conceivable that titanohematites ($y \gtrsim 0.75$), which regularly form in volcanogenic processes by high-temperature deuteric oxidation, predominantly contribute to the observed pattern. Such high-Ti titanohematites were for example identified in marine sediments at the South American continental margin (J. F. L. Garming et al., Low-temperature partial magnetic self-reversal in marine sediments, submitted to *Geophysical Journal International*, 2005).

6.3. Superparamagnetic Components

[44] A rapid decrease of ZFC and FC remanences upon warming from 5 to 50 K as observed for all bulk sediments (Figure 6a) has mostly been attributed to ultrafine grained mineral phases converting into a superparamagnetic state at very low unblocking temperatures [*Banerjee et al.*, 1993]. The phenomenon was observed in oxic to suboxic marine sediments [e.g., *Smirnov and Tarduno*, 2000] but also in the Mediterranean sapropel S1 [*Passier and Dekkers*, 2002]. In the Niger Fan deposits it clearly becomes more pronounced with increasing depth (Figure 6). Assuming that a growing SP fraction originates from the breakdown of larger PSD or SD iron oxides as a consequence of magnetic mineral reduction [*Tarduno et al.*, 1998] appears implausible, because the smallest grains are most vulnerable to dissolution and hence their amount should not build up in the course of a prolonged diagenetic alteration. Therefore the more likely alternative explanation would be minerals formed by progressing diagenetic processes. Rhodochrosite ($MnCO_3$) with a Néel temperature of 34 K [*Frederichs et al.*, 2003] and, particularly in the zone of sulfate reduction [*Burdige*,

1993], siderite ($FeCO_3$) with a Néel temperature of 37 K are potential candidates. However, there is the third option to explain the fast remanence decay between 5 and 50 K in combining the effects of superparamagnetic and diagenetically produced mineral phases. This possibility was considered by *Passier and Dekkers* [2002] who suggested that magnetic iron sulfides of SP grain size control the low-temperature remanence characteristics in the S1 sapropel.

6.4. Magnetic Iron Sulfides

[45] XRD analyses did not yield any indication for the presence of magnetic sulfides in the Niger Fan sediments. A phase transition at around 35 K indicating pyrrhotite [*Dekkers et al.*, 1989; *Rochette et al.*, 1990] was not detected in low-temperature experiments (Figure 6) and high-temperature thermomagnetic cycles (Figure 5) lack the drop in magnetization between 270 and 350°C characteristic for greigite [*Roberts*, 1995]. Hence, if present at all, their concentration should be very low. For the bulk of iron released in the suboxic domain below the Fe redox boundary pyrite, the only stable iron sulfide phase in reducing milieus, is apparently the very predominant sink. As iron limitation directly leads to pyrite formation [*Raiswell and Canfield*, 1996], this scenario should also dominate in the anoxic sediments, where only small amounts of reactive iron compounds remain available. The formation and preservation of greigite or pyrrhotite under these conditions would require an arrested pyritization process. Although no unequivocal evidence could be achieved, low-temperature remanence characteristics bear supporting features that SP grain size magnetic sulfides are in fact present. Moreover, the steadily increasing ARM/IRM ratio in the anoxic sulfidic domain (Figure 4, curve a) should be best explained by a small gradually growing SD fraction of magnetic sulfides. With reference to observations in Mediterranean sapropels [*Roberts et al.*, 1999; *Passier and Dekkers*, 2002] and in shelf sediments from the Korean Strait [*Liu et al.*, 2004] an authigenic formation of greigite should be more likely in this environment than the precipitation of pyrrhotite.

[46] **Acknowledgments.** The authors thank T. Frederichs and C. Hilgenfeldt for technical assistance with the magnetic low-temperature analyses and J. Birkenstock, who provided XRD data. D. Heslop, V. Heuer, A. Kosterov, and M. Zabel are gratefully acknowledged for various discussions and helpful comments. Critical reviews by Andrew Roberts and Mark Dekkers as well as remarks by Associate Editor Carlo Laj substantially improved the manuscript. This study was funded by the Deutsche Forschungsgemeinschaft (Research Center Ocean Margins, contribution RCOM0357).

References

Adegbie, A. T. (2001), Reconstruction of paleoenvironmental conditions in equatorial Atlantic and the Gulf of Guinea basins for the last 245,000 years, *Ber. 178*, 113 pp., Fachber. Geowiss., Univ. Bremen, Bremen, Germany.

Banerjee, S. K., C. P. Hunt, and X.-M. Liu (1993), Separation of local signals from the regional paleomonsoon record of the Chinese loess plateau: A rock-magnetic approach, *Geophys. Res. Lett.*, *20*, 843–846.

Berner, R. A. (1981), A new geochemical classification of sedimentary environments, *J. Sed. Petrol.*, *51*, 359–365.

Berner, R. A. (1984), Sedimentary pyrite formation: An update, *Geochim. Cosmochim. Acta*, *48*, 605–615.

Bleil, U., and T. von Dobeneck (2004), Late Quaternary terrigenous sedimentation in the western equatorial Atlantic: South American versus African provenance discriminated by magnetic mineral analyses, in *The South Atlantic in the Late Quaternary*, edited by G. Wefer et al., pp. 213–236, Springer, New York.

Bloemendal, J., J. W. King, F. R. Hall, and S.-J. Doh (1992), Rock magnetism of late Neogene and Pleistocene deep-sea sediments: Relationship to source, diagenetic processes, and sediment lithology, *J. Geophys. Res.*, *97*, 4361–4375.

Bozorth, R. M., D. E. Walsh, and A. J. Williams (1957), Magnetization of ilmenite-hematite system at low temperatures, *Phys. Rev.*, *108*, 157–158.

Burdige, D. J. (1993), The biogeochemistry of manganese and iron reduction in marine sediments, *Earth Sci. Rev.*, *35*, 249–284.

Canfield, D. E., and R. A. Berner (1987), Dissolution and pyritization of magnetite in anoxic marine sediments, *Geochim. Cosmochim. Acta*, *51*, 645–659.

Canfield, D. E., R. Raiswell, and S. Botrell (1992), The reactivity of sedimentary iron minerals towards sulfide, *Am. J. Sci.*, *292*, 659–683.

Cornell, R. M., and U. Schwertmann (1996), *The Iron Oxides*, VCH Publ., New York.

Day, R. (1977), TRM and its variation with grain size, *J. Geomagn. Geoelectr.*, *29*, 233–265.

Day, R., M. Fuller, and V. A. Schmidt (1977), Hysteresis properties of titanomagnetites: Grain size and compositional dependence, *Phys. Earth Planet. Inter.*, *13*, 260–267.

Dekkers, M. J., J.-L. Mattéi, G. Fillion, and P. Rochette (1989), Grain-size dependence of the magnetic behavior of pyrrhotite during its low-temperature transition at 34 K, *Geophys. Res. Lett.*, *16*, 855–858.

Dekkers, M. J., H. F. Passier, and M. A. A. Schoonen (2000), Magnetic properties of hydrothermally synthesized greigite (Fe_3S_4): II. High- and low-temperature characteristics, *Geophys. J. Int.*, *141*, 809–819.

Dinarès-Turell, J., and M. J. Dekkers (1999), Diagenesis and remanence acquisition in the Lower Pliocene Trubi marls at Punta di Maiata (southern Sicily): Palaeomagnetic and rock magnetic observations, in *Paleaomagnetism and Diagenesis in Sediments*, edited by D. H. Tarling and P. Turner, *Geol. Soc. London Spec. Publ.*, *151*, 53–69.

Dunlop, D. J., and Ö. Özdemir (1997), *Rock Magnetism: Fundamentals and Frontiers*, 573 pp., Cambridge Univ. Press, New York.

Emiroğlu, S., D. Rey, and N. Petersen (2004), Magnetic properties of sediments in the Ría de Arousa (Spain): Dissolution of iron oxides and formation of iron sulphides, *Phys. Chem. Earth.*, *29*, 947–959.

Frederichs, T., T. von Dobeneck, U. Bleil, and M. J. Dekkers (2003), Towards the identification of siderite, rhodochrosite, and vivianite in sediments by their low-temperature magnetic properties, *Phys. Chem. Earth.*, *28*, 669–679.

Froelich, P. N., G. P. Klinkhammer, M. L. Bender, N. A. Luedtke, G. R. Heath, D. Cullen, P. Dauphin, D. Hammond, B. Hartmann, and V. Maynard (1979), Early oxidation of organic matter in pelagic sediments of the eastern equatorial Atlantic: Suboxic diagenesis, *Geochim. Cosmochim. Acta*, *43*, 1075–1090.

Funk, J. A., T. von Dobeneck, and A. Reitz (2004), Integrated rock magnetic and geochemical quantification of redoxomorphic iron mineral diagenesis in late Quaternary sediments from the equatorial Atlantic, in *The South Atlantic in the Late Quaternary*, edited by G. Wefer et al., pp. 237–260, Springer, New York.

Garming, J. F. L., U. Bleil, and N. Riedinger (2005), Alteration of magnetic mineralogy at the sulphate-methane transition: Analysis of sediments from the Argentine continental slope, *Phys. Earth Planet. Inter.*, *151*, 290–308.

Hallam, D. F., and B. A. Maher (1994), A record of reversed polarity carried by the iron sulphide greigite in British early Pleistocene sediments, *Earth Planet. Sci. Lett.*, *121*, 71–80.

Herrero-Bervera, E., R. Ubangoh, F. T. Aka, and J.-P. Valet (2004), Paleomagnetic and paleosecular variation study of the Mt. Cameroon volcanics (0.0–0.25 Ma), Cameroon, West Africa, *Phys. Earth Planet. Inter.*, *147*, 171–182.

Heuer, V. (2003), Spurenelemente in Sedimenten des Südatlantik: Primärer Eintrag und frühdiagenetische Überprägung, *Ber. 209*, 136 pp., Fachber. Geowiss., Univ. Bremen, Bremen, Germany.

Hilgenfeldt, K. (2000), Diagenetic dissolution of biogenic magnetite in surface sediments of the Beguela upwelling system, *Int. J. Earth Sci.*, *88*, 630–640.

Holtvoeth, J., S. Kolonic, and T. Wagner (2005), Soil organic matter export to Quaternary continental margins: Implications from the Niger and Congo deep-sea fans, *Geochim. Cosmochim. Acta*, *69*, 2031–2041.

Horng, C.-S., M. Torii, K.-S. Shea, and S.-J. Kao (1998), Inconsistent magnetic polarities between greigite- and pyrrhotite/magnetite-bearing marine sediment from the Tsailiao-chi section, southwestern Taiwan, *Earth Planet. Sci. Lett.*, *164*, 467–481.

Intergovernmental Oceanographic Commission (1994), GEBCO Digital Atlas [CD-ROM], Intergov. Oceanogr. Comm., Int. Hydrogr. Org., Birkenhead, U. K.

Ishikawa, Y., N. Saito, M. Arai, Y. Watanabe, and H. Takei (1985), A new spin glass system of (1-x)$FeTiO_3$-Fe_2O_3. I. Magnetic properties, *J. Phys. Soc. Jpn.*, *54*, 312–325.

Jiang, W.-T., C.-S. Horng, A. P. Roberts, and D. R. Peacor (2001), Contradictory magnetic polarities in sediments and variable timing of neoformation of authigenic greigite, *Earth Planet. Sci. Lett.*, *193*, 1–12.

Karlin, R. (1990a), Magnetite diagenesis in marine sediments from the Oregon continental margin, *J. Geophys. Res.*, *95*, 4405–4419.

Karlin, R. (1990b), Magnetic mineral diagenesis in suboxic sediments at Betis site W-N, NE Pacific Ocean, *J. Geophys. Res.*, *95*, 4421–4436.

Karlin, R., and S. Levi (1983), Diagenesis of magnetic minerals in recent hemipelagic sediments, *Nature*, *303*, 327–330.

Karlin, R., and S. Levi (1985), Geochemical and sedimentological control of the magnetic properties of hemipelagic sediments, *J. Geophys. Res.*, *90*, 10,373–10,392.

Kasten, S., M. Zabel, V. Heuer, and C. Hensen (2004), Processes and signals of nonsteady-state diagenesis in deep-sea sediments and their pore waters, in *The South Atlantic in the Late Quaternary*, edited by G. Wefer et al., pp. 431–459, Springer, New York.

Kolonic, S. (1999), Eintrag von terrigenem organischen Material durch den Niger in den östlichen äquatorialen Atlantik, M.Sc. thesis, 81 pp., Fachber. Geowiss., Univ. Bremen, Bremen, Germany.

Lee, C. H., and J. H. Jin (1995), Authigenic greigite in mud from the continental shelf of the Yellow Sea, off the southwest Korean peninsula, *Mar. Geol.*, *128*, 11–15.

Leslie, B. W., S. P. Lund, and D. E. Hammond (1990a), Rock magnetic evidence for the dissolution and authigenic growth of magnetic minerals within anoxic marine sediments of the California continental borderland, *J. Geophys. Res.*, *95*, 4437–4452.

Leslie, B. W., D. E. Hammond, W. M. Berelson, and S. P. Lund (1990b), Diagenesis in anoxic sediments from the California continental borderland and its influence on iron, sulphur, and magnetite behavior, *J. Geophys. Res.*, *95*, 4453–4470.

Linssen, J. H. (1988), Preliminary results of a study of four successive sedimentary geomagnetic reversal records from the Mediterranean (Upper Thvera, Lower and Upper Sidufjall, and Lower Nunivak), *Phys. Earth Planet. Inter.*, *52*, 207–231.

Liu, J., R. Zhu, A. P. Roberts, S. Li, and J.-H. Chang (2004), High-resolution analysis of early diagenetic effects on magnetic minerals in post-middle-Holocene continental shelf sediments from the Korean Strait, *J. Geophys. Res.*, *109*, B03103, doi:10.1029/2003JB002813.

Lyle, M. (1983), The brown-green color transition in marine sediments, a marker of the Fe (III)-Fe (II) redox boundary, *Limnol. Oceanogr.*, *28*, 1018–1033.

Maher, B. A. (1988), Magnetic properties of some synthetic sub-micron magnetites, *Geophys. J.*, *94*, 83–96.

Moskowitz, B. M., M. Jackson, and C. Kissel (1998), Low-temperature magnetic behavior of titanomagnetites, *Earth Planet. Sci. Lett.*, *157*, 141–149.

Mullender, T. A. T., A. J. van Velzen, and M. J. Dekkers (1993), Continuos drift correction and separate identification of ferrimagnetic and paramagnetic contributions in thermomagnetic runs, *Geophys. J. Int.*, *114*, 663–672.

Oda, H., and M. Torii (2004), Sea-level change and remagnetization of continental shelf sediments off New Jersey (ODP leg 174A): Magnetite and greigite diagenesis, *Geophys. J. Int.*, *156*, 443–458.

Passier, H. F., and M. J. Dekkers (2002), Iron oxide formation in the active oxidation front above sapropel S1 in the eastern Mediterranean Sea as derived from low-temperature magnetism, *Geophys. J. Int.*, *150*, 230–240.

Passier, H. F., G. J. De Lange, and M. J. Dekkers (2001), Magnetic properties and geochemistry of the active oxidation front of the youngest sapropel in the eastern Mediterranean Sea, *Geophys. J. Int.*, *145*, 604–614.

Petersen, N., and U. Bleil (1982), Magnetic properties of rocks, in *Numerical Data and Functional Relationships in Science and Technology, Landolt-Börnstein V/1b*, edited by G. Angenheister, pp. 366–432, Springer, New York.

Petersen, N., T. von Dobeneck, and H. Vali (1986), Fossil bacterial magnetite in deep-sea sediments from the South Atlantic Ocean, *Nature*, *320*, 611–615.

Raiswell, R., and D. E. Canfield (1996), Rates of reaction between silicate, iron and dissolved sulfide in Peru Margin sediments, *Geochim Cosmochim. Acta*, *60*, 2777–2787.

Reitz, A., C. Hensen, S. Kasten, J. A. Funk, and G. J. de Lange (2004), A combined geochemical and rock-magnetic investigation of a redox horizon at the last glacial/interglacial transition, *Phys. Chem. Earth.*, *29*, 921–931.

Reynolds, R. L., M. L. Tuttle, C. A. Rice, N. S. Fishman, J. A. Karachewski, and D. M. Sherman (1994), Magnetization and geochemistry of greigite-bearing cretaceous strata north slope basin, Alaska, *Am. J. Sci.*, *294*, 485–528.

Roberts, A. P. (1995), Magnetic properties of sedimentary greigite (Fe_3S_4), *Earth Planet. Sci. Lett.*, *134*, 227–236.

Roberts, A. P., and G. M. Turner (1993), Diagentic formation of ferrimagnetic iron sulphide minerals in rapidly deposited marine sediments, South Island, New Zealand, *Earth Planet. Sci. Lett.*, *115*, 257–273.

Roberts, A. P., J. S. Stoner, and C. Richter (1999), Diagenetic alteration of sapropels from the eastern Mediterranean Sea, *Mar. Geol.*, *153*, 103–116.

Robinson, S. G., J. T. S. Sahota, and F. Oldfield (2000), Early diagenesis in North Atlantic abyssal plain sediments characterized by rock-magnetic and geochemical indices, *Mar. Geol.*, *163*, 77–107.

Rochette, P., G. Fillion, L.-J. Mattéi, and M. J. Dekkers (1990), Magnetic transition at 30–34 K in pyrrhotite: Insight into a widespread occurrence of this mineral in rocks, *Earth Planet. Sci. Lett.*, *98*, 319–328.

Schmidbauer, E., and P. W. Readman (1982), Low temperature magnetic properties of Ti-rich Fe-Ti spinels, *J. Magn. Magn. Mater.*, *27*, 114–118.

Schmidt, A. M., T. von Dobeneck, and U. Bleil (1999), Magnetic characterization of Holocene sedimentation in the South Atlantic, *Paleoceanography*, *14*, 465–481.

Schulz, H. D., and Cruise Participants (1998), Report and preliminary results of Meteor cruise M 41/1, *Ber. 114*, 124 pp., Fachber. Geowiss., Univ. Bremen, Bremen, Germany.

Smirnov, A. V., and J. Tarduno (2000), Low-temperature magnetic properties of pelagic sediments (Ocean Drilling Project site 805C): Tracers of maghemitization and magnetic mineral reduction, *J. Geophys. Res.*, *105*, 16,457–16,471.

Stoner, J. S., J. E. T. Channell, and C. Hillaire-Marcel (1996), The magnetic signature of rapidly deposited detrital layers from the deep Labrador Sea: Relationship to North Atlantic Heinrich layers, *Paleoceanography*, *11*, 309–325.

Suttill, R. J., P. Turner, and D. J. Vaughan (1982), The geochemistry of iron in recent tidal-flat sediments of the Wash area, England: A mineralogical, Mössbauer, and magnetic study, *Geochim. Cosmochim. Acta*, *46*, 205–217.

Tarduno, J. A. (1994), Temporal trends of magnetic dissolution in the pelagic realm: Gauging paleoproductivity?, *Earth Planet. Sci. Lett.*, *123*, 39–48.

Tarduno, J. A., W. Tian, and S. Wilkinson (1998), Biogeochemical remanent magnetization in pelagic sediments of the western equatorial Pacific Ocean, *Geophys. Res. Lett.*, *25*, 3987–3990.

Thompson, R., and F. Oldfield (1986), *Environmental Magnetism*, 227 pp., Allen and Unwin, St Leonards, N. S. W., Australia.

Thomson, J., T. R. S. Wilson, F. Culkin, and D. J. Hydes (1984), Nonsteady state diagenetic record in eastern equatorial Atlantic sediments, *Earth Planet. Sci. Lett.*, *71*, 23–30.

Ubangoh, R. U., I. G. Pacca, J. B. Nyobe, J. Hell, and B. Ateba (2005), Petromagnetic characteristics of Cameroon Line volcanic rocks, *J. Volcanol. Geotherm. Res.*, *142*, 225–241.

von Dobeneck, T. (1996), A systematic analyses of natural magnetic mineral assemblages based on modelling hysteresis loops with coercivity-related hyperbolic basis functions, *Geophys. J. Int.*, *124*, 675–694.

Weaver, R., A. P. Roberts, and A. J. Barker (2002), A late diagenetic (syn-folding) magnetization carried by pyrrhotite: Implications for paleomagnetic studies from magnetic iron sulphide-bearing sediments, *Earth Planet. Sci. Lett.*, *200*, 371–386.

Yamazaki, T., A. L. Abdeldayem, and K. Ikehara (2003), Rock-magnetic changes with reduction diagenesis in Japan Sea sediments and preservation of geomagnetic secular variation in inclination during the last 30,000 years, *Earth Planets Space*, *55*, 327–340.

Zabel, M., R. R. Schneider, T. Wagner, A. T. Adegbie, U. de Vries, and S. Kolonic (2001), Late Quaternary climate changes in central Africa as inferred from terrigenous input to the Niger Fan, *Quat. Res.*, *56*, 207–217.

U. Bleil and M. Dillon, Fachbereich Geowissenschaften, Universität Bremen, P.O. Box 330 440, Klagenfurther Straße, D-28334 Bremen, Germany. (mdillon@uni-bremen.de)

GJI Geomagnetism, rock magnetism and palaeomagnetism

Unmixing magnetic remanence curves without *a priori* knowledge

D. Heslop[1,2] and M. Dillon[1]

[1]*Department of Geosciences, University of Bremen,* P.O. Box 330 440, 28344 *Bremen, Germany*
[2]*Research Center Ocean Margins, University of Bremen,* 28334 *Bremen, Germany*

Accepted 2007 February 27. Received 2007 February 26; in original form 2006 October 6

SUMMARY

Many of the natural materials studied in rock and environmental magnetism contain a mixed assemblage of mineral grains with a variety of different origins. Mathematical decomposition of the bulk magnetic mineral assemblage into populations with different properties can therefore be a source of useful environmental information. Previous investigations have shown that such unmixing into component parts can provide insights concerning source materials, transport processes, diagenetic alteration, authigenic mineral growth and a number of other processes. A new approach will be presented that performs a linear unmixing of remanence data into coercivity based end-members using only a minimal number of assumptions. A non-negative matrix factorization (NMF) algorithm for unmixing remanence data into constituent end-members is described with case studies to demonstrate the utility of the approach. The shape of the end-members and their abundances obtained by NMF is based solely on the variation in the measured data set and there is no requirement for mathematical functions or type curves to represent individual components. Therefore, in contrast to previous approaches that aimed to unmix curves into components corresponding to individual minerals and domain states, NMF produces a genetically more meaningful decomposition showing how a data set can be represented as a linear sum of invariant parts. It has been found that the NMF algorithm performs well for both absolute and normalized remanence curves, with the capacity to process thousands of measured data points rapidly.

Key words: magnetic mixtures, non-negative matrix factorization, rock magnetism.

1 INTRODUCTION

The magnetic properties of any given mineral grain are controlled by a number of fundamental factors, such as composition, size, shape and stress (Dunlop & Özdemir 1997). The majority of environmental magnetic investigations are performed on bulk samples and therefore only measure a response integrated over the entire mineral assemblage. Given that many geological materials, for example marine sediments, contain a complex mixture of magnetic minerals with different environmental histories, the bulk response of a sample may provide ambiguous information. For a more complete enviromagnetic interpretation it is necessary to attempt to 'unmix' the behaviour of a given sample material in order to characterize the magnetic mineral assemblage. Such unmixing procedures attempt to decompose the magnetic signal into parts representing specific provenances that provide information on different environmental processes.

Coercivity spectra obtained by the stepwise acquisition or demagnetization of isothermal remanent magnetization (IRM) and anhysteretic remanent magnetization (ARM) curves often act as the basis for unmixing the magnetic mineral assemblages found in environmental materials. Based upon empirical evidence from well classified materials, Robertson & France (1994) hypothesized that bulk IRM acquisition curves could be modelled using a linear mixture of cumulative log-Gaussian (CLG) functions. The individual log-Gaussian elements contained in the model were assumed to represent independent coercivity components with different origins. A number of modelling procedures following this idea have been developed (Stockhausen 1998; Kruiver *et al.* 2001; Heslop *et al.* 2002) and the CLG approach has been applied in a wide variety of settings (Eyre 1996; Kruiver & Passier 2001; van Oorschot *et al.* 2002; Garming *et al.* 2005). Later experimental (Egli 2003) and theoretical (Egli 2004a; Heslop *et al.* 2004) work demonstrated that CLG functions were not sufficient to describe all remanence curves because shape properties, such as skewness and kurtosis were inherent to some coercivity distributions. The skewed generalized Gaussian (SGG) distribution introduced by Egli (2003) provided a more flexible function with which to model the demagnetization curves of ARMs. Both the skewness and the kurtosis of the SGG can be controlled, thus making it more suitable to the modelling of coercivity components that are not log-Gaussian. The applicability of the SGG function to modelling magnetic components has been demonstrated for magnetic populations with a number of provenances including aeolian dust (Spassov *et al.* 2003), urban pollution (Spassov *et al.* 2004), lake and marine sediments (Egli 2004b). Additional work performed by Egli (2004a) revealed a link between

the shape parameters of many coercivity distributions, indicating that kurtosis could be determined as an approximate function of skewness. Both the CLG and SGG approaches represent parametric techniques, which can be applied to single coercivity spectra and each defined component can be described using a relatively small number of parameters.

An alternative non-parametric approach to the unmixing problem is based on simultaneously decomposing a collection of remanence curves into components with constant properties, but varying abundances. Under these conditions such coercivity components can be thought of as end-members and a low-rank approximation of the data set is formed. A collection of methods proposed for such data modelling determine mixing abundances based upon *a priori* knowledge regarding the form of the individual end-members (Thompson 1986; Carter-Stiglitz *et al.* 2001). Therefore, before the unmixing can proceed, 'type curves' are required to represent the end-members. Given the large number of factors which can control the magnetic properties of an assemblage, it is unrealistic to assume that sufficient type curves could be collated to provide a representation of every possible end-member found in nature. An alternative approach is to consider each measured curve in the data set to be a potential end-member in order to find an optimal model (Shankar *et al.* 1994; Peters & Turner 1999). The applicability of such an approach is, however, limited to cases where the sample collection contains at least one pure example of each of the end-members in the mixing system.

The modelling procedure presented in this study uses linear combinations of end-members to represent coercivity spectra and thus does not rely on any specific distribution function. Unlike other end-member models, however, type curves are not required and there is no assumption that pure end-member curves must be contained in the measured data set. Instead, the method determines both the form of the end-members and their abundances using only the input remanence curves. The ideas behind this modelling procedure will be introduced, followed by two case studies that demonstrate the applicability of the method.

2 MAGNETIC ASSEMBLAGES AS LINEAR MIXTURES

The unmixing methods discussed in the previous section are all based on an assumption of linear additivity, however, the question as to whether such a property holds for magnetic mixtures remains open. Previous investigations have shown that magnetostatic interactions can produce non-linear effects in enviromagnetic procedures (Muxworthy *et al.* 2003, 2004; Carvallo *et al.* 2006; Muxworthy *et al.* 2006), but the extent of their influence in natural samples is still poorly understood. Magnetostatic interactions were detected by Heslop *et al.* (2006) in sediment suspensions with various compositions and concentrations, however, their effect was found to be minor. Experimental evidence from Lees (1997) demonstrated the possibility that modifying the magnitude of magnetostatic interactions in artificial mixtures would result in remanence curves that could only be explained with a non-linear mixing model. Using a preparation procedure to minimize grain clumping, Carter-Stiglitz *et al.* (2001) found linear additivity appeared to hold in artificial mixtures of variously sized magnetites.

For most mathematical unmixing procedures, it is assumed that whilst interactions between grains in the same magnetic component will not invalidate the linear model, the existence of magnetostatic interactions between the different components can produce non-linear behaviour. The success of previous unmixing studies based on a variety of different linear approaches provides at least some empirical evidence that the deviations from linear additivity due to magnetostatic interactions are minor in natural materials.

A number of previous studies have assumed that measured magnetization data resulted from a linear mixture of a number of invariant end-members (Shankar *et al.* 1994; Peters & Turner 1999; Carter-Stiglitz *et al.* 2001). A matrix $\mathbf{S}$ can be constructed to represent the form, that is, remanence curve, of each end-member. The matrix must therefore have one row for each of its m end-members and l columns spanning the applied field steps. A second matrix $\mathbf{A}$ represents abundances with n rows, one for the remanence curve of each measured sample and a column for each end-member. If $\mathbf{A}$ is interpreted in terms of abundances then it must be assumed that all of its values are non-negative, that is, $\mathbf{A} \geq 0$. Given an assumption of error-free perfect mixing, the data matrix $\mathbf{X}$ which is composed of n rows corresponding to the sample measurements, and l columns, corresponding to the measured field points, can be described by:

$$\mathbf{X} = \mathbf{AS}. \tag{1}$$

In practise, an observed matrix of remanence data will deviate from $\mathbf{X}$ due to measurement error and any non-linear effects, such as magnetostatic interactions between the components. Therefore, $\mathbf{X}$ will be composed of the remanence values explained by a linear model $\mathbf{AS}$ and an error kernel, $\boldsymbol{\epsilon}$:

$$\mathbf{X} = \mathbf{AS} + \boldsymbol{\epsilon}. \tag{2}$$

To form the data matrix $\mathbf{X}$, all the experimental remanence curves must be measured at the same field values, thus any column in $\mathbf{X}$ represents the remanences of the sample set at a single given field. For most real data sets this means it will be necessary to interpolate the measured curves onto a series of common field values. In addition $\mathbf{X}$ cannot be sparse, therefore it is necessary to have a remanence value for each curve at each field value.

In this study $\mathbf{A}$, $\mathbf{S}$ and $\boldsymbol{\epsilon}$ will be all considered as unknowns, and thus it is necessary to determine both the form of the magnetic coercivity components and their abundances using only the information contained in $\mathbf{X}$.

3 NUMERICAL UNMIXING PROCEDURE

To determine $\mathbf{A}$ and $\mathbf{S}$ numerically requires the definition of a cost function to provide a measure of the difference between the data $\mathbf{X}$ and the model matrix $\hat{\mathbf{X}}$ resulting from $\mathbf{AS}$. The squared Euclidean distance is adopted as a simple cost function which is optimal for systems that contain Gaussian distributed errors (Lee & Seung 2001):

$$\|\mathbf{X} - \hat{\mathbf{X}}\|^2 = \sum_{ij} (\mathbf{X}_{ij} - \hat{\mathbf{X}}_{ij})^2. \tag{3}$$

The key to solving the unmixing problem is the factorization of the matrix $\mathbf{X}$ in eq. (2), in such a manner that $\mathbf{A}$ and $\mathbf{S}$ can be determined simultaneously for a given number of end-members, that is, a specific value of m. To be appropriate to the unmixing problem, the factorization must be constrained in a variety of ways. First, the abundance values in $\mathbf{A}$ must be non-negative, thus $\mathbf{A} \geq 0$. Second, remanence acquisition is expected to proceed monotonically until saturation is achieved. A simple solution to this requirement is to process only remanence gradient data, as used in the gradient of acquisition plots (GAP) of by Kruiver *et al.* (2001). Using the GAP representation, the form of the end-members is expressed as the

derivative of the acquisition and can be constrained by $\mathbf{S} \geq 0$ to ensure monotonicity. To unmix linear or standardized acquisition data (LAP and SAP, respectively) would require more complex constraints to enforce monotonicity that will not be considered here. Finally the end-members in **S** should be linearly independent, in other words, it should not be possible to write any of the end-members as a linear combination of the other end-members.

Lee & Seung (2001) developed an iterative method of non-negative matrix factorization (NMF), to minimize $\|\mathbf{X} - \hat{\mathbf{X}}\|^2$ with respect to **A** and **S**, subject to the constraint **A**, $\mathbf{S} \geq 0$, based on the multiplicative update rules:

$$S_{a\mu} \leftarrow S_{a\mu} \frac{(\mathbf{A}^{\mathrm{T}}\mathbf{X})_{a\mu}}{(\mathbf{A}^{\mathrm{T}}\mathbf{A}\mathbf{S})_{a\mu}}$$

$$A_{ia} \leftarrow A_{ia} \frac{(\mathbf{X}\mathbf{S}^{\mathrm{T}})_{ia}}{(\mathbf{A}\mathbf{S}\mathbf{S}^{\mathrm{T}})_{ia}}$$

where i, a, μ are the indices for the matrices, **A** and **S**, as $i = 1, \ldots, n, a = 1, \ldots, m$ and $\mu = 1, \ldots, l$. The multiplicative update rules will also fulfil the linear independence requirement of **S**. NMF can be applied to both absolute and normalized remanence curves, producing values of **A** that will be expressed in terms of absolute remanences and fractional abundances, respectively.

Lee & Seung (2001) provided a proof to show that under such a multiplicative update approach to NMF, the value of $\|\mathbf{X} - \hat{\mathbf{X}}\|^2$ would descend continually to at least a local minimum. The proof was later shown to be in error and it is possible for the NMF algorithm to descend to a saddle point (Berry *et al.* 2007). It is important to note therefore, that the NMF solution obtained by the presented multiplicative updates is not unique. NMF is still a developing field and recently a number of algorithms have been proposed based on adaptations of the Lee & Seung (2001) method to improve convergence properties (Cichocki *et al.* 2006a; Zdunek & Cichocki 2006).

To initialize the NMF algorithm, the user must define the number of end-members (m) to be included in the model and provide initial estimates of **A** and **S**. The majority of studies employing NMF simply initialize **A** and **S** using random numbers distributed uniformly in the interval [0, 1]. It has been demonstrated however, that the speed and accuracy of the solutions of NMF algorithms can be improved by providing good initializations based on the input data set (Wild *et al.* 2003; Langville *et al.* 2006). One example is to perform cluster analysis on **X** and use the locations of the cluster centres as the initial **S**. Using such an approach, the investigator would still be required to define the number of end-members manually by choosing the number of clusters to be calculated during the initialization procedure. Where appropriate **S** could be populated with predefined type curves, under the multiplicative updates **S** would not remain fixed, but in certain cases such an approach could provide a robust initialization leading to a meaningful convergence. Initializations could also employ CLG or SGG model solutions. For example, the average acquisition curve over an entire data set could be calculated and modelled using either the CLG or SGG methods, with the fitted functions providing an initial estimate of **S**. Using such an approach would still require an estimate of **A** for each measured sample, which given the estimate of **S**, could be found by solving a simple least-squares problem.

The entire iterative NMF algorithm including initialization and multiplicative updates can be written in a compact form using MATLAB® notation:

$\mathbf{S} =$ rand (m, l);

$\mathbf{A} =$ rand (n, m);

for i = 1 : maxiter

$\mathbf{S} = \mathbf{S}. * (\mathbf{A}\text{'}\mathbf{X}). / (\mathbf{A}\text{'}\mathbf{A}\mathbf{S} + \text{eps})$;

$\mathbf{A} = \mathbf{A}. * (\mathbf{X}\mathbf{S}\text{'}). / (\mathbf{A}\mathbf{S}\mathbf{S}\text{'} + \text{eps})$;

end

where *eps* represents some small number, typically of the order 10^{-9} to avoid division by zero (Berry *et al.* 2007).

Here, the NMF approach is presented in its simplest form to demonstrate the applicability of such an approach to the unmixing of remanence curves. A large body of additional work exists, extending the basic NMF algorithm to employ alternative distance measures, control the smoothness of **A** and/or **S**, account for data sparseness and force ϵ to conform to a pre-defined distribution (Hoyer 2004; Cichocki *et al.* 2006a,b; Pauca *et al.* 2006; Zdunek & Cichocki 2006).

As a final point, it is important to consider the minimum number of measured curves that are required to obtain a robust model of the data, that is, what is the practical lower limit of n. This question is difficult to answer because it depends on various factors, such as the number of end-members to be fitted, the intersample variability in end-member abundance, the number of data points in the data curves and noise levels. In general, the investigator should attempt to include as many data curves as possible and run the algorithm a number of times starting from different initializations. Solutions that are clearly meaningless in a rock magnetic context can be discarded and the quality of the remaining solutions can be assessed by the ability to interpret them within the constraints of the specific scenario being investigated. If each separate initialization yields a similar result then it would appear that the algorithm is converging to a consistent minimum each time and the size of the input data set can be deemed to be sufficient. A series of numerical experiments with artificial and real data performed during the present study suggested that for typical remanence curves approximately 50 samples should be considered as the minimum value to ensure a robust unmixing.

3.1 Selecting an appropriate number of end-members

A problem common to remanence unmixing techniques is the decision of how many components should be included in the modelling procedure. A vast body of work exists concerned with the general ideas of model selection criteria (Burnham & Anderson 2002) and the general rules follow the idea that models should employ the minimum number of components that will still provide a good fit to the measured data. A key idea in this approach is that all the resolved components must be interpretable within the natural context of the data, a model which contains inexplicable components is thus deemed to be overly complex.

A number of statistical methods have been applied in the parametric unmixing of remanence data in an attempt to provide an objective estimation of the number of components that should be included in a model. Kruiver *et al.* (2001) adopted an approach based on the statistical testing of the distributions of residuals obtained from fitting with different numbers of CLG functions. An F-test was employed to compare the variance of the residuals from two different models involving m and $m + 1$ components. The more complex $m + 1$ model would be rejected if variance of the residuals from the calculated fit was not significantly lower than the residual variance from the m component model.

Egli (2003) adopted a different approach, employing Pearson's χ^2 goodness of fit test to determine the statistical similarity between measured data and a fitted SGG model. In terms of complexity, Egli (2003) recommended that a model is not overly complex if fitting with less parameters would produce a very different model result.

In this study, we propose a method which is less rigorous statistically than the approaches of Kruiver *et al.* (2001) and Egli (2003), but provides a clear visualization of differences between the measured data and the fitted model, aiding the determination of a suitable number of end-members for NMF models. The basis of the selection criterion lies in fact the NMF is applied to a collection of remanence curves simultaneously. Measured data and a resulting NMF model can be compared by the calculation of the coefficient of determination (r^2) between **X** and **AS** at each measured field value. This approach will provide a measure of how well a given model explains the data variance across the applied field range of the measurements. For the case of a model with insufficient end-members, the variance of the input data cannot be reproduced by the model and the calculated r^2 values will be low at a number of fields. For the optimum model, the r^2 value will be high across all the applied fields and it will be found that the inclusion of additional end-members will have little effect in improving the correlation between the measured and modelled data. The applicability of this approach will be demonstrated in the following case studies.

4 CASE STUDY I: NIGER FAN SEDIMENTS

Gravity core GeoB 4901 was recovered from the southern flank of the Niger deep-sea fan at a water depth of 2184 m. The sediments consisted mainly of clay-bearing diatomaceous nannofossil oozes, without any indications of perturbations (Zabel *et al.* 2001). A stable oxygen isotope chronological framework constructed for the core produced a basal age for the sediments of ∼245 ka, coincident with the transition between marine oxygen isotope stages 8 and 7 (Adegbie 2001).

Terrigenous material dominated the sediment composition, with variations reflecting the climatic history of central Africa, whilst carbonate content was generally low reaching a maximum value of ∼36 wt per cent. Terrigenous input was found to vary rhythmically with orbital parameters, reaching maxima during cold periods when decreased vegetation cover resulted in more intense physical erosion (Zabel *et al.* 2001). Geochemical studies of modern-day conditions indicated that the terrigenous component currently reaching the sampling location contained a maximum of 15 per cent aeolian material and thus was dominated by river-suspended matter. The location of the sampling site close to the Niger river mouth would suggest that a similar situation persisted throughout the history of the core with only minor contributions from aeolian components (Zabel *et al.* 2001).

A geochemical investigation of the core revealed that only the uppermost 10 cm of the sediments were oxic, additionally, based upon the appearance of hydrogen sulphide in the pore water the location of the suboxic/sulphidic transition was set at ∼12.5 m (Heuer 2003). The iron content of the sediment (mean iron concentration of 40.8 g kg^{-1}) was controlled by the lithogenic fraction as evidenced by a strong correlation with the aluminium concentration.

A detailed rock magnetic study of the diagenetically altered sediments from GeoB 4901 was reported recently by Dillon & Bleil (2006). Hysteresis, IRM, ARM, low temperature and thermomagnetic data were combined to provide a comprehensive interpretation of the sedimentary magnetic assemblage and its modification by a variety of diagenetic processes. Dillon & Bleil (2006) suggested that the vast majority of the magnetic assemblage reaching the core location was composed of eroded volcanic material originating from Cameroon. The volcanic assemblage was considered to be of variable composition, containing both titanomagnetites and titanohematites transported via the Niger tributaries. The presence of large numbers of volcanic grains in the sediment has since been confirmed by scanning electron micrographs and energy dispersive X-ray spectroscopy of selected samples.

The modern iron redox boundary was identified at a depth of ∼2.5 m on the basis of a sharp decrease in magnetic mineral content, Fig. 1(a), a shift to coarser grain sizes and a slight softening of the bulk coercivity (Dillon & Bleil 2006). Above the modern iron redox boundary, the ratio of κ_{ARM}/IRM is $\sim 2.0 \times 10^{-3}\ m/A$, which is high enough to be indicative of authigenic minerals including biogenic magnetite (Egli 2004b). Other studies have however reported similar values of κ_{ARM}/IRM from sediments where terrigenous input has been dominated by fine-grained (titano-)magnetites (Frank *et al.* 2003; Frank 2007). As mentioned above, Dillon & Bleil (2006) favoured a terrigenous origin for the magnetic assemblage, supporting their argument with low-temperature remanence data that showed no indication of a Verwey transition when measured on bulk samples and only a weak expression in magnetic extracts. It is however possible for the Verwey transition of bacterial magnetites to be suppressed if they form maghemite rims due to low-temperature oxidation (Smirnov & Tarduno 2000). Subsequent examination of larger terrigenous grains in scanning electron micrographs showed a minimal number of the surface cracks that could be taken as evidence for maghematization (Dunlop & Özdemir 1997), suggesting that the weak Verwey transition observed in the magnetic extracts was due to an absence of bacterial magnetites rather than surface oxidation of magnetosomes. Below the modern iron redox boundary relatively large amplitude variations are still observed in the concentration dependent parameters, beyond the suboxic/sulphidic transition however, these variations disappear and the parameters reach a baseline level.

The rock magnetic investigation of Dillon & Bleil (2006) showed that diagenetic alteration of the detrital titanomagnetites appears to have been dependant on both particle size and titanium content, with the smallest particles dissolving first and the Ti-rich component being the most resistant to the reducing conditions. In an attempt to trace the diagenetic history of the detrital assemblage, NMF unmixing was applied to a collection of 177 backfield curves which were measured during the original study of Dillon & Bleil (2006).

In order that they resembled IRM acquisition curves, the mass normalized backfield data were rescaled (division by a factor of 2), reversed and inverted (Fig. 1b). This pre-processing is necessary because NMF requires **X** to be non-negative, therefore converting backfield curves into pseudo-acquisition curves provides positive remanence values and assuming that the curves are monotonic, positive gradient values. In some cases, the measured curves were treated using a cubic smoothing spline (de Boor 1994), in order to reduce the influence of a relatively high noise contribution. To assess the effect of the smoothing procedure, the percentage residuals between the measured data and the smoothed data were calculated, (Fig. 2). The median of the residual distribution is found at ∼1 per cent, which represents a 1 per cent difference between the measured and smoothed data value. Some much larger residuals exist, in excess of 100 per cent, however they correspond to the very weak remanences where a small absolute change to the measured value during smoothing will produce a large percentage residual. Finally, the GAP

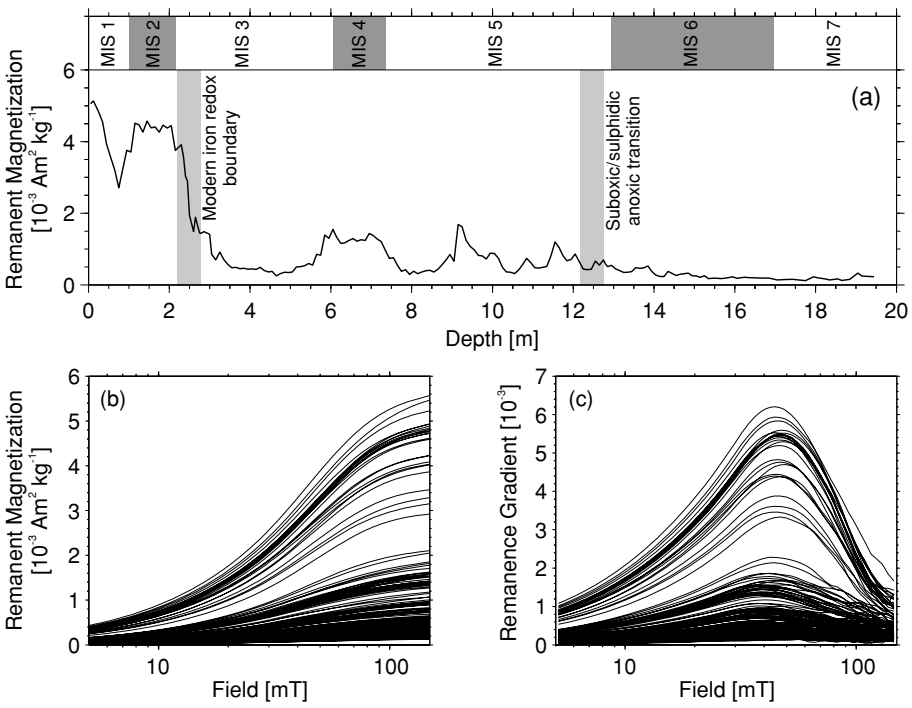

Figure 1. (a) Depth profile of the remanence acquired at 150 mT through the GeoB 4901 core with assigned Marine isotope stage (MIS) positions. (b) Smoothed remanence acquisition curves for all the samples in core GeoB 4901 based on the measured backfield data. (c) Remanence gradient data (GAP) calculated from the smoothed acquisition curves.

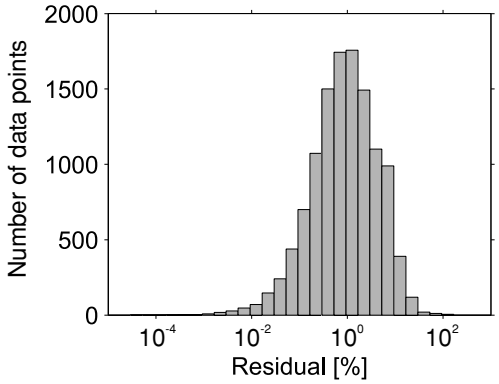

Figure 2. Percentage residuals of the smoothing procedure applied to the remanence curves of the Niger Fan sediments. The median residual is <1 per cent, however larger values are observed for the weak remanences.

data were calculated on a logarithmic field scale. It was found that a number of the GAP curves became noisy at higher fields, therefore the data matrix **X** was truncated at a maximum field of 150 mT (Fig. 1c). Saturated samples are not a requirement of the unmixing procedure, however, truncating the data at low fields will only allow the magnetically soft components of the mineral assemblage to be studied.

The number of end-members to be included in the model was based on the selection process described above. It is important to stress that, although the detrital flux reaching the core location is thought to have had a constant composition through time, the diagenetic processes did not act uniformly across the detrital magnetic mineral assemblage. Thus, a single end-member cannot be used to model the detrital magnetic mineral assemblage, but instead it is necessary to have multiple end-members in order to represent the relative abundance of different parts of the detrital assemblage as the diagenetic processes preferentially remove certain types of grains. It can be seen that a two component fit is not sufficient to model the measured data at a number of fields through the measured spectrum (Fig. 3a). A three component fit provides a great improvement at low fields, however some of the higher field data remains poorly modelled. The addition of an extra component in the 4 end-member model provides only a slight improvement at high fields, thus for the final unmixing, a 3 end-member model was selected. To initialize the NMF algorithm, a GAP model was calculated for a curve formed from the mean acquisition of all the samples, Fig. 3(b), given this estimate of **S**, a first estimate of **A** was made using constrained least squares.

The NMF model produces three negatively skewed distributions with similar forms to the SGG function proposed by Egli (2003). In the upper core, where the detrital assemblage is expected to be pristine, Fig. 4(a), end-member 2 (EM2) makes the greatest contribution to the remanence, followed by end-member 1 (EM1) and finally end-member 3 (EM3). The form of the end-members suggests that the magnetic assemblage is terrigenous in origin and not authigenic/bacterial. The softest two end-members have broad distributions and when modelled individually with SGG functions yield dispersion parameters >0.55, this property points towards a terrigenous origin and is incompatible with the small dispersion expected for bacterial magnetites because of their narrow grain size distributions (Kruiver *et al.* 2001; Egli 2004b). An extra analysis step which could provide additional insights into the data set would be to also perform unmixing of ARM data. In this way κ_{ARM}/IRM could be calculated for each end-member, providing clues to its origin. This idea was first demonstrated by Egli (2004b), who formed SGG models for both IRM and ARM curves and such an approach could be incorporated easily into the NMF procedure. Unfortunately, the ARM data measured for GeoB 4901 was not of sufficient resolution

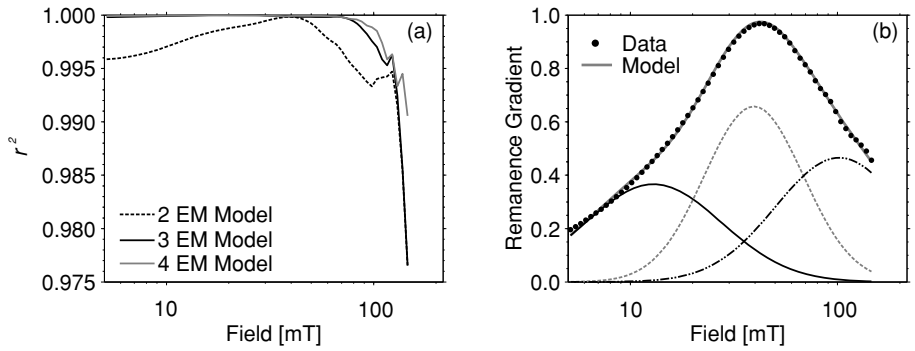

Figure 3. (a) Based on the correlation of the model and measured data as a function of applied field, a three end-member solution was selected as a balance between model quality and complexity. (b) A three component CLG model was formed for the mean acquisition curve to provide an initial **S**, the estimate of **A** for each sample was then obtained by constrained least squares. The CLG model (thick grey line) represents the linear addition of the individual log-Gaussian components and the mean GAP data is shown with closed symbols.

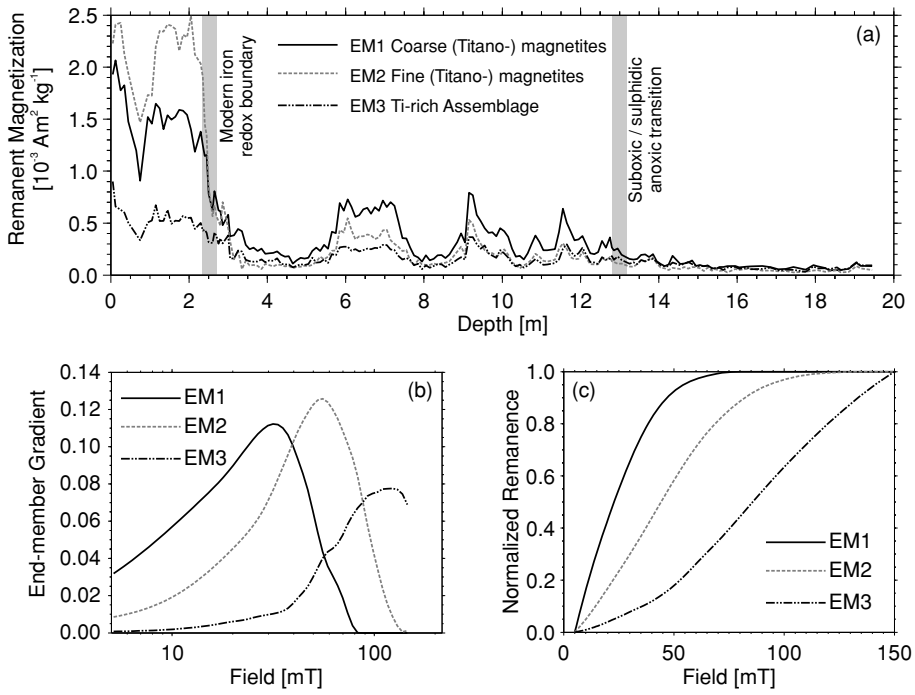

Figure 4. (a) Remanence contributions of the three individual end-members, note that both the absolute and relative proportions of the different end-members vary across the different diagenetic zones of the core. (b) Gradient curves produced as the NMF algorithm output **S**. (c) Remanence acquisition curves for the three end-members calculated from the output of the NMF algorithm. The end-members in **S** have been divided by factors to normalize each acquisition curve to a maximum value of one, absolute remanence values can be calculated for each end-member in each core position by multiplying **A** by the same factors. Because acquisition is non-linear it is not possible to extrapolate the normalized remanence of each end-member back to zero applied field.

to yield robust unmixing results, so interpretation had to be based solely on the backfield data.

At the modern iron redox boundary, a drop in the abundance of all three end-members is observed as dissolution occurs, however the rate at which the individual components decrease differs. A very gradual decrease in EM3 is observed across the modern iron redox boundary, in contrast EM1 is quicker, losing ∼93 per cent of its signal over ∼2.7 m. The greatest and most rapid decrease is seen in EM2, ∼98 per cent of its signal over ∼1.3 m, suggesting it is the end-member most susceptible to dissolution. Below the modern iron redox boundary, the largest contribution to the remanence is made by EM1.

Examination of the end-member coercivity distributions, Fig. 4(b), provides a explanation for the abundance behaviour which is consistent with the interpretation of Dillon & Bleil (2006). EM1 has a lower coercivity than EM2 and appears to have been more resistant to dissolution, this is thought to be a grain size effect, with EM1 composed of large (titano-)magnetite grains and EM2 composed of fine (titano-)magnetite grains which where more readily dissolved by the reducing conditions. It is apparent that EM3 had the greatest resistance to dissolution suggesting a Ti-rich titanomagnetite or titanohematite, this interpretation is supported by the slightly harder nature of this end-member (Day *et al.* 1977).

Below the suboxic/sulphidic transition, further changes are observed in the contributions of the end-members. Diagenetic processes act more slowly in anoxic conditions and all three end-members decrease gradually with depth reaching baseline values. Under certain redox conditions it is possible for new remanence

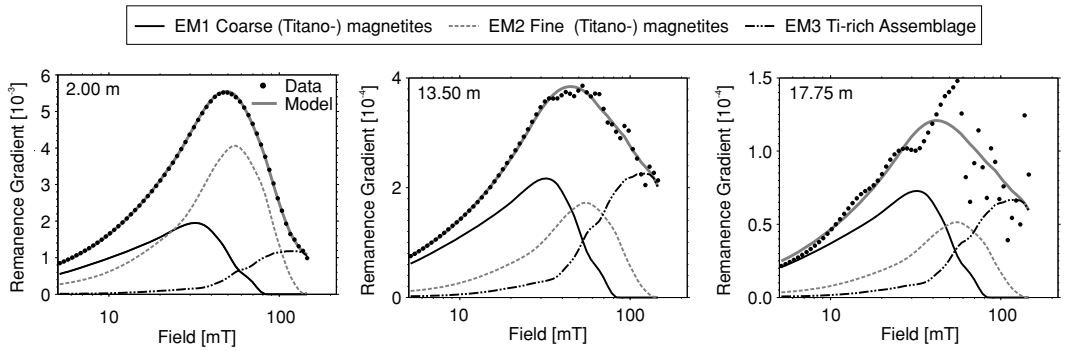

Figure 5. Individual sample fits for three locations through core GeoB 4901 that demonstrate the effect of diagenesis on the detrital input assemblage. In each case, the model (thick grey line) represents the linear addition of the individual end-members and the measured data is shown with closed symbols. The depth of the individual samples is shown in the top left corner of each panel.

bearing phases, such as greigite to be formed (Roberts & Turner 1993; Snowball & Torii 1999). Dillon & Bleil (2006) suggested that minor amounts of single-domain greigite may form in the anoxic zone of the sediments, if this is the case it is not detected in the unmixing, because even with the addition of an extra end-member, none of the resolved components could be interpreted as an authigenic iron sulphide phase.

Individual model fits for three sample horizons in the GeoB 4901 core are shown in Fig. 5. For the first sample (2.00 m), taken above the modern iron redox boundary, the detrital assemblage is dominated by contributions from the coarse and fine components (EM1 and EM2) and a good fit is observed between the data and the model. A sample taken from the lower part of the core (13.50 m), below the suboxic/sulphidic anoxic transition, shows dominant contributions from EM1 and EM3. A good model fit is still achieved when the absolute magnetizations are low, but the data degrades when moving towards high fields because of noise in the measured backfield curve. It is clear, however, that the model follows the general trend of the data and for such noisy curves it is not expected that each point can be fitted exactly. The final example comes from the sample with the worst fit (17.75 m), where there is little correspondence between the data and the model. It can be seen, however, that the data is very noisy, especially at higher fields, and it is not surprising that the model does not fit the data.

The Niger fan sediments can be used to demonstrate an additional point concerning end-member analysis. Because this form of unmixing focuses on forming a low-rank representation of the overall behaviour of a data set, it is possible that samples which deviate from the general pattern cannot be modelled properly. An example of this effect is observed below the modern iron redox boundary. A peak in the median destructive field of ARM was reported by Dillon & Bleil (2006) and attributed to the localized precipitation of bacterial magnetite. Because this zone has unique properties within the sediment sequence, it cannot be accurately modelled using an end-member approach. Shown in Fig. 6 is the data and model for the sample at 2.90 m which is believed to contain bacterial magnetite. A higher coercivity feature is clearly present in the 2.90 m sample, it cannot, however, be modelled with the three calculated end-members. In contrast, neighbouring samples at 2.80 and 3.00 m which are thought to not contain significant amounts of bacterial magnetite and have properties that are more typical of the sediment sequence as a whole can be fitted closely using the end-member model.

5 CASE STUDY II: A YOUNG MID-OCEAN RIDGE BASALT

The cooling rate gradient that exists between the glassy rim of a mid-ocean ridge basalt (MORB) pillow and its interior produces a spatial trend in titanomagnetite size and composition, which can be tracked by a number of rock magnetic procedures (Kent & Gee 1994; Pick & Tauxe 1994; Gee & Kent 1995, 1999; Fabian 2003, 2006). Rapidly cooled MORB samples commonly yield magnetization ratios (M_{rs}/M_s) greater than the value of 0.5 expected for

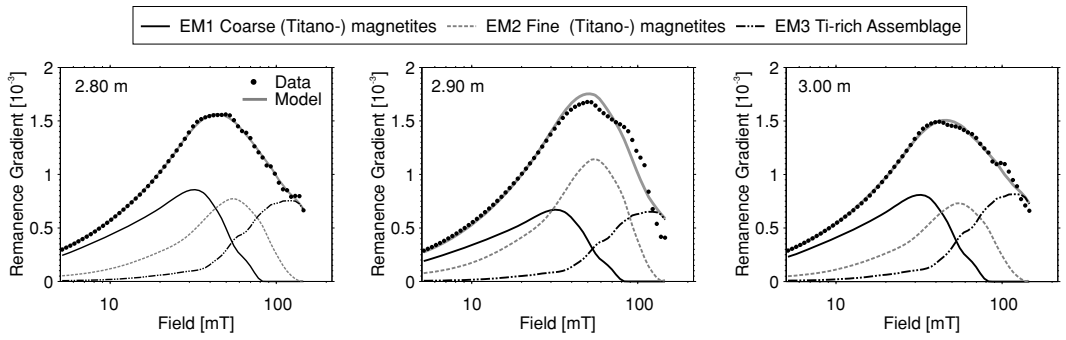

Figure 6. Sample fits spanning the sharp peak in median destructive field of ARM and attributed to bacterial magnetite. The samples above and below the peak, 2.80 and 3.00 m, respectively, can be fitted closely with the three end-member model. In contrast, the sample at the peak (2.90 m) has unique properties within the core and cannot be modelled properly using an end-member approach. In each case, the model (thick grey line) represents the linear addition of the individual end-members and the measured data is shown with closed symbols.

single domain grains dominated by uniaxial anisotropy (Stoner & Wohlfarth 1948). While some authors have suggested that such values are indicative of cubic anisotropy (Gee & Kent 1995, 1999), it has been demonstrated recently that values of $M_{rs}/M_s > 0.5$ were an experimental artifact and a uniaxial system will prevail for titanomagnetite in the presence of moderate internal stress (Fabian 2006).

A densely sampled zero age MORB from the Juan de Fuca Ridge forms the basis of this case study. Pillow specimen T787-R1 (provided by D. Kent) is ∼12 cm long and was cut perpendicular to the glassy margin, producing a transect to the pillow interior. The properties of this MORB have been measured in a number of previous studies and it is thought that the magnetic granulometric trend of the titanomagnetite assemblage is well understood (Zhou *et al.* 1997; Gee & Kent 1999; Zhou *et al.* 2000; Fabian 2003, 2006). Hysteresis loops measured by Fabian (2003) demonstrate the rapid cooling rate of the MORB at the chilled margin resulted in the formation of superparamagnetic (SP) and single-domain (SD) particles. The presence of SP grains is demonstrated by the reduced M_{rs}/M_s values at the rim of the MORB with values subsequently increasing as the SD grains begin to dominate the hysteresis behaviour (Fig. 8a). The slower cooling rate towards the interior of the pillow favoured the production of larger pseudo-single-domain (PSD) and multidomain (MD) particles. As in the previous case study, measured backfield curves (data provided by K. Fabian) were used in the unmixing procedure, therefore no information can be obtained concerning the contribution of SP particles. A total of 68 curves were prepared (rescaled, reversed, inverted and smoothed), however, no mass data were available, therefore the MORB data had to be normalized according to their maximum remanence. Sample locations are only available as positions, which vary only approximately linearly as a function of distance from the chilled margin of the specimen (Fabian 2003).

The composition of titanomagnetites ($Fe_{3-x}\ Ti_xO_4$; $0 \leq x \leq 1.0$) within an individual pillow can vary strongly depending on a number of factors controlled by the cooling rate. Combined magnetic and microscopy investigations (Zhou *et al.* 1997, 2000) identified a subset of titanomagnetite grains that grew up to 40 μm and increased in Ti content from $x \approx 0.3$ at the rim to $x \approx 0.6$ towards the interior of a pillow. A second subset of finer (SD to SP) particles revealed only a slight coarsening towards the interior and a highly variable Ti content ($0 \leq x \leq 0.8$) throughout the pillow.

The evolution of a titanomagnetite assemblage through a MORB pillow must be considered as dynamic and the first step is to determine how many end-members are required to provide a quantification of this behaviour through the T787-R1 specimen. All of the NMF models applied to the MORB data were initialized using only random numbers. We choose this form of initialization to demonstrate that in some cases a robust model can be obtained without a structured input for the NMF algorithm. Dunlop (2002) proposed that the PSD hysteresis properties of titanomagnetites could be modelled using a mixture of SD and MD behaviour. Given this proposition and the fact that SP material will play no role in remanence data, it is possible to imagine that the spatial variation of the magnetic properties within T787-R1 could be explained by a two end-member (SD and MD) model. The two-component model produced by the NMF algorithm yielded a poor fit to the data, this however is not surprising because the spatial evolution of the magnetic assemblage through a MORB pillow is complex. A comparison of 4, 5 and 6 end-member models reveals that sufficient complexity is achieved with a 5 end-member unmixing, Fig. 7, but little improvement is observed with six end-members.

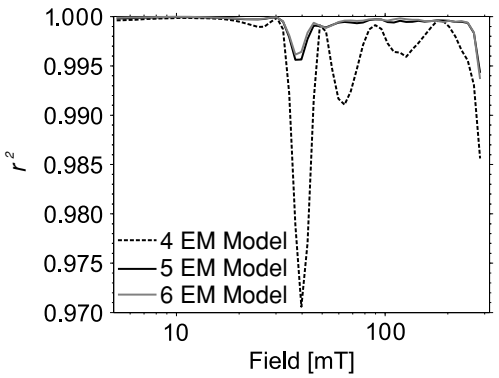

Figure 7. (a) Based on the correlation of the model and measured data as a function of applied field, a five end-member solution was selected as a balance between model quality and complexity. It can be seen that the five end-member solution provides a large improvement over the four end-member model, but the addition of extra components does little to further improve the model quality.

At the pillow interior, EM1 dominates the relative remanence contribution with values >75 per cent (Fig. 8b). Examination of the coercivity distribution, Figs 8(c) and 8(d), shows it is the softest component and reaches saturation just above 50 mT with a maximum in the coercivity spectrum at ∼30 mT. Such characteristics indicate that EM1 is composed of the large (MD) titanomagnetites, which were able to form in the more slowly cooled pillow interior. Based solely upon the coercivity spectrum, it is difficult to estimate the composition of the particles because there is no clear relationship between coercivity of remanence and the level of Ti substitution for coarse grained titanomagnetites (Day *et al.* 1977).

EM5 appears to be composed of particles with a broad distribution of coercivities, it is the hardest of the five components and does not saturate in a field of 300 mT. Because the NMF unmixing procedure is non-parametric, the derived coercivity distributions do not conform to a given mathematical function, therefore it is not possible to predict when a unsaturated component will reach saturation. Day *et al.* (1977) showed that the coercivity of remanence for fine wet-ground titanomagnetites was a function of composition, increasing by a factor of ∼4 from pure magnetite to $x = 0.6$. Such evidence suggests that EM5 represents a fine grained (SD) titanomagnetite assemblage with highly variable composition, possibly as high as $x = 0.8$, formed in the rapidly cooled outer part of the rim. Such a hypothesis is supported by the relative remanence contribution of EM5, which is highest (∼60 per cent) at the rim of the specimen and decreases to <10 per cent within ∼1.5 cm (assuming a linear relationship between position and distance).

EM2, EM3 and EM4 represent transitional assemblages that are required to explain the trends in grain size and composition which follow the cooling gradient of the pillow. It is important to note that because of the linear independence enforced by the NMF algorithm, the transitional end-members cannot be formed by simply mixing together EM1 and EM5. Instead, the transitional end-members allow for the non-linear behaviour of magnetic particle properties as a function of grain size and composition, and it is apparent that the PSD grains cannot be modelled simply as a linear combination of SD and MD behaviour. EM2 is more MD-like with a peak in its coercivity spectrum at ∼40 mT compared to the value of ∼100 mT for the more SD-like EM4. EM3 appears to be a true transitional assemblage with a coercivity peak at ∼55 mT and a shape which contains features similar to both the SD and MD components. Past

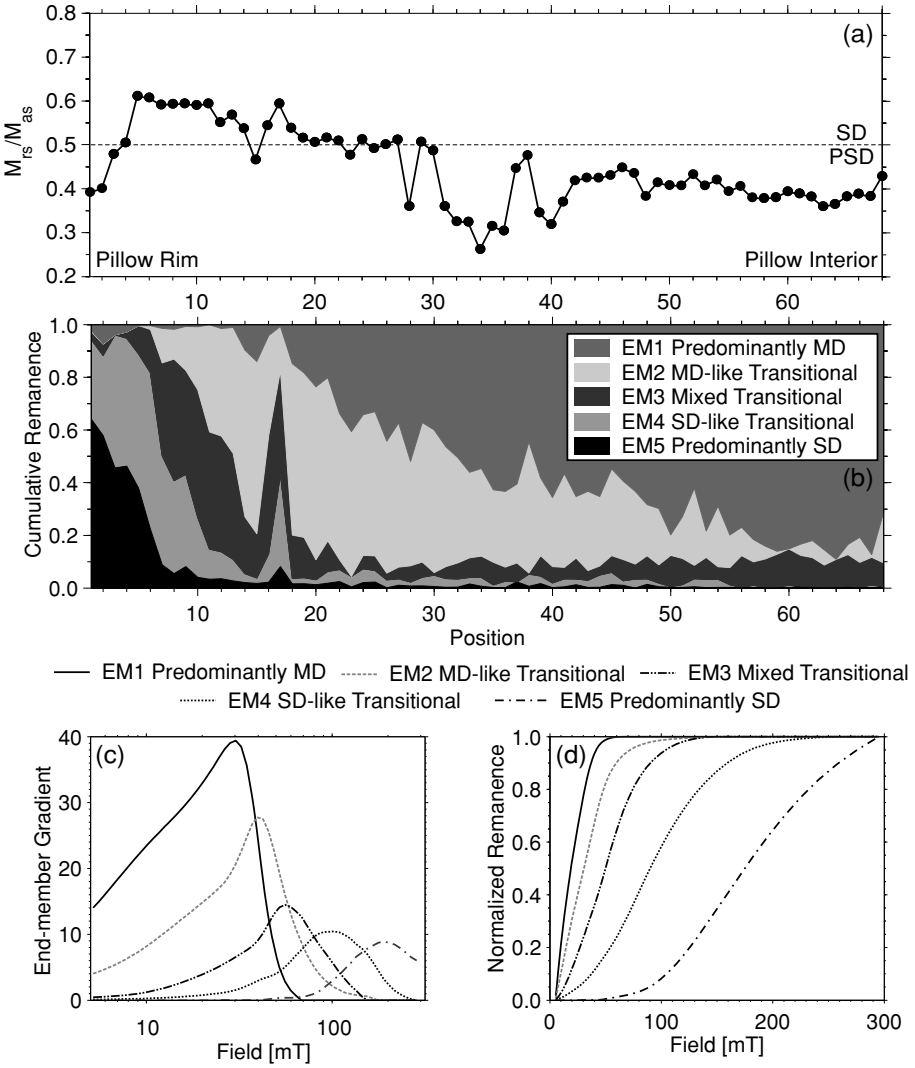

Figure 8. (a) Magnetization ratio measured across the zero age T787-R1 MORB specimen (data provided by K. Fabian). M_{as} corresponds to the 'apparent' saturation which does not take the high field (>1 T) behaviour of the samples into consideration. Sample positions along the ∼12 cm long specimen vary approximately linearly with distance from the chilled margin. (b) End-member abundances shown in a stacked area plot. The data set from T787-R1 was normalized, thus the end-member remanences can only be quoted in relative terms, with the contributions to each sample totalling one. (c) Gradient curves produced as the NMF algorithm output **S**. (d) Remanence acquisition curves for the four end-members calculated from the output of the NMF algorithm, the end-members in **S** have been divided by factors to normalize each curve to a maximum value of one.

a distance of ∼3 cm from the rim (corresponding to position 15 and assuming a linear relationship between position and distance), the SD dominated end-members have almost disappeared from the magnetic assemblage, making a <10 per cent combined contribution to the total remanence. At this position the MD-like components make a significant contribution to the remanence and gradually the full MD component (EM1) becomes dominant towards the interior of the pillow. The model fits for two samples are shown in Fig. 9 to demonstrate the shift from SD-type end-members at the pillow rim to MD-type end-members in the interior.

The presented case study demonstrates the ability of the NMF approach to unmix the variations in the magnetic assemblage of the T787-R1 MORB specimen. The description of the spatial variation of the magnetic properties provided by the end-member model corresponds clearly to the intrapillow processes described by previous authors. In cases, such as T787-R1 where the magnetic mineral inventory is seen to evolve gradually, it is necessary to derive a relatively large number of end-members in order that sufficient transitional assemblages can be defined to produce a good description of the measured data.

6 DISCUSSION AND CONCLUSIONS

The aim of this study was to demonstrate the potential of simple NMF algorithms to unmix remanent magnetization curves. The two presented case studies demonstrate the ability of such an approach to derive both coercivity components and their abundances based solely upon the variability in the measured data set. In the case of sediments from the Niger fan, the effects of diagenetic alteration on the detrital mineral assemblage could be traced in terms of both major changes across geochemical fronts and more gradual modifications as a function of depth. It was also possible to successfully model the evolving titanomagnetite population of the Juan de Fuca Ridge MORB by employing a relatively large number of end-members to

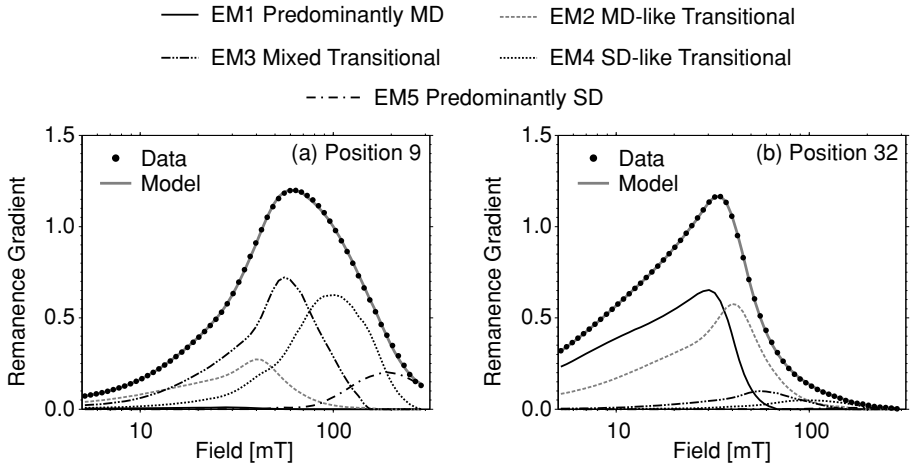

Figure 9. Data fits for two samples taken from the T787-R1 MORB specimen in positions 9 (pillow exterior) and 32 (pillow interior). (a) SD-type end-members are abundant towards the chilled margin of the MORB, whilst the MD end-member (EM1) makes only a very small contribution. (b) Towards the pillow interior, the lower coercivity MD-type end-members dominate whilst the SD end-members are almost entirely absent. In each case, the model (thick grey line) represents the linear addition of the individual end-members and the measured data is shown with closed symbols.

represent transitional assemblages. In both case studies, the number of end-members in each model was selected on the basis of the correlation between the measured and modelled data as a function of field. This approach does not involve statistical testing, but instead the selection criterion were only to keep the model simple, that is, adopting the minimum number of end-members that would provide a good fit to the data, and importantly the environmental origin and implications of each end-member had to be clear.

The potential of NMF based algorithms in the unmixing of rock and environmental magnetic data remains to be fully explored, in particular the question of initialization needs to be addressed in more detail. In principle, many types of magnetic data, both infield and remanence curves, could be analysed where a linear mixing model is thought to hold.

ACKNOWLEDGMENTS

The constructive reviews of M. J. Dekkers and R. Egli helped to improve the manuscript greatly. This work was funded by the DFG Research Centre "Ocean Margins" of the University of Bremen (contribution: 0487). The authors are grateful to K. Fabian who provided backfield data for the T787-R1 MORB specimen.

REFERENCES

Adegbie, A.T., 2001. Reconstruction of paleoenvironmental conditions in equatorial Atlantic and the Gulf of Guinea basins for the last 245 000 years, Tech. Rep. 178, Univ. Bremen, Bremen, Germany.

Berry, M., Browne, M., Langville, A., Pauca, P. & Plemmons, R., 2007. Algorithms and applications for approximate non-negative matrix factorization, *Comput. Stat. Data. Anal.,* in press, doi:10.1016/j.csda.2006.11.006.

Burnham, K.P. & Anderson, D.R., 2002. *Model Selection and Multimodel Inference: A practical Information-Theoretic Approach*, Springer-Verlag Inc, Berlin; New York.

Carter-Stiglitz, B., Moskowitz, B. & Jackson, M., 2001. Umixing magnetic assemblages and the magnetic behaviour of bimodel mixtures, *J. Geophys. Res.,* **106,** 26397–26411.

Carvallo, C., Muxworthy, A.R. & Dunlop, D.J., 2006. First-order reversal curve (FORC) diagrams of magnetic mixtures: Micromagnetic models and measurements, *Phys. Earth Planet. Inter.,* **154,** 308–322.

Cichocki, A., Amari, S., Zdunek, R., Kompass, R., Hori, G. & He, Z., 2006. Extended smart algorithms for non-negative matrix factorization, in *Artificial Intelligence and Soft Computing - ICAISC 2006*, Lecture Notes in Artificial Intelligence.

Cichocki, A., Zdunek, R. & Amari, S., 2006. Csiszar's divergences for non-negative matrix factorization: Family of new algorithms, *Independent component analysis and blind signal separation, Proceedings lecture notes in computer science,* **3889,** 32–39.

Day, R., Fuller, M. & Schmidt, V.A., 1977. Hysteresis properties of titanomagnetites: grain size and compositional dependence, *Phys. Earth Planet. Inter.,* **13,** 260–267.

de Boor, C., 1994. *A practical guide to splines*, Springer Verlag.

Dillon, M. & Bleil, U., 2006. Rock magnetic signatures in diagenetically altered sediments from the Niger deep-sea fan, *J. Geophys. Res.,* **111,** B03105.

Dunlop, D.J., 2002. Theory and application of the Day plot (Mrs/Ms versus Hcr/Hc) 1. Theoretical curves and tests using titanomagnetite data, *J. Geophys. Res.,* **107,** doi:10.1029/2001JB000486.

Dunlop, D.J. & Özdemir, Ö., 1997. *Rock magnetism: fundamentals and frontiers*, Cambridge University Press, Cambridge; UK.

Egli, R., 2003. Analysis of the field dependence of remanent magnetization curves, *J. Geophys. Res.,* **108**(B2), 2081.

Egli, R., 2004a. Characterization of individual rock magnetic components by analysis of remanence curves. 2. Fundamental properties of coercivity distributions, *Phys. Chem. Earth,* **29,** 851–867.

Egli, R., 2004b. Characterization of individual rock magnetic components by analysis of remanence curves, 1. Unmixing natural sediments, *Studia geoph. et geod.,* **48,** 391–446.

Eyre, J.K., 1996. The application of high resolution IRM acquisition to the discrimination of remenance carriers in Chinese loess, *Studia geoph. et geod.,* **40,** 234–242.

Fabian, K., 2003. Some additional parameters to estimate domain state from isothermal magnetization measurements, *Phys. Earth Planet. Inter.,* **213,** 337–345.

Fabian, K., 2006. Approach to saturation analysis of hysteresis measurements in rock magnetism and evidence for stress dominated magnetic anisotropy in yound mid-ocean ridge basalt, *Phys. Earth Planet. Inter.,* **154,** 299–307.

Frank, U., 2007. Rock magnetic studies on sediments from Erlongwan maar lake, Long Gang Volcanic Field, Jilin province, NE China, *Geophys. J. Int.,* **168,** 13–26.

Frank, U., Schwab, M.J. & Negendank, J.F.W., 2003. Results of rock magnetic investigations and relative paleointensity determinations on lacustrine sediments from Birkat Ram, Golan Heights (Israel), *J. Geophys. Res.,* **108**(B8), 2379.

Garming, J.F.L., Bleil, U. & Riedinger, N., 2005. Alteration of magnetic mineralogy at the sulphate–methane transition: Analysis of sediments

from the Argentine continental slope, *Phys. Earth Planet. Inter.,* **151,** 290–308.

Gee, J. & Kent, D.V., 1995. Magnetic hysteresis in Young midocean ridge basalts: dominant cubic anisotropy?, *Geophys. Res. Lett.,* **22,** 551–554.

Gee, J. & Kent, D.V., 1999. Calibration of magnetic granulometric trends in oceanic basalts, *Phys. Earth Planet. Inter.,* **170,** 377–390.

Heslop, D., Dekkers, M.J., Kruiver, P.P. & van Oorschot, I.H.M., 2002. Analysis of isothermal remanent magnetization acquisition curves using the expectation-maximization algorithm, *Geophys. J. Int.,* **148,** 58–64.

Heslop, D., McIntosh, G. & Dekkers, M.J., 2004. Using time and temperature dependant Preisach models to investigate the limitations of modelling isothermal remanent magnetisation curves with cumulative log Gaussian functions, *Geophys. J. Int.,* **157,** 55–63.

Heslop, D., Witt, A., Kleiner, T. & Fabian, K., 2006. The role of magnetostatic interactions in sediment suspensions, *Geophys. J. Int.,* **165,** 775–785.

Heuer, V., 2003. Spurenelemente in Sedimenten des Südatlantik: Primärer Eintrag und frühdiagenetische Überprägung, Tech. Rep. 209, Univ. Bremen, Bremen, Germany.

Hoyer, P.O., 2004. Non-negative matrix factorization with sparseness constraints, *J. Mach. Learn. Res.,* **1457,** 1457–1469.

Kent, D.V. & Gee, J., 1994. Grain size dependent alteration and the magnetization of oceanic basalts, *Science,* **265,** 1561–1563.

Kruiver, P.P. & Passier, H.F., 2001. Coercivity analysis of magnetic phases in sapropel S1 related to variations in redox conditions, including an investigation of the S-ratio., *Geophys. Geochem. Geosyst.,* **2,** doi:10.1029/2001GC000181.

Kruiver, P.P., Dekkers, M.J. & Heslop, D., 2001. Quantification of magnetic coercivity components by the analysis of acquisition curves of isothermal remanent magnetization, *Earth Planet. Sci. Lett.,* **189,** 269–276.

Langville, A.N., Meyer, C.D. & Albright, R., 2006. Initializations for the nonnegative matrix factorization, in *Proceedings of the Twelfth ACM SIGKDD International Conference on Knowledge Discovery and Data Mining*.

Lee, D.D. & Seung, H.S., 2001. Algorithms for non-negative matrix factorization, *Adv. Neural Inform. Process. Syst.,* **13,** 556–562.

Lees, J.A., 1997. Mineral magnetic properties of mixtures of environmental and synthetic materials: linear additivity and interaction effects, *Geophys. J. Int.,* **131,** 335–346.

Muxworthy, A.R., Williams, W. & Virdee, D., 2003. Effect of magnetostatic interactions on the hysteresis parameters of single-domain and pseudo-single-domain grains, *J. Geophys. Res.,* **108,** doi:10.1029/2003JB002588.

Muxworthy, A.R., Heslop, D. & Williams, W., 2004. Influence of magnetostatic interactions on first-order reversal curve (FORC) diagrams: a micromagnetic approach, *Geophys. J. Int.,* **158,** 888–897.

Muxworthy, A.R., King, J.G. & Odling, N., 2006. Magnetic hysteresis properties of interacting and non-interacting micron-sized magnetite produced by electron-beam lithography, *Geophys. Geochem. Geosyst.,* **7**.

Pauca, V.P., Piper, J. & Plemmons, R.J., 2006. Non-negative matrix factorization for spectral data analysis, *Lin. Algebra Appl.,* **416,** 29–47.

Peters, C. & Turner, G., 1999. Lake Paringa: a catchment study using magnetic techniques, *Phys. Chem. Earth,* **24,** 753–757.

Pick, T. & Tauxe, L., 1994. Characteristics of magnetite in submarine basaltic glass, *Geophys. J. Int.,* **119,** 116–128.

Roberts, A.P. & Turner, G.M., 1993. Diagenetic formation of ferrimagnetic iron sulphide minerals in rapidly deposited marine sediments, South Island, New Zealand, *Earth Planet. Sci. Lett.,* **115,** 257–273.

Robertson, D.J. & France, D.E., 1994. Discrimination of remanence carrying minerals in mixtures, using isothermal remanent magnetization aquisition curves, *Phys. Earth Planet. Inter.,* **82,** 223–234.

Shankar, R., Thompson, R. & Galloway, R.B., 1994. Sediment source modelling: Unmixing of artifical magnetization and natural radioactivity measurements, *Earth Planet. Sci. Lett.,* **126,** 411–420.

Smirnov, A.V. & Tarduno, J.A., 2000. Low-temperature magnetic properties of pelagic sediments (Ocean Drilling Program Site 805C): Tracers of maghemitization and magnetic mineral reduction, *J. Geophys. Res.,* **105,** 16457–16471.

Snowball, I.F. & Torii, M., 1999. *Quaternary Climates and Magnetism*, chap. Incidence and significance of ferrimagnetic iron sulphides in Quaternary studies, pp. 199–230, Cambridge University Press.

Spassov, S., Heller, F., Kretzschmar, R., Evans, M.E. & Nourgaliev, L.P.Y. D.K., 2003. Detrital and pedogenic magnetic mineral phases in the loess/palaeosol sequence at Lingtai (Central Chinese Loess Plateau), *Phys. Earth Planet. Inter.,* **140,** 255–275.

Spassov, S., Egli, R., Heller, F., Nourgaliev, D.K. & Hannam, J., 2004. Magnetic quantification of urban pollution sources in atmospheric particulate matter, *Geophys. J. Int.,* **159,** 555–564.

Stockhausen, H., 1998. Some new aspects for the modelling of isothermal remanent magnetization acquisition curves by cumulative log Gaussian functions, *Geophys. Res. Lett.,* **25,** 2217–2220.

Stoner, E.C. & Wohlfarth, E.P., 1948. A mechanism of magnetic hysteresis in heterogeneous alloys, *Phil. Trans. Roy. Soc.,* **240,** 599–642.

Thompson, R., 1986. Modelling magnetization data using SIMPLEX, *Phys. Earth Planet. Inter.,* **42,** 113–127.

van Oorschot, I.H.M., Dekkers, M.J. & Havlicek, P., 2002. Selective dissolution of magnetic iron oxides with the acid-ammonium-oxalate/ferrous-iron extraction technique - II. Natural loess and palaeosol samples, *Geophys. J. Int.,* **149,** 106–117.

Wild, S., Curry, J. & Dougherty, A., 2003. Motivating non-negative matrix factorizations, in *Proceedings of the eighth SIAM conference on applied linear algebra*.

Zabel, M., Schneider, R.R., Wagner, T., Adegbie, A.T., de Vries, U. & Kolonic, S., 2001. Late Quaternary climate changes in central Africa as inferred from terrigenous input to the Niger Fan, *Quat. Res.,* **56,** 207–217.

Zdunek, R. & Cichocki, A., 2006. Non-negative matrix factorization with quasi-Newton optimization, in *Artificial Intelligence and Soft Computing - ICAISC 2006*, Lecture Notes in Artificial Intelligence.

Zhou, W., van der Voo, R. & Peacor, D.R., 1997. Single-domain and superparamagnetic titanomagnetite with variable Ti content in young ocean-floor basalts: No evidence for rapid alteration, *Earth Planet. Sci. Lett.,* **150,** 353–362.

Zhou, W., van der Voo, R., Peacor, D.R. & Zhang, Y., 2000. Variable Ti-content and grain size of titanomagnetite as a function of cooling rate in very young MORB, *Earth Planet. Sci. Lett.,* **179,** 9–20.

Diagenetic alteration of natural Fe-Ti oxides identified by energy dispersive spectroscopy and low-temperature magnetic remanence and hysteresis measurements

Abstract

Low-temperature (LT) magnetic remanence and hysteresis measurements, in the range 300 to 5 K, were combined with energy dispersive spectroscopy (EDS) in order to characterize the magnetic inventory of strongly diagenetically altered sediments originating from the Niger deep-sea fan. On a set of five representative samples, two from the upper suboxic and three from the lower sulfidic anoxic zone, the possibility of distinguishing between different compositions of titanomagnetite and titanohematite is demonstrated. Highly sensitive LT magnetic measurements were performed on magnetic extracts resulting in large differences in the magnetic behavior between samples from the suboxic and anoxic layers, respectively. This emphasizes that both Fe-Ti oxide phases occur in different proportions in the two geochemical environments. Most prominent are the variations in the coercive field B_C. At room-temperature (RT) hysteresis loops for all extracts are narrow and yield low coercivities (6 - 13 mT). With decreasing temperature the loops become more pronounced and wider. At 5 K an approximately 5-fold increase in B_C for the suboxic samples contrasts a 20- to 25-fold increase for the samples from the anoxic zone. We demonstrate that this distinct increase in B_C at LT corresponds to the increasing proportion of the Ti-rich titanohematite phase, while Fe-rich (titano-)magnetite dominates the magnetic signal at RT. This trend is also seen in the room-temperature saturation isothermal remanent magnetization (RT-SIRM) cycles: suboxic samples show remanence curves dominated by Fe-rich mineral phases while anoxic samples clearly exhibit respective curves dominated by Ti-rich particles. We show that the EDS intensity ratios of the characteristic Fe K_α and Ti K_α lines of the Fe-Ti oxides may be used to differentiate between members of the magnetite-ulvöspinel and ilmenite-hematite solid solution series. Furthermore it is possible to calculate an approximate composition for each grain if the intensity ratios of natural particles are linked to well known standards. Thus, element spectra with high Fe/Ti intensity ratios were found to be rather typical for titanomagnetite while low Fe/Ti ratios are indicative for titanohematite. The EDS analyses confirm the LT magnetic results, Fe-rich magnetic phases dominate in the upper suboxic environment whereas Ti-rich magnetic phases comprise the majority of particles in the lower anoxic domain: The mineral assemblage of the upper suboxic environments is composed of magnetite (~19 %), titanomagnetite (~62 %), titanohematite (~17 %) and ~2 % other particles. In the lower anoxic sediments, reductive alteration has resulted in more extensive depletion of (titano-)magnetite phases, resulting in a relative enrichment of the titanohematite phase (~66 %). In these strongly anoxic sediments stoichiometric magnetite is barely preserved and only ~5 % titanomagnetite was detected. The remaining ~28 % comprises Ti-rich particles such as pseudobrookite or rutile.

Keywords: magnetic Fe-Ti oxides, energy dispersive spectroscopy (EDS), marine sediments, scanning electron microscopy (SEM), low-temperature magnetism, early diagenesis.

This chapter is an article in review: Dillon, M. and Franke, C., 2008, Diagenetic alteration of natural Fe-Ti oxides identified by energy dispersive spectroscopy and low-temperature magnetic remanence and hysteresis measurements, *Phys. Earth Planet Int*.

1. Introduction

A detailed rock magnetic study of diagenetically altered sediments from the Niger deep-sea fan (GeoB 4901-8) was reported recently by *Dillon and Bleil* (2006). Room-temperature hysteresis, IRM, ARM, high- and low-temperature data were combined to provide a comprehensive interpretation of the magnetic assemblage and its modification by a variety of diagenetic processes. The authors suggested that the vast majority of the magnetic assemblage reaching the core location was composed of eroded volcanic material originating from the Cameroon Volcanic Line. The volcanic assemblage was considered to be of variable composition, containing Ti-poor and Ti-rich titanomagnetites and titanohematites (*Herrero-Bervera et al.*, 2004, *Ubangoh et al*., 2005).

At gravity core location GeoB 4901 (02°40.7'N / 06°43.2'E, 2184 m water depth, Schulz et al., 1998; Fig. 1) the degradation of organic matter results in a specific redox zonation of the sediment column, with only the upper 10 cm being oxic. Suboxic conditions are characterized by dissolved manganese in the pore water and are established down to 12.50 m. Anoxic conditions prevail below this level where anaerobic oxidation of methane results in free H_2S in the pore water (*Heuer*, 2003). In this distinct redox zonation the magnetic iron oxide mineral inventory undergoes a two-stage diagenetic alteration. The modern iron redox boundary (~2.95 m) is characterized by a drastic decline in magnetic mineral content, a coarsening of the grain size spectrum, and a reduction in coercivity. Such reductive diagenesis in the suboxic zone is a common and frequently studied phenomenon in organic rich marine sediments (e.g. *Karlin and Levi*, 1985; *Canfield and Berner*, 1987). Below the second diagenetic horizon, the suboxic / sulfidic anoxic transition (~12.50 m), a further but less pronounced decrease in magnetic concentration and grain size occurs. The contribution of finer magnetic particles and the proportion of higher coercive magnetic constituents substantially increase in the anoxic environment (*Dillon and Bleil*, 2006).

Diagenetic alteration of the primary detrital mineral inventory was found to be dependent on both, particle size and Ti-content, with the smallest particles dissolving first and the Ti-rich component being most resistant to the reducing conditions. Possible candidates for preservation are titanomagnetite ($Fe_{3-x}Ti_xO_4$) and titanohematite ($Fe_{2-y}Ti_yO_4$) with compositions of $x > 0.75$ and $y > 0.75$. Both mineral phases with Ti-contents > 0.75 are paramagnetic at ambient temperatures and exhibit high magnetic stabilities at low-temperature (*Bozorth et al*., 1957; *Schmidbauer and Readman*, 1982; *Ishikawa et al.,* 1985). Nevertheless, a definite distinction between the two mineral phases remained unresolved. Titanomagnetites with such compositions are rather uncommon as natural compounds, it appears more conceivable that Fe-Ti oxides of $y > 0.75$ constitutes titanohematite.

The role of titanohematite in a magnetic mineral assemblage is often disregarded, although members of this solid solution series exist in a large range of compositions and are frequent constituents of many types of rocks. However, the presence of (titano-)magnetite usually masks the signature of titanohematite when both are present in a sample because the saturation moment of magnetite is at least three times greater than that of titanohematite ($y = 0.63$) at room temperature (*Nord and Lawson*, 1989).

At room temperature titanohematites are either para-, ferri-, or antiferromagnetic, depending on their individual cation ordering and spin structure (e.g. *McEnroe et al.*, 2000). Titanohematites with compositions of $0 < y < 0.5$ are antiferromagnetic at room temperature and their magnetic moments are aligned as in hematite (*Warner et al*., 1972).

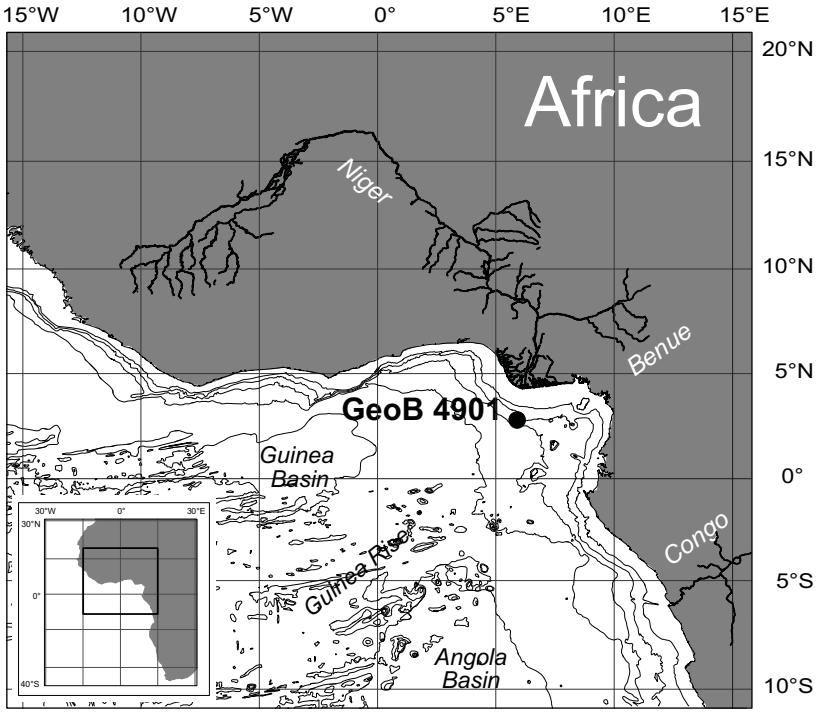

Fig. 1 Location of sediment coring site GeoB 4901 in 2184 m water depth on the southeastern flank of the Niger deep-sea fan (02°40.7'N / 06°43.2'E). Isobaths are shown at 1000 m intervals according to *Intergovernmental Oceanographic Commission* (1994).

Ferrimagnetic ordering occurs for intermediate compositions ($0.5 < y < 0.75$) and is related to the ordering of Fe and Ti on separate sublattices (*Ishikawa*, 1985). Compositions with $y > 0.75$ are paramagnetic at room temperature, but magnetic ordering does occur at lower temperatures, e.g. the end-member ilmenite is antiferromagnetic below its Néel temperature of ~63 K (*Lagroix et al*., 2004).

This study has two aims: first to identify low-temperature remanence and hysteresis characteristics that help discriminate between members of the magnetite-ulvöspinel and ilmenite-hematite solid solution series and which will expand the low-temperature database for such natural samples. Second, by demonstrating the compositional changes of the magnetic mineral assemblage during progressive sub- and anoxic diagenesis, the applied low-temperature magnetic measurements give insight into the environmental implications for the core retrieved from the Niger deep-sea fan. The magnetic results are linked to findings of SEM energy dispersive spectroscopy analyses. In particular, the intensity ratios of the characteristic Fe K_α and Ti K_α lines are used to differentiate between the mineral phases of the magnetite-ulvöspinel and ilmenite-hematite solid solution series.

2. Materials and methods

The magnetic extraction method of *Petersen et al*. (1986) was applied to obtain magnetic concentrates for five representative samples along the depth profile of the gravity core from (a) the upper suboxic sediments above the Fe-redox boundary (1.65 m), (b) the upper suboxic sediments below the Fe-redox boundary (2.95 m), and (c) to (e) from the anoxic sulfidic sediments (13.25, 14.55 and 15.25 m; Fig. 2). Mass determination is not practical here, since the typical amount for these magnetic extracts is below the precision of a microbalance ($d = 10^{-5}$ g). The sample from 1.65 m depth represents the zone where diagenetic

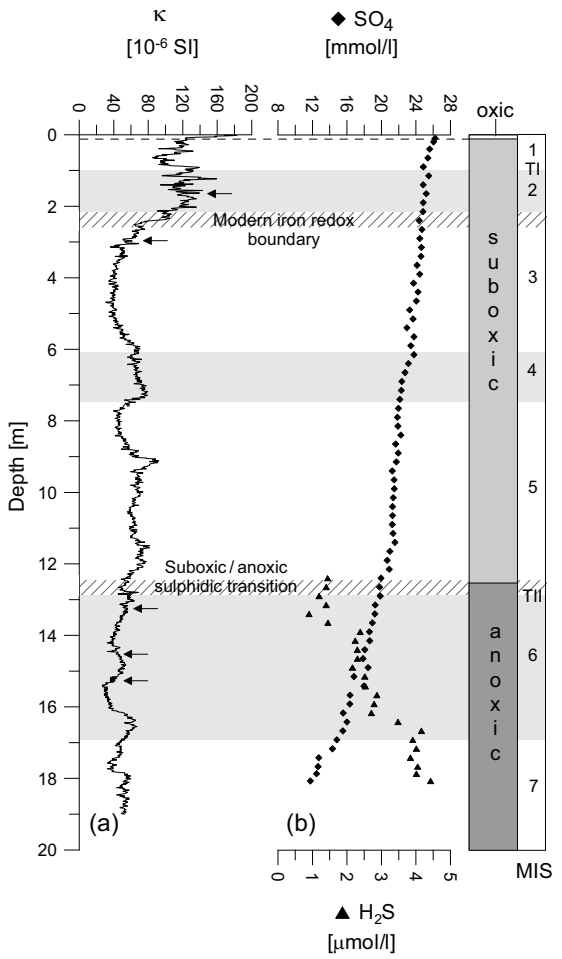

Fig. 2 (a) Depth profile of the volume specific bulk susceptibility κ delineating variations in the concentration of magnetic minerals. (b) Pore water chemistry at Site GeoB 4901 (*Heuer*, 2003). All parameters are plotted against a linear depth scale and a non-linear age scale (*Adegbie*, 2001) including marine oxygen isotope stages (MIS) and terminations (T). Grey shading indicates cold periods. Horizontal hatched bars mark the modern iron redox boundary (~2.85 m) and the suboxic / sulfidic anoxic transition (~12.5 m). Arrows at the κ profile denote the horizons, where detailed magnetic analyses have been performed.

influences are minimal and hence characterizes the primary magnetic mineralogy. The main interest of sampling at 2.95 m was to detect the existence of biogenic magnetite, which possibly formed around the modern Fe-redox boundary (*Hilgenfeldt*, 2000). Samples between 13.25 m and 15.25 m were selected to characterize the magnetic mineral assemblage in the anoxic sediments (Fig. 2).

2.1. Scanning electron microscopy

SEM analysis included back scatter electron (BSE) imaging (*Lloyd*, 1985) performed on the magnetic extracts of selected unconsolidated samples from 1.65, 14.55 and 15.25 m depth, using a *FEI XL30 SFEG* scanning electron microscope at the EMU (Electron Microscopy Utrecht, The Netherlands). The SEM was operated at an acceleration voltage between 12 and 30 kV with a ~2 nA beam current. Sample preparation for SEM analysis was carried out as described in *Franke* (2006). The elemental composition was acquired using energy X-ray dispersive spectroscopy (EDS; *Goldstein et al*., 1992). The obtained element spectra were (semi-) quantified using the 'Remote SEM Quant Phiroz' program version 3.4. All element spectra are normalized to the height of their oxygen peak. Background noise was subtracted before calculation of the element composition. The SEM analyses are restricted to the resolvable µm-particle fraction of the extracts and EDS was performed for about 40 to 50 particles per sample. The upper suboxic environment is represented by the sample from 1.65 m depth. Samples from 14.55 m and 15.25 m depth represent the anoxic zone. In the following the SEM results of the two samples from 14.55 m and 15.25 m depth are combined and will be referred to as anoxic samples.

2.2. Low-temperature magnetic measurements

Low-temperature magnetic measurements were performed on a superconducting *Quantum Design Magnetic Property Measurement System* (MPMS), with an instrumental noise level of ~10^{-11} Am^2. Two types of low-temperature measurements were performed in this study: (1) Saturation isothermal remanent magnetization imparted at room temperature (RT-SIRM), applying a

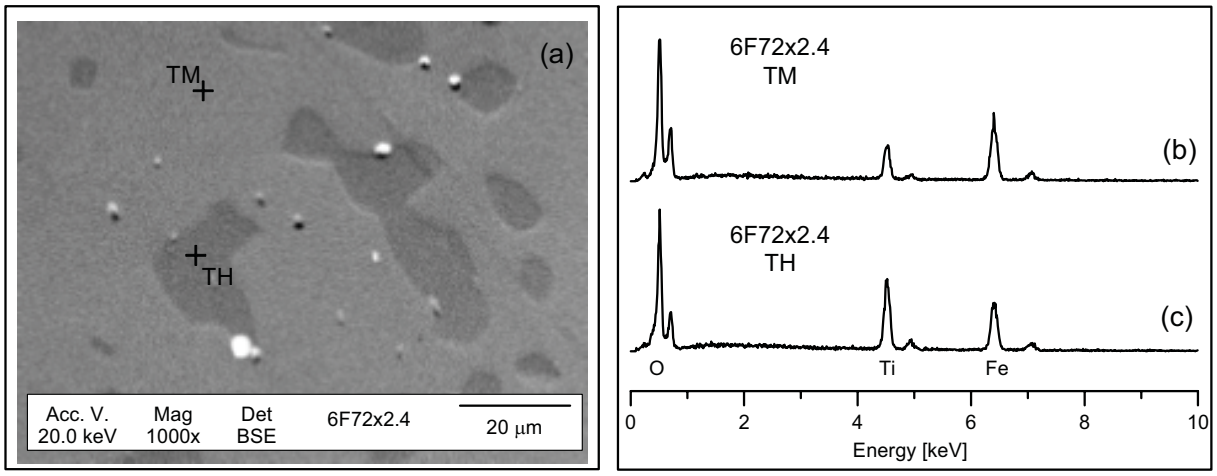

Fig. 3 (a) Backscattered electron micrograph of synthetic sample 6F72x2.4, light grey areas correspond to TM63 (Fe-richer) and darker grey areas correspond to TH76 (Fe-poorer). (b) EDS spectrum of the TM63 phase from the spot marked in (a). (c) EDS spectrum of the TH76 phase from the spot marked in (a).

maximum field of 5 T at 300 K followed by continuous cooling in zero field to 5 K and subsequent continuous warming back to 300 K. (2) Hysteresis loops measured between magnetic peak fields of ± 5 T at 15 distinct temperatures between 5 and 295 K. From these loops the temperature dependence of the standard hysteresis parameters such as saturation magnetization (M_S), saturation remanent magnetization (M_{RS}) and coercive force B_C were determined.

3. Scanning electron microscopic results

3.1. Discrimination between titanomagnetite and titanohematite

Studies such as *Franke et al*. (2007a) and *Lattard et al*. (2005) have shown that the EDS intensity ratios of the characteristic Fe K_α and Ti K_α lines can be used under certain conditions to differentiate between mineral phases of the magnetite-ulvöspinel and ilmenite-hematite solid solution series. Element spectra with high Fe/Ti intensity ratios were found to be rather typical for titanomagnetite while low Fe/Ti ratios are indicative of titanohematite. With increasing Ti-content the Fe/Ti ratio decreases for both solid solution series, the lowest possible value is Fe/Ti = 2 for the magnetite-ulvöspinel solid solution series and Fe/Ti = 1 for the ilmenite-hematite solid solution series according to their respective stoichiometric formulas. Therefore particles with ratios of Fe/Ti > 2 can be either titanomagnetite or -hematite, while particles with ratios of Fe/Ti < 2 can only be titanohematites.

To test this method, EDS spectra were taken from a defined synthetic sample (6F72x2.4) of known composition, which was provided by the Mineralogical Institute of the University Heidelberg. The sample was synthesized at 1300°C in the Fe-Ti-O system and contains titanomagnetite (TM63) and titanohematite (TH76). This sample can then subsequently be used as a standard to compare to the EDS peak intensities of the unconsolidated natural particles of this study. Another advantage of the synthetic sample is its ideal flat polished surface, which means that scattering errors can be neglected.

The element spectra were derived on the same SEM instrument for both, synthetic and natural samples. Fig. 3a shows a backscatter electron (BSE) micrograph of the sample 6F72x2.4. The gray tones in the BSE image reflect the different chemical compositions of the two mineral phases, with lighter areas corresponding to TM (Fe-richer) and darker areas corresponding to TH (Fe-poorer). Completely black or

white spots mark pores in the polished sample, where surface charging might have an effect due to poor carbon coating. The two mineral phases can be discriminated by their EDS element spectra (Figs. 3b and 3c), since the intensity ratios of the characteristic Fe K_α and Ti K_α lines are distinct. In Table 1 the semi-quantified Fe and Ti contents are listed for ten spot checks analysed on the polished section of the synthetic sample. The values were used to calculate the Fe/Ti ratios and the resulting titanomagnetite (TM) and titanohematite (TH) compositions. Spectra from TM (lighter area) show Fe/Ti ratios > 2, whereas spectra from TH (darker areas) have ratios Fe/Ti < 2. The average composition was calculated as TM68 and TH78. These values are slightly higher than the compositions (TM63 and TH76) derived from electron microprobe (EMP) analyses and inductively coupled plasma atomic emission spectrometry (ICP-AES) reported by *Lattard et al*. (2005; 2006). This discrepancy is presumably due to slightly inhomogeneous chemical compositions within the sample from the rim to the center of the synthesized pellet (*R. Engelmann*, pers. comm., 2006). These results underline that it is in principle possible to discriminate between titanomagnetite and titanohematite phases on the basis of the element intensity ratio Fe/Ti and hence that it is possible to calculate a close approximate composition for each particle.

3.2. Magnetic particle discrimination

Fig. 4a and 4b show the cation element content in at% for the main elements Fe and Ti and the minor abundant elements Mg and Al for all particles examined, divided into suboxic and anoxic environments. Mg and Al constitute as the most common cation impurities in natural titanomagnetites and –hematites found in igneous rocks (*Creer et al*., 1975). To consider the effect of substitution of Fe with either Mg or Al, the total of the three elements Fe, Mg and Al was calculated and will be referred to as Fe_Σ (equals to Fe+Al+Mg) in the following. The magnetic mineral assemblage of the upper suboxic environment is dominated by Fe-rich mineral phases with fairly low Ti-contents (Fig. 4a). In contrast, the Ti-content increases notably and even exceeds the Fe-content in the particles of the lower anoxic samples (Fig. 4b). In Fig. 4c and Fig. 4d representative element spectra of typical particles from the magnetic extracts are shown, originating from the upper suboxic and lower anoxic domain. These EDS analyses clearly show that the natural magnetic grains contain a minor amount of metal ions other than Fe and Ti. The

Table 1
Cation element content in at% for the elements Fe and Ti of the synthetic sample 6F72x2.4.

Sample Name	Spot		Ti [at%]	Fe [at%]	Fe/Ti	TM calculated	TH calculated
6F72x2.4	lighter area	TM	4.70	17.51	3.73	63	
6F72x2.4	darker area	TH	8.53	12.67	1.49		80
6F72x2.4	lighter area	TM	4.75	16.51	3.48	67	
6F72x2.4	darker area	TH	8.06	12.53	1.55		78
6F72x2.4	darker area	TH	7.96	12.62	1.59		77
6F72x2.4	lighter area	TM	4.83	16.25	3.36	69	
6F72x2.4	lighter area	TM	5.20	17.53	3.37	69	
6F72x2.4	lighter area	TM	5.23	18.57	3.55	66	
6F72x2.4	darker area	TH	7.96	12.73	1.60		77
6F72x2.4	lighter area	TM	4.81	17.28	3.59	65	

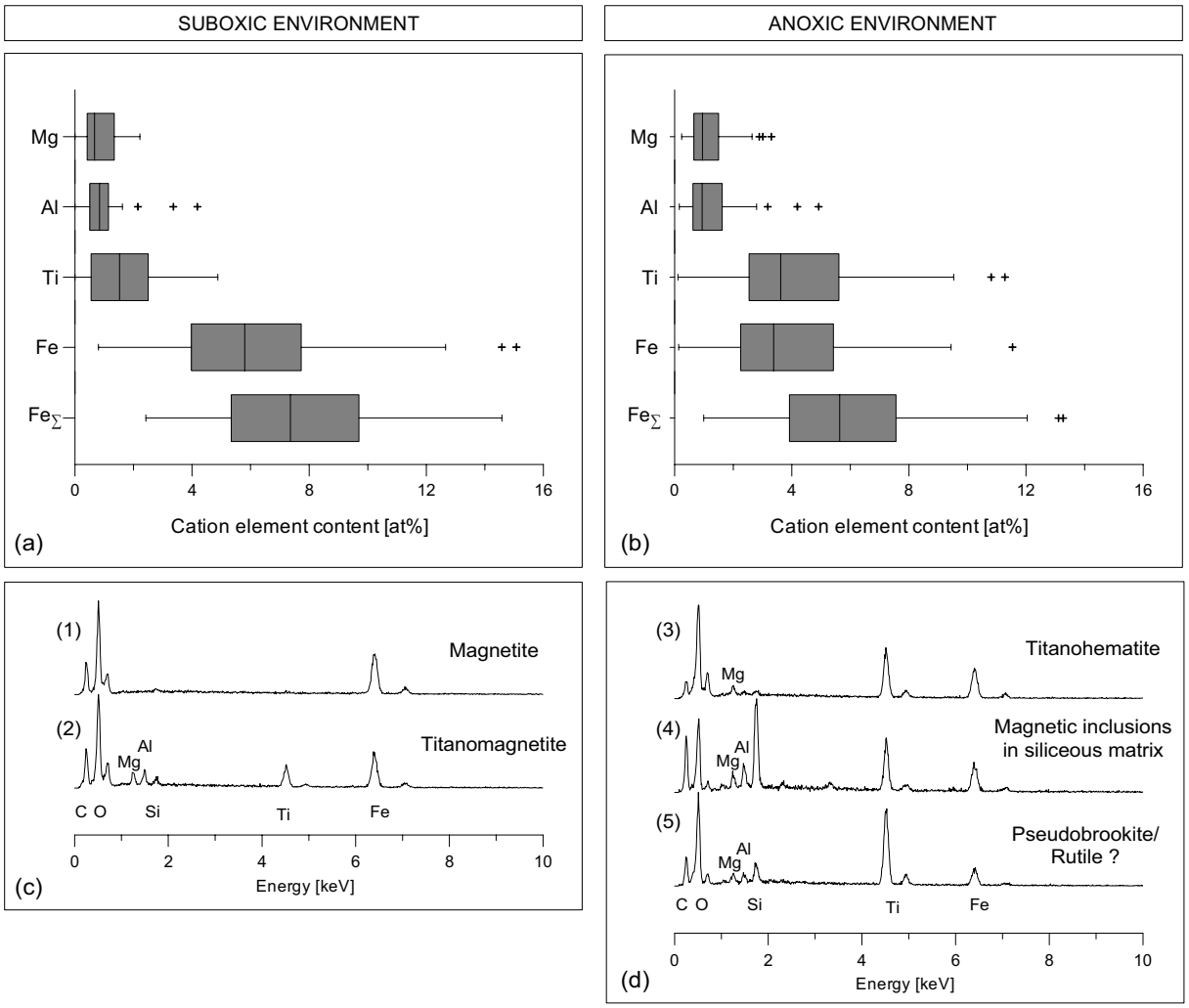

Fig. 4 Univariate box-and-whisker plots of the cation element content for the main elements Fe and Ti and minor contributions of Mg and Al of magnetic extracts from (a) the suboxic and (b) the anoxic sediments. Fe_{Σ} equals the sum of the three elements Fe, Mg and Al. The boxes represent the median values and the interquartile range, the whiskers mark the total data range. Symbols (+) display outlier samples from the respective data group. (c) and (d) show typical element spectra for particles representing the different Fe-Ti oxide phases detected in the two geochemical environments.

presence of the supplementary elements, such as Na, Mg, Al and Si support the assumption of the detrital origin of these particles. Small amounts of Al and Si are most likely also due to clay mineral coatings on the grains.

In Table 1 the element ratios of Fe_{Σ}/Ti for every analysed particle are divided into the $Fe_{\Sigma}/Ti \geq 2$, $1 \leq Fe_{\Sigma}/Ti < 2$, $0.5 \leq Fe_{\Sigma}/Ti < 1$ and $Fe_{\Sigma}/Ti < 0.5$ fractions. In the upper suboxic zone ~19% of the examined particles exhibit spectra without any Ti-content, comparable to spectrum (1) in Fig. 4c. They represent detrital magnetite, a common component in the upper suboxic core section. However, the majority of the magnetic particles contain Ti, with an element ratio Fe_{Σ}/Ti varying between 0.75 and 13.89. 79% of these particles have Fe_{Σ}/Ti ratios ≥ 2, only 2% have Fe_{Σ}/Ti ratios < 1 (Table 2). According to the semi-quantitative EDS spectra, the Ti-content for particles with $Fe_{\Sigma}/Ti \geq 2$ varies between 0.4 and 4.9 at%. This would either correspond to a titanomagnetite composition between TM20 and TM90 or a titanohematite composition between TH13 and TH60. However, titanomagnetites with $x > 0.75$

Table 2
Distribution of the Fe_{Σ}/Ti ratio for N particles examined.

	N	Fe_{Σ}/Ti *< 0.5*	Fe_{Σ}/Ti *< 1*	Fe_{Σ}/Ti *< 2*	Fe_{Σ}/Ti *≥ 2*	Ti/Fe_{Σ} *= 0*
Suboxic particles	53	-	2 %	-	79 %	19 %
Silicates	3	-	-	-	100 %	-
Anoxic particles	74	3 %	26 %	47 %	24 %	-
Silicates	12	-	8 %	-	92 %	-

are quite uncommon in nature (*Petersen and Bleil*, 1982). Instead it is more likely that such grains represent titanohematites, which would correspond to compositions between TH50 and TH60. Titanohematites of such compositions are typical for volcanogenic rocks which underwent high-temperature deuteric oxidation processes.

Additionally, magnetic inclusions in silicates were observed. They make up ~5% of the magnetic assemblage in the upper suboxic zone. The major elements in the measured spectra are Si and O, which are accompanied by Fe and Ti as minor components. Calculated element compositions for the magnetic inclusions show Fe_{Σ}/Ti ratios of ≥ 2, resulting in either TM15 to TM60 or TH9 to TH40. Such typical composites have been found in various sedimentary environments as described by e.g. *Garming et al*. (2005).

Shrinking cracks are evidence for a mild maghemitization (*Dunlop and Özdemir*, 1997), but only a small number were observed in the upper suboxic sample. This suggests that (titano-)maghemite is of low importance in these samples. In addition to the observed microparticles, a considerable number of much smaller grains in the nm-range are present in the sample from the upper suboxic zone. These grains are beyond the spatial resolution of the used SEM. This is indicative for the presence of small PSD/SD particles.

In contrast to the analyses of the suboxic sample, only tributary amounts of nm-sized particles were observed in the magnetic extracts from 14.55 and 15.25 m depth. These samples mainly consist of somewhat "coarser" grains in the grain-size range from ~2 to 5 μm. Non-magnetic particles, such as silicates and feldspars are more abundant than in the upper suboxic sample. This has to be kept in mind for the interpretation of the hysteresis data.

The average Ti-content of all particles examined is notably higher for the anoxic samples (~4.06 at%) compared to the suboxic samples (~1.61 at%) and even exceeds the meager Fe content (Fig. 4b). When taking the Mg and Al concentrations into account, the mean value of Fe_{Σ} is slightly higher than the average Ti-content. In terms of numbers of grains the Ti-rich mineral phases clearly dominate the (magnetic) mineral inventory in the lower anoxic sediments. Here the ratios Fe_{Σ}/Ti vary between 0.21 and 4.87, particles without any Ti-content were no longer observed. Only 24% of the examined grains exhibit Fe_{Σ}/Ti ratios ≥ 2. These particles would either refer to titanomagnetite compositions between TM51 and TM99 or to titanohematite compositions of TH34 to TH66. Particles with $1 \leq Fe_{\Sigma}/Ti < 2$ (47%) resemble most abundant members of the ilmenite-hematite solid solution series. Their

Ti-content varies between 0.95 and 7.04 at%, corresponding to TH68 and TH99.

Additionally, a considerable number of particles yield $Fe_{\sum}/Ti$ ratios of < 1 (26%) or even < 0.5 (3%). The element spectra for this particle type exhibit much higher Ti- than Fe-content (Fig. 3; compare spectrum (5)). This composition corresponds rather to the pseudobrookite-ferropseudobrookite (Fe_2TiO_5)-($FeTi_2O_5$) solid solution series. Pseudobrookite may be present in the detrital Fe-Ti oxide assemblage as minor constituents within titanomagnetite and –hematite grains as a result of high-temperature oxidation during the initial cooling of igneous rocks (*Reynolds and Goldhaber*, 1978; *Frost and Lindsley*, 1991). Another possibility for the genesis of such Ti-rich mineral phases is the further alteration of members of the ilmenite-hematite solid solution series towards hematite with fine rims of anatase (*Houston and Murphy*, 1962). This would enrich the elemental bulk composition of the grains in terms of their TiO_2 content.

The number of silicates with magnetic inclusions was found to be reasonably higher (14%) in the anoxic sediments than in the suboxic sample (5%). The majority of these inclusions (92%) have $Fe_{\sum}/Ti$ ratios ≥ 2 (resulting in compositions of TM9 to TM75 or TH6 to TH50, respectively), only 8% of the inclusions show $Fe_{\sum}/Ti$ ratios of < 1.

3.3. Summary of SEM results

As mentioned above, titanomagnetites with $x > 0.75$ are quite rare in nature (*Petersen and Bleil*, 1982). The range of the composition for titanohematites strongly relates to the bulk chemistry of the rock, but lies typically above $y = 0.5$ (*Petersen and Bleil*, 1973). Considering these restrictions, the approximate abundances of the various Fe-Ti oxides in the magnetic mineral assemblage of the investigated samples can be estimated (Table 3).

The mineral assemblage of the upper suboxic environment constitutes ~19% magnetite, ~62% titanomagnetite (TM20-TM70), ~17% titanohematite (TH50-TH60) and ~2% other particles. The composition of magnetic inclusions in the siliceous matrix varies between TM15 and TM60. The main magnetic mineral component in the assemblage of the lower suboxic environment is titanohematite with an abundance of ~66% and compositions varying between TH53 and TH99. Pure magnetite is no longer present and only ~5% titanomagnetite was found. The remaining ~28% comprise Ti-rich particles, such as pseudobrookite or rutile. When titanomagnetite is preserved as inclusions in a siliceous matrix it apparently withstands diagenetic alteration even in the anoxic environment.

Table 3
Relative abundances of mineral components in the upper suboxic and lower anoxic magnetic extracts.

Component	Suboxic	Anoxic
Magnetite	18.9%	0%
Titanomagnetite	62.3%	5.4%
Titanohematite	16.9%	66.2%
Others	1.9%	28.4%

4. Low-temperature magnetic results

4.1. Room-temperature SIRM (RT-SIRM)

Fig. 5 shows the RT-SIRM curves normalized to their initial value at 300 K and the respective derivatives for all analyzed samples. The samples from the suboxic zone (Fig. 5a-b) clearly show ferrimagnetic dominated curves typical of (titano-)magnetite as described by *Özdemir and Dunlop* (2003) and *Kosterov* (2003). The RT-SIRM first increases with cooling, reaching a maximum around 220 K (Fig. 5a) and 230 K (Fig. 5b). According to *Danker*s (1978) such an increase upon cooling is related to an increase in the spontaneous magnetization of titanomagnetite phases whose Curie temperature is above the temperature where the remanence is acquired. For such

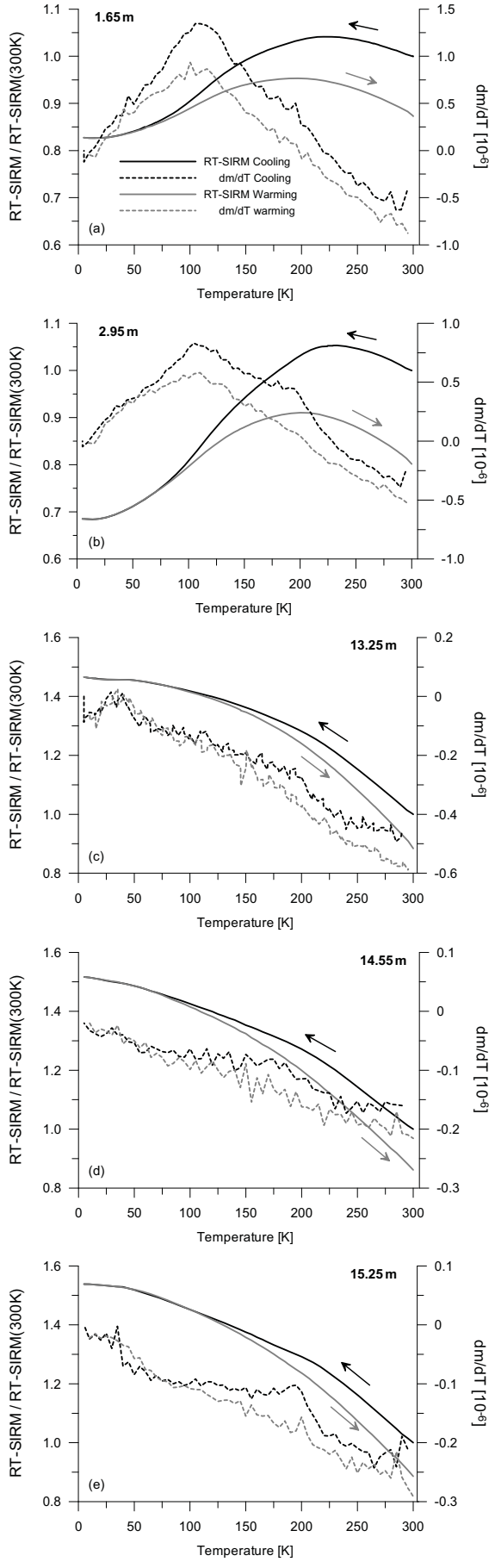

cases the spontaneous magnetization has not reached its maximum intensity at 300 K, which results in an increase upon cooling. Upon cooling further the RT-SIRM curves decrease with decreasing temperature. At 5 K some 83% (Fig. 5a) and 69% (Fig. 5b), respectively of the initial RT-SIRM is demagnetized. The maximal gradient is reached at 100 to 110 K, corresponding to the temperature interval which is indicative for the Verwey structural phase transition of magnetite. This complies with results from zero field cooling (ZFC) and field cooling (FC) thermal demagnetization curves, described by *Dillon and Bleil* (2006), which revealed partially suppressed Verwey transitions in the same temperature interval. During warming from 5 to 300 K the RT-SIRM retraces the cooling curve between 5 and 50 K. Upon further warming only limited remanence recovery is observed when passing through the Verwey transition. At 300 K about 87% (Fig. 5a) and 80% (Fig. 5b) of the initial RT-SIRM is recovered.

The RT-SIRM behavior of samples from the anoxic zone contrasts strongly the behavior of the samples from the suboxic layers. However, internally the anoxic samples (Fig. 4 c-d) reveal very similar low-temperature behaviour with comparable remanence memory. The RT-SIRM cooling curves show a continuous gradual increase between 300 and 5 K, where the RT-SIRM is 46 to 69% higher than the initial remanence. On warming the curves resemble the corresponding cooling curves back to ~ 100 K. Above 100 K the warming curves proceed below the cooling curves. The remanence loss back at 300 K is 86 to 89% compared to the initial RT-SIRM. No specific magnetic transitions were observed, though the first derivatives

Fig. 5 Temperature variation of RT-SIRM during zero field cooling from 300 to 5 K (black solid line) and zero field warming back to 300 K (grey solid line). First derivative curves of the RT-SIRM curves are shown as dashed with the proceeding color code

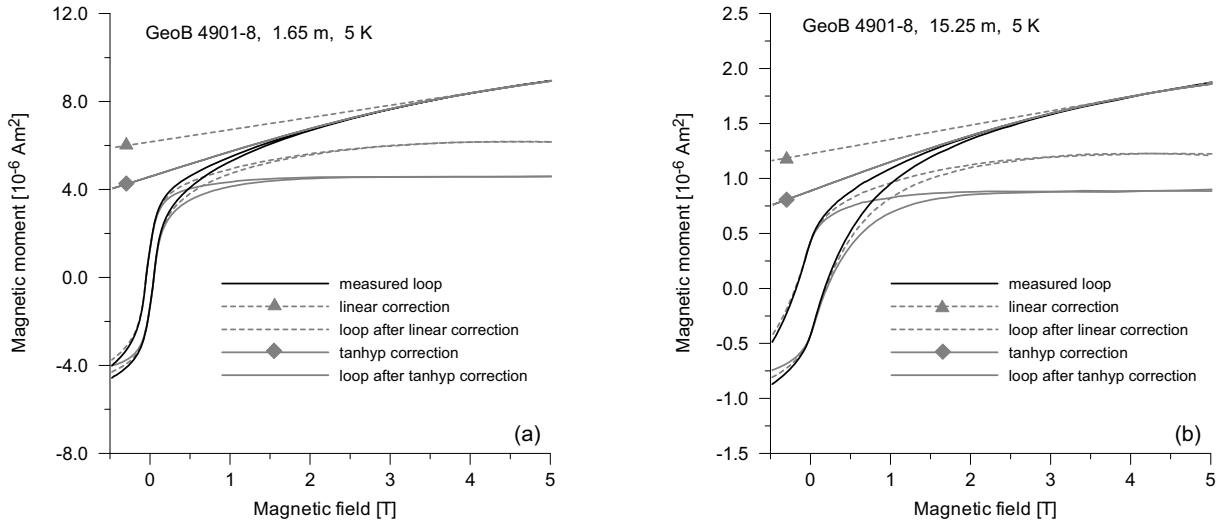

Fig. 6 Uncorrected (black solid line), linear slope corrected (grey solid line) and paramagnetic slope corrected (grey dashed line) hysteresis data shown for samples from (a) 1.65 m and (b) 15.25 m core depth measured at 5 K. Filled triangles indicate high field slope determined by least squares fit of data measured between 4 and 5 T; filled diamonds depict the paramagnetic slope derived from the equation m(B,T) = a·tanh (B/b).

of samples 13.25 and 15.25 m display an inflection around 210 K. This may be indicative of the transition of titanohematite with an approximate composition of y = 0.85 from antiferromagnetism to paramagnetism (*Garming et al*., 2007).

4.2. Low-temperature magnetic hysteresis

For all five magnetic extracts the temperature dependence of hysteresis loops was examined between 5 and 295 K. The measured hysteresis loops contain diamagnetic contributions originating from the sample holder (gelantine capsule) and non-ferromagnetic sediment constituents in the extracts such as feldspars and silicates, which to a certain extent were included in the extract. The temperature dependence of the paramagnetic contribution was calculated, using the relationship m(B,T) = a · tanh (B/b), where m(B,T) equals the measured magnetic moment in the applied field B at the temperature T, and a and b are constants (*Dunlop and Özdemir*, 1997). This approach was necessary since the induced magnetization of paramagnetic constituents begins to saturate in high fields at low-temperatures and cannot be approximated with a linear function. Using this approach, excellent fits to the magnetization curves were achieved (Fig. 6).

The results of hysteresis measurements for the suboxic and anoxic samples are largely different. To represent the suboxic and anoxic environments, the temperature evolution of the hysteresis loops is shown for the samples from 1.65 m (Fig. 7a) and 15.25 m (Fig. 7b) depth. For the sake of clarity only six selected temperature steps (295 K, 195 K, 110 K, 50 K, 20 K and 5 K) are given. The hysteresis loops systematically change in shape with decreasing temperature and increasing sediment depth. At room temperature hysteresis loops for all extracts are quite narrow and yield low coercivities. Saturation magnetization is usually reached in low to moderate fields (< 500 mT), which is indicative of the presence of a soft ferrimagnetic phase. With decreasing temperature the loops become more pronounced and wider, in particular, the samples from the anoxic zone exhibit distinct hysteresis at lower temperatures. This effect is most pronounced in the temperature dependence of B_C (Table 4).

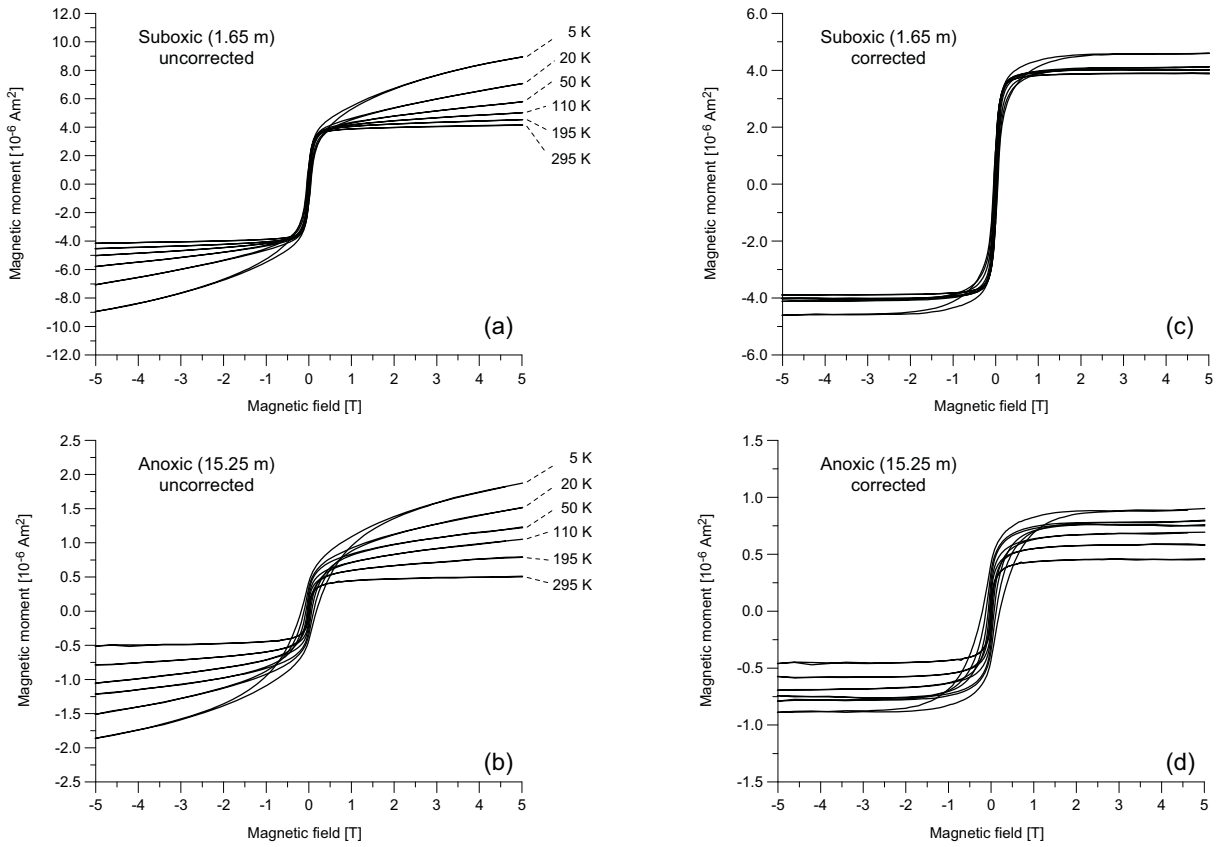

Fig. 7 Low-temperature evolution of hysteresis loops for magnetic extracts from samples of the upper suboxic (a, b) and lower anoxic (c, d) core sections. For the sake of clarity, hysteresis loops at six selected temperatures are shown, indicated by small numbers in the left side panel. Data shown on the left are uncorrected, data on the right are corrected for dia- and paramagnetic contributions.

The temperature dependence of the hysteresis properties quantified after dia- and paramagnetic correction are shown in Fig. 8. Due to the inability of mass determination, the parameters have been normalized to their respective value at 5 K in order that the samples can be compared. The absolute values are summarized in Table 4.

The saturation magnetization M_S (Fig. 8a) for the suboxic samples shows only subtle temperature variations between 295 and 30 K. Upon further cooling to 5 K an increase of about 20% is observed. In contrast a quasi-continuous increase for M_S with decreasing temperature can be seen for the anoxic samples. At 5 K the values for M_S are about a factor of two to three higher for the anoxic and 1.15 for the suboxic samples than at room temperature. However, the complexity of the paramagnetic correction may effect the accurate determination of M_S and thus the results should be treated with caution.

Saturation remanence M_{RS} (Fig. 8b) for the suboxic samples increases slightly between 295 and 50 K and even steeper below 50 K. M_{RS} seems to reach saturation at very low temperatures. However, the overall increase of two to three times is relatively small. For the anoxic samples a continuous increase with decreasing temperature is observed, with an overall seven fold increase between 295 and 5 K. At room temperature, values of B_C (Fig. 8c) range between 6 and 13 mT for all samples. *Thompson and Oldfield* (1986) report this as a typical value for multi-domain magnetite. Upon cooling, B_C varies little between 295 and 50 K. Below 50 K the coercive field starts to increase sharply, reaching values of 50 – 67 mT at 5 K for the suboxic samples and up to 140 – 233 mT for the anoxic samples. This equals a four and seven fold increase for

Table 4. Temperature-dependent values for hysteresis parameters saturation magnetization M_S, saturation remanence M_{RS} and coercive force B_C.

	1.65 m			*2.95 m*			*13.25 m*			*14.55 m*			*15.25 m*		
T [K]	M_s [10^{-6} Am^2]	M_{rs} [10^{-6} Am^2]	B_c [mT]	M_s [10^{-6} Am^2]	M_{rs} [10^{-6} Am^2]	B_c [mT]	M_s [10^{-6} Am^2]	M_{rs} [10^{-6} Am^2]	B_c [mT]	M_s [10^{-6} Am^2]	M_{rs} [10^{-6} Am^2]	B_c [mT]	M_s [10^{-6} Am^2]	M_{rs} [10^{-6} Am^2]	B_c [mT]
295	3.98	0.67	12.56	1.59	0.25	10.31	0.78	0.13	9.47	0.36	0.05	6.80	0.46	0.06	9.17
245	3.98	0.74	15.05	1.71	0.30	12.96	0.93	0.19	13.56	0.42	0.07	10.15	0.52	0.09	12.87
195	4.02	0.81	17.54	1.72	0.35	16.28	1.06	0.26	19.65	0.48	0.10	14.82	0.58	0.12	18.97
145	4.00	0.87	19.98	1.74	0.39	20.67	1.19	0.34	29.77	0.51	0.12	21.79	0.65	0.17	28.32
110	4.02	0.91	22.19	1.76	0.43	24.89	1.28	0.40	40.72	0.53	0.15	29.44	0.69	0.20	38.54
75	4.04	0.98	25.54	1.75	0.47	30.74	1.35	0.48	56.32	0.56	0.18	39.62	0.73	0.24	52.20
60	4.03	1.01	27.05	1.75	0.49	33.58	1.37	0.52	65.08	0.57	0.20	45.40	0.74	0.26	60.00
50	4.02	1.03	28.30	1.75	0.50	35.96	1.39	0.55	73.26	0.57	0.21	50.55	0.75	0.28	68.20
40	4.03	1.08	30.56	1.75	0.53	39.82	1.41	0.58	84.67	0.58	0.22	57.60	0.76	0.29	77.89
35	4.04	1.12	31.93	1.75	0.55	41.95	1.43	0.61	93.12	0.59	0.23	62.39	0.76	0.30	84.98
30	4.05	1.18	34.41	1.76	0.57	46.09	1.45	0.63	104.25	0.59	0.24	69.05	0.77	0.32	93.69
25	4.10	1.23	36.93	1.78	0.60	49.68	1.47	0.67	118.51	0.60	0.25	78.13	0.78	0.33	104.76
20	4.12	1.27	39.73	1.80	0.61	54.41	1.49	0.70	135.97	0.60	0.27	87.98	0.79	0.35	118.60
15	4.19	1.29	43.60	1.84	0.62	57.71	1.51	0.74	163.73	0.62	0.28	102.12	0.81	0.37	140.50
10	4.36	1.28	46.65	1.89	0.63	62.33	1.58	0.80	195.91	0.64	0.30	119.85	0.83	0.39	171.30
5	4.60	1.30	49.81	1.98	0.65	66.60	1.68	0.86	233.50	0.67	0.31	140.45	0.89	0.42	205.10

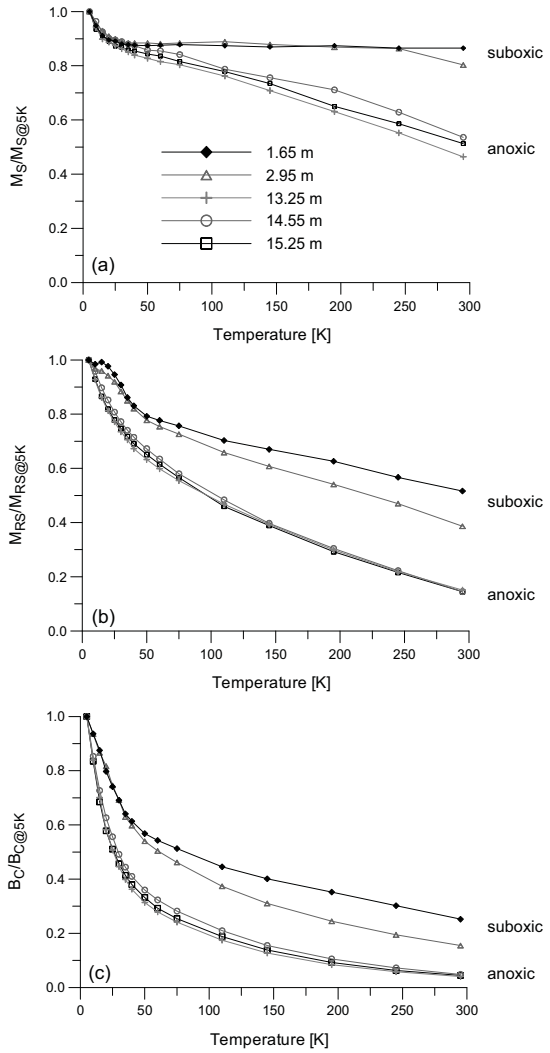

Fig. 8 Results of normalized hysteresis parameters: low-temperature dependence of (a) saturation magnetization M_S, (b) saturation remanent magnetization M_{RS}, and (c) coercive field B_C.

the suboxic samples and on average 25-fold higher coercivities for all anoxic samples. No ordering temperature could be determined from the temperature dependence of the coercivity (such as the magnetic ordering transition from antiferromagnetism to paramagnetism at 210 K for TH80, as seen before in the RT-SIRM cycling experiments, compare Fig. 5).

The hysteresis loops at certain low-temperatures exhibit a peculiar wasp-waisted shape, which is more pronounced for the anoxic than for the suboxic samples (Fig. 9). *Roberts et al*. (1995) and *Tauxe* (1996) describe this phenomenon as being indicative of a mixture of relatively high- and low-coercive material. Such a mixture could consist of either distinct magnetic minerals or a bi-modal grain-size distribution of a single magnetic component.

Large quantities of superparamagnetic magnetite or hard coercivity particles (such as hematite or goethite) are commonly assumend to be the main reason for wasp-wasited hysteresis loops. In this study these options appear implausible for several reasons: the applied extraction method tend to favor the collection of low-coercivity components (*Franke et al*. 2007b). Moreover, hematite and/or geothite must be a hundred times more abundant in the sediment to rival the magnetization of (titano-)magnetite. Secondly, the observed hysteresis loops become more constricted with decreasing temperature. Super-paramagnetic (magnetite) particles would be expected to cause constriction in the room-temperature rather than low-temperature loops because they block at lower temperatures and become stable single domain grains (*Dunlop*, 1973).

An alternative explanation for the wasp-waisted hysteresis loops at low-temperature are the observed Ti-rich titanohematites with compositions $0.85 < y < 1$. These members of the ilmenite-hematite solid solution series are paramagnetic at room-temperature but exhibit superparamagnetic properties between their spin glass freezing temperature and their Néel or Curie temperature, respectively (*Ishikawa*, 1962). The endmember ilmenite for example exhibits superparamagnetic behavior between 40 and 60 K (*Brown et al*., 1993).

5. Discussion

SEM analyses have shown, that the predominant magnetic minerals in the upper suboxic sediments are (titano-) magnetites of variable Ti composition. Titanohematites are also present, but relative to (titano-)magnetite they are

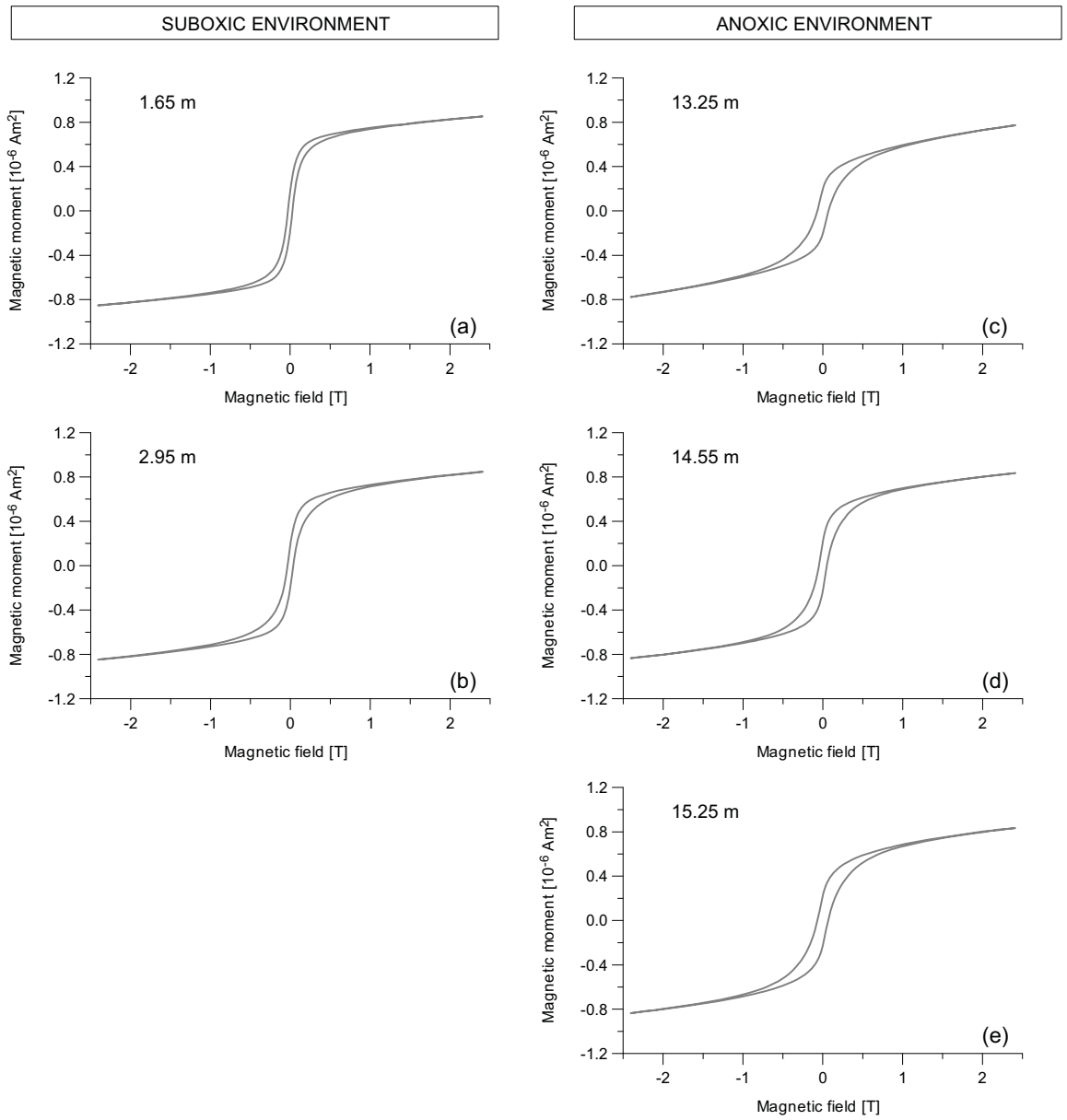

Fig. 9 Uncorrected hysteresis loops measured at 50 K; suboxic samples (a) and (b) show slightly wasp-waisted characteristics, whereas anoxic samples (c) to (e) show a distinct wasp waisted shape.

less abundant and thus less important in this depth interval. *Dillon and Bleil* (2006) already suggested that the vast majority of the magnetic assemblage reaching the core location was composed of eroded volcanic material originating from the Cameroon Volcanic Line. *Herrero-Bervera et al*. (2004) and *Ubangoh et al*. (2005) reported titanomagnetites, both poor and rich in Ti, as the principal magnetic minerals in rocks from the Cameroon volcanics in the drainage area of the Niger River tributaries. *Ubangoh et al.* (2005) also observed rocks with abundant ilmenite lamellae in the titanomagnetites. Both investigations used Curie temperature experiments above room-temperature for the discrimination of the magnetic particles. Titanohematites with high Ti-contents could not be determined by these former studies, as they may have Curie temperatures below room-temperature. Combined with our microscopy findings, which show that titanohematite is only a minor component in the primary magnetic mineral assemblage compared to (titano-) magnetite, sub-room temperature Curie

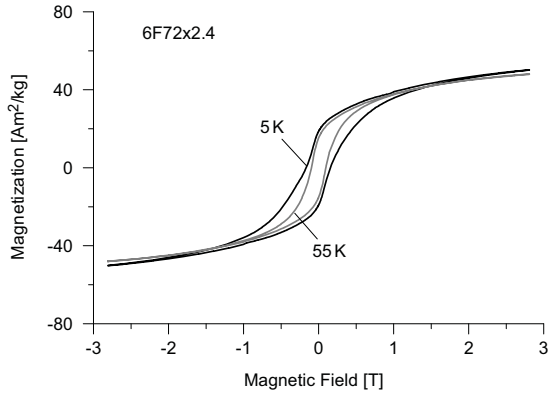

Fig. 10 Low-temperature hysteresis loops for synthetic sample 6F72x2.4 measured at 55 K (black solid line) and 5 K (grey solid line), showing slightly (55 K) and pronounced (5 K) wasp-waisted shapes (R. Engelmann et al., unpublished data).

points provide a possible explanation why titanohematite has not been identified previously. In the lower anoxic sediments the alteration has resulted in a more complete depletion of (titano-)magnetite phases, arising in a relative enrichment of the titanohematite phase in the strongly diagenetically altered section so that the relative abundance of the titanohematite particles increases to ~66%. The change in abundance can be interpreted in terms of selective diagenetic effects on the magnetic mineral assemblage. *Dillon and Bleil* (2006) reported that reductive diagenesis has extensively affected the magnetic mineral inventory of these organic-rich late Quaternary sediments in the Niger deep-sea fan. The rock magnetic investigation showed that the diagenetic processes did not act uniformly across the detrital magnetic mineral assemblage, but instead strongly depend on particle size and Ti-content, with the smallest particles dissolving first and the Ti-rich component being the most resistant to the reducing conditions.

Due to the already considerable strong alteration of the upper suboxic sediments, one of the main challenges in this study is the generally low magnetic mineral content. Therefore the concentration of magnetic carriers is even lower in the anoxic sediments and only relicts of the primary magnetic mineral assemblage remain. Highly sensitive low-temperature magnetic measurements on the magnetic extracts were therefore required. They result in large contrasts between the samples from the suboxic and anoxic layers. This emphasizes that the Fe-Ti oxide phases occur in different proportions in the two different geochemical environments, which is also reflected in the magnetic behavior of the samples.

5.1. Suboxic samples

In the upper suboxic sediments (titano-) magnetite particles dominate the low-temperature magnetic characteristics. The increase in the RT-SIRM cooling curves shortly below room-temperature and the broad decrease around 120 K were described as characteristic behavior for a (Ti-poor) titanomagnetite dominated mineral assemblage by *Özdemir and Dunlop* (2003) and *Kosterov* (2003) (Fig. 3). Additionally, the low-temperature hysteresis measurements confirm the presence of a soft ferrimagnetic mineral phase, documented in the relatively small increase in hysteresis parameters with decreasing temperature. The value of the coercive force, with an overall increase by a factor of four to seven between 300 and 5 K, is comparable with results obtained from synthetic magnetites by *Özdemir et al*. (2002). *Harrison and Putnis* (1995) analyzed the low-temperature dependence of the magnetite-spinel solid solution series and observed low coercivities (10 mT) for the magnetite-rich (Fe-rich) endmembers at low-temperatures (4.4 K). The synthetic submicron magnetites in the study of *Özdemir et al*. (2002) yield coercivities of ~15 mT at room temperature and ~50 mT at 15 K, which equals a similar increase in B_C by a factor of three to four. The coercivity for the synthetic samples increases sharply when crossing the Verwey transition, since they show compositions close to stoichiometry. The lack of the Verwey transition in the suboxic samples of this study is

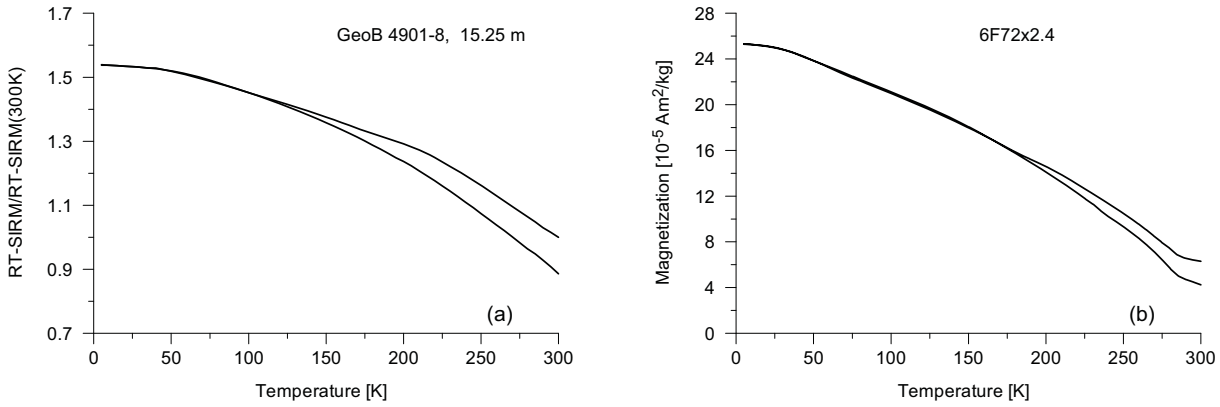

Fig. 11 Low-temperature variation of RT-SIRM for (a) the magnetic extract from 15.25 m depth and (b) the synthetic sample 6F72x2.4 (*R. Engelmann et al.*, unpublished data).

presumably due to their Ti-content, since at fairly low Ti-contents of $x > 0.04$ the transition is suppressed (*Kakol et al.*, 1994). The small amount of observed shrinking cracks is indicative of a small degree of maghemitization, which may additionally subdue the Verwey transition. *Tucker* (1981) reported low-temperature magnetic hysteresis properties for two multi domain titanomagnetite single crystals with compositions of $x = 0.52$ and $x = 0.65$. The first titanomagnetite ($x = 0.52$) shows values for B_C (~25 mT) and M_{RS}/M_S (0.29) at 77 K which are comparable with our results at 75 K of $B_C = 25$ mT and a M_{RS}/M_S ratio of 0.25. When calculating the average titanomagnetite composition for our suboxic mineral assemblage, its value of TM55 is very close to the composition of the respective single crystal of *Tucker* (1981). For the TM65 the reported values are higher ($B_C = 58$mT; $M_{RS}/M_S = 0.58$). As an explanation for the increase in coercivity the author suggested an increase in magnetic anisotropy. At even lower temperatures of 4.2 K, *Schmidbauer and Readman* (1982) observed coercivity values of comparable magnitude for titanomagnetites with compositions of $x = 0.5$ ($B_C \sim 31$ mT) and $x = 0.6$ ($B_C \sim 70$ mT).

The hysteresis loops of the suboxic samples show wasp-waisted shapes at lower temperatures. The presence of an intermediate titanomagnetite phase in paragenesis with a titanohematite phase as described by *Krása et al.* (2005) would offer a reasonable explanation for this behaviour. According to *Buddington and Lindsley* (1964) the ilmenite content of a titanohematite phase coexisting with a titanomagnetite phase with a composition of $x > 0.5$ would be $y > 0.85$. Since titanohematite phases of such composition exhibit superparamagnetic properties at low-temperatures (*Ishikawa*, 1962), it would explain the constriction which was observed in the hysteresis loops of the suboxic samples. This is also consistent with the SEM and EDS analyses, which revealed the presence of titanohematite as minor constituents (~17%) in the primary magnetic mineral assemblage of the suboxic samples.

Nevertheless, the Ti-contents derived from the SEM analysis are not overly high. However, the hysteresis loop for the synthetic sample 6F72x2.4 clearly shows wasp-waisted characteristics at temperatures ≤ 55 K (Fig. 10), even though the composition of the titanohematite phase is below $y = 0.8$. With $y = 0.76$ the titanohematite composition of 6F72x2.4 is still higher than in our natural sample, but it generally shows that wasp-waisted shapes do occur for such Ti-contents. The distribution of the two phases in the synthetic sample is comparable (79% TM : 21% TH) to the

derived distribution in our natural suboxic sample (82% Mt/TM : 17% TH). Therefore the wasp-waisted shape in the hysteresis loops here is most likely attributed to the interaction between titanomagnetite and -hematite.

5.2. Anoxic samples

The results of the low-temperature measurements from the anoxic layers lead to the conclusion, that titanomagnetite can not be the predominant magnetic mineral phase in this depth interval. Here, Ti-rich titanohematites dominate the magnetic mineral assemblage. This was also confirmed by the findings of *Heslop and Dillon* (2007), who used a non-negative matrix factorization (NMF) algorithm to unmix remanence data into constituent end-members from the same Niger deep-sea fan sediments. Based on the coercivity distribution, fine and coarse grained (titano-)magnetite was found to make the greatest contribution to the remanence signal in the upper sediments. However, a third component was needed to successfully model the detrital magnetic mineral assemblage. This third component comprised the hardest coercivity and was argued to be Ti-rich titanomagnetite or –hematite. It could be shown by the study, that below the anoxic/sulphidic transition, this Ti-rich component had the greatest resistance to reductive dissolution and dominates the magnetic mineral assemblage, whereas the coarse and fine (titano-)magnetite fraction almost disappears completely towards the base of the core.

During cooling, the RT-SIRM increases continuously with decreasing temperature. *Franke et al*. (2007b) considered two possibilities for this phenomenon, either the presence of a high-coercive mineral such as goethite or a Ti-rich oxide phase. Due to their assumption that high-coercivity minerals are generally under-represented in magnetic extracts, it appears more probable for the natural samples in this study that a Ti-rich mineral phase is responsible for the observed increase of RT-SIRM during cooling. The assumption that this behavior can be attributed to the presence of titanohematites is therefore reasonable, although the interpretation of low-temperature RT-SIRM curves from comparable natural samples is still lacking in the literature (*Kosterov*, 2007).

Fig. 11 shows a direct comparison of the low-temperature measurements of the natural sample from core GeoB 4901-8 (15.25 m; Fig. 11a) and the well defined synthetic sample 6F72x2.4 (Fig. 11b). The continuous increasing trend in the RT-SIRM curves with decreasing temperature can be seen for both samples. Since the composition of the synthetic sample is well known, goethite can be excluded as a possible reason for this low-temperature behavior. Here this phenomenon can be rather attributed to the presence of a Ti-rich mineral phase. The RT-SIRM curve of another well-defined single phase titanomagnetite of synthetic origin (TM60) (not shown here; *R. Engelmann*, unpublished data) shows a rather similar RT-SIRM curve progression as the suboxic samples of this study, with a large decrease around 190 K. This particular sample does not contain any titanohematite. Therefore we suggest that in the two-phase synthetic sample 6F72x2.4 the distinct low-temperature increase refers to the presence of a Ti-rich titanohematite phase. The magnetically harder nature of this mineral phase suggests that a higher coercitivity magnetic component than (titano-)magnetite must be present to create such a low-temperature increase in the RT-SIRM.

In particular the EDS results of the SEM analyses confirm an overall higher content of Ti-rich particles in the lower anoxic part of the sediment series. The main component here is titanohematite (~66%) with compositions between TH50 up to nearly pure ilmenite (TH99). The unusually high coercivities of the anoxic samples at low-temperatures also concur with the presence of titanohematite, rather than titanomagnetite. The stability at low-temperatures with B_C values up to 220 mT

is remarkable. For titanomagnetites such high coercivities at low-temperatures have been rarely published in the literature. *Schmidbauer and Readman* (1982) reported on coercive forces of 500 mT for synthetic titanomagnetites with a composition of x = 0.8 at 4.2 K, which is twice as high as the natural samples of our study.

Brown et al. (1993) also reported coercivity values for members of the ilmenite-hematite solid solution series. For synthetic titanohematites with compositions of y = 0.2 and y = 0.4 to 0.6 they observed values between 170 mT and 260 mT at temperatures of 125 K. They also found that samples quenched at high-temperatures have significantly higher coercivities than those annealed at temperatures below the order-disorder transition of titanohematite. *Nord and Lawson* (1992) correlate this behavior with the development of twin domain boundaries during quenching from high-temperature. According to them, annealing above the order-disorder transition temperature results in a substantial increase in twin-domain boundaries and a drastic increase in the coercivity of the material.

Gehring et al. (2007) studied micromagnetic properties of titanohematite particles originating from an alluvial soil. X-ray diffraction revealed titanohematite grains with an ilmenite mole fraction of y = 0.86. The hysteresis loops at 20 K yielded B_C = 92 mT, at 15 K reached B_C = 144 mT and at 6 K, B_C = 244 mT. These values are clearly consistent with the results of our study (compare Table 2). Here, the calculated average titanohematite composition is TH77. In metamorphic ilmenite-hematite bearing rocks from Norway stable natural remanences have been identified by *McEnroe et al*. (2001). Such natural ilmenite-hematite phases show high coercivities which are attributed to their small grain-sizes due to exsolution that results from chemical alteration (*Merrill*, 1968, *McEnroe et al*., 2001).

Besides the unusually high coercivities of the natural samples, the wasp-waisted shape of the low-temperature hysteresis loops hints at the presence of Ti-rich titanohematite phases. For the suboxic samples the wasp-waisted shape could be explained by the interaction between titanomagnetite and –hematite. In the anoxic sediments titanomagnetite is only present in very minor amounts (~5%), but wasp-waisted hysteresis loops are still observed. These are most pronounced in the temperature interval between 30 and 50 K. Apparently, another mechanism must be responsible for this phenomenon. The hysteresis loops measured by *Gehring et al.* (2007) showed typical wasp-waisted shapes at temperatures between 150 and 30 K. The behaviour also became more pronounced with decreasing temperature. They explained the wasp-waisted shape by the generation of short-range ordered areas in the superparamagnetic state within the titanohematite particles.

Titanohematites with $y \geq 0.8$ are known to exhibit superparamagnetic behavior at temperatures below 50 K (*Ishikawa et al*., 1985) and thus can account for the wasp-waisted shape of the hysteresis loops at low-temperatures. Such Ti-rich phases are rather untypical as individual homogenous grains, but more likely present as intergrown exsollution lamellae within the Ti-poor titanohematite matrix. *Dunlop and Özdemir* (1997) report that if the cooling of a melt is slow enough, titanohematites of intermediate composition tend to exsolve into intergrown Ti-poor (near hematite) and Ti-rich (near ilmenite) phases. However, compositions with $y > 0.8$ were identified in the magnetic extracts of this study. Whether they consist of either homogenous grains or of intergrown exsolved phases cannot be verified by the technique used for our unconsolidated samples. *Nord and Lawson* (1992) reported that titanohematites with $y > 0.5$ are magnetically inhomogeneous and consist of cation-ordered ferrimagnetic microstructures which are separated by boundary layers. Earlier on, *Lawson and*

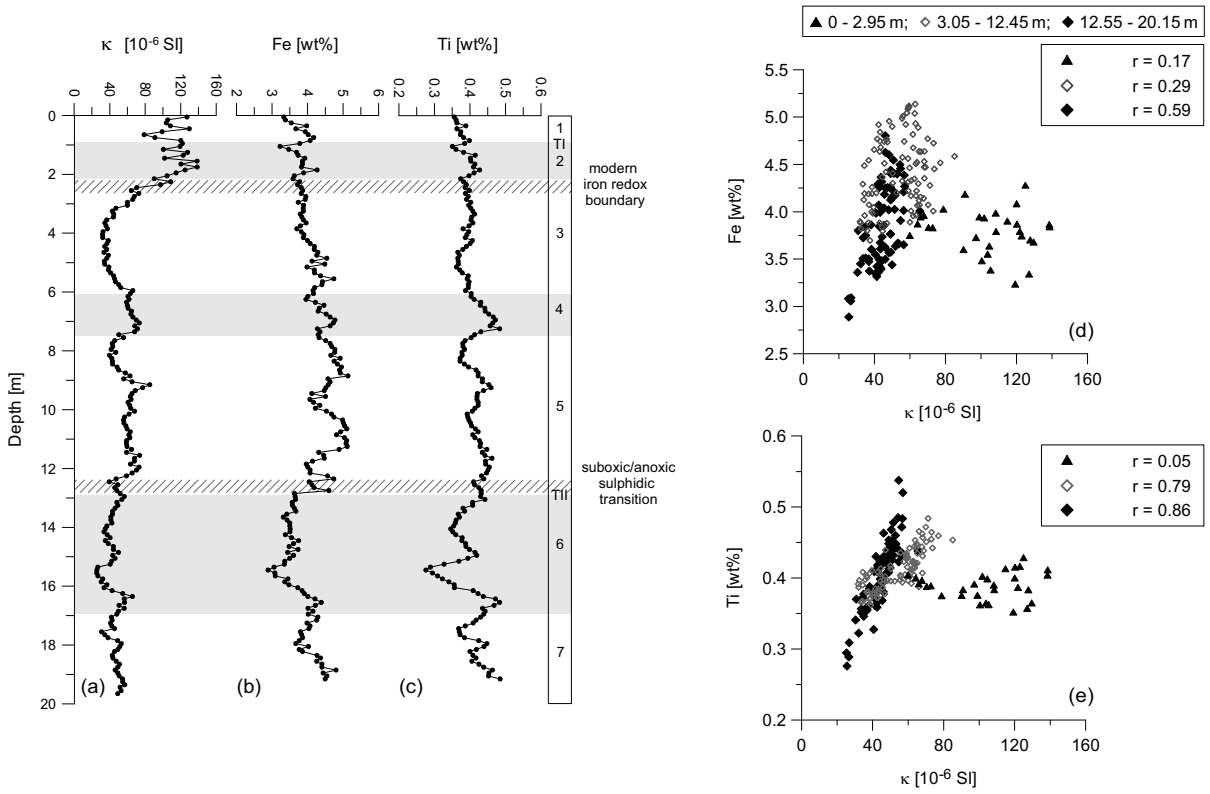

Fig. 12 (left) Downcore profiles of (a) volume magnetic susceptibility κ and solid phase concentrations of (b) Fe and (c) Ti (*Zabel et al*., 2001). All parameters are plotted on a linear depth scale and a non-linear age scale (*Adegbie*, 2001) including marine oxygen isotope stages (MIS) and terminations (TI, TII). Grey shading indicates cold periods. For further details see also Figure 2. (right) Correlation of (d) κ vs. Fe-content, and (e) κ vs. Ti-content. Symbols indicate data points for the upper three metres (black triangles), the depth interval from 3.0 m to 12.5 m (open grey diamonds) and below 12.5 m (filled black diamonds). Pearson´s correlation coefficients r are given for the respective depth intervals.

Nord (1984) showed that synthetic Ilm80-Hem20 (y = 0.8) samples had remanence properties that can be explained by the presence of a single SD-like magnetic carrier, even though Ilm80-Hem20 should be paramagnetic at room-temperature. The source of the measured remanence is argued to be SD-like material within the grains themselves, resulting from the generation of transformation induced domain boundaries, which are partly enriched in the hematite component relative to the bulk composition of the grain.

Specific low-temperature magnetic measurements can be used to differentiate between Fe and Ti dominated magnetic mineral assemblages. If Fe-rich mineral phases prevail, RT-SIRM cycles in the low-temperature range show a distinct decrease around the Néel temperature and/or Verwey transition of magnetite. For Ti-rich particles the RT-SIRM curves continuously increase with decreasing temperature. However, solely on the basis of the RT-SIRM experiments it is not possible to differentiate unambiguously between the magnetite-ulvöspinel ($Fe_{3-x}Ti_xO_4$) and ilmenite-hematite solid solution series ($Fe_{2-y}Ti_yO_3$). The hysteresis parameters reveal additional diagnostic features that can help to differentiate between Fe-rich and Ti-rich oxide mineral phases. The characteristic evolution of the measured loops with decreasing temperature points towards two distinct mineral phases in the different environments. In particular the coercive force was found to be a helpful indicative parameter, with a 25-fold increase in the

coercive force values characteristic for phases of the ilmenite-hematite solid solution series. Such high values were not found for any Fe-rich mineral phase. The high coercivities most likely result from exsolution or lamellar magnetism in titanohematite grains.

5.3. Environmental implication: correlation of Fe and Ti vs. κ

SEM and EDS analysis have clearly shown, that Fe-rich particles dominate in the upper suboxic environment, whereas Ti-rich particles prevail in the lower anoxic section. The dominance of Ti-rich magnetic particles in the lower anoxic environments is also strongly reflected in the downcore profile of the volume magnetic susceptibility κ. Fig. 12 (left) shows the downcore profiles of κ compared to the solid phase concentrations of Fe and Ti in the bulk sediments derived from ICP-EAS analysis (*Zabel et al.,* 2001).

The correlation between κ and Fe is in general clear throughout the whole depth profile, as is the correlation between κ and Ti. Only for the depth interval from the top of the core to the modern Fe redox boundary (upper three metres) is the correlation not significant. However, for this section the correlation is higher between κ and Fe ($r = 0.17$, Pearson; Fig. 12d) relative to the correlation between κ and Ti ($r = 0.05$; Fig. 12e). Below the modern Fe-redox boundary the correlation between κ and Ti is consistently higher than between κ and Fe. Not including the upper three metres, Pearson´s correlation coefficient between κ and Ti ($r = 0.70$) is noticeably higher than between κ and Fe ($r = 0.51$).

Between 3.0 and 12.5 m core depth the correlation of κ and Ti is considerably higher ($r = 0.79$) than for κ and Fe ($r = 0.29$) (Fig. 12d-e). This suggests that below the modern Fe-redox boundary the relative contribution of Ti-rich mineral phases to the magnetic susceptibility signal increases notably. The transition from suboxic to anoxic sedimentary conditions is located at 12.5 m core depth. Below this transition the highest correlation of $r = 0.86$ exists between κ and Ti. For the same depth interval the correlation also increases slightly again for κ and Fe ($r = 0.59$; Fig. 12d). Here, the iron is mainly bound to non-magnetic phases such as pyrite, which was identified in previous high-temperature thermomagnetic measurements (*Dillon and Bleil*, 2006). This concurs well with the fact that the magnetic susceptibility of titanohematites ($\chi = 100 - 100000 \cdot 10^{-8}$ m^3/kg; *Bleil und Petersen,* 1982) is at least one magnitude higher compared to the magnetic susceptibility of pyrite ($\chi = 30 \cdot 10^{-8}$ m^3/kg; *Thompson and Oldfield*, 1982).

In the uppermost core section above the modern Fe-redox boundary, the good correlation between κ and Fe implies that reactive Fe is bound in Fe-rich magnetic mineral phases. These phases dominate the magnetic mineral assemblage, both in concentration and concerning their magnetic properties. In the subsequent lower suboxic and anoxic intervals the clear correlation between κ and Ti and the less pronounced correlation between κ and Fe demonstrates that most of the Fe bound to phases that are non-magnetic at room-temperature or is present in its reduced state. Here reactive Fe was subsequently depleted, relocated and the formation of secondary Fe minerals took place. As a consequence the influence of the Ti-rich phases on the magnetic signal increases significantly. This is also reflected in the magnetic susceptibility record. Therefore we conclude that the degree of correlation between κ and Fe and κ and Ti, represents whether the magnetic assemblage is dominated rather by Fe-rich magnetic mineral phases, components of intermediate Ti-content, depleted in reactive Fe, or by Ti-rich magnetic phases, including mainly non-reactive Fe.

6. Conclusions

In this study the different magnetic components in sediments from the Niger deep-sea fan were determined in detail by a combination of low-temperature measurements with scanning electron microscopy analyses applied to magnetic extracts from various geochemical zones. The magnetic analyses indicate a fairly complex mineralogy of the primary magnetic mineral assemblage, which is dominated by (titano-)magnetite of variable composition derived from the Cameroon volcanics in the drainage area of the Niger River tributaries (*Herrero-Bervera et al.*, 2004; *Ubangoh et al.*, 2005). Above the modern redox boundary titanohematite originating from the same source area is also present. Magnetically this phase does not play such an important role here because the concentration is too low and the magnetic moment is too weak.

Nevertheless, below 3.0 m core depth, processes of reductive diagenesis start to influence the composition of the magnetic mineral assemblage. The portion of pure Fe-oxides decreases almost to zero and Ti-bearing mineral phases become more important in this depth interval. Although titanohematites are abundant, titanomagnetites are still the major contributor to the magnetic signal. Below the sulfidic transition, located in a depth of 12.5 m, grains of the ilmenite-hematite solid solution series are found to be the prevailing contributor to the magnetization of the anoxic sediments. In the course of reductive diagenesis, alteration has resulted here in a more complete depletion of titanomagnetite. (Titano-)magnetite is most likely replaced by paramagnetic iron sulphide minerals. Titanohematite is therefore much more resistant against reductive diagenesis due to its low content of reactive iron.

The study has also shown that even when remanence transitions and susceptibility peaks are not obviously apparent in low-temperature data - which is the case for most marine sediment samples - careful investigations of the data reveal important relevant information. This can be used to characterize magnetic mineral phases in a sediment sample and results therefore in a detailed paleo-environmental understanding.

Acknowledgements

The synthetic sample 6F72x2.4 and the respective unpublished data were provided by Ralf Engelmann and Dominque Lattard (University Heidelberg, Germany), the authors are grateful for their support and various discussions. We would like to thank T. Frederichs (University of Bremen, Germany) for technical assistance and annotation of the low-temperature MPMS analyses. The SEM and EDS analyses were performed at the Electron Microscopy Utrecht (Utrecht University, the Netherlands). U. Bleil is gratefully acknowledged for constructive criticism of the manuscript. This study was funded by the Deutsche Forschungsgemeinschaft (Research Centre Ocean Margins, contribution RCOMxxxx).

References

Adegbie, A.T., 2001. Reconstruction of paleoenvironmental conditions in equatorial Atlantic and the Gulf of Guinea Basins for the last 245,000 years. Berichte, Fachbereich Geowissenschaften, Universität Bremen, 178: 113 pp.

Bleil, U., and Petersen, N., 1982. Magnetic properties of minerals. In: G. Angenheister (Editor). Numerical Data and Functional Relationships in Science and Technology, Landolt-Börnstein V/1b. Springer-Verlag, Berlin, Heidelberg, 308-365.

Bozorth, R.M., Walsh, D.E., and Williams, A.J., 1957. Magnetization of ilmenite-hematite system at low temperatures. Phys. Rev., 108: 157-158.

Brown, N.E., Navratsky A., Nord Jr., G.L., and Banerjee, S.K., 1993. Hematite-ilmenite (Fe_2O_3-$FeTiO_3$) solid solutions: Determination of the Fe-Ti order from magnetic properties. Am. Mineral., 78: 941-951.

Buddington, A., and Lindsley, D., 1964. Iron-titanium oxide minerals and synthetic equivalents. J. Petrol., 5: 310–357.

Canfield, D.E., and Berner, R.A., 1987. Dissolution and pyritization of magnetite in anoxic marine sediments. Geochim. Cosmochim. Acta, 51: 645-659.

Creer, K.M., and Like, C.B., 1967. A low temperature investigation of the natural remanent magnetization of several igneous rocks. Geophys. J. R. Astr. Soc., 12: 301-312.

Dankers, P.H.M., 1978. Magnetic properties of dispersed natural iron-oxides of known grain-size. Ph.D thesis, State University of Utrecht, 142 pp.

Dillon, M., and Bleil, U., 2006. Rockmagnetic signatures in diagenetically altered sediments from the Niger deep-sea fan. J. Geophys. Res., 111, B03105, doi:10.1029/2004JB003540.

Dunlop, D.J., 1973. Superparamagnetic and single-domain threshold sizes in magnetite. J. Geophys. Res., 78: 1780-1793.

Dunlop, D.J., and Özdemir, Ö., 1997. Rock Magnetism: Fundamentals and Frontiers. Cambridge University Press, Cambridge, 573 pp.

Franke, C., 2006. Investigating lithologic characteristics of marine magnetic proxy parameters. Geologica Ultraiectina, 263, Ph.D. Thesis, Utrecht Univ., 146pp.

Franke, C., Pennock, G.M., Drury, M.R., Engelmann, R., Lattard, D., Garming, J.F.L., von Dobeneck, T., and Dekkers, M.J., 2007a. Identification of magnetic Fe-Ti oxides in marine sediments by electron backscatter diffraction in scanning electron microscopy. Geophys. J. Int., 170 (2): 545-555. doi:10.1111/j.1365-246X.2007.03410.x.

Franke, C., Frederichs, T., and Dekkers, M.J., 2007b. Efficiency of heavy liquid separation to concentrate magnetic particles. Geophys. J. Int., 170 (3): 1053-1066. doi: 10.1111/j.1365-246X.2007.03489.x.

Frost, B.R., and Lindsley, D.H., 1991. Occurrence of iron-titanium oxides in igneous rocks: Rev. Mineral., 25: 433-468.

Garming, J.F.L., Bleil, U., and Riedinger, N., 2005. Alteration of magnetic mineralogy at the sulphate-methane transition: Analysis of sediments from the Argentine continental slope. Phys. Earth Planet. Inter., 151: 290-308.

Garming, J.F.L., von Dobeneck, T., Franke, C., and Bleil, U., 2007. Low-temperature partial magnetic self-reversal in marine sediments by magnetostatic interaction of titano-magnetite and titanohematite intergrowths. Geophys. J. Int., 170 (3): 1067-1075. doi:10.1111/j.1365-246X.2007.03504.x.

Gehring, A.U., Fischer, H., Schill, E., Granwehr, J., and Luster, J., 2007. The dynamics of magnetic ordering in a natural hemo-ilmenite solid solution. Geophys. J. Int., 169 (3): 917-925. doi: 10.1111/j.1365-246X.2007.03326.x.

Goldstein, J.I., Newbury, D.E., Echlin, P., Joy, D.C., Romig Jr., A.D., Lyman, C.E., Fiori, C., and Lifshin, E., 1992. Scanning electron microscopy and X-ray microanalysis, 2nd edition. Plenum Press, New York, 820 pp.

Harrison, R.J., and Putnis, A., 1995. Magnetic properties of the magnetite-spinel solid solution: Saturation magnetization and cation distribution. Am. Mineral., 80: 213-221.

Herrero-Bervera, E., Ubangoh, R., Aka, F.T., and Valet, J.-P., 2004. Paleomagnetic and paleosecular variation study of the Mt. Cameroon volcanics (0.0-0.25 Ma), Cameroon, West Africa. Phys. Earth Planet. Int., 147: 171-182.

Heslop, D., and Dillon, M., 2007. Unmixing magnetic remanence curves without *a priori* knowledge. Geophys. J. Int., 170 (2): 556–566. doi:10.1111/j.1365-246X.2007.03432.x.

Heuer, V., 2003. Spurenelemente in Sedimenten des Südatlantik. Primärer Eintrag und frühdiagenetische Überprägung. Berichte, Fachbereich Geowissenschaften, Universität Bremen, 209: 136 pp.

Hilgenfeldt, K., 2000. Diagenetic dissolution of biogenic magnetite in surface sediments of the Beguela upwelling system. Int. J. Earth Sci., 88: 630-640.

Houston, R.S., and Murphy, J.F., 1962. Titaniferous black sandstone deposits of Wyoming. Geol. Soc. Wyoming Bull., 49: 120 pp.

Intergovernmental Oceanographic Comission, 1994. GEBCO Digital Atlas [CD-ROM]. Intergov. Oceanogr. Comm., Int. Hydrogr. Org., Birkenhead, U.K.

Ishikawa, Y., 1962. Magnetic properties of ilmenite-hematite system at low temperature. J. Phys. Soc. Jpn., 17, 1835-1844.

Ishikawa, Y., Saito, N., Arai, M., Watanabe, Y., and Takei, H., 1985. A new spin glass system of (1-x)$FeTiO_3$–Fe_2O_3. I. Magnetic Properties. J. Phys. Soc. Jpn., 54: 312-325.

Kakol. Z., Sabol, J., Kozlowski, A., and Honig, J.M., 1994. Influence of titanium doping on the magnetocrystalline anisotropy of magnetite. Phys. Rev. B, 49: 12,767-12,772.

Karlin, R., and Levi, S., 1985. Geochemical and sedimentological control of the magnetic properties of hemipelagic sediments. J. Geophys. Res., 90: 10,373-10,392.

Kosterov, A., 2003. Low-temperature magnetization and AC susceptibility of magnetite: effect of thermomagnetic history. Geophys. J. Int., 154: 58-71.

Kosterov, A., 2007. Low-temperature magnetic properties. In: D. Gubbins and E. Herrero-Bervera (Editors). Encyclopedia of Geomagnetism and Paleomagnetism, Springer, Dortrecht, The Netherlands, 515-525.

Krása, D., Shcherbakov, V.P., Kunzmann, T., and Petersen, N., 2005. Self-reversal of remanent magnetization in basalts due to partially oxidized titanomagnetites. Geophys. J. Int., 162: 115–136.

Lagroix, F., Banerjee, S.K., and Jackson, M.J., 2004. Magnetic properties of the Old Crow Tephra: Identification of a complex iron titanium oxide mineralogy. Geophys. Res., 109, B01104, doi:1029/2003JB002678.

Lattard, D., Sauerzapf, U., and Käsemann, M., 2005. New calibration data for the Fe-Ti oxide thermo-oxybarometers from experiments in the Fe-Ti-O systems at 1 bar, 1,000-1,300°C and a large range of oxygen fugacities. Contrib. Mineral Petrol., 149: 735-754.

Lattard, D., Engelmann, R., Kontny, A., and Sauerzapf, U., 2006. Curie temperatures of synthetic titanomagnetites in the Fe-Ti-O system: Effects of composition, crystal chemistry, and thermomagnetic methods. J. Geophys. Res., 111, B12S28. doi:10.1029/2006JB004591.

Lawson, C.A., and Nord, G.L. Jr., 1984. Remanent magnetization of a "paramagnetic" composition in the ilmenite-hematite solid solution series. Geophys. Res. Lett., 11: 197-200.

Lloyd, G.E., 1985. Review of instrumentation, techniques and applications of SEM in mineralogy. In: J.C. White (Editor). Application of electron microscopy in Earth Sciences. Min. Ass. of Canada short courses, 11: 151-188.

McEnroe, S.A., Robinson, P., and Panish, P., 2000. Detailed chemical and petrographic characterization of ilmenite-and magnetic-rich cumulates of the Sokndal Region, Rogaland, Norway. Norwegian Geolog. Survey Bull., 426: 49–56.

McEnroe, S.A., Robinson, P., and Panish, P.T., 2001. Aeromagnetic anomalies, magnetic petrology, and rock magnetism of hemo-ilmenite- and magnetite-rich cumulate rocks from the Sokndal Region, South Rogaland, Norway. Am. Mineral., 86: 1447-1468.

Merrill, T.M., 1968. A possible source for the coercivity of ilmenite-hematite minerals. J. Geomagn. Geoel., 20: 181-185.

Nord., G.L. Jr., and Lawson, C.A., 1989. Order-disorder transition induced twin domains and magnetic properties in ilmenite-hematite. Amer. Min., 74: 160-176.

Nord, G.L., Jr., and Lawson, C.A., 1992. Magnetic properties of $ilmenite_{70}$-$hematite_{30}$: Effect of transformation-induced twin boundaries. J. Geophys. Res., 97: 10897-10910.

Özdemir, Ö., and Dunlop, D.J., 2003. Low-temperature behavior and memory of iron-rich titanomagnetites (Mt. Haruba, Japan and Mt. Pinatubo, Phillipines). Earth Planet. Science Lett., 216: 193-200.

Özdemir, Ö., Dunlop, D.J., and Moskowitz, B.M., 2002. Changes in remanence, coercivity and domain state at low temperatures in magnetite. Earth Planet. Science Lett., 194: 343-358.

Petersen, N., and Bleil, U., 1973. Self reversal of remanent magnetization in synthetic titanomagnetites, Z. Geophys., 39: 965-977.

Petersen, N., and Bleil, U., 1982. Magnetic properties of rocks. In: G. Angenheister (Editor). Numerical Data and Functional Relationships in Science and Technology, Landolt-Börnstein V/1b. Springer-Verlag, Berlin, Heidelberg, 366-432.

Petersen, N., von Dobeneck, T., and Vali, H., 1986. Fossil bacterial magnetite in deep-sea

sediments from the South Atlantic Ocean, Nature, 320: 611-615.

Reynolds, R.L., and Goldhaber, M.A., 1978. Iron-titanium minerals and associated alteration phases in some uranium bearing sandstones. J. Res. U.S. Geol. Surv., 6: 707-714.

Roberts, A.P., Cui, Y., and Verosub, K.L., 1995. Wasp-waisted hysteresis loops: Mineral magnetic characteristics and discrimination of components in mixed magnetic systems. J. Geophys. Res., 100: 17909-17924.

Schmidbauer, E., and Readman, P.W., 1982. Low temperature magnetic properties of Ti-rich Fe-Ti spinels. J. Magn. Magn. Mat., 27: 114-118.

Schulz, H.D., and cruise participants, 1998. Report and preliminary results of Meteor Cruise M 41/1, Berichte, Fachbereich Geowissenschaften, Universität Bremen, 114: 124 pp.

Tauxe, L., Mullender, T.A.T., and Pick, T., 1996. Potbellies, wasp-waists, and super-paramagnetism in magnetic hysteresis. J. Geophys. Res., 101: 571-583.

Thompson, R., and Oldfield, F., 1986. Enviromental Magnetism. Allen and Unwin, London, 227 pp.

Tucker, P., 1981. Low-temperature magnetic hysteresis properties of multidomain single-crystal titanomagnetite. Earth Planet. Sci. Lett., 54: 167-172.

Ubangoh, R.U., Pacca, I.G., Nyobe, J.B., Hell, J., and Ateba, B., 2005. Petromagnetic characteristics of Cameroon Line volcanic rocks. J. Volc. Geothem. Res., 142: 225-241.

Warner, B.N., Shive, P.N., Allen, J.L., and Terry, C., 1972. A study of the hematite-ilmenite series by the Mössbauer effect. J. Geomag. Geoelec., 24: 353-367.

Zabel, M., Schneider, R.R., Wagner, T., Adegbie, A.T., de Vries, U., and Kolonic, S., 2001. Late Quaternary climate changes in central Africa as inferred from terrigenious input to the Niger Fan. Quat. Res., 56: 207-217.

Sediment magnetic characteristics of marine deposits from the upwelling region off NW Africa

Abstract

Detailed rock magnetic analyses were performed on a sedimentary sequence recovered from the continental margin region off Cape Ghir (Morroco) in order to investigate the impact of early diagenesis on the primary magnetic mineral assemblage. These environmental processes are related to the upwelling system off NW Africa. The primary detrital magnetic mineralogy in this region is dominated by ferrimagnetic magnetite of variable degrees of oxidation as indicated by Curie points of around 580°C and a broad, blurred Verwey transition in the temperature range from 95-120 K. The ARM/IRM ratio hints at high amounts of fine-grained particles. The gradual convergence of the field cooling (FC) and zero field cooling (ZFC) warming curves measured between 5 K and 300 K suggests the additional presence of a high coercivity component, such as goethite. Restricted to a distinct depth interval between ~ 1.50 m and 3.80 m, typical diagenetic alteration features are encountered such as a clear reduction in the total magnetic mineral content, a marked overall coarsening of the grain-size spectrum and lower coercivities. Within this confined diagenetic interval not only the ferrimagnetic but also the antiferromagnetic iron oxide minerals have been reduced in concentration. Although reductive diagenesis has caused significant alterations of the remanence properties, nearly stoichiometric magnetite remains the dominant magnetic phase in these reduced sediments. This was demonstrated by the occurrence of a distinct Verwey transition close to 120 K and approximately identical ZFC and FC warming curves. Magnetite apparently survived the reductive diagenetic processes, which contradicts typical findings for such reducing environments. However, these results clearly show that reductive diagenesis driven by the upwelling system off NW Africa, is expressed only as a relatively slight alteration of the magnetic mineral inventory in the Cape Ghir region.

This chapter is in preparation for publication as M. Dillon, Sediment magnetic characteristics of marine deposits from the upwelling region off NW Africa.

1. Introduction

The Canary Island region accommodates one of the World's most prominent upwelling systems, which gives rise to an intense biological primary productivity in the surface waters promoting high fluxes of organic material (C_{org}) to the sea floor. In such marine environments microbial degradation of organic matter takes place in the sediments. This leads to reducing conditions in the sediment column, which in turn results in strong diagenetic effects on the primary magnetic mineral components. As a consequence the stability of various minerals is reduced, leading to dissolution, alteration and remineralization. The degradation of organic matter by microorganisms proceeds according to a well defined sequence, as proposed by *Froelich et al*. (1979). The microorganisms maintain energy for there metabolism by emplying different terminal electron acceptors in the sediment column, starting with oxygen in the top layer, nitrate, Mn-oxides, Fe-oxides and sulfate at depth, followed by methane fermentation. Early diagenesis, driven by microbially degradation of organic matter, is well known to affect the magnetic

mineral assemblage in marine sediments. In the iron reduction zone, magnetite and other oxides of detrital or biogenic origin become unstable and dissolve (*Karlin and Levi*, 1985; *Leslie et al*., 1990). Then, under sulphate reducing conditions dissolved ferrous (Fe^{2+}) ions react with H_2S to form secondary, authigenic iron sulphide phases, which are stable under reducing conditions (*Robinson,* 2000).

The terrestrial influence on sedimentation in the eastern North Atlantic adjacent to the semi-arid and arid NW African continent is mainly dust (*Sarntheim et al.,* 1982). The dust is transported over NW Africa and the eastern tropical Atlantic by strong trade winds blowing in south westerly directions. The supply of terrigenous material to the NW African continental slope experienced several distinct changes, in particular during Holocene times. Most significant was the environmental turnover between 14.8 and 5.5 cal. ka BP, a well-defined period of low influx associated with the African Humid Period, when the now-hyperarid Sahara desert was fully vegetated and supported numerous perennial lakes (*Jolly et al.*, 1998). An arid interval corresponding to the Younger Dryas punctuates this humid period. The African Humid Period has been attributed to a strengthening of the African monsoon due to gradual increases in summer season insolation (*DeMenocal et al*., 2000). Climate reconstructions by *Claussen et al.* (1999) reflect an abrupt climate change in the mid Holocene some four to six thousand years before present associated with the start of the desertification of the Sahara.

The main objective of this study is to apply rock magnetic proxy parameters to characterize the sedimentary deposits derived from the marginal zone of the upwelling system. There, most of all critical steering factors driving the early diagenetic processes are expected to display steepest gradients. Conventional room-temperature rock magnetic methods were performed in order to describe the extent of dissolution, alteration and re-mineralization of magnetic minerals. High and low-temperature magnetic experiments have been performed in order to identify the magnetic mineral inventory in detail.

2. Investigation Area

For the NW African region aeolian dust is the most important contributor of lithogenic material to marine sediments, thus reflecting environmental conditions in the continental source areas as well as properties of the atmospheric circulation. Aeolian dust transport over the NW African continent and the eastern tropical Atlantic is driven by two main wind systems: the Saharan Air Layer (SAL) and the NE trade winds (*Mayewski et al.,* 1997). The SAL is a mid-tropospheric zonal wind system related to the African Easterly Jet and occurrs at altitudes between 1500 and 5000 m (*Prospero,* 1990), which accounts for the transport of Saharan and Sahelian dust (*Bergametti et al.,* 1989*; Torres-Padrón et al.,* 2002). The lower altitudes (< 1500 m) are dominated by the seasonal NE trade winds, blowing parallel to the African coast. The dust load of these trade winds originates mainly from the northern Sahara and the Atlas Mountains (*Chiapello et al.,* 1995). Aeolian input was generally stronger during glacial times (e.g. *Sarntheim,* 1982*; Balsam et al.,* 1995*; Stuut et al.,* 2005).

Recent studies have discussed river discharge as the second important input factor for the transport of lithogenic material to the NE Atlantic Ocean (e.g. *Holz et al.,* 2004). Sediments recovered near the Moroccan coast at Cape Ghir were found to have received a significant portion of terrigenous matter from river discharge throughout the last 130 kyrs. This indicates an enhanced river activity during interglacial time intervals (*Kuhlmann et al.,* 2004). Fluvial input of terrigenous material transported into the North Atlantic Ocean originates from river systems draining the Atlas Mountains

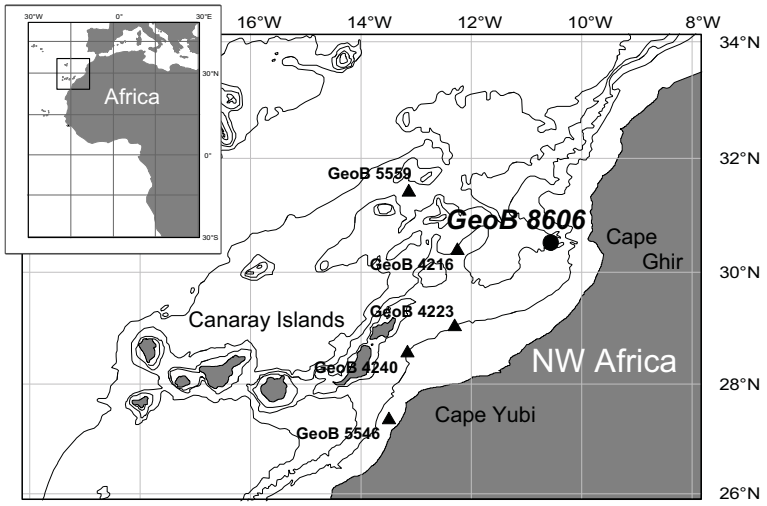

Fig. 1 Location of Site GeoB 8606 (filled circle) in 1223 m water depth from the upwelling region off Cape Ghir (31°00.2´N; 10°44.6´W). The five stratigraphic reference cores from which the Canary magnetic susceptibility stack (CAMS; *Kuhlmann et al.,* 2004) was derived are shown as filled triangles. Isobaths are given at 1000 m intervals according to *Intergovernmental Oceanographic Commission* (1994).

(*Millman & Meade,* 1983). The Souss River, which reaches the North Atlantic Ocean at Cape Ghir has a drainage area with seasonal runoff mainly induced by Mediterranean winter precipitation (*Hsu & Wallace,* 1976*; Watkins and Maher,* 2003).

3. Study Materials

Gravity core GeoB 8606-6 (31°00.2´N; 10°44.6´W) was recovered during R/*V Meteor Cruise M 58/2* from 1223 m water depth in the upwelling region off Cape Ghir (Fig. 1) (*Bleil et al.,* 2004). The sediment series comprises a total length of 9.20 m and consist of olive brown soft and fine-grained mud alternating with grayish brown forambearing nannofossil clay. Small amounts of quartz grains, rock and shell fragments indicate a sediment supply from the nearby African shelf (*Bickert et al.,* 2004). The sediments display no evidence of coring induced or other disturbances.

Site GeoB 8606 is located within the path of the Canary Current, which flows southwards along the NW African coast as far as ~ 15°N where it turns westwards towards the open tropical Atlantic, forming the North Equatorial Current (NEC; *Stramma & Siedler,* 1988). Triggered by Ekman transport, the trade winds force the upwelling of colder water at the continental shelf area (*Hagen,* 2001). These water masses contain a higher nutrient concentration, which promotes enhanced marine primary productivity (*Sarnthein et al.,* 1982).

4. Analytical Methods

4.1 Magnetic susceptibility measurements

Bulk rock magnetic measurements have been performed on oriented cubic specimens (6.2 cm^3) sampled at a 5 cm depth interval. Magnetic volume susceptibility κ, was determined using a *Bartington MS2* spot sensor on the split core archive halves. Additional frequency dependent susceptibility measurements were carried out on the cubic samples, with the same *Bartington* meter with a dual-frequency head.

4.2 Laboratory induced remanence experiments

Acquisition of isothermal remanent magnetization (IRM) in 18 steps to 0.3 T and anhysteretic remanent magnetization (ARM), imparted by superimposing a gradually decaying alternating field of

0.3 T maximum amplitude on a constant biasing field of 40 μT was followed by incremental triaxial IRM and ARM alternating field demagnetization. All remanences were measured using a *2G Enterprises 755R DC SQUID cryogenic magnetometer*, the applied fields were generated by its built-in facilities. A number of indicative rock magnetic parameters characterizing the low coercivity ferrimagnetic (titano-)magnetite mineral fraction was derived from these data, including the median destructive fields MDF_{IRM} and MDF_{ARM}.

To estimate the concentration of the high coercitivity components hematite and goethite from the hard isothermal remanent magnetization (HIRM) (*Stoner et al.,* 1996) detailed IRM acquisition was continued for a set of 21 selected samples to 2.5 T, which constitutes the maximum field available of the external *2G Enterprises 660 pulse magnetizer*. A back field of –0.3 T was subsequently imparted to calculate the $S_{-0.3\,T}$-ratio following the method of *Bloemendal et al.* (1992).

4.3 Magnetic hysteresis measurements

Magnetic hysteresis and backfield measurements both limited to a maximum field of 0.3 T were performed using a *PMC* M2900 *alternating-gradient force magnetometer*. A subset of 50 samples (in varying depth resolution of 10 and 20 cm) was prepared following the technique described by *von Dobeneck* (1996). For data processing, the program '*Hystear*' (*von Dobeneck*, 1996) was used to determine mass specific saturation magnetization (σ_s), remanent saturation magnetization (σ_{rs}), coercive force (B_c) and remanent coercivity (B_{cr}). These parameters help to quantify the concentration, magnetic grain-size and coercivity of the ferrimagnetic mineral components.

4.4 Thermomagnetic measurements

Eight representative dry bulk sediment samples were subjected to further high- and low-temperature magnetic experiments. High-temperature magnetic measurements between room temperature and 720°C were performed at Utrecht University (The Netherlands) using a horizontal translation-type Curie balance (*Mullender et al.,* 1993) with heating and cooling rates of 5°C per minute.

Low-temperature experiments were performed on a *Quantum Design Magnetic Property Measurement System* (MPMS) at the University of Bremen. Three different measurements have been performed in the following order; first, the samples were cooled in zero field to 5 K where a 5 T magnetic field was applied. Subsequently the instrumental magnet was reset to zero and thermal demagnetization of zero field cooling (ZFC) remanence was monitored in 2 K increments during warming to room temperature. In a second run, the samples were cooled to 5 K in the presence of a 5 T magnetic field. At 5 K the magnet was reset to zero and the field cooling (FC) remanence was monitored during warming in 2 K increments back to room temperature. The third experiment consists of a room temperature saturation isothermal remanent magnetization (RT-SIRM), which was imparted to the samples using a magnetic field of 5 T at ambient temperature. The thermal dependence of the remanence was measured in zero field in increments of 5 K upon continuous cooling down to 5 K and subsequent warming back to 300 K. Samples for MPMS analyses have been prepared using the techniques described by *Frederichs et al.* (2003).

4.5 SEM analyses of magnetic concentrates

Backscattered electron (BSE) (*Lloyd*, 1985) and secondary electron (SE) imaging of magnetic extracts and heavy liquid separates were performed using a *FEI XL30 SFEG* scanning electron

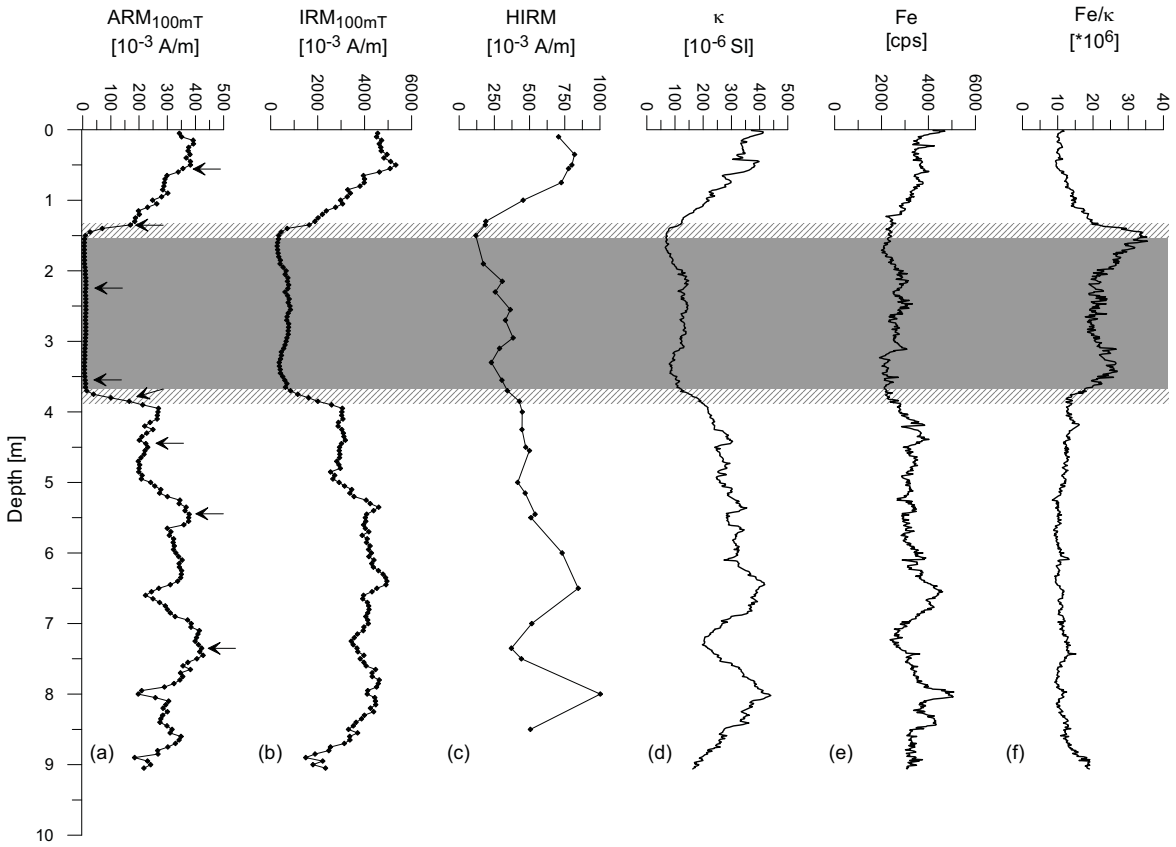

Fig. 2 Depth profiles of rock magnetic parameters delineating variations in magnetic mineral content. (a) Volume specific anhysteretic remanent magnetization ARM, (b) isothermal remanent magnetization IRM, (c) hard isothermal remanent magnetization HIRM and (d) magnetic susceptibility κ. Also shown is (e) the solid phase iron concentration and (f) the diagenesis parameter Fe/k after *Funk et al*. (2004). Arrows at the ARM profile denote horizons where high- and low temperature magnetic analyses have been performed. The grey area represents the approximate extent of the diagenetic zone. Hatched horizontal bars mark the intervals which exhibit the strongest gradients in the magnetic properties.

microscope (SEM) at Utrecht University (The Netherlands). The SEM was operated at an acceleration voltage between 12 and 30 kV with a ~2 nA beam current.For magnetic extraction the technique of *Petersen et al.* (1986) was applied. Additionally heavy liquid separates were derived using the method described by *Franke et al.* (2007a). The sample preparation for SEM analysis was carried out as described in *Franke et al*. (2007b). The element composition was acquired by using energy dispersive spectroscopy (EDS, e.g. *Goldstein et al*., 1992). The obtained element spectra were (semi-)quantified using the EDAY software '*Remote SEM Quant Phiroz'* version 3.4. Peaks were detected automatically and the background contribution was subtracted before calculation of the element composition. The intensities for all elemental peaks were normalized by the respective oxygen peaks.

4.6 XRF measurements

Solid phase Fe concentrations were determined by X-ray Fluorescence Spectroscopy (XRF) at a depth resolution of 1 cm on surfaces of archive core halves using a non-destructive XRF core logging system developed especially for marine sediments (*Röhl and Abrams*, 2000). Resulting element data are relative abundances given in counts per second (cps).

5. Room Temperature Magnetic Analyses

5.1 Concentration and Mineralogy

Depth profiles of the concentration dependent magnetic parameters of anhysteretic remanent magnetization ARM, isothermal remanent magnetization IRM, hard isothermal remanent magnetization HIRM, and volume magnetic susceptibility κ are shown in Fig. 2, together with the solid phase Fe concentration and the diagenesis parameter Fe/κ of *Funk et al*. (2004). All concentration related magnetic attributes document a substantial progressive reduction of the magnetic mineral content within a distinct depth interval between 1.35 and 3.85 m depth.

Most pronounced is the drop in the ARM (Fig. 2a), which is predominantly carried by the single-domain (SD) and fine pseudo-single-domain (PSD) grain-size fractions of (titano-)magnetite. Compared to $227.5 \cdot 10^{-3}$and $229.8 \cdot 10^{-3}$ A/m in the upper and lower core section respectively, ARM intensities display a distinct decrease between 1.35 m and 3.85 m depth to on average $5.7 \cdot 10^{-3}$ A/m. This decrease to less than 5 % of its initial value is clearly indicative of reductive dissolution of the fine-grained ferrimagnetic mineral fraction. It also implies that only a tiny fraction of fine-grained minerals is present in this depth interval.

The IRM (Fig. 2b), which quantifies the complete magnetic grain-size spectrum of all ferrimagnetic remanence carriers, shows a similar but less pronounced drop (2455 to $357 \cdot 10^{-3}$ A/m). This indicates that not only the fine particles fraction has been dissolved, but PSD and multi-domain (MD) particles are also affected by dissolution. This concurs with previous findings, that fine grained magnetite undergoes diagenetic dissolution more rapidly than coarse grained magnetite due to its larger surface area to volume ratio (*Karlin and Levi*, 1983).

The HIRM generally quantifies contributions of high coercivity iron oxides (hematite, hemoilmenite) and oxyhydroxides (goethite) to the total remanence (*Stoner et al.,* 1996). The drop in the HIRM (Fig 2c) signal from on average 639 to $281 \cdot 10^{-3}$ A/m at ~1.35 m depth indicates that the high-coercivity fraction was also depleted diagenetically, but to a much lesser extent than the low-coercivity fraction. With a hematite saturation remanence of 1 kA/m (*Thompson and Oldfield*, 1986) the antiferromagnetic mineral content can be estimated to diminish from approximately 0.07 wt% in the top sediments to 0.03 wt% in the depleted interval. This provides only minimum estimates, because the 2.5 T field applied is insufficient to saturate hematite and in particular goethite.

The magnetic volume susceptibility κ (Fig. 2d) reflects the overall content of magnetic minerals, but also contains contributions from the dia- and paramagnetic mineral components of the

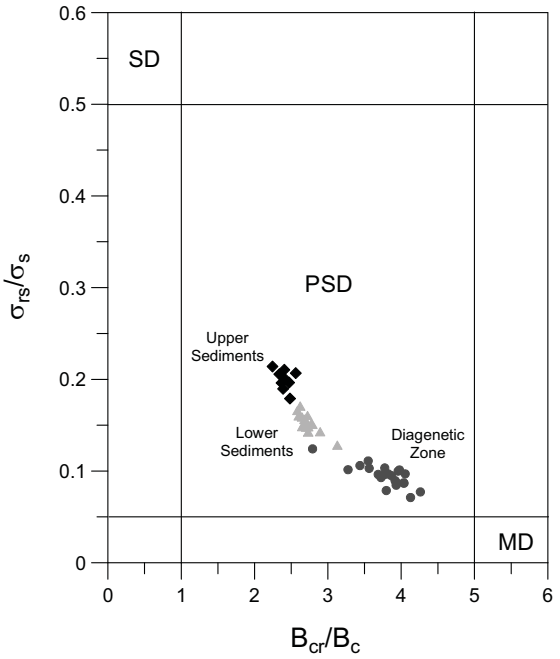

Fig. 3 Bulk magnetogranulometric ratios of saturation remanence to saturation magnetization, σ_{rs}/σ_s, and coercivity of remanence to coercive field, B_{cr}/B_c, plotted in the *Day et al*. (1977) standard diagram for samples from the upper sediments (diamonds), the diagenetic zone (circles) and the lower sediments (triangles).

sediment matrix. Lowest κ values are observed between ~1.35 and ~3.85 m, but the decline is less pronounced and extends more gradually over a broader depth interval than IRM and ARM. In contrast, κ and HIRM exhibit distinct, closely related variations (Pearson´s correlation coefficient r = 0.95). Mass specific saturation magnetization σ_S (not shown here) and κ display notably similar variations (r = 0.98) throughout the core. Using a room-temperature specific saturation magnetization of 92 Am^2/kg (*Thompson and Oldfield*, 1986) for magnetite, the ferrimagnetic mineral content can be estimated to diminish from a mean of 0.02 wt% in the top and bottom sediments to 0.009 wt% in the diagenetic zone.

Downcore solid phase Fe concentrations are shown in Fig. 2e. Similar to the magnetic susceptibility, Fe corresponds to terrigenous content. Therefore, Fe should essentially mirror the variations of κ. A correlation coefficient of r = 0.88 supports this assumption. Overall very high Fe concentrations are observed in the core.

The parameter Fe/κ (Fig. 2f) is suitable for the identification of diagenetic influences in sediment sequences (*Funk et al.*, 2004, *Hofmann et al.,* 2005). Post-depositional reductive diagenesis is capable of reducing ferrimagnetic iron minerals to paramagnetic iron compounds whereby κ is noticeably diminished. Since diffusion rates are small, the local Fe concentration remains nearly constant during this process (*Hofmann et al*., 2005). Consequently, reductive diagenesis increases the Fe/κ ratio above the characteristic value for the undisturbed terrigenous phase. Here, average values of Fe/κ are lowest in the sediments from the core top to 0.50 m and the lower sediments from 3.85 m to the bottom of the core at 9.20 m depth with values of $\sim 11 \pm 1 \cdot 10^6$ cps (Fig. 2f). This value is therefore defined as the characteristic background value for the studied sediments of GeoB 8606-6. Highest values, with a maximum of $\sim 35 \cdot 10^{-6}$ cps at ~1.60 m depth, are reached in the distinct depth interval between 1.35 and 3.85 m depth. The distinct drop in magnetic mineral content in both, ferri- and antiferromagnetic mineral fractions, correlates with the highest values in Fe/κ.

Therefore the sediment sequence can be subdivided into three sections: (1) the upper core section from top to 1.35 m, (2) the diagenetic zone ranging from 1.35 to 3.85 m and (3) the lower core section from 3.85 m to the bottom of the core at 9.20 m depth. In Table 1 the respective arithmetic means of sediment magnetic parameters for the three sections are listed. The intervals which exhibit the strongest gradients in the magnetic properties have been excluded from these calculations (compare horizontal hatched bars in Fig. 2).

5.2 Grain-size

The bulk magnetogranulometric ratios of saturation remanence to saturation magnetization, σ_{rs}/σ_s, and coercivity of remanence to coercive field, B_{cr}/B_c, are plotted in the standard diagram after *Day et al*. (1977) (Fig. 3). All samples lie within the pseudo-single-domain (PSD) field and show distinct depth dependent clustering. The samples from the upper sediment section show average σ_{rs}/σ_s ratios of 0.20 and B_{cr}/B_c ratios of 2.41. Samples from the lower part have σ_{rs}/σ_s values of 0.15 and B_{cr}/B_c values of 2.73. Both fall into the medium PSD field. The slightly coarser grain-sizes of samples from the lower part compared to samples from the upper part, document a mild alteration of the fine grained ferrimagnetic oxides in the deeper sediment layers. Samples from the diagenetic zone clearly fall in the coarsest observed PSD grain-size range with on average values of 0.09 for σ_{rs}/σ_s and 3.88 for B_{cr}/B_c.

Respective coarsening and fining trends were also observed in the magnetic grain-size indicative ratio ARM/IRM (*Maher*, 1988), which delineates variations in the

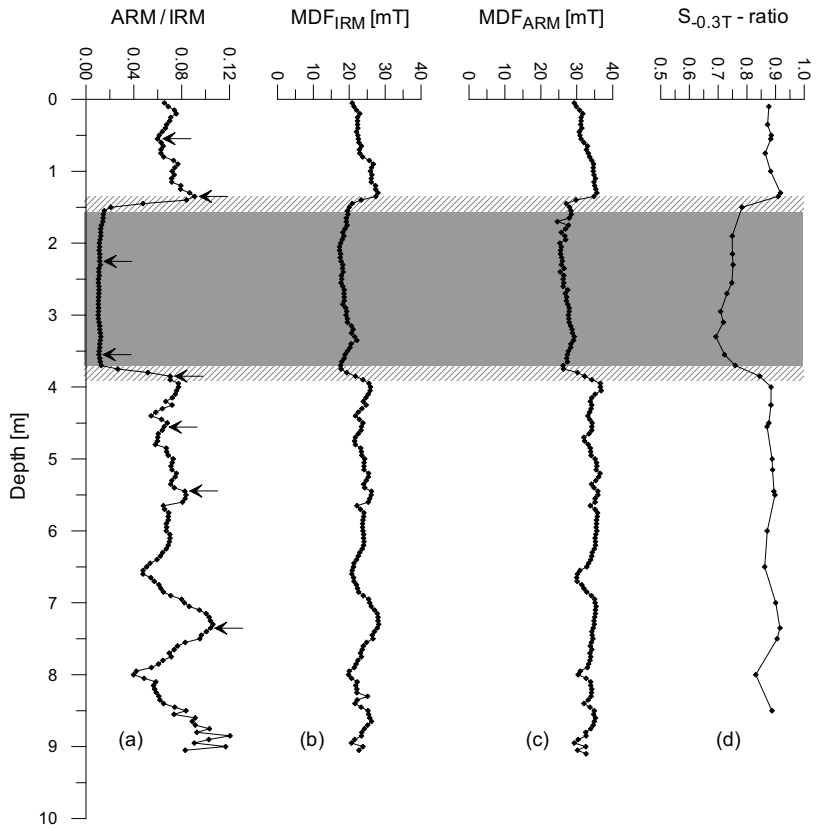

Fig. 4 Depth profiles of rock magnetic parameters characterizing variations in magnetic grain-size, coercivity and mineralogy. (a) Magnetogranulometric ratio of anhysteretic to isothermal remanent magnetization ARM/IRM, coercivity parameters median destructive fields of IRM and ARM (b) MDF_{IRM} and (c) MDF_{ARM}. Also shown is (d) the $S_{-0.3T}$-ratio which provides an estimate of the relative proportions of hard and soft magnetic minerals (*Bloemendal et al.,* 1992). Arrows at the ARM/IRM profile denote horizons, where high- and low temperature magnetic analyses have been performed. The grey area represents the approximate extent of the diagenetic zone. Hatched horizontal bars mark the intervals which exhibit the strongest gradients in the magnetic properties.

distribution of the fine particle fraction, in particular in the SD/PSD range of (titano-) magnetite. The sediments from above and below the diagenetic zone are characterized by much higher portions of PSD/SD (titano-)magnetite (Fig. 4a) than within the narrow interval starting at ~ 1.35 m. At this depth a distinct shift towards much coarser grain-size spectra documents the almost complete loss of the fine grained ferrimagnetic fraction. At 3.85 m depth a subsequent fining is observed, reaching values identical to those at the very top of the sediment core.

5.3 Coercivity

The coercivity parameters MDF_{IRM} and MDF_{ARM}, are useful for describing the magnetic stability of all remanence carrying particles (MDF_{IRM}) and the fine-grained fraction (MDF_{ARM}) in particular. Here these parameters comprise a rather uniform bulk magnetic stability of the ferrimagnetic mineral assemblage above and below the diagenetic zone with mean MDF_{IRM} of 23.8 ± 1.9 mT and mean MDF_{ARM} of 33.8 ± 1.7 mT. Both parameters increase slightly from the sediment surface downcore and drop on average 5-6 mT in the diagenetic zone. The values recover completely below the depth of 3.85 m (Fig. 4b-c). This characteristic low between 1.35 m and 3.85 m complies with the observed general coarsening of the (titano-)magnetite component (compare Fig. 2a), assuming that the coercivity is predominantly grain-size controlled, since

the coercivity for MD magnetite is smaller than for SD/PSD magnetite (*Thompson and Oldfield, 1988*).

The $S_{-0.3T}$-ratio provides an estimate of the relative proportions of hard and soft magnetic minerals in a given assemblage (*Bloemendal et al.,* 1992). Average values of 0.89 for the upper and 0.88 for the lower sediment layers reveal the presence of a significant portion of high coercive minerals throughout the entire core. In the diagenetic zone the $S_{-0.3T}$ -ratio drops to ~0.74, due to the diminishing content of the ferrimagnetic fraction. The relative contribution of high coercivity minerals to the remanence increases here from on average 11% to 25% (Fig. 4d).

6. Scanning Electron Microscopy

Figure 5 shows backscattered (a, b) and secondary electron (c) micrographs of particle clusters from magnetic extracts and (d) heavy liquid separates obtained from the diagenetic zone at a depth of 2.25 m. Overall 100 grains from the μm-particle fraction were examined as spot checks by EDS, the obtained element spectra were normalized to their oxygen peaks. The most common particles found were magnetite (Fig. 5a-3, Fig. 5b-4, Fig. 5b-6)) and titanomagnetites (Fig. 5a-1, Fig. 5a-2, Fig. 5b-5) showing various degrees of maghemitization. Additionally the heavy liquid concentrate contains framboidal pyrite (Fig. 5d).

7. Thermomagnetic Analysis

7.1 High-temperature cycling

Sediments from the top layer (0.55 m) revealed a single significant Curie temperature in the heating curve of ~580°C, pointing to magnetite as being the major primary magnetic mineral component (Fig. 6). Minor inflections in the temperature range between 300 and 400°C in the heating curves hint to the additional presence of titanomagnetite and / or -maghemite (*DeBoer and Dekkers,* 1996). In samples from depths below 0.55 m pyrite was identified by its oxidation to magnetite, maghemite and finally hematite. The oxidation of pyrite results in a distinct increase and subsequent decrease in magnetization between 400 and 500°C. Euhedral pyrite should be present when the sulfidic phase oxidises above 450°C. For samples between 1.35 m and 3.55 m a second peak below 450°C was observed, which is characteristic for the oxidation of framboidal pyrite (*Passier et al.,* 2001). Framboidal pyrite has also been positively identified by SEM analysis (Fig. 4d). At 720ºC both, primary ferrimagnetic Fe-oxides and secondary pyrite oxidation products are largely altered to hematite. Lower magnetizations prevail upon cooling, except for samples from 1.35 m and 3.55 m depth. Their cooling curves undergo a rapid increase in magnetization towards room temperature below ~320°C. A possible explanation for the observed

Table 1
Average rock magnetic parameters for the upper core section (0 – 1.30 m), the diagenetic zone (1.50 – 3.75 m) and the lower core section (3.95 – 9.20 m) of the studied sediment sequence. The intervals which exhibit the strongest gradients in the magnetic properties have been excluded from this calculation (cf. horizontal hatched bars in Fig. 2 and Fig. 4).

Parameter	Upper core section	Diagenetic zone	Lower core section
κ (10^{-6} SI)	258.7	103.3	273.8
IRM (10^{-3} A/m)	2455	357	2360
ARM (10^{-3} A/m)	227.5	5.7	229.8
HIRM (10^{-3} A/m)	639	281	548
MDF_{IRM} (mT)	24.0	18.9	23.8
MDF_{ARM} (mT)	32.8	27.1	34.0
$S_{-0.3T}$ - ratio	0.88	0.74	0.88
ARM/IRM	0.09	0.02	0.10
B_{cr}/B_c	2.43	3.95	2.73
σ_{rs}/σ_s	0.20	0.09	0.15

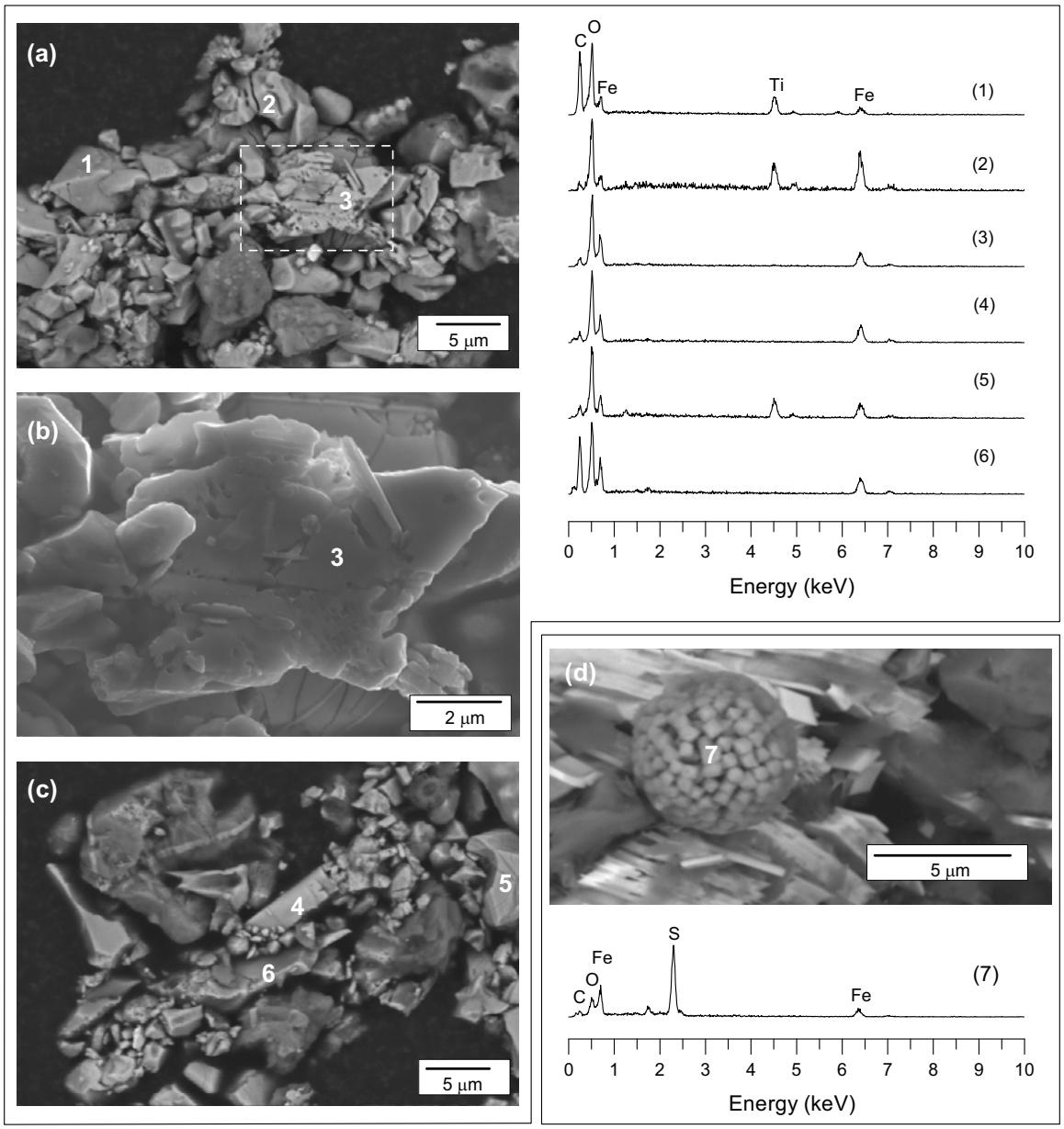

Fig. 5 Backscatter electron (BSE) (a, c) and secondary electron (SE) micrographs (b) of magnetic extracts from 2.25 m depth. (d) Image obtained in BSE mode from the heavy liquid extracts from the same depth interval. All EDS spectra are normalized to their oxygen maxima, they correspond to spot analyses on the respective numbered particle. (1, 2) Titanomagnetites with shrinking cracks. (3) Magnetite grain showing strong reductive diagenetic dissolution marks. (4, 6) Detrital magnetite. (5) Detrital titanomagnetite. (7) Framboidal pyrite.

increase is the formation of fine-grained, superparamagnetic (e.g. ferrihydrid?) Fe-oxides at higher temperatures (*Passier et al.,* 2001).

7.2 Low-temperature cycling: LT-SIRM after zero field and field cooling

Low-temperature SIRM obtained in a 5 T field at 5 K after ZFC and FC were monitored upon warming to 300 K (Fig. 7). To place an emphasis on specific temperature dependent features, the first derivatives (dm/dT) of the ZFC and FC remanences are also shown in Fig. 7. Thermal demagnetization curves for selected samples from the upper (above 1.35 m) and lower sediment sections (below 3.85 m) decrease steadily during

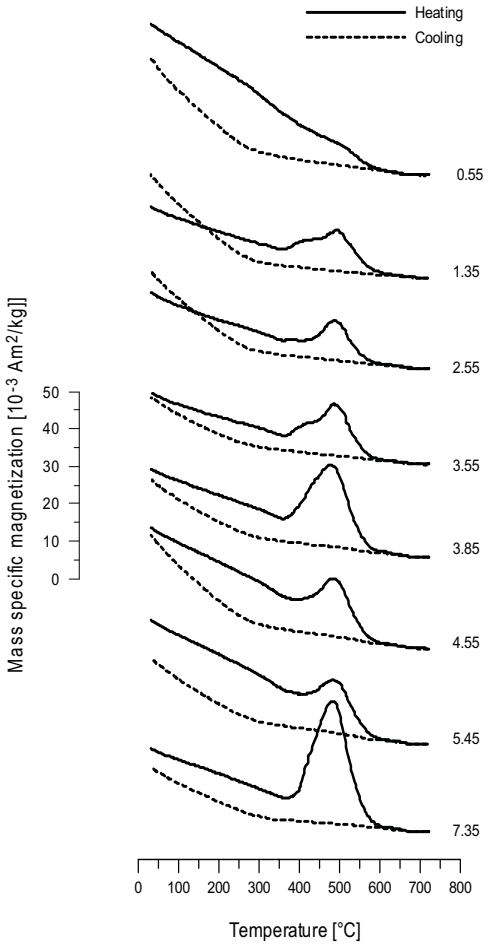

Fig. 6 High-temperature thermomagnetic cycles measured on a translation type Curie balance in air. Numbers on the right denote sample depths in metre.

warming to 300 K with two distinct Verwey structural phase transitions, one at ~95 K and a second close to 120 K (Fig. 7a-b;e-h). The two samples from within the diagenetic zone display only the Verwey transition close to 120 K (Fig. 7c-d). The temperature of 120 K is diagnostic of pure, stoichiometric magnetite (*Verwey,* 1939). The transition at 95 K clearly indicates a second non-stoichiometric magnetite phase. This temperature shift may either be a result of minor titanium substitution (*Kakol et al.,* 1994) or more likely from surface oxidation, forming a shell of maghemite around a magnetite core (*Özdemir et al.,* 1993).

A Verwey transition below 100 K for titanomagnetites is very unlikely, since even low Ti^{4+} concentrations ($x > 0.04$) result in the diasappearance of the Verwey transition (*Kakol et al.,* 1994). In contrast, *Özdemir et al.* (1993) showed a shift to temperatures below 100 K for partially oxidized magnetites ($z < 0.3$). Thus the Verwey transition at ~ 95 K reflects rather maghemitization than Ti substitution. In nature, low-temperature oxidation of magnetite towards maghemite is probably one of the most common oxide mineral alterations. Additionally, SEM analyses of magnetic extracts from 2.25 m depth show coarse grained titanomagnetites (Fig. 5B, (4)) and magnetites with clear indications of maghemitization (Fig. 5B, (5)).

We did not observe any features consistent with hematite, such as the Morin transition, $T_{Morin,}$ at ~258 K (*Liebermann and Banerjee*, 1971). But like the Verwey transition, T_{Morin} is very sensitive to cation substitution and grain-size. Small amounts of Ti impurities depress the Morin transition and for very small particles the transition vanishes completely (*Bando et al.,* 1965).

A diagnostic feature in the low-temperature range for goethite is an apparent discrepancy between ZFC and FC warming curves at low temperatures, which shrinks continuously upon warming back to 300 K (*Franke et al.,* 2007b). Such a discrepancy is most pronounced for the uppermost sample, less strong for the sample from 1.35 m and samples from below 3.85 m depth. This suggests that goethite is present in sizable amounts only in the uppermost sediments.

In contrast, the samples from the diagenetic zone yield nearly no differences between FC and ZFC remanences in the complete temperature range between 5 K and room-temperature. *Brachfeld et al.,* (2002) obtained similar results from natural and synthetic magnetites. They found that multi-domain MD magnetite yields even higher ZFC remanences than FC remanences at 5 K. Coarse grained PSD/MD nearly stoichiometric magnetite

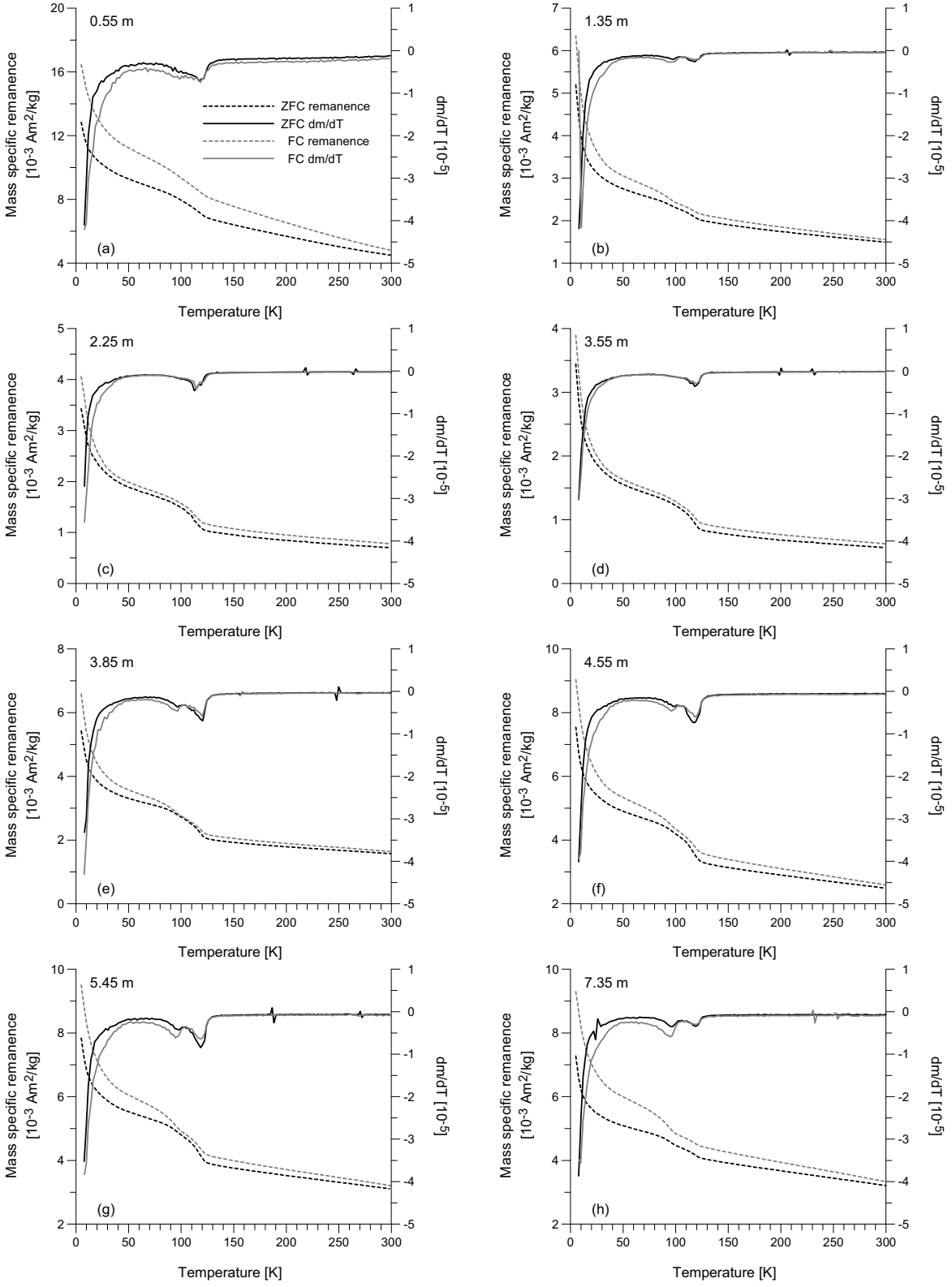

Fig. 7 Low temperature thermal demagnetization of mass specific remanences acquired by applying a 5 T field at 5 K after cooling from room-temperature in the absence (zero field cooling (ZFC), black dashed line) and presence of a 5 T field (field cooling (FC), grey dashed line). The first derivatives of the demagnetization curves of ZFC and FC remanences are given as black and grey solid lines, respectively. Numbers in the upper left corners correspond to the sample depth in meter.

is therefore most likely to be the predominant magnetic mineral present in the zone of low magnetization. The transition at 95 K was detected for samples from the upper and lower core sections, but is more pronounced for samples from below the diagenetic zone (Fig. 7e-h). This might hint at a change in the source origin of the magnetic material or at changing environmental conditions during sedimentation. After cooling in the presence of a magnetic field, this transition becomes even more pronounced than after zero-field cooling (cp. Fig. 7g-h). Apparently the presence of a field during cooling has a lasting effect on (e.g. the internal structure of) the maghemite phase.

The increase of ZFC and FC remanences upon warming, which occurs in the temperature range between 30 and 5 K is usually attributed to the presence of superparamagnetic (SP) mineral fractions, because ultrafine grained mineral phases convert into a stable SD state at very low unblocking temperatures (*Banerjee et al*., 1993). This phenomenon was observed in oxic to suboxic marine sediments (e.g., *Smirnov and Tarduno*, 2000) but also in the Mediterranean sapropel S1 (*Passier and Dekkers*, 2002). Since the measurements of this study were performed on bulk sediment samples, the increase can also be attributed to paramagnetic constituents of the sediment matrix (e.g. iron-bearing silicates or clay minerals), which are paramagnetic at room-temperature, but order magnetically at very low temperatures (*Coey,* 1988).

7.3 Low-temperature cycling: RT-SIRM

Thermal variations of room-temperature SIRM cycles during zero-field cooling from 300 K to 5 K and zero-field warming back to 300 K are shown in Fig. 7 for bulk sediment samples. During cooling RT-SIRM increases with a broad peak around 200 - 250 K, followed by a distinct decrease, with a maximum gradient near 120 K (Fig. 8), the characteristic Verwey temperature for magnetite. Between 100 K and 50 K a broad minimum is reached. Further cooling below 50 K results in a distinct remanence increase. When warming the samples back to room temperature, the SIRM retraces the cooling curve in the range between 5 - 50 K. Warming back through the Verwey transition results in a temporary increase in remanence, followed by a continuous final decrease. Between 83% and 93% of the original RT-SIRM is recovered at 300 K for samples from the upper and lower sediments and ~ 78 % for samples from the diagenetic zone. The decrease in remanence when cooling through the Verwey transition is largest for samples from the diagenetic zone, which is characteristic for coarse magnetite (*Dunlop,* 2002). The maximum drop amounts to -20% of the initial RT-SIRM. During warming back to room temperature a similar distinct transition was not observed.

In clear contrast to the low-temperature ZFC and FC remanence curves, the RT-SIRM curves do not show any evidence for the transition at 95 K. As in the LT-SIRM curves a steep increase in remanence is observed at temperatures below 30 K, presumably caused by ferrimagnetic ordering of paramagnetic sediment components and superparamagnetic particles acquiring a thermal remanence by passing through their SP/SD threshold.

8. Discussion and Conclusions

8.1 Primary Magnetic Mineralogy

The rock magnetic measurements reflect three zones of differing magnetic mineral content. Sediments from the upper core section from 0 to 1.35 m and the lower core section from 3.85 m to the bottom of the core display similar magnetic characteristics (cf. Table 1), suggesting, that similar conditions prevailed during sedimentation. The primary magnetic mineral inventory comprises ferrimagnetic (titano-)magnetite and maghemite within the pseudo single domain (PSD) grain size

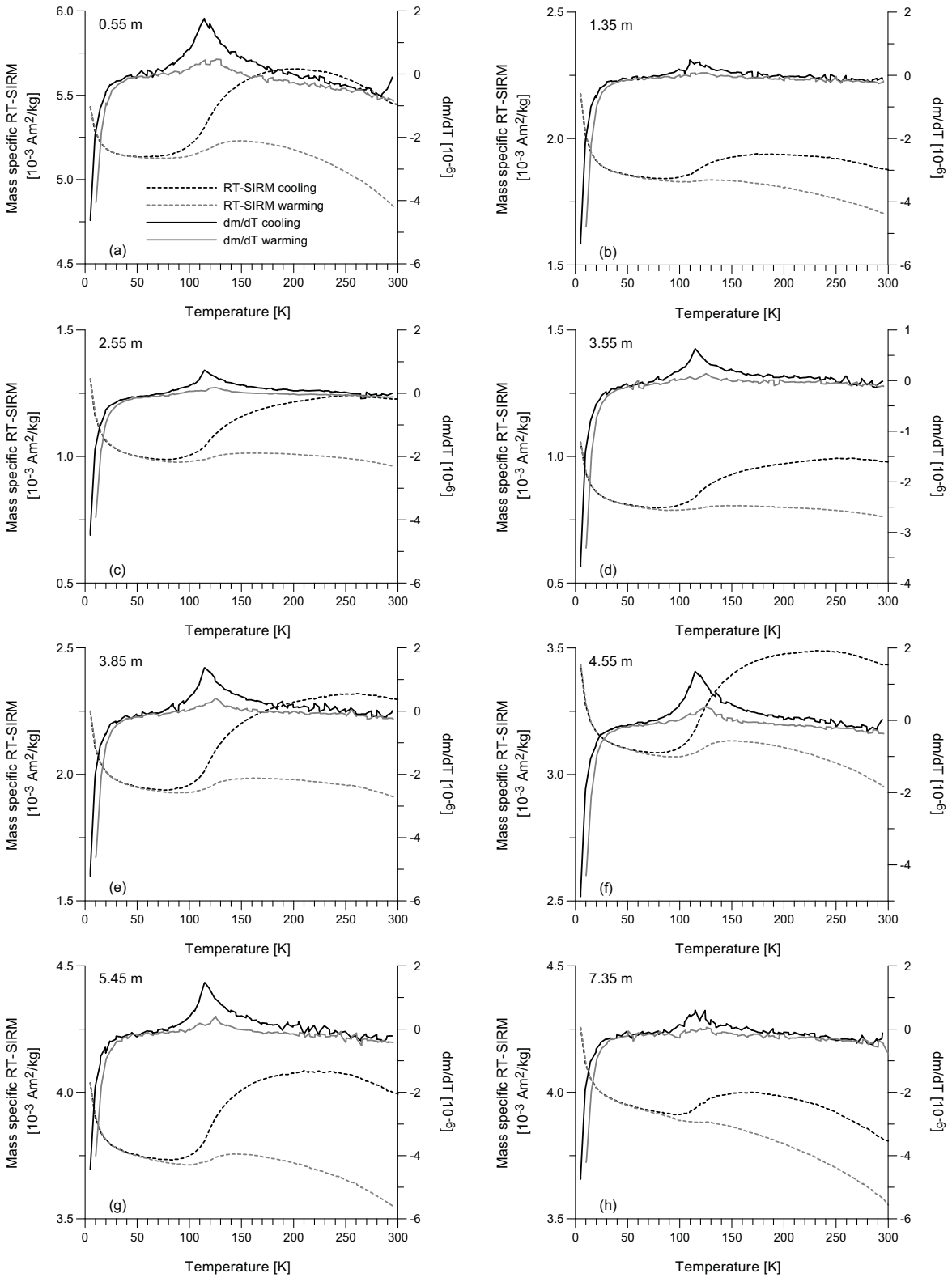

Fig. 8 Bulk sediment cooling (black dashed line) and warming curves (grey dashed line) of room-temperature saturation isothermal remanent magnetization RT-SIRM acquired by applying a maximum field of 5 T. Their respective first derivatives are given as solid lines of respective color coding. Numbers in the upper left corners correspond to the sample depth in meters.

range (Fig. 3). The high-coercivity fraction is thought to be dominated by hematite. IRM acquisition up to 2.5 T (not shown) revealed curves close to saturation at fields of 2.5 T and also low-temperature measurements revealed only limited diagnostic features for the presence of goethite. If at all, sizable amounts of goethite are present in the younger sediments.

Estimates based on saturation magnetization and saturation remanence data yield 0.02 wt% and 0.07 wt% of the bulk sediment to be magnetite and hematite, respectively. Apparently the concentration of high coercivity antiferromagnetic components is higher than those of magnetite, which also explains the close relation between the volume susceptibility κ and HIRM ($r = 0.95$). The HIRM expressed as a percentage of the saturation remanence SIRM acquired at 2.5 T reaches an average values of HIRM% ≈ 11. This value also complies with the results reported by *Watkins and Maher* (2003) for surface sediments from the study area. There the haematite/goethite input has been associated with aeolian transport of soils from the sub-Saharan/Sahel region of Africa.

The low-temperature magnetic measurements revealed the presence of magnetite in form of the Verwey transition, but they are lacking the Morin transition indicative for hematite. The two distinct Verwey transitions, one present at ~95 K and the second one close to 120 K suggest two discrete populations of maghemite and magnetite, respectively (Fig. 7a-b,e-h) above 1.35 m and below 3.85 m. The ARM/IRM ratio (Fig. 4a) documents the presence of a substantial fraction of fine-grained ferrimagnetic (titano-)magnetite in the primary magnetic mineralogy (*Maher*, 1988). Superparamagnetic components were estimated from the frequency dependence of magnetic susceptibility and are on average $\kappa_{fd} = 2\%$, therefore of minor importance in the upper and lower core sections. In the magnetically depleted sediments this method could not be applied, because of its limited resolution.

8.2 Modern iron redox boundary

The downcore profiles of the rock magnetic parameters (Fig. 2) delineate variations in the magnetic mineral content, suggesting that the modern iron redox boundary is situated just above a depth of 1.35 m. A drastic decline in magnetic mineral content, lower coercivities and a marked overall coarsening of the grain-size spectrum, which were observed here, are typical features of diagenetic alteration in suboxic environments (*Karlin and Levi,* 1983*,* 1985; *Robinson et al.,* 2000). Finer magnetic grains are more sensitive to dissolution than larger grains due to their larger surface to volume ratio. The ARM delineates concentrations of SD/PSD low coercivity components such as magnetite or maghemite and drops to very low values at 1.35 m (Fig. 2c) thus indicating a coarsening of the magnetic grain-size within a narrow depth interval of a few decimetres (Fig. 3a). Standard criteria for the exact position of the modern iron redox boundary such as a change in sediment color (*Lyle,* 1983) or the precipitation of biogenic magnetite just above the iron redox boundary (*Hilgenfeldt,* 2000) were not observed at Site GeoB 8606. Looking closely at the concentration related parameters, a minor drop in magnetic mineral concentration is already observable in κ, ARM and IRM at ~60 cm depth. A gradual increase in the diagenesis sensitive parameter Fe/κ (*Funk et al.,* 2004; Fig. 2f) concurs with these findings. Between 0.60 m and 1.35 m, Fe/κ increases continuously from values of $\sim 10 \cdot 10^{-6}$ cps to the overall maximal value of $35 \cdot 10^{-6}$ cps at 1.60 m depth. Another important aspect is the presence of pyrite, which was positively identified by thermomagnetic analyses at a depth of 1.35 m. The authigenic formation of pyrite takes place below the iron reduction zone, as this is the depth where fine-grained iron oxides are no longer stable and dissolve

whilst iron sulphides precipitate (*Karlin and Levi,* 1985).

In contrast to this depletion trend in the magnetic mineral content, no such characteristics were found in the grain-size dependent magnetic parameters ARM/IRM, MDF_{ARM} and MDF_{IRM} (Fig. 3). In fact, an opposite trend was observed for the depth interval between 0.60 and 1.35 m depth. Instead of a slight coarsening of the magnetic grain-sizes, a fining was observed here in all three parameters. This implies that in case of diagenetic alteration the effect on the magnetic mineral assemblage is only mild down to a depth of 1.35 m depth. Alteration is not strong enough to dissolve a subsatntial amount of the primary magnetic assemblage present and to cause a notable coarsening effect in the magnetic grain-size distribution.

A possible explanation might be given by a mild maghemitization of the present magnetite grains. This low-temperature alteration process starts at the crystal surfaces, leaving the core of the particle unaltered, which would also explain the observed fining of the grain-size spectrum. MD particles convert into PSD, PSD to SD and SD accordingly to SP particles. These ultrafine magnetic grains are not able to carry a remanent magnetization and thus do not contribute to IRM or ARM. As a result a decrease in concentration is observed. While *Torii* (1997) suggested that maghemitization occurs mainly at the water-sediment interface, *Smirnov and Tarduno* (2000) proposed that it may also occur deeper in the suboxic zone of marine sediments.

The oxidation of magnetite to maghemite is also a plausible explanation for the distinct double peak of the observed Verwey transition. Mild maghemitization is known to shift the Verwey transition to lower temperatures (from 120 K to 95K) (*Özdemir et al.,* 1993*, Kosterov,* 2003). For grains with an oxidation parameter of $z > 0.3$ the transition is completely suppressed (*Özdemir et al.,* 1993). The mildly oxidized grain rims would therefore show a Verwey transition at 95 K, the unaltered magnetite core of an oxidized grain depicts a Verwey transition at ~120 K, provided that the core of the grain is still large enough (SD-like).

8.3 Diagenetic alteration

The extent of the diagenetic zone (1.35 to 3.85 m) has primarily been delineated from variations of the fine-grained mineral components (ARM/IRM ratio; Fig. 4) as they are the most sensitive to diagenetic dissolution. Within this confined diagenetic interval the ferrimagnetic and also the antiferromagnetic iron oxide minerals have been drastically reduced in their total concentration, as illustrated by variations in volume magnetic susceptibility (κ), isothermal remanent magnetization (IRM) anhysteretic remanent magnetization (ARM) and hard isothermal magnetization (HIRM) (compare Fig. 2). About 85% of the ferrimagnetic and 54% of the antiferromagnetic components are lost within this diagenetic interval. Additionally, the increase in the Fe/κ ratio (Fig. 2f) depicts the combined effects of magnetic iron oxide dissolution and the concurrent precipitation of paramagnetic iron sulphides such as pyrite, which has been positively identified by SEM analyses (Fig. 5) and thermomagnetic measurements (Fig. 6).

In the diagenetic depth interval stoichiometric magnetite is still preserved as demonstrated by a single Verwey transition close to 120 K (Fig. 7; Fig. 8). The remarkable similarity of the ZFC and FC warming curves (Fig. 7) concurs with the findings of *Brachfeld et al.* (2001) holding PSD to MD grains responsible for this phenomenon.

The absence of the second transition at 95 K (Fig. 7c,d) can be explained by a further oxidation of the maghemite rim to a phase with an oxidation parameter $z > 0.3$. Although *Smirnov and Tarduno* (2000) stated that this process may also occur in the suboxic zone of marine sediments, this explanation seems rather implausible in this depth interval of strongly reducing

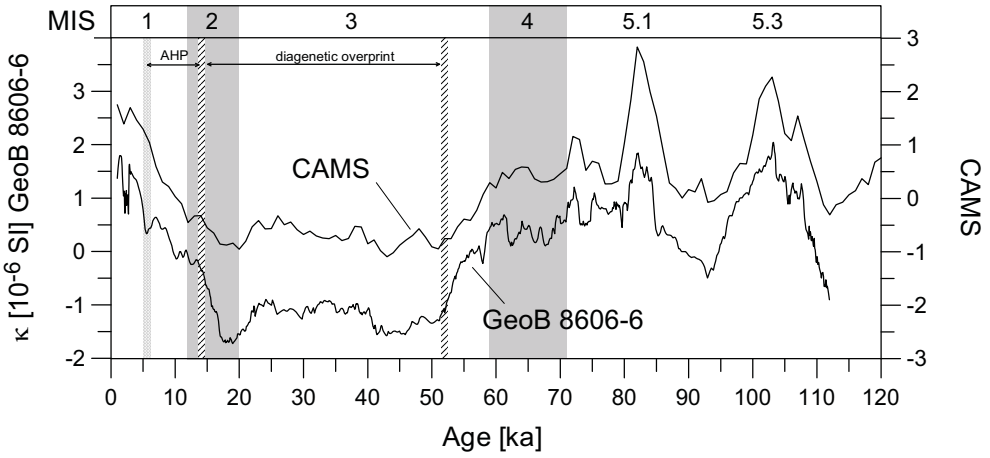

Fig. 9 Correlation of the magnetic susceptibility record of gravity core GeoB 8606-6 to the Canary Magnetic Susceptibility Stack (CAMS) (*Kuhlmann et al.,* 2004). Also shown are the marine oxygen isotope stages (MIS), grey shading indicates cold periods. Hatched horizontal bars mark the extent of the diagenetic zone identified from the rock magnetic parameters (cf. Fig 2 and Fig. 4). The dotted horizontal bar marks the end of the African Humid Period (AHP).

conditions. A more conceivable explanation is the progressive dissolution of these oxidized coatings. While very fine grains are most likely completely dissolved it seems plausible that for larger grains mainly the particle rim is dissolved, leaving the relatively unaltered magnetite core behind. The dissolution of the maghemite coatings may be further associated with a partial transformation into pyrite as reported by *Canfield and Berner* (1987). Thus, the inner magnetite core might be protected against progressive dissolution by a pyrite crust given that pyrite was clearly detected by Curie balance and also by SEM analyses on unconsolidated particle samples. However, for clear evidence a flat polished section of the sample would be needed.

No evidence for hematite was found in the low-temperature measurements, even though the relative concentration of high coercivity components increases notably from on average HIRM% =11 to HIRM% = 25 in the diagenetic zone. However, the presence of magnetite usually masks the signature of hematite when both phases are present in a sample because the saturation moment of MD magnetite is still greater than that of hematite at room temperature (*Thompson and Oldfield*, 1988).

The sediments above and below this specific horizon were found to be relatively unaltered by reductive dissolution processes. For the depth interval of enhanced magnetic mineral dissolution, a sudden change to higher biological productivity rates would be reasonable. Possibly an increased non-steady state accumulation rate and subsequent degradation of organic matter may be the reason for the identified geochemical zonation. This however is rather speculative and needs to be investigated in more detail.

8.4 Age model

An approximate age model was derived for gravity core GeoB 8606-6 by correlating its magnetic susceptibility record to the Canary Magnetic Susceptibility Stack (CAMS) (*Kuhlmann et al.,* 2004). CAMS is a magnetic susceptibility stack on the basis of five stratigraphic reference cores from that region (compare Fig. 1), for which a stratigraphic age model was derived from $\delta^{18}O$ and ^{14}C analyses on planktonic foraminifera. For this stack a generally enhanced productivity during glacial times with highest values during the deglaciation was observed.

Applying the CAMS age model to Site GeoB 8606, this study represents a quasi complete sequence of the last 5 marine oxygen isotope stages (MIS). The bottom of the core reaches an age of about 110 ka (Fig. 9). Hence the estimated sedimentation rate varies between about 3 to 16 cm/kyr with a mean value of 8 cm/kyr. The chronological uncertainty is relatively high, due to the difficulties to correlate the depth interval between 1.35 and 3.85 m to CAMS. To obtain an even more precise age model a multi-parameter correlation as described by *Hofmann et al*. (2005) would be required.

However, the confined diagenetically overprinted interval roughly starts at ~52 ka and lasts until ~14 ka, highlighted as hatched horizontal bars in Fig 9. No obvious correlation with an MIS transition is apparent for the lower diagenetic front. Interestingly, the decrease in κ starts already at the boundary of MIS 4/3. In contrast the upper diagenetic front corresponds roughly with the onset of the African Humid Period (AHP), the well-defined time interval between 14.8 and 5.5 cal. ka BP, which is characterized of generally low terrigenous influx. The depth of 60 cm (~5.85 ka) corresponds to the end of the African Humid Period (Fig 9, dotted line). The decrease in magnetic mineral content between ~0.60 m and ~1.35 m depth can thus be associated with the event of the AHP and not necessarily to a magnetic mineral dissolution as assumed earlier on (cf. 8.1).

8.5 Summary and Outlook

One of the most striking features noticed in the sediments from the upwelling region off NW Africa is certainly the depth dependent appearance of the double Verwey transition observed in the low-temperature measurements. While the transition at ~120 K was observed throughout the entire core, the transition at 95 K was not detected for the samples from the diagenetic zone. This depth dependent appearance of the Verwey transition at 95 K is interpreted as follows: The primary magnetic mineralogy of the sediments is dominated by nearly stoichiometric magnetite. The rims of the magnetite particles are oxidized to maghemite at the sediment/water interface, while pure magnetite still remains in the central part of the grain. As the chemical environment of the sediment turns into a reducing one, the maghemite rim is dissolved first, and the stoichiometric magnetite core remains present.

So far it has been assumed that the sediments from the upwelling region off NW Africa were affected too strongly by reductive diagenesis, so that the alteration of the primary magnetic signal does not allow for in particular palaeointensity studies. However, this study has shown that the magnetic signal in the sediments from this marginal region is only partially affected by reductive diagenesis. The overprint is restricted to a confined interval of the sediment section. The majority of the sediment sequence remains unaffected by dissolution effects and thus qualify for such delicate high temporal resolution investigations, as reported in the following chapter 6 (*Bleil and Dillon*, in press).

Acknowledgements

The author would like to thank T. Frederichs, D. Heslop and C. Franke for their technical assistance and helpful comments. High-temperature measurements and SEM analyses were carried out at the ´Fort Hoofdijk` and the EMU at Utrecht University (The Netherlands).

References

Balsam, W. L., B. L. Otto-Bliesner, and B. C. Deaton (1995), Modern and last glacial maximum eolian sedimentation patterns in the Atlantic Ocean interpreted from sediment iron oxide content, *Paleoceanography, 10,* 493-507.

Banerjee, S. K., C. P. Hunt, and X.-M. Liu (1993), Seperation of local signals from the regional paleomonsoon record of the Chinese

loess plateau: A rock-magnetic approach, *Geophys. Res. Lett., 20*, 843-846.

Bando, Y., M. Kiyama, N. Yamamoto, T. Takada, T. Shinjo, and H. Takaki (1965), The magnetic properties of α-Fe_2O_3 fine particles, *J. Phys. Soc. Jpn.* 20, p. 2086.

Bergametti, G., L. Gomes, G. Coude-Gaussen, P. Rognon, and M.-N. le Coustumer (1989), African dust observed over Canary Islands: Source-regions identification and transport pattern for some summer situations, *J. Geophys. Res., 94*, 14855-14864.

Bickert, T., H. Paulsen, and R. Tjallingii (2004), Lithologic core summary, in Bleil, U., and cruise participants, Report and preliminary results of Meteor Cruise M 58/2, Las Palmas – Las Palmas (Canary islands, Spain, 15.05 – 08.06.2003), Berichte, Fachbereich Geowissenschaften, Universität Bremen, 227, 20-64.

Bleil, U., and cruise participants (2004), Report and preliminary results of Meteor Cruise M 58/2, Las Palmas – Las Palmas (Canary islands, Spain, 15.05 – 08.06.2003), Berichte, Fachbereich Geowissenschaften, Universität Bremen, 227, 123 pp.

Bloemendal, J., J. W. King, F. R. Hall, and S.-J. Doh (1992), Rock magnetism of late Neogene and Pleistocene deep-sea sediments: relationship to source, diagenetic processes, and sediment lithology, *J. Geophys. Res., 97*, 4361-4375.

Brachfeld, S. A., S. K. Banerjee, Y. Guyodo, and G. D. Acton (2002), A 13200 year history of century to millennial-scale paleo-environmental change magnetically recorded in the Palmer Deep, western Antarctic Peninsula, *Earth Planet. Sci. Lett., 194*, 311-326.

Canfield, D. E., and R. A. Berner (1987), Dissolution and pyritization of magnetite in anoxic marine sediments, *Geochim. Cosmochim. Acta, 51*, 645-659.

Chiapello, I., G. Bergametti, L. Gomes, B. Chatenet, F. Dulac, J. Pimenta, and E. Santos Suares (1995), An additional low layer transport of Sahelian and Saharan dust over the North-Eastern Tropical Atlantic, *Geophys. Res. Lett., 22*, 3191-3194.

Claussen, M., C. Kubatzki, V. Brovkin, A. Ganopolski, P. Hoelzmann, and H.-J. Pachur (1999), Simulation of an abrupt change in Saharan vegetation in the mid-Holocene. *Geophys. Res. Lett., 26*,2037-2040.

Coey J. M. D. (1988), Magnetic properties of iron in soil iron oxides and clay minerals, in *Iron in soils and clay minerals*, edited by Stucki, J. W. et al., Reidel, Dordrecht.

Day, R., M. Fuller, and V. A. Schmidt (1977), Hysteresis properties of titanomagnetites: grain size and compositional dependence, *Phys. Earth Planet. Int., 13*, 260-267.

DeBoer, C. B. and M. J. Dekkers (1996), Grain-size dependence of the rock magnetic properties for a natural maghemite, *Geophys. Res. Lett., 23*, 2815-2818.

DeMenocal, P. B., J. Ortiz, T. Guilderson, and M. Sarnthein (2000), Coherent high- and low-latitude climate variability during the Holocene warm period, *Science, 288*, 2198-2202.

Dunlop, D. J. (2002), Theory and application of the Day plot (M_{rs}/M_s versus H_{cr}/H_c) 1. Theoretical curves and tests using titanomagnetite data, *J. Geophys. Res.*, *107*(B3), 2056, doi:10.1029/2001JB000486.

Franke, C., G. M. Pennock, M. R. Drury, R. Engelmann, D. Lattard, J. F. L. Garming, T. von Dobeneck, and M. J. Dekkers (2007a), Identification of magnetic Fe-Ti oxides in marine sediments by electron backscatter diffraction in scanning electron microscopy, Geophys. J. Int., 170, 545-555, doi:10.1111/j.1365-246X.2007.03489.x.

Franke, C., T. Frederichs, and M. J. Dekkers, (2007b), Efficiency of heavy liquid separation to concentrate magnetic particles, *Geophys. J. Int., 170(3)*, 1053-1066, doi: 10.1111/j.1365-246X.2007.03489.x.

Frederichs, T., T. von Dobeneck, U. Bleil, and M. J. Dekkers (2003), Towards the identification of siderite, rhodochrosite, and vivianite in sediments by their low-temperature magnetic properties, *Phys. Chem. Earth., 28*, 669-679.

Froelich, P. N., G. P. Klinkhammer, M. L. Bender, N. A. Luedtke, G. R. Heath, D. Cullen, P. Dauphin, D. Hammond, B. Hartmann, and V. Maynard (1979), Early oxidation of organic matter in pelagic sediments of the eastern equatorial Atlantic: suboxic diagenesis, *Geochim. Cosmochim. Acta, 43*, 1075-1090.

Funk, J. A., T. von Dobeneck, and A. Reitz (2004), Integrated rock magnetic and geochemical quantification of redoxomorphic iron mineral diagenesis in late Quaternary sediments from the

equatorial Atlantic, in *The South Atlantic in the Late Quaternary*, edited by G. Wefer et al., pp. 237-260, Springer-Verlag, Berlin, Heidelberg.

Goldstein, J. I., D. E. Newbury, P. Echlin, D. C. Joy, A. D. Romig Jr., C. E. Lyman, C. Fiori, and E. Lifshin (1992), *Scanning electron microscopy and X-ray microanalysis, 2nd edition*, 820 pp., Plenum Press., New York.

Hagen, E. (2001), Northwest African upwelling scenario, *Oceanol. Acta, 24*, 113-128.

Hilgenfeldt, K. (2000), Diagenetic dissolution of biogenic magnetite in surface sediments of the Beguela upwelling system, *Int. J. Earth Sci., 88*, 630-640.

Hofmann, D. I., K. Fabian, F. Schmieder, B. Donner, and U. Bleil (2005), A stratigraphic network across the Subtropical Front in the central South Atlantic: Multi-parameter correlation of magnetic susceptibility, density, X-ray fluorescence and d18O records, *Earth Planet. Sci. Lett., 240*, 694–709.

Holz, C., B. Stuut, Z. Finenko, and D. Larkin (2004), Terrigenous sedimentation along the continental margin off NW Africa: Implications from grain-size analyses of surface sediments, *Sedimentol., 51*, doi:10.1111/j.1365-3091.2004.00665.x.

Hsu, C. P. F., and J. M. Wallace (1976), The global distribution and annual and semiannual cacles in precipitation, *Monthly Weather Rev., 104*, 1093-1101.

Intergovernmental Oceanographic Comission (1994), GEBCO Digital Atlas [CD-ROM], Intergov. Oceanogr. Comm., Int. Hydrogr. Org., Birkenhead, U.K.

Jolly, D., S. P. Harrsion, B. Damnati, and R. Bonnefille (1998), Simulated climate and biomes of Africa during the late quaternary: Comparison with pollen and lake status data, *Quat. Sci. Rev., 17*, 629-657.

Kakol, Z., J. Sabol, A. Kozlowski, J. M. Honig (1994), Influence of titanium doping on the magnetocrystalline anisotropy of magnetite, *Phys. Rev. B, 49*, 12,767-12,772.

Karlin, R., and S. Levi (1983), Diagenesis of magnetic minerals in recent hemipelagic sediments, *Nature, 303*, 327-330.

Karlin, R., and S. Levi (1985), Geochemical and sedimentological control of the magnetic properties of hemipelagic sediments, *J. Geophys. Res., 90*, 10373-10392.

Kosterov, A. (2003), Low temperature magnetization and AC susceptibility of magnetite: effect of thermomagnetic history, *J. Geophys. Int., 154*, 58-71.

Kuhlmann, H., H. Meggers, T. Freudenthal, and G. Wefer (2004), The transition of the monsoonal and the N Atlantic climate system off NW Africa during the Holocene, *Geophys. Res. Lett., 31,* doi:10.1029/2004GL021267.

Leslie, B. W., S. P. Lund, and D. E. Hammond (1990a), Rock magnetic evidence for the dissolution and authigenic growth of magnetic minerals within anoxic marine sediments of the California continental borderland, *J. Geophys. Res., 95*, 4437-4452.

Liebermann, R. C., and S. K. Banerjee (1971), Magnetoelastic interactions in hematite—implications for geophysics, *J. Geophys. Res., 76*, 2735–2757.

Lloyd, G. E. (1985), Review of instrumentation, techniques and applications of SEM in mineralogy, in *Application of electron microscopy in Earth Sciences*, edited by J. C. White, pp. 151-188, Min. Ass. of Canada short courses, 11.

Lyle, M. (1983), The brown-green color transition in marine sediments, a marker of the Fe(III)-Fe(II) redox boundary, *Limnol. Oceanogr., 28*, 1018-1033.

Maher, B. A. (1988), Magnetic properties of some synthetic sub-micron magnetites, *J. Geophys. Res., 94*, 83-96.

Mayewski, P. A., L. D. Meeker, M. S. Twickler, S. Whitlow, Q. Yang, W. B. Lyons, and M. Prentice (1997), Major features and forcing of high-latitude northern hemisphere atmospheric circulation using a 110,000-year-long glaciochemical series, *J. Geophys. Res., 102*, 26345-26366.

Millman, J. D., and R. H. Meade (1983), World-wide delivery of river sediment to the oceans, *J. Geol., 91*, 1-21.

Mullender, T. A. T., A. J. van Velzen, and M. J. Dekkers (1993), Continuos drift correction and separate identification of ferrimagnetic and paramagnetic contributions in thermomagnetic runs, *Geophys. J. Int., 114*, 663-672.

Özdemir, Ö., D. J. Dunlop, and B. M. Moskowitz (1993), The effect of oxidation

on the Verwey transition in magnetite, *Geophys. Res. Lett., 20*, 1671-1674.

Passier, H. F., and M. J. Dekkers (2002), Iron oxide formation in the active oxidation front above sapropel S1 in the eastern Mediterranean Sea as derived from low-temperature magnetism, *Geophys. J. Int., 150*, 230-240.

Passier, H. F., G. J. De Lange, and M. J. Dekkers (2001), Magnetic properties and geochemistry of the active oxidation front of the youngest sapropel in the eastern Mediterranen Sea, *Geophys. J. Int., 145*, 604-614.

Petersen, N., T. von Dobeneck, and H. Vali (1986), Fossil bacterial magnetite in deep-sea sediments from the South Atlantic Ocean, *Nature, 320*, 611-615.

Prospero, J. M., (1990), Mineral-aerosol transport to the North Atlantic and North Pacific: The impact of African and Asian sources, in *The long-range atmospheric transport of natural and contaminant substances, Mathematical and Physical Sciences*, edited by A. H. Knap, Kluwer Academic Publishers, Dodrecht, pp.59-86.

Robinson, S. G., J. T. S. Sahota, and F. Oldfield (2000), Early diagenesis in North Atlantic abyssal plain sediments characterized by rock-magnetic and geochemical indices, *Mar. Geol., 163*, 77-107.

Röhl, U., and L. J. Abrams (2000), High-resolution downwhole and non-destructive core measurements from Sites 999 and 1001 in the Caribbean Sea: Application to the Late Paleocene thermal maximum, in *Proc ODP Sci. Results,* edited by R. M. Leckie et al., pp. 191-203, College Station, TX.

Sarnthein, M., J. Thiede, U. Pflaumann, H. Erlenkeuser, D. Fütterer, B. Koopmann, H. Lange, and E. Seibold (1982), Atmospheric and oceanic circulation patterns off Northwest Africa during the past 25 million years, In *Geology of the Northwest African Continental Margin*, edited by U. von Rad et al., pp. 545-604, Springer, Berlin, Heidelberg.

Smirnov, A. V., and J. Tarduno (2000), Low-temperature magnetic properties of pelagic sediments (Ocean Drilling Project Site 805C): Tracers of maghemitization and magnetic mineral reduction, *J. Geophys. Res., 105*, 16457-16471.

Stoner, J. S., J. E. T. Channell, and C. Hillaire-Marcel (1996), The magnetic signature of rapidly deposited detrital layers from the deep Labrador Sea: Relationship to North Atlantic Heinrich layers, *Paleoceanography, 11,* 309-325.

Stramma, L., and G. Siedler (1988), Seasonal changes in the North Atlantic Subtropical Gyre, *J. Geophys. Res.*, 93, 8111-8118.

Stuut, J.-B., M. Zabel, V. Ratmeyer, and P. Helmke (2005), Provenance of present-day eolian dust collected off NW Africa, *J. Geophys. Res., 110*, D04202, doi:10.1029/2004JD005161.

Thompson M., and F. Oldfield (1986), Environmental Magnetism, Allen & Unwin, London, pp. 1-227.

Torii, M. (1997), Low-temperature oxidation and subsequent downcore dissolution of magnetite in deap-see sediments, ODP Leg 161 (Western Mediterranean), *J. Geomag. Geoelectr., 49*, 1233-145.

Torres-Pádron, M. E., M. D. Gelado-Caballero, C. Collado-Sanchez, V. F. Siruela-Matos, P. J. Cardona-Castellano and J. J. Hernandez-Brito (2002), Variability of dust inputs to the CANIGO zone, *Deep-Sea Res., Part 2, Top. Stud. Oceanogr.,* 49, pp. 3455–3464.

Verwey, E. J. W. (1939), Electronic conduction of magnetite (Fe_3O_4) and its transition point at low temperatures, *Nature, 44*, 327-328.

von Dobeneck, T. (1996), A systematic analyses of natural magnetic mineral assemblages based on modelling hysteresis loops with coercivity-related hyperbolic basis functions, *Geophys. J. Int., 124*, 675-694.

Watkins, S. J., and B. M. Maher (2003), Magnetic characterisation of present-day deep-sea sediments and sources in the North Atlantic, *Earth Planet. Sci. Lett., 214*, 379-394.

Holocene Earth's magnetic field variations

recorded in marine sediments of the NW African continental margin

Abstract

Holocene records documenting variations in direction and intensity of the geomagnetic field during the last about seven and a half millennia are presented for Northwest Africa. High resolution paleomagnetic analyses of two marine sediment sequences recovered from around 900 meter water depth on the upper continental slope off Cape Ghir (30°51'N, 10°16'W) were supplemented by magnetic measurements characterizing composition, concentration, grain-size and coercivity of the magnetic mineral assemblage. Age control for the high sedimentation rate deposits (~60 cm/kyr) was established by AMS radiocarbon dates. The natural remanent magnetization (NRM) is very predominantly carried by a fine grained, mostly single domain (titano-)magnetite fraction allowing the reliable definition of stable NRM inclinations and declinations from alternating field demagnetization and principal component analysis. Predictions of the *Korte and Constable* (*2005*) geomagnetic field model CALS7K.2 for the study area are in fair agreement with the Holocene directional records for the most parts, yet noticeable differences exist in some intervals. The magnetic mineral inventory of the sediments reveals various climate controlled variations, specifically in concentration and grain-size. A very strong impact had the mid-Holocene environmental change from humid to arid conditions on the African continent which also clearly affects relative paleointensity (RPI) estimates based on different remanence normalizers. To overcome this problem the pseudo-Thellier RPI technique has been applied. The results represent the first Holocene record of Earth's magnetic field intensity variations in the NW Africa region. It displays long term trends similar to those of model predictions, but also conspicuous millennium scale differences.

This chapter is an article in press: Bleil U. and Dillon, M., 2008, Holocene Earth´s magnetic field variations recorded in marine sediments of NW African continental margin, *Studia Geophysica & Geodaetica*.

Introduction

Major progress has been made in recent years to unravel the Holocene history of the Earth's magnetic field. In particular, novel high resolution records of intensity variations were reported from archeomagnetic studies as well as analyses of lake and marine sedimentary series.

With new results obtained from French potteries (*Genevey and Gallet, 2002; Gallet et al., 2005*), complemented by older data sets, archeointensity is now documented in fair detail for the last about 3,000 years in Western Europe. In Eastern Europe, where this was already achieved earlier (see e.g., *Valet, 2003* for a comprehensive review), secular variation of the geomagnetic intensity has been determined for the last approximately eight millennia in several regions by archeomagnetic investigations (*Genevey et al., 2003* and references therein). Holocene archeointensity records comprising similar long periods of time were recently also presented for Central Asia (*Nachasova and Burakov, 2000*) and the Middle East (*Genevey et al., 2003*).

Relative paleointensity (RPI) derived from a number of annually laminated Swedish and Finnish lake sediment sequences has been summarized in a stack for Fennoscandia extending over the last about 10,000 years (*Snowball et al., 2007* and references therein). As noted by various authors (e.g., *Genevey et al*., *2003; Snowball and Sandgren, 2004*), a collective evaluation of these data sets suggests that prominent changes and long term trends in Earth's magnetic field intensity occur synchronously over Western Europe, the Middle East and Central Asia, i.e., an area of some 60° of longitude and 30° of latitude. The Scandinavian intensity stack also compares favorably with the geomagnetic field model of *Korte and Constable (2005)* for millennial scale characteristics. However, at higher frequency sub-millennial scale variations, quite clear differences are observed. The agreement between model predictions and respective Fennoscandian Holocene stacks of declination and inclination overall appears not very convincing.

Very high resolution Holocene RPI records reported for sediment series from the St. Lawrence Estuary (Eastern Canada) are broadly consistent in shape and amplitude with several United States lake sediment data sets (*St-Onge et al., 2003* and references therein) for the last about 3,700 years. In detail, multiple discrepancies exist and older sections display no coherent trends. The most prominent feature in worldwide Holocene paleointensity, a maximum between 3,000 and 2,000 before present, is clearly recognized both in North America and Eurasia as well as in global absolute paleointensity compilations (e.g., *Yang et al., 2000*).

Holocene geomagnetic intensity variations essentially still remain inadequately constrained due to various intrinsic limitations. Archeomagnetic studies are likely to produce the most reliable data. Yet, they are of course regionally and temporally much too restricted to ever provide a sufficiently detailed global coverage. Precise enough dating of natural materials has always been problematic. This is particularly true for volcanic rocks which, because of their irregular mode of formation, typically yield highly discontinuous records. On the other hand, as with the artifacts used for archeointensity determinations, volcanic rocks carry a well defined magnetic signal from which, at least in principle, paleointensity can reliably be reconstructed. For sedimentary deposits typically just the opposite situation is encountered. While appropriate age control can often be achieved for continuous and high accumulation rate sediment sequences, the fidelity of their magnetic signal is regularly disputed. So far, there is no technique available to determine absolute paleointensities from sedimentary deposits and critical problems arise from the fact that processes leading to the acquisition and preservation of a natural remanent magnetization in sediments are still poorly understood. Hence, there is always the question whether RPIs represent true paleofield behavior or are partially influenced, in worse case scenarios even totally controlled, by environmental factors during and after sediment deposition.

Despite these well known severe restrictions a lot more RPI records are required especially from the marine realm to attain increasingly improved information about the past Earth's magnetic field on a global scale. The present study is to contribute to this goal with new high resolution Holocene RPI data from the so far unstudied NW Africa region.

Study Area

General Setting

An intense marine productivity combined with large amounts of terrigenous material delivered from the continent result in high sedimentation rates at the NW African

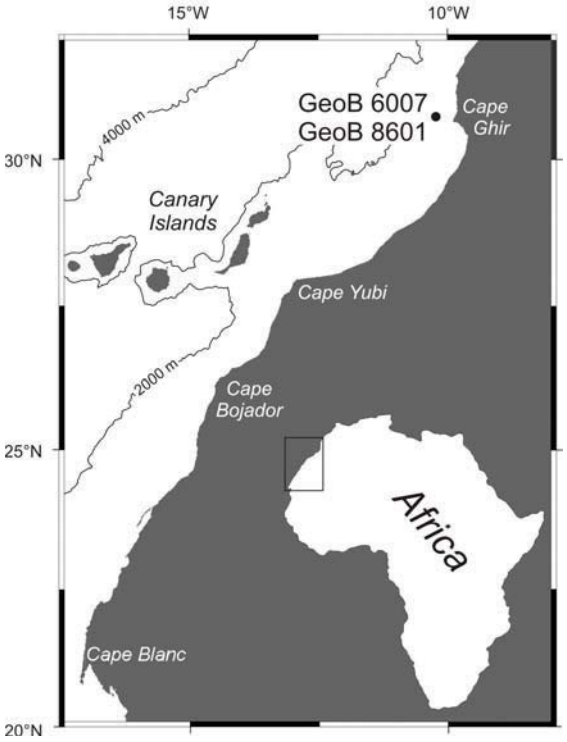

Fig. 1 Study area with coring sites GeoB 6007 and GeoB 8601 in around 900 m water depth at the upper NW African continental slope off Cape Ghir.

continental margin (*Kuhlmann et al.,2004a*). Trade wind induced upwelling near the coast controls the primary marine productivity which is transported by filaments to the open ocean at cape locations. The elevated flux of organic matter thus reaching the ocean floor is potentially important for the sediment magnetization through two different processes. First, it substantially improves the living conditions of magnetotactic bacteria (*Petermann and Bleil, 1993*), but on the other hand may cause diagenetic alteration which can severely affect the sediment magnetic mineral assemblage. The supply of terrigenous material to the NW African continental slope, the main source of magnetic minerals, was subject to several distinct changes during Holocene times. Most significant was the environmental turnover from the early Holocene 'African Humid Period' (*deMenocal et al., 2000*) to the late Holocene arid conditions about 5,000 years ago (*Claussen et al., 1999*).

Sampling Sites

The two investigated sediment sequences were recovered with gravity cores (GeoB 6007; 30°51.0'N, 10°16.1'W; water depth 900 m (*Neuer et al., 2000*) and GeoB 8601; 30°50.9'N, 10°16.1'W; water depth 921 m (*Bleil et al., 2004*)) on the upper NW African continental slope, just north of the Agadir Canyon and west of Cape Ghir (Fig. 1, see *Weaver et al.*, 2000 for a detailed physiographic map of the NW African continental margin). The hemipelagic deposits consist of olive brown to, in the deeper layers, dark greenish grey, homogeneous fine grained nannofossil clay with small quantities of foraminifera shells and quartz grains.

Although the coring locations were directly adjacent to each other, the sediment series retrieved had remarkably different lengths, around 11 and 8 m, respectively (Fig. 2). As indicated by the magnetic susceptibility profiles and confirmed by visual inspection, the core GeoB 8601 sequence is disrupted at about 680 cm depth. Most likely, the gap results from an incomplete recovery. For the paleomagnetic analyses this drawback had no consequences, however, because it turned out that below about 480 cm depth the sediments of both cores are strongly affected by diagenetic alteration (Fig. 2) making them a poor choice for RPI studies.

The intense down slope transport within the Agadir Canyon system provides large amounts of suspended material which deposits on its levees. The hemipelagic sediments of core GeoB 6007 thus allowed to document the Holocene terrigenous influx at a high time resolution (*Kuhlmann et al., 2004b*). At around 8,500 years before present (in the following all ages are reported as calendar years before present, cal. yrs B.P.), a significant change in sedimentation rate (Fig. 2) and periodicity of the terrigenous signal occurred. Further south, the continental mid-Holocene climate and vegetation transition

(*Claussen et al., 1999*) is very clearly reflected in sediment characteristics, such as a rapid increase of eolian terrigenous input at the open ocean ODP Site 658 (21°N off Cape Blanc; *deMenocal et* al., 2000) or a similar drastic decrease of fluvial terrigenous input closer to the coast (27°N off Cape Yubi; *Kuhlmann et al., 2004b*). In the study area at 31°N these shifts appear to be more gradual and a periodic oscillation of about 900 years controls the Holocene terrigenous input since around 8,500 cal. yrs B.P (*Kuhlmann et al., 2004b*). These findings are interpreted as indicating a strong influence of the N Atlantic climate system to at least the Cape Ghir region, whereas at lower latitudes the W African monsoonal system predominates and causes a major abrupt change of terrigenous discharge in mid-Holocene times.

Age Control

Age control for the sediment series of core GeoB 6007 was established by 18 Accelerator Mass Spectroscopy (AMS) radiocarbon dates (*Kuhlmann et al., 2004b*). As no precise reservoir correction is available for the study area, ^{14}C dates have been converted to calendar years assuming a moderate estimate of 400 years reservoir time (*Stuiver et al., 1998*). On the basis of these data two distinct depositional regimes can be distinguished during the Holocene. High average sedimentation rates of ~ 170 cm/kyr in the earlier part of the sequences rapidly decreased to ~ 60 cm/kyr at around 8,500 cal. yrs B.P. (Fig. 2). Extrapolations yield ages of ~ 50 cal. yrs B.P. for the surface layer and ~ 12,800 cal. yrs B.P. for the sediments at the base of GeoB 6007.

For the upper 5 m, where the magnetic mineral inventory is unaltered by diagentic processes, the age model of core GeoB 6007 was transferred to the core GeoB 8601 sediments by visually matching distinct peaks and troughs in both high resolution (1 cm spacing) magnetic susceptibility profiles (23 tie points; Fig. 3). Their depth positions typically agree within less than 10 cm. Maximum differences in the age-depth succession amount to about 250 years.

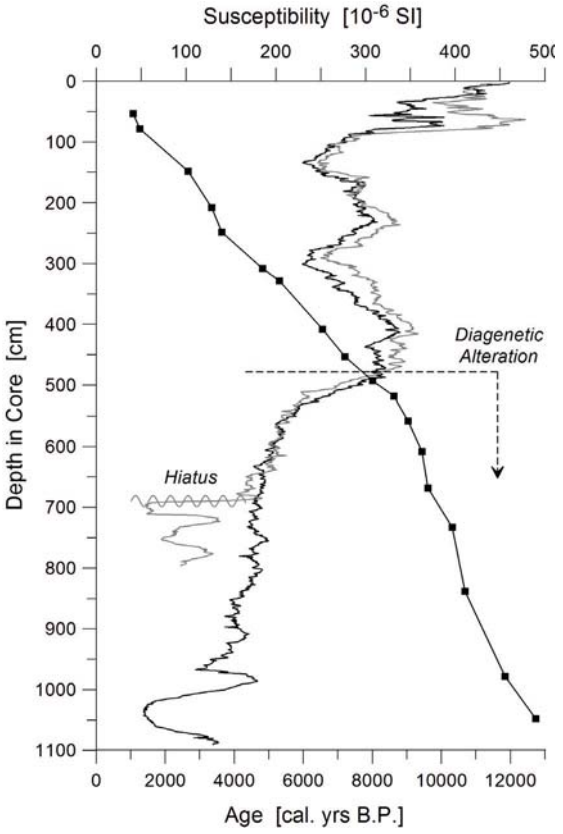

Fig. 2 High resolution (1 cm spacing) magnetic susceptibility profiles of cores GeoB 6007 (black) and GeoB 8601 (grey) together with the age succession (calendar years before present; 0 referring to AD 1950) in core GeoB 6007 (full squares) based on AMS radiocarbon data (*Kuhlmann et al., 2004b*). Note the hiatus at about 680 cm depth in core GeoB 8601, presumably originating from the coring process, and the iron redox diagenetic front at around 480 cm which systematically affects the magnetic mineral assemblage in both cores.

Data Acquisition

Paleomagnetic Analysis

Paleomagnetic measurements were performed on cube specimens (6.2 cm^3) sampled on average at 5 cm depth intervals. Incremental triaxial alternating field demagnetization (15 steps to a maximum alternating field of 100 mT) and

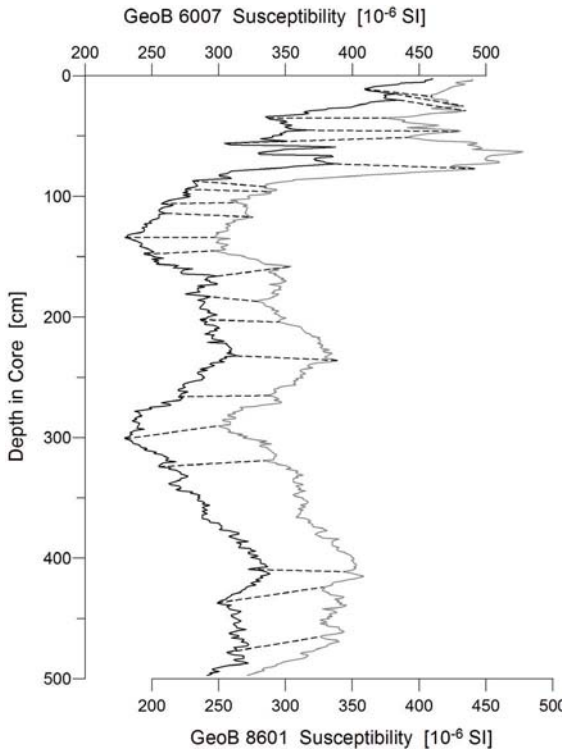

Fig. 3 Susceptibility correlation scheme (23 tie points) applied to transfer the core GeoB 6007 (black) age model to core GeoB 8601 (grey). Note that the core GeoB 8601 susceptibility scale has been shifted by 50 units to improve clarity.

principal component analysis (*Kirschvink, 1980*) have been applied to determine the characteristic stable inclinations and declinations of the natural remanent magnetization (NRM).

Sediment Magnetic Measurements

Magnetic volume susceptibility κ was determined with a *Geofyzica Kappabridge* KLY-2 supplementing quasi continuous κ logs recorded with a *Bartington* MS2F spot sensor on the split core halves (Figs. 2 and 3). Acquisition of anhysteretic remanent magnetization (ARM), imparted by superimposing gradually decaying alternating fields (the same 15 steps scheme to a maximum of 100 mT as used for NRM demagnetization) on a constant biasing field of 40 μT, and saturation isothermal remanent magnetization (SIRM) in 18 steps to 0.3 T was followed by incremental triaxial SIRM and ARM alternating field demagnetization (again 15 steps to maximum fields of 100 mT). All magnetizations have been measured on a *2G Enterprises* 755R DC SQUID cryogenic magnetometer system, the various fields were generated with its build-in facilities. Diagnostic sediment magnetic parameters deduced from the laboratory remanences, include the median acquisition fields MAF_{SIRM} and MAF_{ARM} and the median destructive fields MDF_{SIRM} and MDF_{ARM}. To estimate high coercitivity antiferromagnetic hematite and goethite mineral concentrations, 2.5 T hard isothermal remanent magnetizations, HIRM (*Stoner et al., 1996*) were imparted with a pulse magnetizer and subsequently 300 mT backfields applied. A complete environmetal magnetism evaluation of the sediment magnetic data sets, particularly in view of alteration phenomena, will be given elsewhere (*Dillon et al., manuscript in preparation, 2007*).

Sediment Magnetic Characteristics

Concentration

With the experimental setting selected, saturation isothermal remanent magnetization primarily quantifies total concentration of ferrimagnetic (titano-)magnetite, anhysteretic remanent magnetization its finer grained fractions. Hard isothermal remanent magnetization imparted at 2.5 T (not shown) is overall fairly constant. As a rough estimate, on average %HIRM ˜ 10 indicate that concentrations of high coercivity antiferromagnetic components (hematite and goethite) are at least equal, most likely higher than those of magnetite. This complies with results reported for surface sediments from the working area (*Watkins and Maher, 2003*), but much lower HIRM were found in turbidites from the NW African continental slope (*Robinson et al., 2000*).

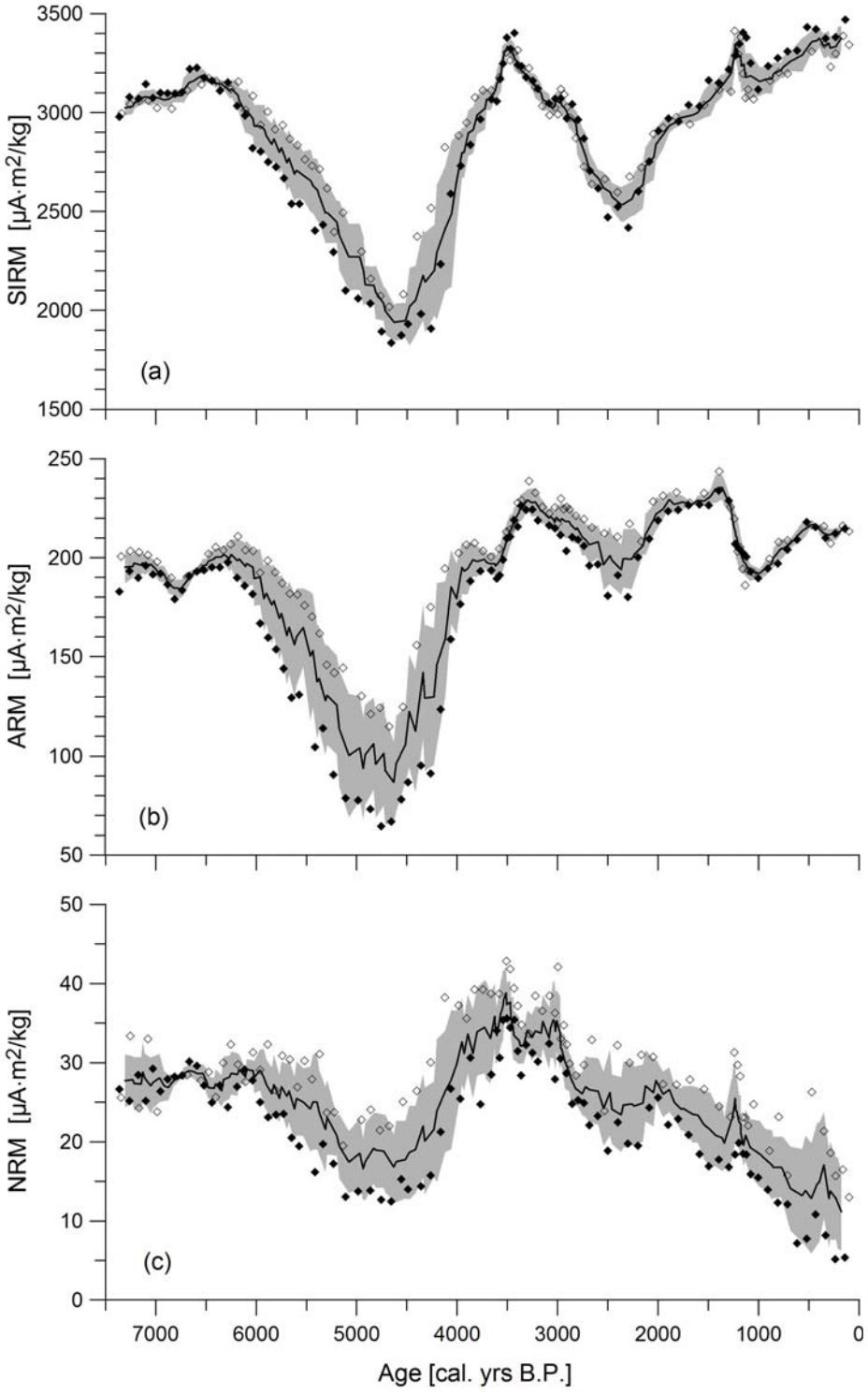

Fig. 4 Saturation remanent magnetization, SIRM (a), anhysteretic remanent magnetization, ARM (b), and natural remanent magnetization, NRM (c) of cores GeoB 6007 (full diamonds) and GeoB 8601 (open diamonds) as function of age. Black lines denote 150 year running window averages, grey shading ± one standard deviation.

SIRM (Fig. 4a) and ARM (Fig. 4b) exhibit distinct, closely related (Pearson's r = 0.83) temporal variations. The outstanding feature, a prominent minimum between about 6,000 and 4,000 cal. yrs B.P., is evidently associated with the environmental shift from the early Holocene humid period to late Holocene arid conditions on the African continent. However, the striking decrease of magnetic mineral concentrations rather resembles the pattern of total terrigenous material transport to the ocean in more southern regions of the African continental margin than that observed at the actual coring site *(Kuhlmann et al., 2004b)*. Also different from the total terrigenous fluxes, magnetic mineral accumulation declines slightly earlier and then remarkably returns to about its previous level. The drastic reduction in the amount of magnetic minerals has the strongest impact clearly on the fine grained components and also influences NRM intensity (Fig. 4c). The observed change should essentially reflect a transition from predominant fluvial to eolian discharge. A possible scenario to explain the minimum in magnetic mineral concentrations during the transition could be a relatively rapid closure of the fluvial drainage systems, while the vegetation in the hinterland diminished much more gradual. The wind systems that prevail to the present day hence became fully effective only over a prolonged time span, at least as the transport mode for magnetic minerals. Similar proportions of fine grained and bulk (titano-)magnetite concentrations before and after the transition may hint at persistent source characteristics of the magnetic mineral inventory. Both SIRM and ARM also show a number of minor fluctuations. However, spectral analyses (not shown) revealed no statistically significant periodicities, particularly, the about 900 year oscillations observed for the Holocene terrigenous influx at the coring site *(Kuhlmann et al., 2004b)* could not be detected in any of the sediment magnetic attributes.

Despite the discussed major shifts, the variations in magnetic remanences are still well within the limits of acceptance for sediment paleointensity studies as noted by *King et al. (1983)* and *Tauxe (1993)*.

Over large parts of the records, and most clearly manifest in the 6,000 to 4,000 cal. yrs B.P. interval of reduced intensities, ARM is systematically higher in core GeoB 8601 than in core GeoB 6007 sediments, on average ~10%. For SIRM respective differences are much smaller, on average ~2%, and essentially confined to the low intensity period. As the cores were recovered from neighboring sites, the local depositional regime must be responsible for this bias in magnetic mineral distribution. Most likely, strong gradients in bottom water velocity, which are typical in continental slope environments, have caused an elevated accumulation especially of finer grained (titano-)magnetite at site GeoB 8601. Support for this assumption comes from the fact that NRM intensities, which mostly reside in this mineral fraction, are higher at site GeoB 8601 by on average ~30% (Fig. 4c). Between about 7,500 and 3,000 cal. yrs B.P. NRM intensities display the same relative variations as ARM and SIRM. In the youngest part NRM systematically decreases, a trend which has no parallel in ARM or SIRM. Another interesting observation is the noticeable contrast between ARM and NRM intensities. While they reach about the same level in Scandinavian lake deposits (*Snowball and Sandgren, 2004*), ARM/NRM ratios > 5 in cores GeoB 6007 and GeoB 8601 (Fig. 5a) are quite typical for most marine sediments. ARM/NRM ratios are quite stable with a mean of 7.5 in the deeper parts of both cores, but highly variable in the upper layers with an average of about 20 and a trend to increase toward the tops. It appears that progressively less of the fine grained magnetic mineral fractions actually contribute to the natural remanence in sediments younger than about 1,000 cal. yrs B.P., because they are above the lock-in depth.

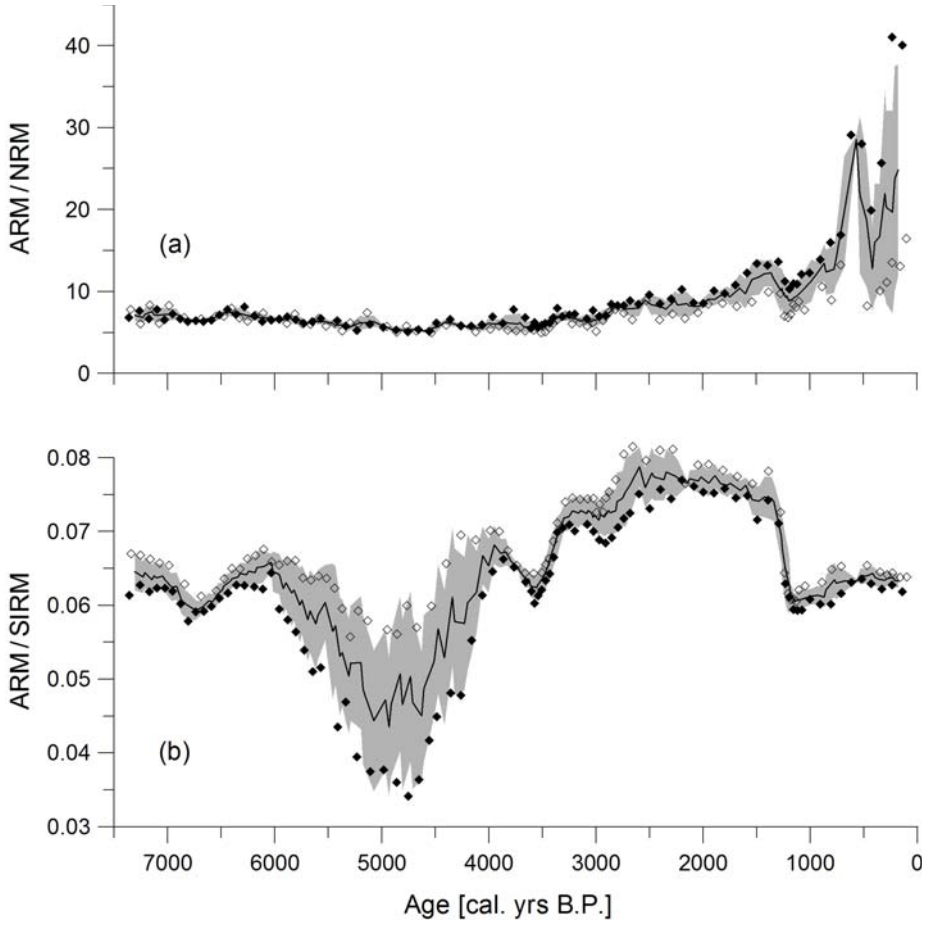

Fig. 5 ARM/NRM ratio (a) estimating the fraction of fine grained (titano-)magnetite which contributes to the natural remanence and granulometric ARM/SIRM ratio (b) of cores GeoB 6007 (full diamonds) and GeoB 8601 (open diamonds) as function of age. Black lines denote 150 year running window averages, grey shading ± one standard deviation.

Grain Size and Coercivity

Granulometric ARM/SIRM ratios > 0.05 document single-domain (SD) magnetite grain-sizes < 0.1 µm (*Maher, 1988*). Core GeoB 8601 sediments exclusively fall into this range (Fig. 5b). Consistently lower ARM/SIRM ratios (on average ~10%) of core GeoB 6007 sediments indicate markedly coarser grain-sizes. However, only in the interval around 5,000 cal. yrs B.P. do pseudo-single-domain states dominate. Grain-sizes show mostly similar temporal variations as remanent magnetizations. As expected, a significant correlation exists between ARM intensities and ARM/SIRM ratios (r = 0.85).

Median destructive fields of SIRM (Fig. 6a) and ARM (Fig. 6b) display minor variabilities. In the 6,000 and 4,000 cal. yrs B.P. interval small reductions in magnetic stability are observed, slightly more pronounced is a step like decrease at around 1,200 cal. yrs B.P. which also appears in the granulometric ARM/SIRM ratio (Fig. 5b). Mean MDF_{SIRM} (23.3 ± 1.8 and 23.8 ± 2.1 mT) and mean MDF_{ARM} (33.9 ± 1.8 and 36.0 ± 2.4 mT) in core GeoB 8601 and GeoB 6007, respectively, confirm overall quite uniform coercivities. Though small, the MDF differences between the cores are remarkable as they do not simply conform to the grain-size data (Fig. 5b) which clearly hint at on average coarser magnetic minerals in the core GeoB 6007 sediments. These estimates apparently do not represent approximately normal grain-size distributions. Relatively higher concentrations towards the coarse ends of the mineral spectra carrying SIRM and

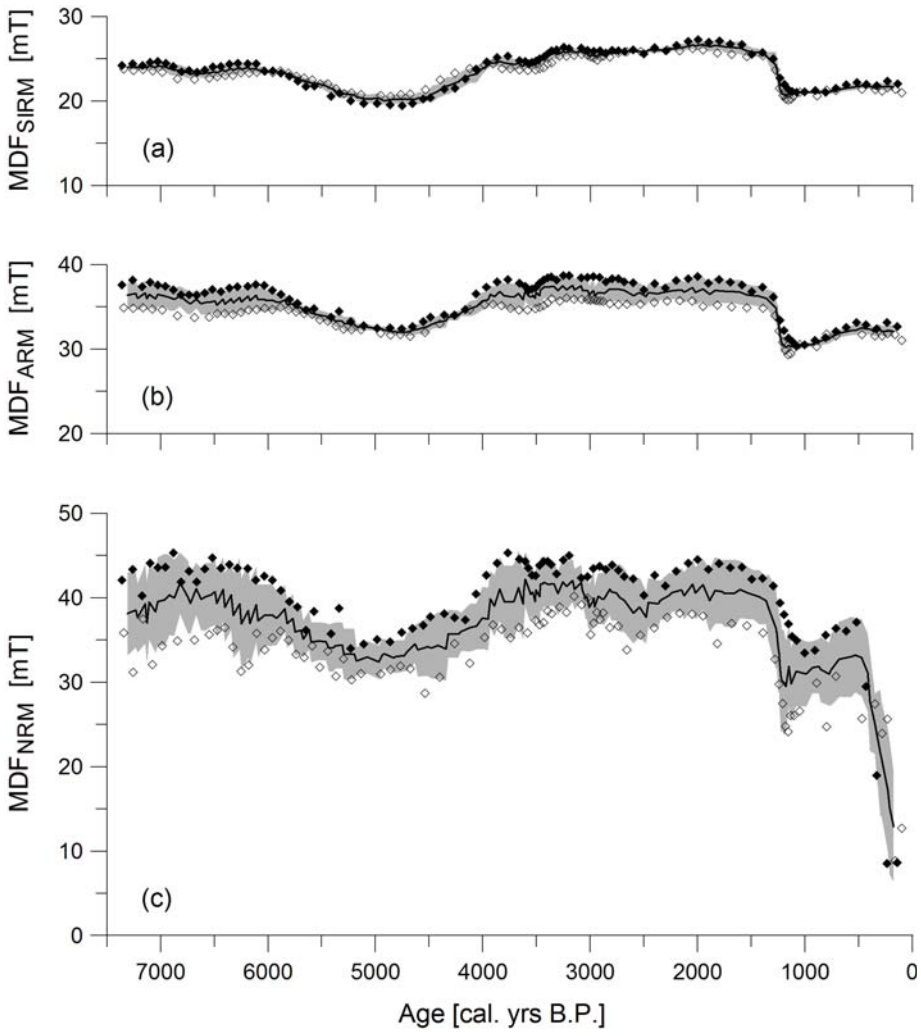

Fig. 6 Cores GeoB 6007 (full diamonds) and GeoB 8601 (open diamonds) median destructive fields of SIRM (a), ARM (b), and NRM (c) AF demagnetization as function of age. Black lines denote 150 year running window averages, grey shading ± one standard deviation.

ARM could reduce the median destructive fields in core GeoB 8601. As discussed above for the differences in magnetic mineral concentrations between both cores, the discrepancies most probably result from local gradients in bottom water activity.

Not including the upper parts younger than about 500 cal. yrs B.P., median destructive fields of NRM (Fig. 6c) and ARM yield identical means of 34.1 mT in core GeoB 8601. In core GeoB 6007 MDF_{NRM} (41.1 mT) is on average even higher than MDF_{ARM} (36.2 mT). $MDF_{NRM} < MDF_{SIRM}$ observed for the very young sediments indicate that coarse grained minerals substantially contribute to the depositional remanence (DRM), whereas processes leading to the acquisition of a post-depositional remanence (PDRM) are not yet completed, i.e. the lock-in zone extends to a deeper depth. Both the ARM/NRM ratios (Fig. 5a) and median destructive fields of NRM (Fig. 6c) hint at variable lock-in depths in the core GeoB 6007 and GeoB 8601 sediments. Of course, coring induced disturbances could considerably reduce the preservation of the NRM record in the top sections of the cores.

In summary, sediment magnetic characteristics demonstrate that the magnetic mineral inventory is dominated by fine grained (titano-)magnetite fractions which, except for the uppermost layers,

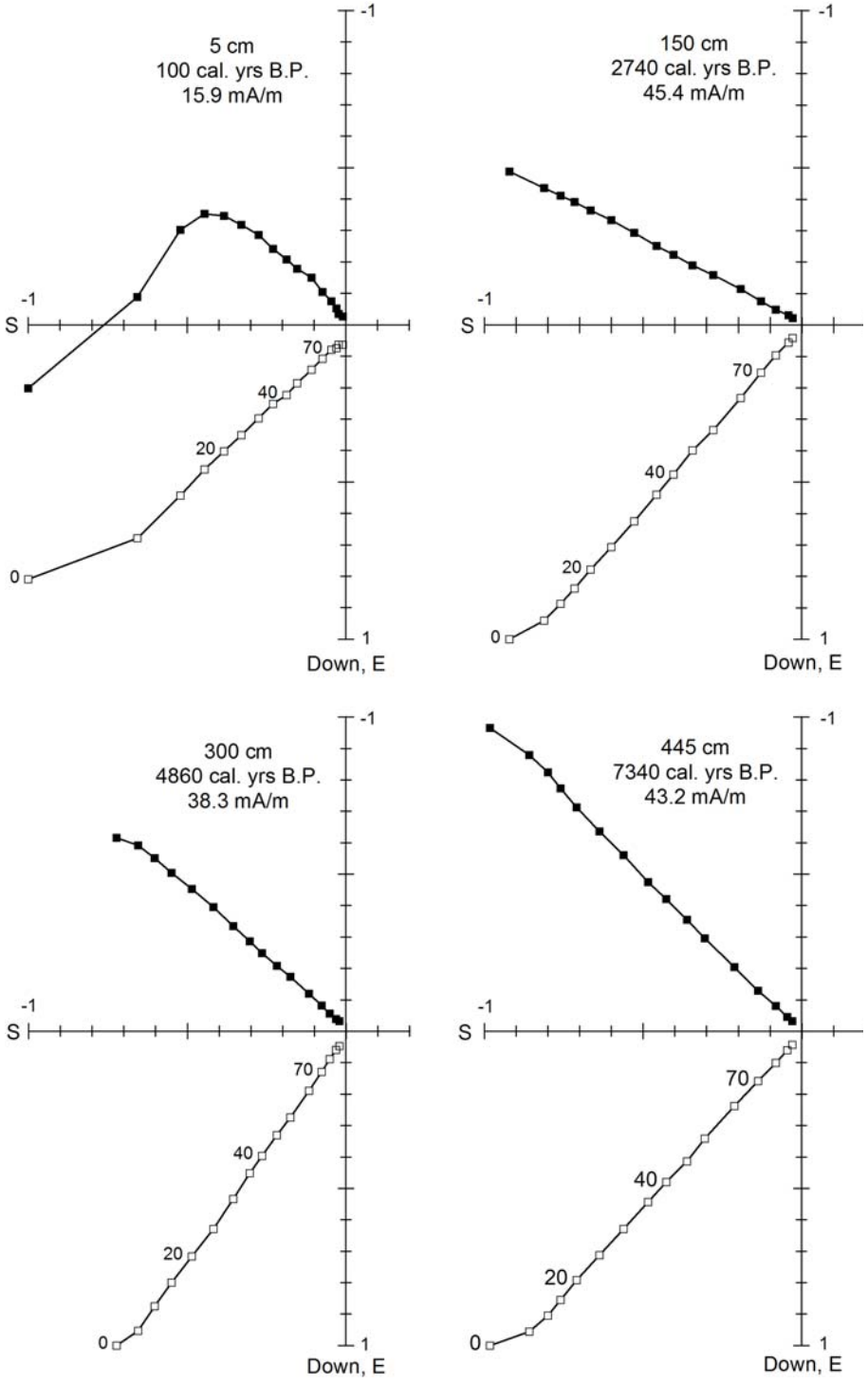

Fig. 7 Orthogonal diagrams illustrating typical AF demagnetization results of core GeoB 8601 natural remanent magnetizations. Full and open squares represent NRM projections onto horizontal and vertical planes, respectively, accompanying numbers are AF amplitudes in mT. Intensities are normalized. Initial NRM intensity is specified together with depth position and age for each sample. Note that declinations are uncorrected.

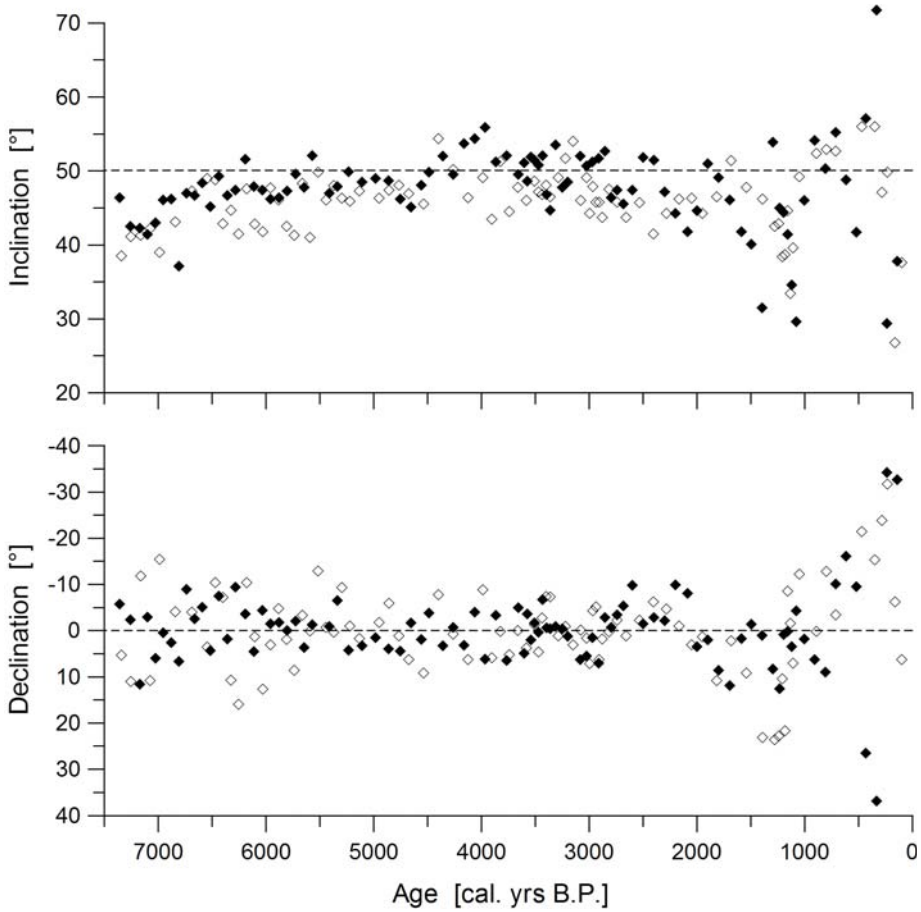

Fig. 8a ChRM inclinations and declinations of core GeoB 6007 (full diamonds) and GeoB 8601 (open diamonds) sediments as function of age. Broken lines denote geomagnetic axial dipole (GAD) directions. Core means of original relative declinations (Fig. 7) have been rotated to zero assuming that the record is long enough to represent the GAD declination.

carry natural remanent magnetizations of high stability. On the other hand, all bulk magnetic attributes show considerable variations during Holocene and in addition, noticeable discrepancies exist between the sediment series recovered from directly adjacent sites. Hence there is no doubt that regional and also local environmental factors had a strong impact on the magnetic mineral assemblages.

NW African Holocene Earth' Magnetic Field Variations

Directional Record

Typical AF demagnetization characteristics of the sediments are illustrated in Figure 7. Minor spurious components, which possibly result from the coring process or subsequent handling and storage of the samples, could mostly be removed by 10 mT AF fields. Only in the uppermost layers of the sediment columns somewhat higher fields (≥ 20 mT) were necessary to isolate stable single component inclinations and declinations. After 100 mT AF demagnetization on average about 5% of the initial NRM remain. Despite relatively high concentrations, hematite (and/or goethite) is thus of subordinate importance as carrier of the natural remanent magnetization in the core GeoB 6007 and GeoB 8601 sediments. Remarkably uniform directions up to high AF levels (Fig. 7) indicate that hematite and magnetite fractions demagnetized to 100 mT essentially contain the same paleomagnetic information. The high directional stability generally corresponds to high NRM median destructive fields

(Fig. 6). Even for the sediments younger than about 500 cal. yrs B.P. with low NRM_{MDF} in both cores, characteristic remanent magnetization (ChRM) directions could reliably be determined. Mostly five or more demagnetization steps were used for principal component analysis, giving maximum angular deviations of typically <2°.

Holocene variations of ChRM declinations and inclinations are shown in Figure 8a. There are no persistent disparities between the directional data of both cores. Original declinations (Fig. 7) refer to a continuous straight line along which the core liner segments were cut into archive and working halves. Core means of these data have been rotated to zero assuming that the record is long enough to represent the geomagnetic axial dipole (GAD) declination. This premise should be essentially justified as inclination averages of both cores agree to GAD inclination for the coring sites (50.1°) within one standard deviation of the mean. Applying a 150 year running window average to the combined data sets of both cores yields the final paleomagnetic result (Fig. 8b).

Both our record and the model prediction of *Korte and Constable* (*2005*) for the study area show relatively constant declinations within ±10° of GAD declination between about 7,000 and 2,000 cal. yrs B.P.. As there are no confidence limits available for the model results, possible disagreements in minor details are not sufficiently documented. The paleomagnetic data indicate considerably higher variations in declination since about 2,000 cal. yrs B.P. which largely do not conform to the model predictions. However, there may be undetected coring disturbances in the top parts and for the last millennium our age model is of limited resolution. These restrictions also apply to the inclination record which not only during this interval but for most of the last 7,000 cal. yrs B.P. considerably disagrees with the paleofield model. In particular, the model trend towards much shallower inclinations before about 5,000 cal. yrs B.P. is not confirmed by our data set. Such a comparison has to consider that the model evaluation could not yet rely on actual data of the study area, but had to be extrapolated from distant neighboring regions.

Relative Paleointensity Records

Relative paleointensity estimates of the geomagnetic field from sedimentary records are mostly based on ratios of the natural remanent magnetization and a normalizer which should quantify the magnetizability of the sediment sequence. Ideally, normalization should employ the magnetizability of the NRM acquisition process, but this is not achievable in reality. ARM, SIRM (IRM) and susceptibility which are generally used as normalizers all have their specific limitations (*King et al., 1983; Tauxe, 1993*). To discard viscous and other spurious magnetization components of relatively low magnetic stability, *Levi and Banerjee* (*1976*) have proposed to derive RPI estimates from NRM and also ARM and SIRM (IRM) after AF demagnetization to some tens of mT. This method has since become common praxis.

According to the AF demagnetization characteristics of NRM directions (Fig. 7) we have chosen the 20 mT level to quantify RPI estimates. Figure 9 shows the NRM_{20mT}/ARM_{20mT} and $NRM_{20mT}/SIRM_{20mT}$ results as 150 year running window averages combining the core GeoB 6007 and GeoB 8601 data. A close agreement between RPI records using ARM, SIRM (IRM) or susceptibility for normalization has been proposed as an indispensable prerequisite of reliable sediment relative paleointensities (*King et al., 1983; Tauxe, 1993; Lund and Schwartz, 1999*). On the other hand, even a perfect match will not prove that the past geomagnetic field intensity has been correctly determined. Although closely correlated ($r = 0.90$), our NW African records do not adequately meet the criterion of uniformity. Taking

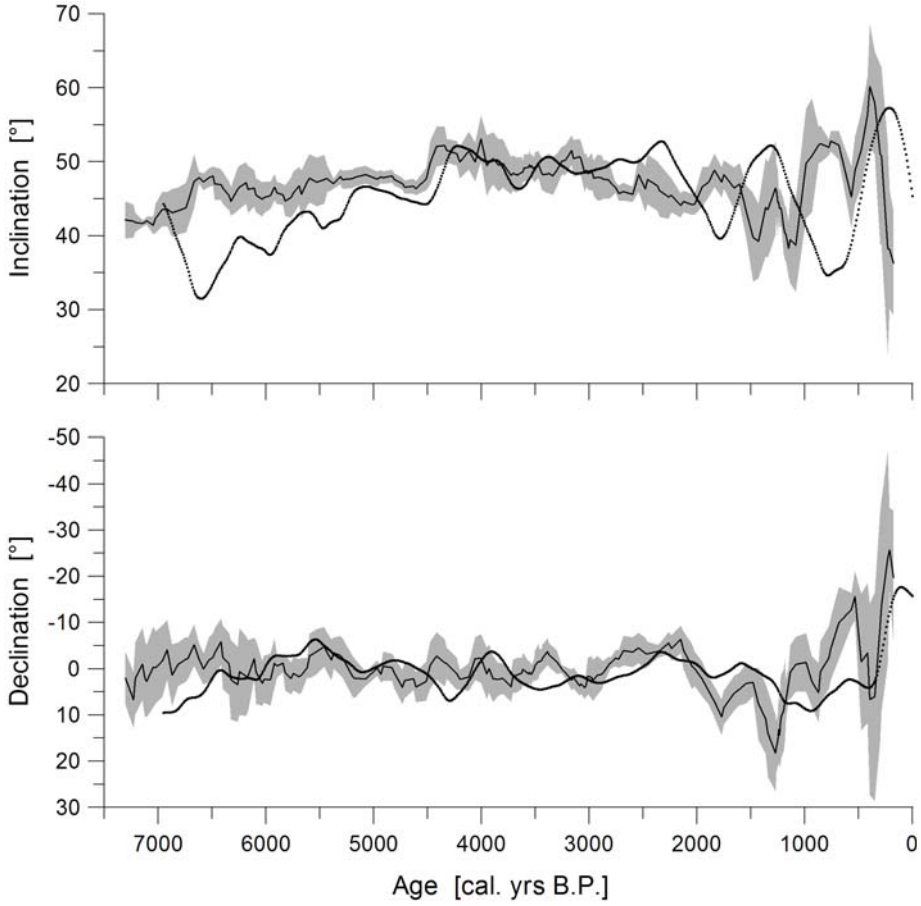

Fig. 8b 150 year running window averages combining core GeoB 6007 and GeoB 8601 ChRM declination and inclination data shown in Figure 8a (black line). Grey shading denotes 95% confidence limits. Dotted lines show the CALS7K.2 model predictions of *Korte and Constable* (*2005*) for the study area at 10 year resolution.

the 95% confidence limits into account, significant discrepancies between NRM_{20mT}/ARM_{20mT} and $NRM_{20mT}/SIRM_{20mT}$ exist in the intervals from about 5,400 to 4,500, around 3,200 and about 2,900 to 2,600 cal. yrs B.P. The mismatch in the older part evidently results from the fact that during the mid-Holocene environmental transition on the African continent SIRM decreases proportionally less than ARM (Fig. 4). Consequently $NRM_{20mT}/SIRM_{20mT}$ ratios are lower. The opposite trend observed in the younger intervals is caused by a relative minimum in ARM and maximum in SIRM without corresponding features in the other data set. A complete agreement between RPI records based on different normalizers would require a perfect covariance of ARM, SIRM (IRM) and susceptibility (or preferably their constancy) over time. Susceptibility not only refers to the remanence carrying magnetic mineral fractions, but also depends on paramagnetic and diamagnetic sediment components. In the present study area, where the influx of terrigenous material was extremely variable during the entire Holocene, its application as a normalizer (not shown) yields a basically similar RPI record as ARM and SIRM. Differences to the remanence normalized data in several intervals have the same order of magnitude as the discrepancies between these two records. Note that the overall about constant, relatively small hematite (or goethite) contributions to NRM intensities as well as to ARM, SIRM intensities and κ

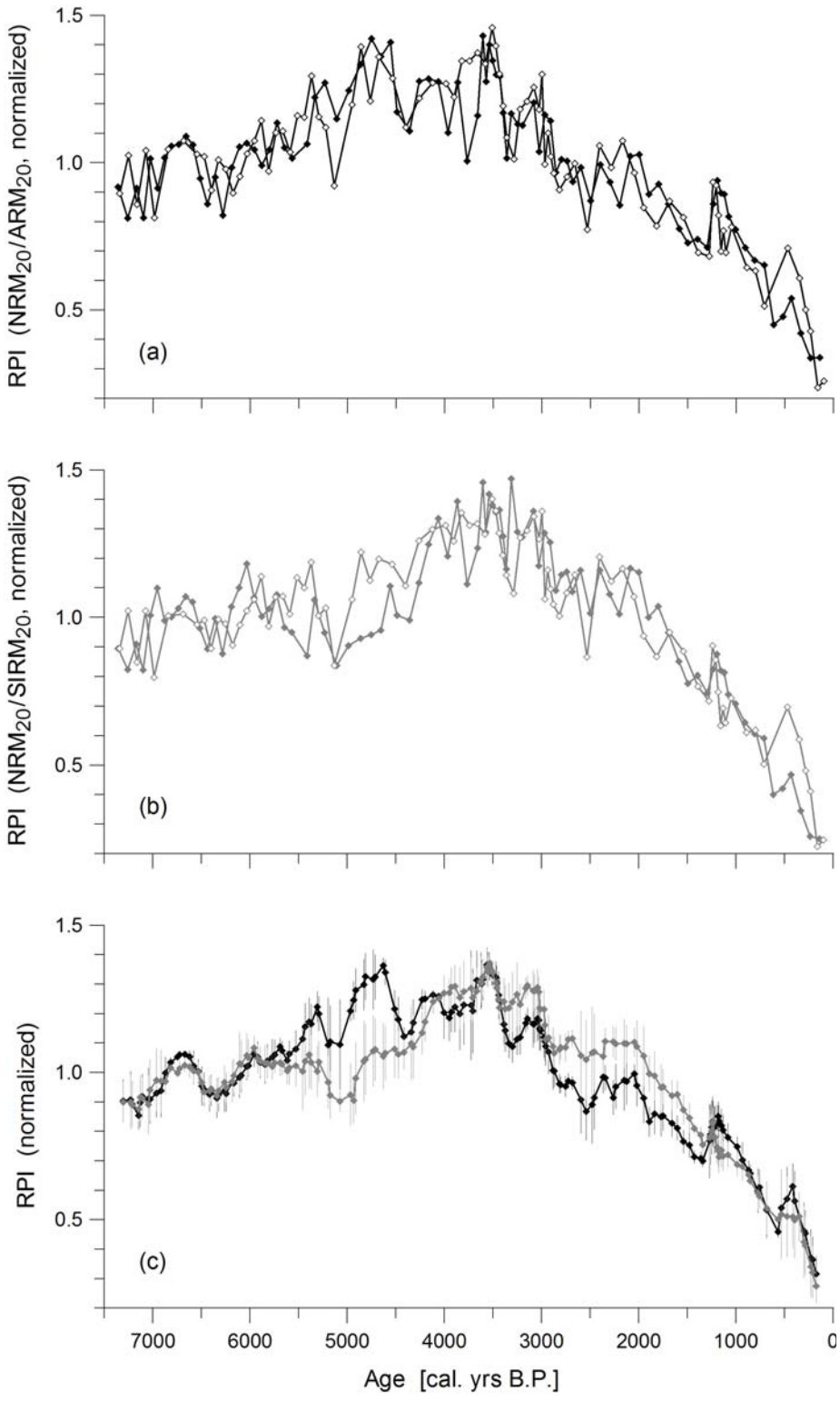

Fig. 9 (a) NRM_{20}/ARM_{20} and (b) $NRM_{20}/SIRM_{20}$ relative paleointensity estimates based on NRM, ARM and SIRM data after 20 mT AF demagnetization of cores GeoB 6007 (full diamonds) and GeoB 8601 (open diamonds) as function of age. (c) 150 year running window averages combining core GeoB 6007 and GeoB 8601 NRM_{20}/ARM_{20} (black) and $NRM_{20}/SIRM_{20}$ (grey) results; vertical bars denote 95% confidence limits. All records have been normalized to a mean of unity.

will not significantly influence the RPI records normalized to unity.

The data from the 5,400 to 4,500 cal. yrs B.P. period impose a moderate negative correlation (r = -0.446) between NRM_{20mT}/ARM_{20mT} and ARM which is significantly reduced (r = -0.138) if they are excluded. Hence, climatic factors influence at least parts of this RPI record. Some impact also on the $NRM_{20mT}/SIRM_{20mT}$ ratios is indicated by their correlation of r = -0.279 to SIRM.

To further evaluate the relative paleointensity information in our sediment series, the so-called pseudo-Thellier technique has been employed. This method introduced by *Tauxe et al*. (*1995*) was used in a number of recent studies (e.g., *Kruiver et al., 1999; Snowball and Sandgren, 2004*). The basic principles are similar to those successfully applied to obtain absolute paleointensities from thermal remanences of volcanic rocks or archeologic artifacts. It also extends on ideas of *Jackson et al.* (*1988*) that normalizing the partial NRM demagnetized within a particular alternating field interval by the partial ARM acquired in the same AF range will combine a specific, identical coercitivity window. The pseudo-Thellier technique seeks to objectively define an optimal coercitivity window for RPI estimates by plotting the NRM remaining versus the ARM acquired in the same sequence of alternating fields, in general 10 to 15 steps between 5 and 100 mT (Fig. 10). At low AF levels such Arai-type diagrams mostly show a distinct curvature indicating that relatively higher proportions of NRM are removed than ARM acquired. This pattern reflects the demagnetization of gradually diminishing amounts of low coercivity, possibly viscous components (*Tauxe et al., 1995*). Concave shapes observed towards high AF levels, i.e. proportionally less NRM remains than ARM is acquired, imply the presence of additional stable magnetic mineral fractions which do not contribute to NRM. In between a more or a less linear segment exists. RPI estimates based on NRM/ARM ratios, which correspond to the slope of the Arai plot, refer to the same coercivity spectra of the magnetic mineral assemblage in this interval. Although ARM relates to the total fine grained fraction, its relative portion carrying NRM remains essentially unchanged there.

The interval of optimal linearity in the Arai plot has been established individually for each sample as the best fitting regression (minimal standard error of the slope) within four consecutive field steps between 15 and 90 mT (Fig. 10). This objective routine should be given preference above the pilot sample method and has the additional advantage to provide an estimate of uncertainty for every pseudo-Thellier relative paleointensity (PT-RPI) determination (*Tauxe et al., 1995*). The best fitting four field step interval for the majority of samples falls into the 25 to 40, 30 to 45 or 35 to 50 mT range. Only for a small number of samples from all parts of the cores was the best fit obtained at intermediate fields of 40 to 55 and 45 to 60 mT. For about 25% of the samples from core GeoB 8607 and 36% from core GeoB 6007 the best fitting intervals were 50 to 80 or 60 to 90 mT. Some of these samples are unsystematically distributed over both cores, but most, and particularly in core GeoB 6007, originate from the 6,000 to 4,000 cal. yrs B.P. period of environmental turnover.

Figure 11 summarizes the PT-RPI results. Individual estimates show a quite high scatter, yet no consistent differences are present over the entire records or longer intervals of both cores. The 95% confidence limits of the 150 year running window averages combining the data reflect this relatively broad distribution. Nevertheless, several distinct variations and trends can be clearly identified. Most prominent is the maximum around 3,600 cal. yrs B.P.. It suggests an approximately 60% increase of the geomagnetic field intensity in the study area since the beginning of the record at about

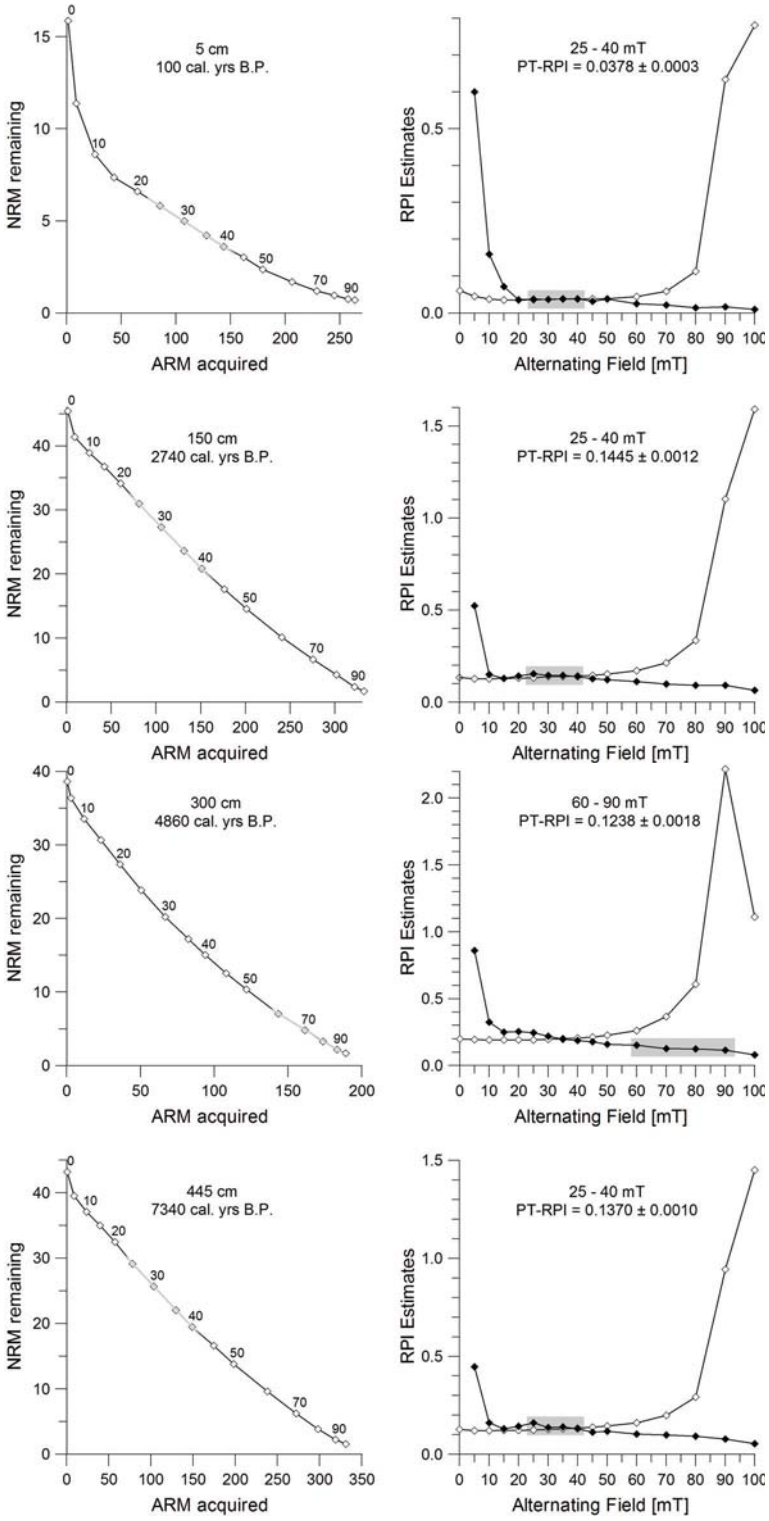

Fig. 10 Examples illustrating PT-RPI estimates of core GeoB 8601 sediments. (left) ARM acquired in specified (mT) alternating fields versus NRM remaining after AF demagnetization in the same fields. PT-RPI is determined as the best fitting regression (minimal standard error of the slope) for four consecutive field steps between 20 and 90 mT (grey line). (right) RPI estimates of NRM/ARM ratios as a function of demagnetization field (open diamonds) and PT-RPI estimates of two consecutive field steps (full diamonds). Grey bars denote the best fitting four field step interval. Respective PT-RPI estimate is specified together with depth position and age for each sample. (Results of NRM demagnetization of the same sample set are shown in Fig. 7).

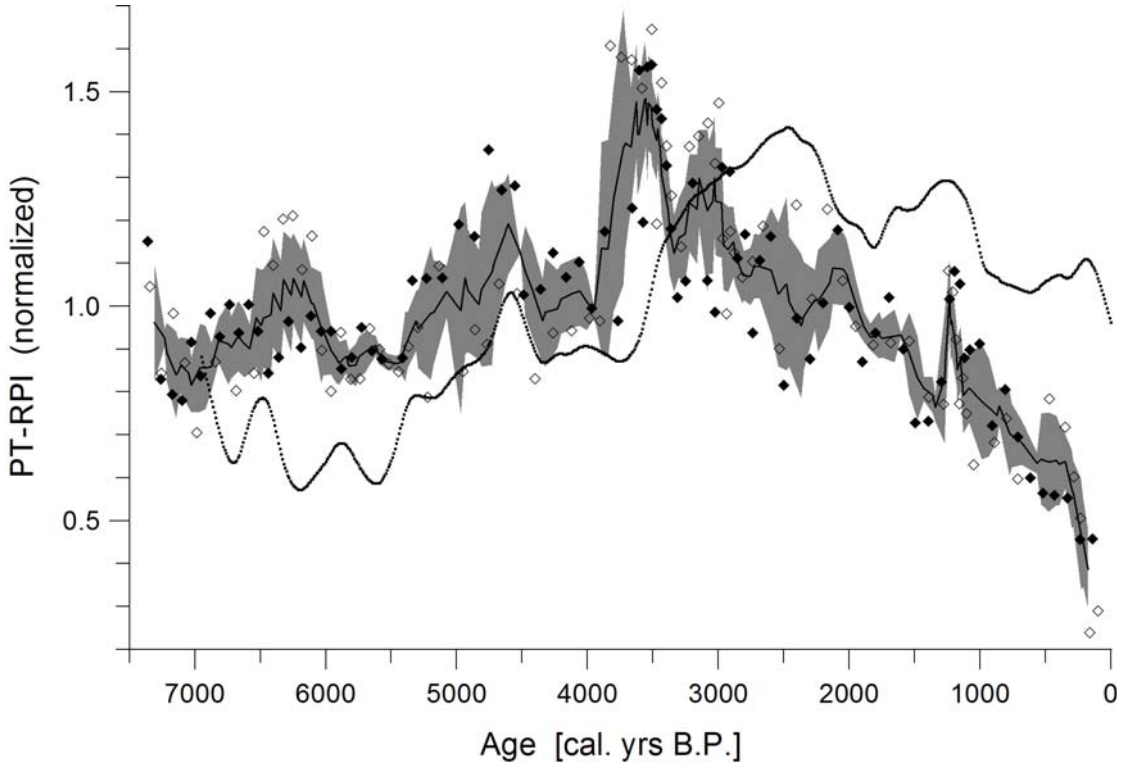

Fig. 11 PT-RPI estimates of core GeoB 6007 (full diamonds) and GeoB 8601 (open diamonds) sediments as function of age. Black line shows 150 year running window averages combining the data of both cores. Grey shading denotes 95% confidence limits. Dotted line represents the CALS7K.2 model predictions (*Korte and Constable, 2005*) of the geomagnetic field intensity for the study area at 10 year resolution. All records have been normalized to a mean of unity.

7,500 cal.yrs B.P.. This rise has not been continual, but took place over two local maxima at about 6,300 and 4,600 cal. yrs B.P. separated by local minima at about 5,700 and 4,200 cal. yrs B.P., respectively. From the maximum at around 3,600 cal. yrs B.P. to the present, PT-RPI estimates more or less steadily decrease. For the last 500 years our age model may be inadequate. Moreover, the respective PT-RPI data are questionable, because of the incomplete paleomagnetic lock-in. Before this interval, the regional geomagnetic field intensity should already have declined to less than half of its preceding maximum. Different from the standard NRM_{20mT}/ARM_{20mT} RPI estimates, the PT-RPI record does not show any correlation ($r = 0.002$) to ARM implying that climatically controlled influences have been successfully eliminated. Our PT-RPI record shows basically similar long term trends as the global CALS7K.2 model of *Korte and Constable* (*2005*), which is based on archeomagnetic as well as lake sediment data (Fig. 11). A marked intensity increase since the early Holocene to a maximum is followed by a decrease to the present. Our data peak at around 3,600 cal. yrs B.P., while the model intensities reach the maximum only about 1,100 years later, a difference which should be well beyond the accuracy limits of age dating. Other detailed archeomagnetic and RPI records from the northern hemisphere (Fig. 12) also consistently report the highest Holocene geomagnetic intensities around 2,500 cal. yrs B.P. In global compilations of absolute paleointensity data (*Valet, 2003* and references therein) the maximum appears very broad, extending from about 3,500 to 1,500 cal. yrs B.P.

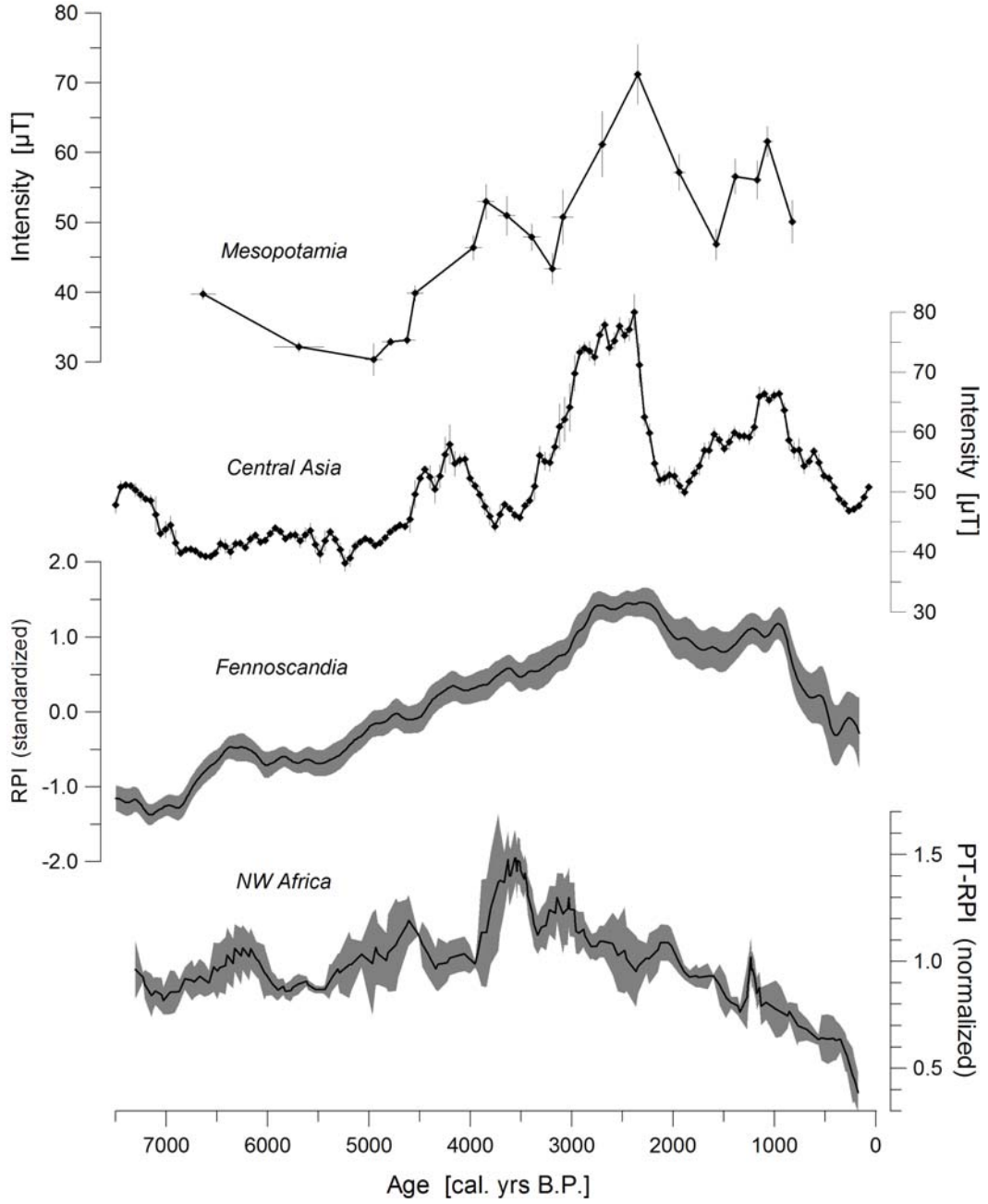

Fig. 12 Comparison of the NW Africa relative paleointensity record with the Fennoscandian relative paleointensity stack (*Snowball et al., 2007*) and absolute paleointensity records for Central Asia (*Nachasova and Burakov, 2000*) and the Middle East (*Genevey et al., 2003*) derived from archeomagnetic analyses.

The global model predicts a major intensity low around 6,000 cal. yrs B.P. (Fig. 11) corresponding to shallow inclination estimates in the directional record (Fig. 8b). Both features clearly contradict our actual observations. It is interesting to note that paleomagnetic data of lacustrine sediments from Cameroon (*Thouveny and Williamson, 1988*) also do not show shallow inclinations in this period. In the younger part, the model intensities are systematically higher, their decline towards the present much less steep. As mentioned before, our record is likely unreliably for the last 500 years, possibly even the last millennium. Excluding this period does not substantially reduce the notable

dissimilarities, however. As matters stand, there should presently be little sense in discussing disagreements or agreements (which obviously exist) at millennium scales. What is definitely needed to solve the apparent problems, are more data from the study area. Variations in paleomagnetic lock-in depth observed even at closely adjacent sedimentary sites (*Sagnotti et al., 2005*) and likely also affecting the core GeoB 6007 and GeoB 8601 results should preclude any adequate resolution within some hundreds of years.

Summary

The magnetic mineral inventory of Holocene marine sediment series from the NW African continental margin is clearly dominated by a fine grained (titano-)magnetite fraction which exhibits distinct, apparently climate induced variations in grain-size related attributes. They are particularly manifest during the about 6,000 to 4,000 cal. yrs B.P. shift from humid to arid condition on the African continent.

Notwithstanding these influences, paleomagnetic analyses of the sediments could establish a high quality declination and inclination record, documenting the directional variability of the Earth's magnetic field in the study area during Holocene. Its comparison to predictions of the CALS7K.2 global geomagnetic field model reveals certain agreements, but also remarkable inconsistencies in some intervals for which there is no other sound explanation at present than a lack of data.

Conventional relative paleointensity estimates based on NRM_{20mT}/ARM_{20mT} and $NRM_{20mT}/SIRM_{20mT}$ ratios are clearly affected by climatic factors, at least during critical periods such as the mid-Holocene environmental transition. The pseudo-Thellier method to determine RPI estimates apparently overcomes this problem. Yet, to a large extent its results do not compare favourably to the global geomagnetic model predictions.

Acknowledgements

We thank Ian Snowball and Monika Korte for providing their original data sets. Discussions with Karl Fabian, David Heslop and Tilo von Dobeneck and critical comments by Nicolas Thouveny and an anonymous reviewer were of very substantial support in improving the manuscript. This article contributes to the Project C1 '*Sedimentary Signatures and Diagenetic Processes of Ocean Margin Deposits*' of the DFG Research Center Ocean Margins as publication no. RCOM 05535.

References

Bleil, U. and cruise participants, 2004. Report and preliminary results of Meteor Cruise M 58/2. *Berichte*, **227**, Fachbereich Geowissenschaften, Universität Bremen.

Claussen, M., Kubatzki, C. and Petoukhov, V., 2003. Climate change in northern Africa: the past is not the future. *Clim. Change*, **57**, 99-118.

deMenocal, P., Ortiz, J., Guilderson, T., Adkins, J., Sarnthein, M., Baker, L. and Yarusinsky, M., 2000. Abrupt onset and termination of the African Humid Period: rapid climate responses to gradual insolation forcing. *Quat. Sci. Rev.*, **19**, 347-361.

Gallet, Y., Genevey, A. and Fluteau, F. 2005. Does Earth's magnetic field variation control centennial climate change? *Earth Planet. Sci. Lett.*, **236**, 339-347.

Genevey, A., Gallet, Y. and Margueron, J.-C., 2003. Eight thousand years of geomagnetic field intensity variations in the eastern Mediterranean. *J. Geophys. Res.*, **108**, 2228, doi: 10.1029/2001JB001612.

Genevey, A. and Gallet, Y., 2002. Intensity of the geomagnetic field in western Europe over the past 2000 years: new data from ancient French potteries, *J. Geophys. Res.*, **107**, 2285, doi: 10.1029/2001JB000701.

Jackson, M., Gruber, W., Marvin, J. and Banerjee, S.K., 1988. Partial anhysteretic remanence and its anisotropy: applications and grainsize-dependence. *Geophys. Res. Lett.*, **15**, 440-443.

King, J.W., Banerjee, S.K. and Marvin, J., 1983. A new rock-magnetic approach to

selecting sediments for geomagnetic paleointensity studies: application to paleointensity for the last 4000 years. *J. Geophys. Res.*, **88**, 5911–5921.

Kirschvink, J.L., 1980. The least-squares line and plane and the analysis of palaeomagnetic data. *Geophys. J. R. Astron. Soc.*, **62**, 699-718.

Korte, M. and Constable, C.G., 2005. Continuous geomagnetic field models for the past 7 millennia: 2. CALS7K, *Geochem. Geophys. Geosyst.*, **6**, Q02H16, doi: 10.1029/2004GC000801.

Kruiver, P.P., Ko, Y.S., Dekkers, M.J., Langereis, C.G. and Laj, C., 1999. A pseudo-Thellier relative paleointensity record, and rock magnetic and geochemical parameters in relation to climate during the last 276 kyr in the Azores region. *Geophys. J. Int.*, **136**, 757-770.

Kuhlmann, H., Freudenthal, T., Helmke, P. and Meggers, H., 2004a. Reconstruction of paleoceanography off NW Africa during the last 40,000 years: influence of local and regional factors on sediment accumulation. *Mar. Geol.*, **207**, 209-224.

Kuhlmann, H., Meggers, H., Freudenthal, T. and Wefer, G., 2004b. The transition of the monsoonal and the N Atlantic climate system off NW Africa during the Holocene. *Geophys. Res. Lett*, **31**, L22204, doi: 10.1029/2004GL021267.

Levi, S. and Banerjee, S.K., 1976. On the possibility of obtaining relative paleointensities from lake sediment. *Earth Planet. Sci. Lett.*, **29**, 219-226.

Lund, S.P. and Schwartz, M., 1999. Environmental factors affecting geomagnetic field paleointensity estimates from sediments. In: B.A. Maher, and R. Thompson (Eds.), *Quaternary Climates, Environments and Magnetism,* Cambridge University Press, Cambridge, U.K., 324-351.

Maher, B.A., 1988. Magnetic properties of some synthetic sub-micron magnetites. *Geophys. J.*, **94**, 83-96.

Neuer, S. and cruise participants, 2000. Report and preliminary results of Meteor Cruise M45/5. *Berichte*, **163**, Fachbereich Geowissenschaften, Universität Bremen.

Nachasova, L.E. and Burakov, K.S., 2000. The geomagnetic field intensity in Central Asia from 6000 to 3000 B.C., *Izv. Russ. Acad. Sci. Phys. Solid Earth*, **36**, 358-363 (Engl. Transl.).

Petermann H., and Bleil, U., 1993. Detection of live magnetotactic bacteria in South Atlantic deep-sea sediments. *Earth Planet. Sci. Lett.*, **117**, 223-228.

Robinson, S.G., Sahota, J.T.S. and Oldfield, F., 2000. Early diagenesis in North Atlantic abyssal plain sediments characterized by rock-magnetic and geochemical indices. *Mar. Geol.*, **163**, 77-107.

Sagnotti, L, Budillon, F., Dinarès-Turell, J., Iorio, M., and Macri, P., 2005. Evidence for a variable paleomagnetic lock-in depth in the Holocene sequenze from the Salerno Gulf (Italy): Implications for "high-resolution" paleomagnetic dating. *Geochem. Geophys. Geosyst.*, **6**, Q11013, doi: 10.1029/2005GC001043.

Snowball, I. and Sandgren, P., 2004. Geomagnetic field intensity changes in Sweden between 9000 and 450 cal BP: extending the record of "archaeomagnetic jerks" by means of lake sediments and the pseudo-Thellier technique. *Earth Planet. Sci. Lett.*, **227**, 361-376.

Snowball, I., Zillén, L., Saarinen, A., Ojala, A. and Sandgren, P., 2007. FENNOSTACK and FENNORPIS: Varve dated Holocene palaeomagnetic secular variation and relative palaeointensity stacks for Fennoscandia. *Earth Planet. Sci. Lett.*, 55, 106-116.

Stoner, J.S., Channell, J.E.T. and Hillaire-Marcel, C., 1996. The magnetic signature of rapidly deposited detrital layers from the deep Labrador Sea: relationship to North Atlantic Heinrich layers. *Paleoceanography*, **11**, 309-325.

St-Onge, G., Stoner, J.S. and Hillaire-Marcel, C., 2003. Holocene paleomagnetic records from the St. Lawrence Estuary, eastern Canada: centennial- to millennial-scale geomagnetic modulation of cosmogenic isotopes. *Earth Planet. Sci. Lett.*, **209**, 113-130.

Stuiver, M., Reimer, P.J., Bard, E., Beck, J.W., Burr, G.S., Hughen, K.A., Kromer, B., McCormac, G., van der Plicht, J. and Spurk, M., 1998. INTERCAL98 rardiocarbon age calibration, 24,000 – 0 cal BP. *Radiocarbon*, **40**, 1041-1083.

Tauxe, L., 1993. Sedimentary records of relative paleointensity of the geomagnetic

field: theory and practice. *Rev. Geophys.*, **31**, 319–354.

Tauxe, L., Pick, T. and Kok, Y.S., 1995. Relative paleointensity in sediments: a pseudo-Thellier approach. *Geophys. Res. Lett.*, **22**, 2885-2888.

Thouveny, N. and Williamson, D., 1988. Palaeomagnetic study of the Holocene and Upper Pleistocene sediments from Lake Barombi Mbo, Cameroun: first results. *Phys. Earth Planet. Inter.*, **52**, 193-206.

Valet, J.-P., 2003. Time variations in geomagnetic intensity. *Rev. Geophys.*, **41**, 1004, doi: 10.1029/2001RG000104.

Watkins, S.J. and Maher, B.A., 2003. Magnetic characterisation of present-day deep-sea sediments and sources in the North Atlantic. *Earth Planet. Sci. Lett.*, **214**, 379-394.

Weaver, P.P.E., Wynn, R.B., Kenyon, N.H. and Evans, J., 2000. Continental margin sedimentation, with special reference to the north-east Atlantic margin. *Sedimentology*, **47**, 239-256.

Yang, S., Odah, H. and Shaw, J., 2000. Variations in the geomagnetic dipole moment over the last 12 000 years. *Geophys. J. Int.*, **140**, 158-162.

Conclusions

This study was conducted within the framework of the Research Center Ocean Margins (RCOM), University of Bremen, in the scope of subproject C1: "*Gauging diagenetic processes versus terrigenous and biogenic influx from physical, chemical and mineralogical attributes of sedimentary deposits in high productivity systems*", funded by the German Research Foundation (DFG).

The presented work focuses on the magnetic characteristics of natural iron oxide minerals in suboxic and anoxic marine sediments recovered from continental margin regions of western Africa. These regions, which are characterized by high marine productivity in the surface waters that result in elevated biogenic accumulation rates, are often associated with the occurrence of diagenetic processes, which can severely affect the sediment magnetic mineral assemblage. Iron oxides are redox sensitive minerals, which react very easily and in specific ways in response to reducing conditions and thus have an important role to play in proxy based paleo-environmental reconstructions. Therefore it is of great interest to know how the primary sediment composition can be reconstructed and how the role of diagenetic processes are reflected in the magnetic characteristics of the preserved sediments. Further it is of interest to see to what extent these sediments are suitable for paleomagnetic investigations. The interpretation of the magnetic signal is not always straightforward. However, a variety of rock-magnetic techniques, including conventional room-temperature rock-magnetic methods and high- and low-temperature magnetic measurements are available to facilitate a robust rock-magnetic interpretation and to unravel environmental signals.

The results of this thesis are based mainly on such high-resolution rock-magnetic analyses, which allow for a detailed classification of natural iron minerals of different compositions and grain-sizes. Due to diagenetic alteration the magnetic mineral concentration, especially in anoxic environments, is found to be rather low. To obtain a stronger signal for the subsequent thermomagnetic analysis magnetic minerals have been concentrated by extraction. Changes in the magnetic mineralogy were investigated, in particular which magnetic phases are responsible for the magnetic characteristics under anoxic geochemical conditions.

The complexity of the mechanisms driving the diagenetic alteration of the magnetic inventory means it is necessary to integrate methods from different scientific disciplines. Therefore geochemical pore water and solid phase analyses and electron microscopic techniques were combined with the rock-magnetic methods. With the results of this multidisciplinary approach a more complete understanding of the magnetic signal in ocean margin sediments, its origin and particularly its post-depositional alterations is obtained.

The presented investigations in this thesis are concerned with the sediments of the Niger deep-sea fan and the upwelling area off Cape Ghir. At first I would like to focus on the methods that were developed and how they were employed to unravel the paleo-environmental history of the studied sediments. The applicability of the developed methods is demonstrated in terms of the information which can be obtained from the magnetic properties of continental margin sediments. At the end of the section a short outlook is provided.

The investigations have revealed that low-temperature measurements performed on magnetic mineral extracts are suitable to characterize the magnetomineralogical composition of a sediment sample. It was shown that even when remanence transitions and characteristic susceptibility peaks are not obviously apparent in low-temperature curves, careful investigation of the data reveal important

environmental information. This can be used to characterize the magnetic mineral phases in a given sediment sample providing a much more detailed paleo-environmental understanding of the study area.

The highly sensitive low-temperature magnetic measurements combined with scanning electron microscopy provided an even more complete picture of the magnetic mineral inventory. Thus, a powerful tool was established to identify and quantify the magnetic mineral phases present in the sediment samples. This approach also provided the possibility to distinguish between compositionally similar particles, e.g. between titanomagnetite and titanohematite phases and to calculate an approximate composition for individual particles. The classification of individual magnetic particles allows a more detailed interpretation concerning aspects such as the source areas of the primary magnetic assemblage.

Low-temperature magnetometry has become increasingly popular over recent years for the identification of complex Fe-Ti oxide assemblages in rocks and/or sediments. The main advantage of magnetic measurements at low-temperatures is that they are non-destructive and highly sensitive. This becomes particularly important when the magnetic mineral content in a bulk sample is very low and the availability of sample material is limited. Unfortunately the published database of low-temperature magnetic measurements mainly consists of experiments made on synthetic materials of well-known composition and grain-size or on natural samples with relatively simple compositions. Only a few studies included natural samples in which the domain state and composition of the magnetic minerals is more complex. With the results of this thesis this database can be expanded significantly with, for example, complex low-temperature hysteresis measurements performed on natural samples. The characteristic evolution of the measured loops and in particular the coercive force was found to be a particularly indicative parameter, which could be applied for the identification of the main magnetic mineral phase in the sediment.

A non-negative matrix factorization (NMF) algorithm was employed for unmixing rock and environmental magnetic data. This algorithm provides a new approach that performs a linear unmixing of remanence data into coercivity based end-members and thus does not rely on any specific distribution function. This method provided a detailed picture of the magnetic inventory in the different geochemical zones of sediments from the Niger Fan. It was shown, that the primary magnetic signal is dominated by fine and coarse grained Ti-poor (titano-) magnetite, but Ti-rich titanomagnetite and/or –hematite was found to be also present in the primary magnetic mineral inventory. Yet its magnetic properties are masked by magnetite and the Ti-poor magnetic mineral phases. The analysis demonstrated that the dominant presence of Ti-rich magnetic mineral phases in the anoxic sediments is therefore related to the primary source signal and the strong dissolution of pure and Ti-poor iron oxides rather than to the formation of authigenic magnetic mineral phases. The potential of this method remains to be fully explored, in particular the question of initialization of the algorithm. However, in general rock magnetic data can be analysed with this approach where the assumption of linear mixing is thought to hold.

In the Niger deep-sea fan area the dissolution of magnetic minerals in the sediments was found to be strongly related to grain-size, with the smallest particles dissolving first, due to their larger surface area to volume ratio. Additionally the Ti content plays an important role during the reductive dissolution process because Ti bearing oxides have generally a higher stability relative to pure iron oxides. As a result of their high intrinsic stability, titanohematite phases persist as the

predominant magnetic mineral fraction in the sulfidic anoxic sediments of the Niger deep-sea fan. On the other hand findings in the upwelling region off NW Africa suggest that maghemitization can also be an important process in the preservation of pure magnetite. This low-temperature oxidation process starts at the crystal surfaces, and proceeds towards the centre of the particle, due to preferential diffusion of ferrous ions (Fe^{2+}) from (titano-)magnetite. A relatively mild maghemitization process e.g. at the sediment/water interface has the effect that the rim of the magnetite particle is converted into maghemite, protecting the central part of the grain against further alteration. In case of a change of the chemical conditions in the sediment into a reducing milieu, the maghemite rim dissolves first and the stoichiometric magnetite core remains present in the sediment for longer.

The Niger Fan and the Canary Island region exhibit quite similar environmental conditions, with surface waters characterized by an intense biological productivity and high fluxes of organic material to the sea floor leading to extensive diagenetic processes in their sedimentary deposits. However, the diagenetic effects on the primary magnetic mineral assemblage are vastly different. The main difference concerning the magnetic material is the different origin and input pathways of the deposited material in each study area. The Niger fan deposits are dominated by terrigenous components supplied by the Niger River. Here the aeolian contributions are of minor importance (7 to 15% of the lithogenic fraction). The vast majority of the magnetic assemblage reaching the gravity core location is composed of eroded volcanic material originating from the Cameroon Volcanic Line. In contrast in the Canary Island region the influx of terrigenous magnetic components into the sediments is strongly influenced by an aeolian fraction transported westwards from the modern semi-arid to arid areas of the African continent. The weathering conditions in the source area (Sahara) favour the presence of the high coercivity minerals hematite and goethite in the dust fraction. This leads to the conclusion, that the postdepositional conditions in the sediment column are not the only important steering factors, but also the nature of the magnetic terrigenous fraction plays an important role in the preservation and subsequent modifications after sediment deposition.

Diagenetic alteration can severely affect the primary sediment magnetic mineral assemblage as shown in the deposits from the eastern Niger deep-sea fan. Here, the magnetic signal is strongly affected by reductive dissolution so that the remaining signal does not allow reliable paleointensity information to be recovered from the sediments. However, this thesis has also shown that sediments from upwelling regions are not necessarily unsuitable for paleomagnetic studies. The overprint of the deposits from the marginal region off NW Africa is restricted to a very confined interval of the sediment column. The majority of the sediment sequence remains practically unaffected by dissolution effects and thus qualifies for delicate high temporal resolution paleomagnetic investigations. A high quality declination and inclination record was established, documenting the directional variability of the Earth's magnetic field for the last seven ka for NW Africa.

Continental margin sediments are a particularly interesting environment in which to study modifications of the primary magnetic mineralogy in the course of reductive diagenesis. This work has shown, that the extent of iron dissolution and consequent effects on magnetic properties depend on the degree of the reducing conditions, as well as on the origin of the magnetic material. The alteration can obscure and even erase paleomagnetic information stored in the sedimentary record, but on the other hand, relicts of geochemical processes reveal

paleo-environmental information and the diagenetic history of the sediments, e.g. by using the magnetic titano-phases present in the sediment.

For further identification and quantification of these individual components e.g. Mössbauer spectroscopy or electron backscatter diffraction (EBSD) are recommended. These methods provide more details on the exact chemical composition, crystallographic structure and concentration of each particle type. This additional information also helps to "clarify" the physical mechanisms, which are responsible for the low-temperature behaviour observed in natural samples. Such detailed information is necessary because the (physical) effects in natural samples are usually much more complex than for synthetic samples, which are described in the published data. However, Mössbauer spectroscopy and EBSD analyses are relatively time consuming and not practical for large scale studies. Therefore the method outlined in chapter 4 of this thesis by using the characteristic Fe K_α and Ti K_α lines derived from elemental dispersive spectroscopy should be further developed in future. A larger number of well defined standards are required to establish a database, to which the experimental EDS spectra of the natural samples can be compared.

It was shown, that the magnetic signal in rapidly deposited sediments can also be a source of information on the geomagnetic field. Yet, comparisons of the derived Holocene relative paleointensity record to model predictions of the geomagnetic field intensity for the study area revealed certain agreements, but also remarkable inconsistencies in some intervals, which at present can not be explained because of a lack of comparable data from this region. A logical pursuit would be to retrieve further records from the region, to validate the relative paleointensity determinations derived for this study area and to identify and exclude potential artefacts in the relative paleointensity determinations.

Zusammenfassung in deutscher Sprache

Diese Studie wurde im Rahmen des Forschungszentrums „Research Center Ocean Margins“ (RCOM) an der Universität Bremen, im Teilbereich C1 “*Gauging diagenetic processes versus terrigenous and biogenic influx from physical, chemical and mineralogical attributes of sedimentary deposits in high productivity systems*” durchgeführt. Sie befasst sich mit der detaillierten Untersuchung diagenetisch überprägter Sedimente aus dem östlichen Äquatorialatlantik (Nigerfächer). Ergänzt werden die Arbeiten durch Untersuchungen an Sedimenten aus dem Auftriebsgebiet vor Nordwest (NW) Afrika (Kap Ghir). Hierzu sind insbesondere die magnetischen Eigenschaften natürlicher Eisenminerale im suboxischen und anoxischen Milieu untersucht worden. Eisenoxide sind redox sensitive Minerale, die sensibel und charakteristisch auf reduzierenden Porenwasserchemismus reagieren. Zusätzlich ist überprüft worden, ob und in welchem Maße paläomagnetische Untersuchungen an Sedimenten aus Hochproduktionsgebieten möglich sind.

Durch den Aufstieg nährstoffreichen Zwischenwassers entlang des Kontinentalhanges sind die Primärproduktionsraten im Oberflächenwasser beider Arbeitsgebiete insgesamt stark erhöht. Es bilden sich große Mengen organischen Materials, die zum Meeresboden absinken und in den Sedimenten eingelagert werden. Der anschließende Abbau durch reduzierende Bakterien führt zu intensiven diagenetischen Prozessen in den sedimentären Ablagerungen, in deren Folge auch gut kristallisierte ferrimagnetische Oxide instabil werden können. Damit verbunden sind signifikante Veränderungen der magnetischen Eigenschaften des Sedimentes.

Ziel dieser Arbeit war es, mit den Methoden der Sedimentmagnetik das primäre magnetische Signal zu identifizieren und die Auswirkungen frühdiagenetischer Prozesse auf dieses Signal zu quantifizieren. Als Grundlage dienten dabei unterschiedliche sedimentmagnetische Parameter, gemessen bei Raum-, Hoch- und Tieftemperatur, mit deren Hilfe differenzierte Aussagen über die magnetischen Mineralfraktionen möglich sind. Zum weiteren Verständnis der komplexen Mechanismen, die für die diagenetische Überprägung des magnetischen Mineralinventars verantwortlich sind, wurden geochemische Porenwasser- und Festphasendaten sowie rasterelektronenmikroskopische (REM) Analysen bei der Interpretation der sedimentmagnetischen Parameter mit einbezogen.

Aufgrund der reduktiven Lösung der Eisenoxide ist die Konzentration magnetischer Partikel, insbesondere im anoxischen Sedimentmilieu, sehr gering. Um ein ausreichend starkes Signal für die Tieftemperaturmessungen zu erhalten, wurden die magnetischen Minerale aus dem Gesamtsediment mit Hilfe der magnetischen Extraktion angereichert. Gesteinsmagnetische Messungen an einem „Magnetic Property Measurement System“ (MPMS) im Temperaturbereich zwischen 300 und 5 K an magnetischen Extrakten haben sich als erfolgreich erwiesen, die magnetomineralogische Zusammensetzung in einer Sedimentprobe zu charakterisieren. So ließen sich aus der sorgfältigen Analyse der magnetischen Tieftemperaturkurven Informationen ableiten, mit denen die einzelnen magnetischen Mineralphasen spezifiziert werden konnten. Insbesondere temperaturabhängige Hysteresemessungen haben sich dabei als sehr hilfreich erwiesen. Die charakteristische Veränderung der Messkurven und die daraus abgeleitete Koerzitivkraft konnten als indikative Parameter genutzt werden, um die verschiedenen magnetischen Eisen-Titanoxide im Sediment zu unterscheiden.

Die Kombination mit REM Untersuchungen und „Energie dispersiver Spektroskopie“ (EDS) vervollständigt das umfassende Bild des magnetischen

Mineralinventars. So konnten die Mineralphasen, die hauptsächlich für die magnetischen Eigenschaften unter reduzierenden anoxischen Bedingungen verantwortlich sind, eindeutig bestimmt werden. Zudem bietet dieser Ansatz die Möglichkeit, chemisch sehr ähnliche, aber mineralogisch unterschiedliche Phasen, wie zum Beispiel Titanomagnetit ($Fe_{3-x}Ti_xO_4$; $0 \leq x \leq 1$) und Titanohämatit ($Fe_{2-y}Ti_yO_3$; $0 \leq y \leq 1$), voneinander zu unterscheiden. Durch den Vergleich natürlicher Sedimentproben mit gut definierten Standards war es möglich, für individuelle Partikel eine genaue Elementzusammensetzung zu berechnen. Solch eine Klassifizierung einzelner magnetischer Teilchen kann verwendet werden, um Beziehungen zwischen Quellen und Senken der magnetischen Partikel herzustellen und die umweltmagnetischen Parameter für ein bestimmtes Arbeitsgebiet genauer zu interpretieren.

Zur Komponentenanalyse von gesteins- und umweltmagnetischen Daten ist ein „nicht-negativer Matrix-Faktorisierungs-Algorithmus“ (NMF-Algorithmus) entwickelt worden. Dieser ermöglicht eine lineare Trennung der magnetischen Remanenz-daten in Endglieder bezüglich ihrer Koerzitivität und ist damit nicht auf spezifische Verteilungsfunktionen angewiesen. Mit Hilfe dieser Methode konnte das Schicksal des magnetischen Mineralinventars in den unterschiedlichen geochemischen Zonen in den Sedimenten des Nigerfächers genauer nachvollzogen werden. Es wurde gezeigt, dass das primäre magnetische Signal hier von reinem Magnetit und titanarmen Eisenoxiden dominiert wird, dass aber titanreiche Titanomagnetite und/oder -hämatite ebenfalls im primären Mineralinventar vertreten sind. Deren magnetische Eigenschaften werden jedoch von Magnetit und den titanarmen Komponenten überlagert. Nach den intensiven anoxischen Lösungsprozessen bleiben jedoch nur noch die titanreichen Mineralphasen im Sediment erhalten.

Zusammengefasst zeigen die Ergebnisse aus dem Nigerfächer, dass die reduktive Lösung magnetischer Mineralphasen im Sediment stark von der Korngröße abhängig ist, da kleinere Partikel aufgrund ihres größeren Verhältnisses von Oberfläche zu Volumen bevorzugt gelöst werden. Zusätzlich spielt auch der Titangehalt während des reduktiven Lösungsprozesses eine wichtige Rolle, da titanhaltige Eisenoxide im Vergleich zu reinen Eisenoxiden eine höhere Koerzitivität aufweisen. Aufgrund ihrer hohen intrinsischen Stabilität sind Titanohämatitphasen daher resistenter gegenüber reduktiver Diagenese und bleiben somit als dominierende magnetische Mineralfraktion in den anoxischen Sedimenten des Nigerfächers erhalten.

Im Gegensatz dazu deuten die Ergebnisse aus dem Auftriebsgebiet vor NW Afrika darauf hin, dass Maghemitisierung ein wichtiger Prozess hinsichtlich der Erhaltung von titanfreiem Magnetit sein kann. Dieser Tieftemperatur-Oxidationsprozess beginnt an der Kristalloberfläche und schreitet von dort weiter in Richtung Partikelzentrum vor. Ein relativ milder Maghemitisierungsprozess, zum Beispiel an der Sediment/Wasser Grenze, bewirkt, dass das Äußere des Magnetitpartikels in Maghemit umgewandelt wird und den Kern des Partikels vor weiterer Alteration schützt. Ändern sich die chemischen Parameter im Sediment von oxischen zu reduzierenden Bedingungen, wird zuerst der Maghemitrand weggelöst während der Magnetitkern zunächst erhalten bleibt.

Trotz ähnlicher geochemischer Bedingungen in der Sedimentsäule sind die Auswirkungen der diagenetischen Alteration auf das primär eingetragene magnetische Material in den beiden Arbeitsgebieten sehr unterschiedlich ausgeprägt. Entscheidend sind dabei die magnetischen terrigenen Mineralfraktionen, die durch unterschiedliche Herkunftsgebiete und Eintragsmechanismen charakterisiert sind. Die Sedimente des Nigerfächers werden von

einer terrigenen Fraktion dominiert, die über das Flusssystem des Niger in den östlichen Äquatorialatlantik eingetragen wird. Das äolisch transportierte Material ist dort mit ~7 – 15 % gegenüber der fluviatil eingetragenen Fraktion von untergeordneter Bedeutung. Dagegen ist der Eintrag des terrigenen Materials in das Auftriebsgebiet vor NW Afrika stark von einer äolischen Fraktion beeinflusst, die mit den Passatwinden hauptsächlich aus den ariden Gebieten des afrikanischen Kontinents eingetragen wird. So begünstigen die Witterungsbedingungen in dieser Quellregion die Entstehung hochkoerzitiver Mineralphasen wie Hämatit oder Goethit, während das magnetische Mineralinventar im Nigerfächer vorwiegend aus erodiertem vulkanischen Material besteht, das von der Vulkankette der Kamerunlinie stammt. Offensichtlich sind also nicht nur die geochemischen Bedingungen in der Sedimentsäule wichtige Kriterien für die Erhaltung bzw. Veränderung der magnetischen Eigenschaften des Mineralinventars durch postsedimentäre Prozesse, sondern im großen Maß bereits die primäre Beschaffenheit der magnetischen terrigenen Fraktion selbst.

Wie anhand der Sedimente des Nigerfächers gezeigt wurde, können diagenetische Prozesse das primäre magnetische Mineralinventar erheblich beeinflussen. Dort wurde das magnetische Signal so stark durch reduktive Lösung verändert, dass das verbleibende Signal keine verlässlichen Informationen mehr hinsichtlich der Paläointensität des Erdmagnetfeldes enthält. Dennoch sind Sedimente aus Auftriebsgebieten nicht grundsätzlich für solche wichtigen paläomagnetischen Untersuchungen zu verwerfen. Die diagenetische Überprägung der Ablagerungen am Kontinentalhang vor NW Afrika ist beispielsweise nur auf ein bestimmtes Tiefenintervall begrenzt. Der Großteil des Sediments bleibt von Lösungseffekten unbeeinflusst und ist daher durchaus verwendbar für hochauflösende paläomagnetische Studien. So konnte für diese Region ein hochwertiger Datensatz für die relative Paläointensität gewonnen werden, der die nur ungenau bekannte Variabilität des geomagnetischen Feldes für die letzten sieben tausend Jahre detailliert dokumentiert. Vergleiche der relativen Paläointensität mit Modellvorhersagen der geomagnetischen Feldintensität für NW Afrika zeigen deutliche Übereinstimmungen, allerdings auch einige Unstimmigkeiten, deren Ursachen aufgrund des Fehlens vergleichbarer Datensätze aus diesem Arbeitsgebiet zum jetzigen Zeitpunkt nicht zu erklären sind. Daher ist es notwendig, die Datenbasis zum Verlauf der relativen Paläointensität des Erdmagnetfeldes in dieser Region zu verbreitern. Die Arbeiten haben gezeigt, dass die dortigen Sedimente in weiten Teilen dazu geeignet sind.

Acknowledgements

Die vorliegende Arbeit wurde in der Arbeitsgruppe Marine Geophysik im Fachbereich Geowissenschaften der Universität Bremen erstellt. Für die Vergabe und Betreuung, sowie für die stete Gesprächs- und Diskussionsbereitschaft, bedanke ich mich ganz herzlich bei Herrn Prof. Dr. Ulrich Bleil. Des weiteren möchte ich mich bei Frau PD. Dr. Sabine Kasten für die Übernahme des Zweitgutachtens bedanken.

Ein besonderer Dank geht an alle aktuellen und ehemaligen Mitarbeiter der Arbeitsgruppe Marine Geophysik der Universität Bremen, die mir mit Rat und Tat bei der Durchführung der magnetischen Messungen, bei technischen Problemen im Labor und bei der Beantwortung zahlreicher Fragen zur Seite standen und damit maßgeblich zum Gelingen dieser Arbeit beigetragen haben.

Ich möchte mich an dieser Stelle auch bei den Mitgliedern des paläomagnetischen Labors ´Fort Hoofdijk` an der Universität Utrecht (Niederlande) bedanken, wo ich freundlicherweise einen Teil der thermomagnetischen Messungen durchführen durfte. Die elektronenmikroskopischen Analysen wurden ebenfalls an der Universität Utrecht am EMU angefertigt. Ein großer Dank geht auch an die AG Kristallographie und der AG Geochemie der Universität Bremen, die mir z.T. unveröffentlichtes Datenmaterial zur Verfügung gestellt haben und mich damit in meiner Arbeit hilfreich unterstützt haben. Bei Dominique Lattard und Ralf Engelmann von der Universität Heidelberg möchte ich mich dafür bedanken, dass sie die synthetische Proben 6F72x2.4 inklusive unveröffentlichter Daten zur Verfügung gestellt hat.

Ganz besonders bedanke ich mich bei Christine für ihre riesengroße Hilfe und ihre unendliche Geduld gerade in der Endphase. Danke für deine uneingeschränkte Unterstützung und dass du immer für mich da warst und hoffentlich auch in Zukunft bist.

Mein persönlicher Dank gilt meiner Familie, ohne die es niemals möglich gewesen wäre, meinem Kind und dieser Arbeit die Aufmerksamkeit zukommen zu lassen, die beides verlangt. Und auch mit dieser Hilfe war es nicht immer einfach allem und jedem gerecht zu werden.

Ich danke meinen Eltern, die mir uneingeschränkt ihre Unterstützung gegeben haben und immer für mich da waren und sind. Ganz lieben Dank auch an meine Großeltern, die in ihrem hohen Alter sich noch tapfer als Babysitter geschlagen haben. Immer wenn ich diesbezüglich ihre Hilfe brauchte, haben sie sie mir gegeben, ohne sich auch nur einmal zu beschweren.

Last but not least I owe special thanks to Conor und Tony for constantly supporting me and for just being there. I know it was not always easy, yet we stuck together. Thanks.

Bibliography

Chapter 2

Dillon, M., and U. Bleil (2006), Rock magnetic signatures in diagenetically altered sediments from the Niger deep-sea fan, J. Geophys. Res., 111, B03105, doi:10.1029/2004JB003540.

Chapter 3

Heslop, D., and M. Dillon (2007), Unmixing magnetic remanence curves without a priori knowledge, Geophys. J. Int. 170 (3), doi: 10.1111/j.1365-246X.2007.03432.x.

Chapter 4

Dillon, M., and C. Franke, Diagentic alteration of natural Fe-Ti oxides identified by energy dispersive spectroscopy and low-temperature magnetic remanence and hysteresis measurements, submitted to Physics of the Earth and Planetary Interiors.

Chapter 5

Dillon, M., Sediment magnetic characteristics of marine deposits from the upwelling region off NW Africa, in preparation for publication.

Chapter 6

Bleil U., and M. Dillon (2008), Holocene Earth´s magnetic field variations recorded in marine sediments of NW African continental margin, Studia Geophysica & Geodaetica, in press.

N a m e :..……..…… Datum ……..

Anschrift :……...

Erklärung

Hiermit versichere ich, dass ich

1. die Arbeit ohne unerlaubte fremde Hilfe angefertigt habe,

2. keine anderen als die von mir angegebenen Quellen und Hilfsmittel benutzt habe und

3. die den benutzten Werken wörtlich oder inhaltlich entnommenen Stellen als solche kenntlich gemacht habe.

_____, den …….

_____
(Unterschrift)